ABSTRACT

Title of Document: TEMPLATED SYNTHESIS OF GLYCOLURIL OLIGOMERS AND MONOFUNCTIONALIZED CUCURBIT[6]URIL DERIVATIVES

Derick Lucas, Ph.D., 2011

Directed by: Professor, Lyle Isaacs
Department of Chemistry and Biochemistry

The molecular recognition properties exhibited by molecular containers have inspired supramolecular chemists to generate diverse and specialized macrocycles. The family of hosts known as cucurbiturils (CB[n]) have become a popular platform for molecular recognition due to their high binding affinities and selectivity in water. As CB[n] branch into increasingly complex applications it becomes important to find efficient pathways to prepare monofunctionalized CB[n] derivatives bearing reactive functional groups.

Chapter 1 presents a literature review of the synthesis, properties, mechanism of formation, and applications of the CB[n] family. We use this background information to explain our key hypothesis, that templated reactions offer potential routes to obtain glycoluril oligomer building blocks that allow the preparation of monofunctionalized

CB[n] compounds.

Chapter 2 describes the templated synthesis of glycoluril hexamer (**6C**) in a one step synthetic procedure on the gram scale using the *p*-xylylenediammonium ion (**II-11**). Hexamer **6C** undergos cyclization with (substituted) phthalaldehdyes **II-12**, **II-14**, **II-15**, **II-18** under acidic conditions at room temperature to deliver monofunctionalized CB[6] derivatives **II-13**, **II-15**, **II-16**, and **II-19**. Furthermore, the reaction kinetics for CB[6] cyclization between hexamer and formaldehyde or phthalaldehyde is influenced by the size and shape of ammonium ion templates. The larger size of the *p*-xylylenediammonium ion (**II-11**) allows it to act as a *negative template* by discouraging transformation of hexamer and paraformaldehyde to form CB[6]. However, **II-11** and hexanediammonium ion (**II-20**) act as *positive templates* during the reaction of **6C** and phthalaldehyde **II-12** by giving (±)-**II-21** as an intermediate along the mechanistic pathway to CB[6] derivative **II-13**. Finally, a fluorescence turn-on assay was investigated using the fluorophore and metal-ion binding (e.g., Eu^{3+}) of naphthalene-CB[6] derivative **II-19**. The synthesis of monofunctionalized CB[6] derivatives in high yields has broad implications toward tailor-made approaches to CB[n] derived functional systems in the future.

Chapter 3 describes the high yield synthesis of glycoluril pentamer (**5C**) by the 3,5-dimethylphenol induced fragmentation of bis-*ns*-CB[10] under acid conditions. The access to large quantities of **5C** and **6C** and previously reported tetramer **III-4** allowed for a comparison of host-guest recognition properties of acyclic CB[n]-type receptors

toward alkaneammonium ions in water.

TEMPLATED SYNTHESIS OF GLYCOLURIL OLIGOMERS AND MONOFUNCTIONALIZED CUCURBIT[6]URIL DERIVATIVES

By

Derick Lucas

Dissertation submitted to the Faculty of the Graduate School of the
University of Maryland, College Park, in partial fulfillment
of the requirements for the degree of
Doctor of Philosophy
2011

Advisory Committee:
Professor Lyle Isaacs, Chair
Professor Philip DeShong
Professor Jeffery Davis
Professor Daniel Falvey
Associate Professor Volker Briken, Dean's Representative

Dedication

To my parents Larry Lucas and Carol Lucas
and my soon to be wife, Jennifer.

Acknowledgements

I would like to express my sincere gratitude to my Ph.D. advisor Professor Lyle Isaacs for his guidance and support throughout my graduate career. Lyle has devoted his time and energy to teach me invaluable lessons as a researcher that will accompany me throughout my professional life.

I'd like to thank my undergraduate chemistry Professor Lindy Harrison for making me a better chemist, inspiring me to persue my Ph.D., and her continued encouragment over the last several years.

Thank you to all the former Isaacs group members for teaching me the essential techniques necessary to succeed in our lab. Regan, Wei, Shome, and Da Ma were always willing to devote their time and knowledge to help me excel at my research.

Thank you to all my current group members for your support and creative input, especially Jimmy who has been a great teammate and friend throughout my graduate career. I'd like to thank former undergraduate researcher Greg Iannuzzi for his dedicated efforts in the lab and his continued support over the last several years. I would like to thank Dr. Yui-Fai Lam and Dr. Yinde Wang for providing their expertise with various NMR experiments.

I would never have been able to accomplish any of my life goals without the constant inspiration and encouragement of my loving parents and soon to be wife. Thank you for your patience, understanding, and enduring the good and bad over all these years.

Table of Contents

List of Tables

Chapter 1

Chapter 2

Chapter 3

List of Figures

Chapter 1

Chapter 2

Chapter 3

List of Schemes

Chapter 1

Chapter 3

Chapter 4

List of Charts

Chapter 1

Chapter 2

List of Abbreviations

Ac	acetyl
anh.	anhydrous
aq.	aqueous
br. s	broad singlet
t-Bu	tertiary butyl
calcd	calculated
CB[n]	cucurbit[n]uril
d	doublet
dd	doublet of doublets
dec	decomposition
DMSO	dimethyl sulfoxide
EI	electron ionization
EtOAc	ethyl acetate
h	hour(s)
H_2SO_4	sulfuric acid
HCl	hydrochloric acid
Hz	hertz
i	inverted
IR	infrared
J	coupling constant
M	molar
m	multiplet

m	meta
mM	millimolar
M^+	molecular ion
m/z	mass-to-charge ratio
Me	methyl
MHz	megahertz
min	minute(s)
M.p.	melting point
MS	mass spectroscopy
NMR	nuclear magnetic resonance
o	ortho
OAc	acetate
p	para
Ph	phenyl
q	quartet
s	singlet
t	triplet
TFA	trifluoroacetic acid
v	volume

I. Chapter 1: Pathways Toward Macrocycles for use in Supramolecular Chemistry.

1.1 Introduction.

Interest in molecular containers has exploded in recent years as industry and researchers alike have investigated their ability to encapsulate molecules of interest. As the field expands and more specialized systems become desirable, it is crucial to find efficient pathways for their construction. This chapter discusses the synthesis, mechanism, applications, and progress towards functionalized derivatives in the family of supramolecular containers known as cucurbiturils.

1.2 Synthesis and Structure of Cucurbit[n]uril.

The investigation of glycoluril (**1**) based polymers began in 1905 when Behrend et. al. performed a condensation reaction between one equivalent of **1** and two equivalents of formaldehyde in HCl.[1] The resulting compound was referred to as "Behrend's polymer" and recrystallization from concentrated H_2SO_4 gave a crystalline substance that demonstrated its ability to form complexes with a variety of compounds including $KMnO_4$, $AgNO_3$, and methylene blue. The structure of this compound remained uncharacterized until it was reinvestigated over 70 years later by Mock.[2] He discovered a highly symmetrical macrocycle consisting of six glycoluril units linked by twelve methylene bridges that create two electron rich, carbonyl lined portals. Due to the molecules resemblance to a pumpkin, he named the compound cucurbituril, now

commonly known as cucurbit[6]uril and abbreviated as CB[6] (Scheme I-1). The steady development of the cucurbituril field over the past 30 years by Mock,[3,4] Buschmann,[5,6] Day,[7] Isaacs,[9-11] and Kim,[12,13] have lead to the isolation of CB[5], CB[7], CB[8], and CB[10] and an understanding of their formation from glycoluril oligomers **2C** to **8C** (Scheme I-2).

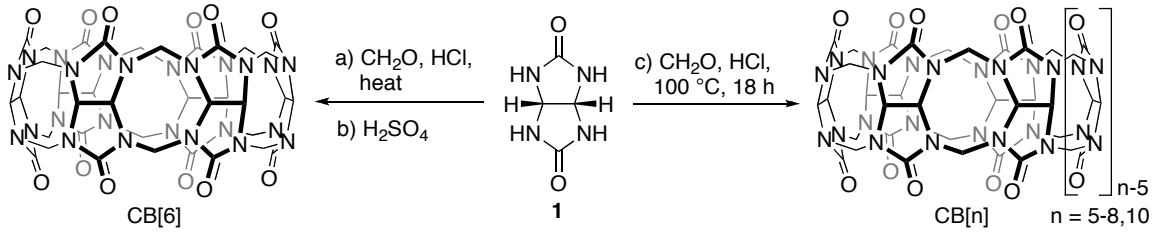

Scheme I-1. Synthesis of CB[6] and homologues CB[5] to CB[10].

1.3 Recognition Properties of Cucurbit[n]urils.

The remarkably high binding affinity and selectivity of cucurbiturils towards a wide variety of guests distinguishes them from other families of molecular containers such as cyclodexterins and calixarenes.[14-16] These exceptional binding properties can be attributed to their two ureidyl carbonyl lined portals and comparatively wider hydrophobic cavity. The cooperative hydrogen bonding, hydrophobic binding, and ion-dipole interactions (Figure I-1) make cucurbiturils ideal for sequestering cationic species, especially alkyl and aryl ammonium guests.[3-6] The diverse cavity sizes provided by the CB[n] homologues provide excellent selectivity toward ammonium guests such as **I-9** to **I-17** (Figure I-1). For example, the binding constant measured for CB[7]•**I-16** is 4.2×10^{12} M^{-1}, however, the binding constant is reduced to 8.2×10^{8} M^{-1} for CB[8] and the guest is too large to enter the CB[6] sized cavity.[17] Binding constants for selected

ammonium guests are listed in Table I-1 demonstrating the binding preference of larger hosts (CB[7] and CB[8]) towards bulkier guests and the preference of smaller host (CB[6]) towards alkyl diammonium salts.

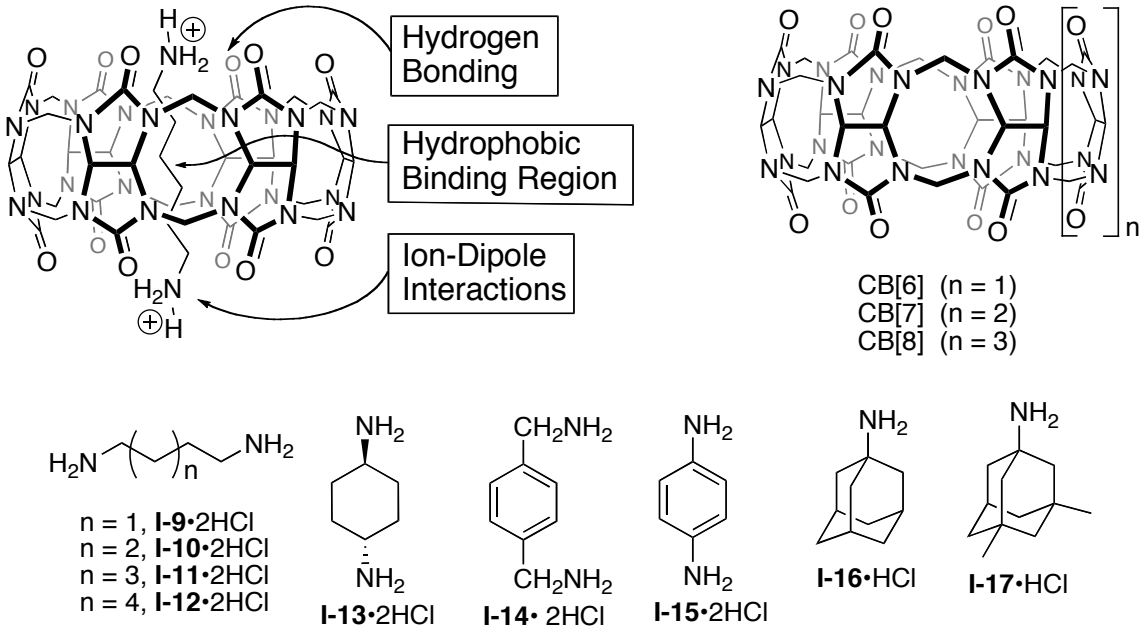

Figure I-1. Binding of CB[n] with alkyl and aryl ammonium cations.

Table I-1. Ammonium guests with CB[6], CB[7], and CB[8]: a) K_a values taken from ref 3, b) K_a values taken from ref 17, c) K_a values taken from ref 18, d) no binding.

Guest	CB[6][a]	CB[7][b]	CB[8][b]
I-9	1.5×10^5	-	-
I-10	2.4×10^6	-	-
I-11	2.8×10^6	$(9.0 \pm 1.4) \times 10^7$	-
I-12	4.3×10^4	-	-
I-15	$(1.9 \pm 0.1) \times 10^{3}$ [b]	$(2.1 \pm 0.3) \times 10^6$	-
I-14	550 ± 30[b]	$(1.8 \pm 0.3) \times 10^9$	-
I-13	1.4×10^{6} [c]	$(2.3 \pm 0.4) \times 10^7$	-
I-16	n.b.[d]	$(4.2 \pm 1.0) \times 10^{12}$	$(8.2 \pm 1.8) \times 10^8$
I-17	n.b.	$(2.4 \pm 0.4) \times 10^4$	$(4.3 \pm 1.1) \times 10^{11}$

1.4 Mechanism of Cucurbit[n]uril Formation.

The ongoing discovery of new CB[n] analogues, homologues, and derivatives has driven investigations regarding the mechanism of formation for these remarkable macrocycles. While the reaction of glycoluril and formaldehyde under mild conditions (100 °C, conc. HCl; 75 °C, 9M H_2SO_4) yields the family of CB[n] homologues, CB[6] remains the major component of the reaction and the isolation of CB[5], CB[7], CB[8], and CB[10] require time consuming washing and recrystallization procedures.[12,19] The groups of Isaacs and Day have been heavily involved in the elucidation of these mechanistic details, not only to satisfy their scientific curiosity, but to uncover ways to manipulate reactions conditions that can potentially deliver specific CB[n] homologues and derivatives.[20-24]

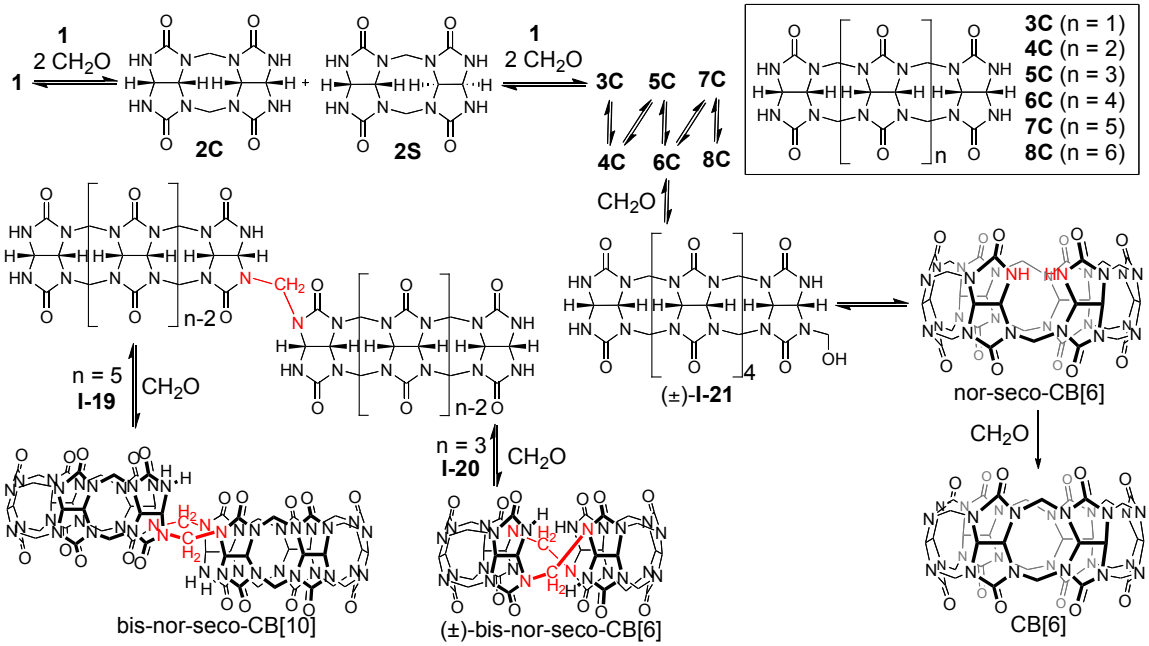

Scheme I-2. Mechanistic pathway for CB[n] formation via glycoluril oligomers **2C**-**8C**.

Previous mechanistic studies by Day and Isaacs demonstrated that 2 equivalents of glycoluril and 2 equivalents of formaldehyde react to give glycoluril dimers **2C** and **2S**.[10,20] It was thought that these dimers would undergo further oligomerization via **3C**-**8C** (Scheme I-2) and form an ill-defined glycoluril polymer ribbon known as "Behrend's polymer". The polymer chain would then form C and S-shaped polymer subunits that could cyclize to deliver CB[n] homologues via an end-to-end cyclization mechanism (e.g. **6C** to CB[6]) (Scheme I-3).

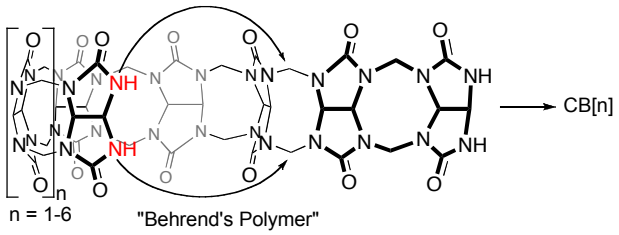

Scheme I-3. "Behrend's polymer" cyclizing to give CB[n] homologues.

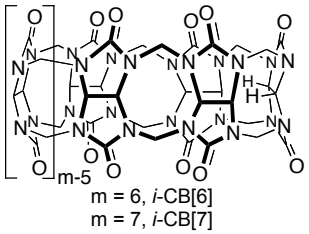

Chart I-1. Structures of i-CB[6] and i-CB[7].

Although this mechanistic theory is very likely to occur, another level of detail surfaced with the isolation of C-shaped glycoluril oligomers **3C**-**6C** by Isaacs.[11] These oligomers were separated from a reaction of one equivalent of **1** and one equivalent of formaldehyde using a low yielding purification procedure based on Dowex ion-exchange

chromatography and recrystallization. Therefore, it is possible to arrive at kinetically controlled intermediates as the reaction progresses towards CB[n] by depriving the reaction of formaldehyde (< 2 equiv.). As shown in Scheme I-2, it is likely that oligomers **2C**-**6C** proceed by a chain-growth mechanism where the stepwise addition of **1** to the oligomer gives a new oligomer chain one glycoluril unit longer. Scheme I-2 also presents the oligomers heptamer (**7C**) and octamer (**8C**) as likely mechanistic intermediates although they have not been isolated to date. As the oligomer chain grows it is likely that its intrinsic C-shape brings the reactive NH tips of oligomers **5C**-**8C** in close proximity and allows condensation with formaldehyde to form *nor*-*seco*-CB[n][25,26] (*ns*-CB[n]) and then ring closure to CB[n]. For example, as shown in Scheme I-2, **6C** reacts with one equivalent of formaldehyde to form (±)-**I-21** and undergoes intramolecular cyclization to form the isolable species *ns*-CB[6]. Finally, one more formaldehyde unit condenses with *ns*-CB[6] to complete the cyclization and forms the CB[6] product. While CB[5], CB[6], and CB[7] are considered thermodynamically controlled products since they do not undergo decomposition under acidic conditions with heat, resubmission of CB[8] undergoes ring contraction to form smaller CB[n].[20] It has also been shown that the inverted glycoluril unit of i-CB[6] and i-CB[7] (Chart I-1) can flip to give CB[n] under similar acidic conditions.[27] It was evident from the isolation of (±)-bis-*ns*-CB[6][25] and bis-*ns*-CB[10][26] that a step-growth mechanistic pathway was also at play. In CB[n] chemistry, step-growth processes occur when the condensation of two oligomers give a longer oligomer or kinetically controlled intermediates en route to CB[n]. For example, two molecules of **3C** can combine to form CB[6] or two molecules of **4C** can combine to give CB[8]. This was further examined by resubmission

experiments using **2C**-**6C** to form CB[n].[11] The results showed a strong preference for the formation of CB[6], but especially in reactions containing **6C** (100% CB[6] formation). However, it was also evident that specific CB[n] could be delivered in significant amounts using the appropriate oligomers such as **3C** + **4C** to give CB[7] (42%) and **4C** + **4C** to give CB[8] (40%). The mechanistic details highlighted in this chapter are significant for several reasons: 1) Reactions of glycoluril that are deprived of formaldehyde deliver kinetically controlled intermediates including oligomers **2C**-**6C**, 2) The C-shaped oligomers have proved to be highly reactive species and can be used to influence the CB[n] product distribution, 3) The reactivity and shape of these oligomers may be exploited for the synthesis of new and useful CB[n] derivatives.

1.5 Cucurbit[n]uril Functionalization.

Despite the promise that CB[n] show in supramolecular applications, the lack of synthetic pathways toward their selective functionalization has hindered the progress of CB[n] chemistry in specialized applications. Unlike the functionalization of other macrocycles such as cyclodextrins[28,29] and calixarenes,[30,31] the robust structures, complicated purification, and delicate equilibria exhibited in CB[n] chemistry leaves very few accessible pathways for synthesizing useful functional scaffolds.

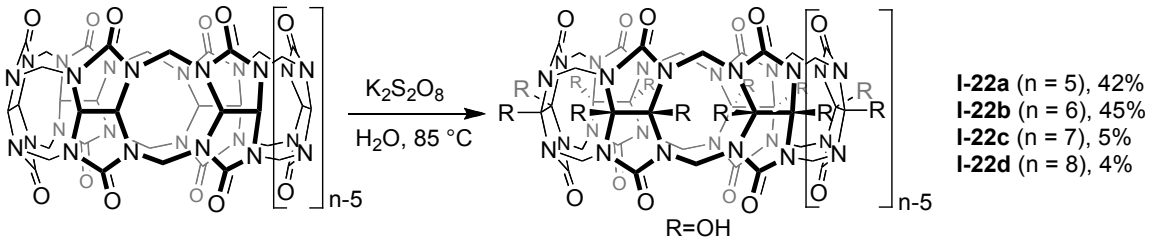

Scheme I-4. Kim's hydroxylation of CB[5], CB[6], CB[7], and CB[8].

The most accepted functionalization pathway to date was discovered by Kim and coworkers in 2003.[32] Using preformed CB[5], CB[6], CB[7], and CB[8], Kim is able to replace the glycoluril C-H groups with hydroxyl groups via direct functionalization using potassium persulfate in water at 85 °C (Scheme I-4). The new CB[n] derivative **I-22b** has the expected hydroxyl groups around the periphery as revealed by X-ray crystallography and results in low distortion of the carbonyl lined portals.

The most important feature of these new derivatives is their ability to undergo further reactions using standard organic chemistry in polar organic solvents such as DMSO and DMF. For example, treatment of **I-22b** with NaH in DMSO followed by addition of allyl bromide gives the perallyloxy CB[6] **I-22b1** (Scheme I-5). The allyl ether functional group is especially appealing due to its reactivity for further transformations as shown in Scheme I-5 with the transformation of **I-22b1** to thioether CB[6] **I-22b3**.

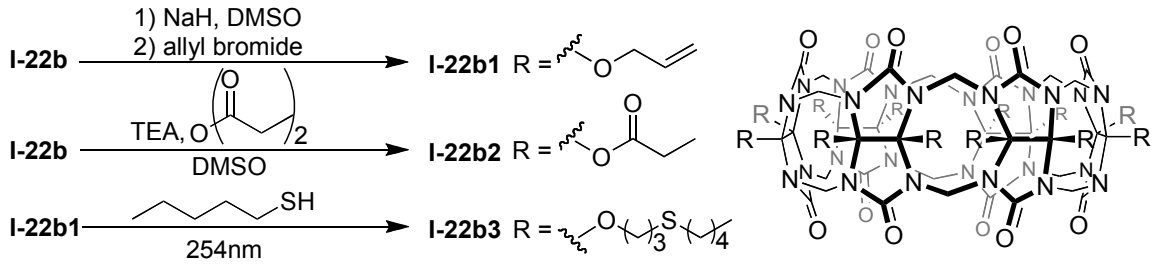

Scheme I-5. Methods for post-functionalization of CB[6] derivatives **I-22b** and **I-22b1**.

Although the perhyroxylation of CB[n] allows access to new functionalized derivatives, the synthetic route comes with many drawbacks. The perhydroxylation reaction gives moderate yields for CB[5] and CB[6] derivatives (42 and 45% respectively) but very low yields for CB[7] and CB[8] derivatives (5 and 4% respectively). This is discouraging since CB[7] and CB[8] show the most interesting host-guest interactions with larger molecules of interests such as anti-cancer drugs in drug delivery devices,[42] dyes in indicator displacement assays,[52,53] and other practical applications. Another pitfall of Kim's perhydroxylation is the lack of control during post-functionalization reactions with the CB[n] surface. Since the synthesis of the perhydroxy CB[n] leaves the surface polyfunctionalized, subsequent reactions give product mixtures where the CB[n] is polyfunctionalized to various degrees. This lack of functionalization control makes it unusable for specialized applications where functionalized macrocycles are crucial. This has lead to limited theoretical use of polyfunctionalized CB[n] in drug delivery,[33,34] biomimetic systems,[35] and on solid surfaces.[36,37] It is therefore imperative that new and efficient methods are developed for synthesizing monofunctionalized CB[n] in order to create a new wave of CB[n] for specialized applications.

1.6 Cucurbit[n]uril Applications.

The family of CB[n] has been widely exploited for its excellent binding affinities and selectivity in numerous applications.[22,23] While many applications have generated interest in CB[7] due to its preferable cavity size, several other applications require the smaller cavity of CB[6] or the large cavities of CB[8] and CB[10]. The functionalization

of CB[n] by Kim expanded the range of applications available to the CB[n] family and further highlights the benefits of selectively functionalized CB[n].

1.6.1 Drug Delivery.

The CB[n] family has shown particular promise in their application as drug delivery vehicles, especially considering similar macrocycles, such as cyclodextrins, are being used commercially for the same purpose.[38] Supramolecular containers are especially desirable for drug delivery applications due to their ability to enhance the solubility of poorly soluble drugs and drug stability.[39-43] The binding selectivity exhibited by CB[n] give them a distinguishing advantage that may propel them as the drug delivery platform of choice in the future.

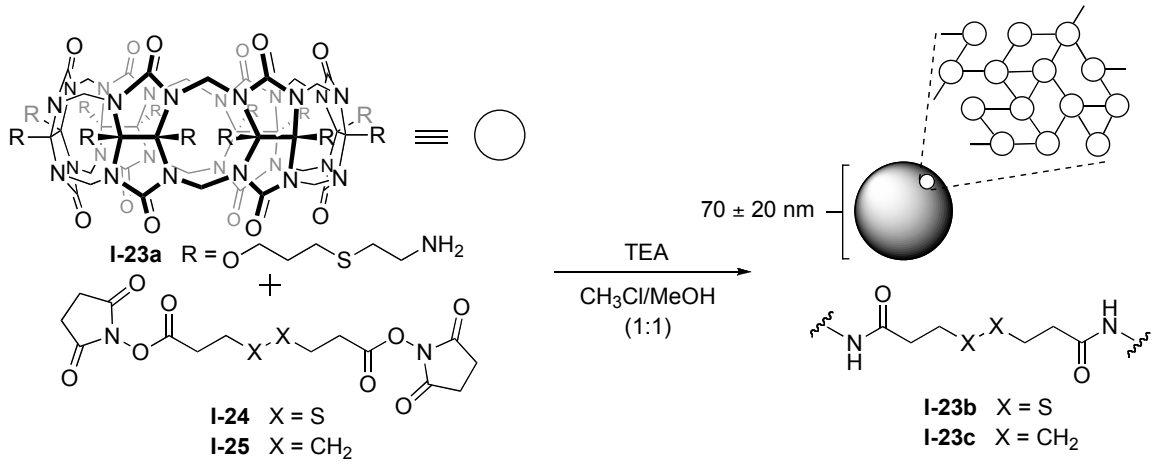

Scheme I-6. The synthesis of hollow polymer nanocapsules used for drug delivery.

Although several publications have used CB[n] homologues, particularly CB[7], in toxicology[44,45] and drug delivery applications,[33,34,42,43] very few have used functionalized CB[n] for accomplishing this goal. One method of using functionalized

CB[n] in drug delivery has been developed by Kim and group using their perhydroxy CB[6]. Unlike conventional methods that are designed to bind one drug molecule inside one container, Kim has been able to tailor perhydroxy CB[6] in order to form nanocapsules capable of holding cargo in the core.[33,34] His more recent method is accomplished by reacting a thioamine functionalized CB[6] (**I-23a**) with diester **I-24** to create a polymer network that assembles into a spherical nanocapsule (**I-23b**) (Scheme I-6).[33] The key features that make this nanocapsule desirable as a drug delivery device include: 1) the hollow core capable of being loaded with cargo, 2) the disulfide linker used in **I-23b** can be cleaved under reductive conditions to collapse the nanocapsule releasing the cargo, and 3) the CB[6] macrocycles covering the surface can encapsulate a targeting ligand to enhance the nanocapsules cell targeting.

As shown in Scheme I-7, the carboxyfluorescein dye (**I-26**) loaded nanocapsule (**I-23b1**) was covered with a galactose-spermine conjugated targeting ligand (**I-27**) in order to target HepG2 hepatocellular carcinoma cells with over-expressed galactose receptors. Upon arrival of the polymer nanocapsule (**I-23b2**) into the cytosol the disulfide linkers were cleaved by naturally occurring reducing agents such as glutathione, thereby inducing intracellular release of the cargo dye **I-26**.

The use of CB[n] nanocapsules as drug delivery vehicles may show promise for the *in vitro* theoretical studies illustrated, but need to be expanded to *in vivo* studies using appropriate drugs as cargo. Modifications to this system include the covalent attachment of targeting ligands or fluorophores that would demonstrate direct evidence for the CB[n]

crossing the cell membrane. Covalently attaching substrates to the outside of the CB[n] would also leave the cavity empty and capable of holding the cargo without the assembly of large nanocapsules.

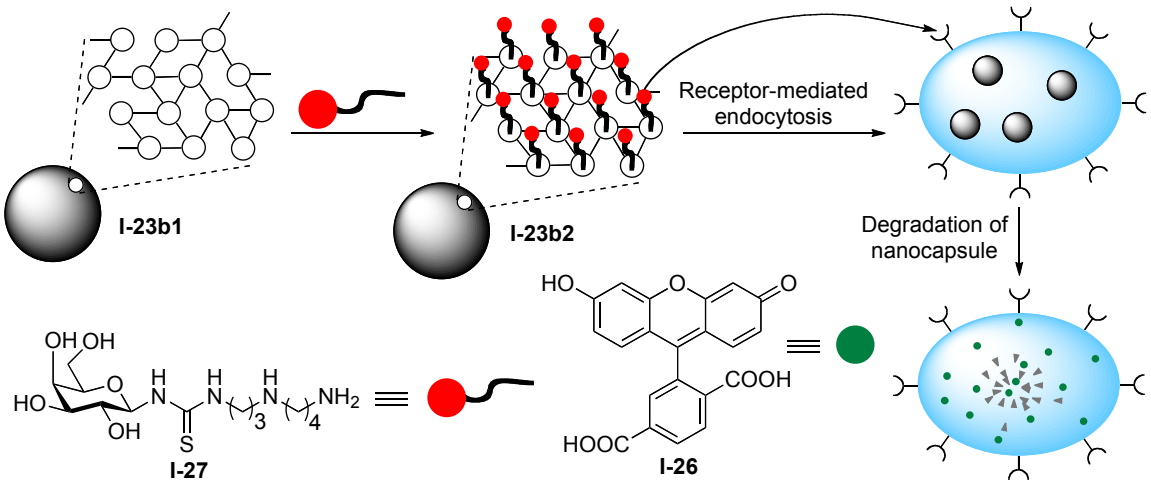

Scheme I-7. Targeting of hepG2 cells and intracellular release of cargo molecules **I-26**.

1.6.2 Biomimetic Systems.

Supramolecular macrocycles have been largely accepted as artificial receptors that in many ways simulate the processes undergone in biological systems through their use of non-covalent interactions.[46,47] The use of various CB[n] hosts including i-CB[n], CB[10], nor-seco-CB[n], bis-ns-CB[10], (±)-bis-*ns*-CB[6], *ns*-CB[6]) in biomimetic systems have been investigated over the past few years by the Isaacs group.[26,48-51] Such studies exploit the high binding affinities and selectivities of CB[n] to create systems that act as metalloenzyme mimetics,[49] demonstrate homotropic allostery in duel cavity systems,[26] and examine metal-ion triggered folding.[50]

Another example by Isaacs in 2010 demonstrated control over biological catalysis using a competition between CB[7] and the enzyme, bovine carbonic anhydrase (BCA).[51] When BCA is catalytically active it is known to catalyze the hydrolysis of *p*-nitrophenylacetate (**I-28**) to form *p*-nitrophenolate (**I-29**) which gives a UV/Vis absorption maximum at 400 nm. When the catalytic activity of BCA is inhibited, **I-29** is not formed and no absorbance is observed. However, the catalytic activity of BCA is directly related to the rate of hydrolysis to form **I-29**, which can be monitored by the UV/Vis absorbance at 400 nm. It was found that guest **I-30** almost completely inhibits the enzymatic activity of BCA due to the favorable interaction with the sulfonamide to form BCA•**I-30** (Scheme I-8). Addition of CB[7] into the solution regenerated the catalytic activity due to the tighter binding affinity of CB[7] towards the trimethylsilylamine unit on guest **I-30** ($K_a \approx 10^9$ M^{-1}) thereby dissociating the BCA•**I-30** complex and formation of CB[7]•**I-30**. Catalytic activity was once again turned off by the addition of **I-31** due to its significantly higher binding affinity towards CB[7] ($K_a > 10^{12}$ M^{-1}) and forced the release of guest **I-30** and formed the CB[7]•**I-31** and BCA•**I-30** complexes. This on-off switch could be repeated for several cycles by the addition of CB[7] and **I-31** in alternating sequences. The demonstration of remarkable control over a biological system hints at the great potential CB[n] receptors have as biological tools in future applications especially with the emergence of functionalized CB[n] that allow for targeting and imaging in these complex systems.

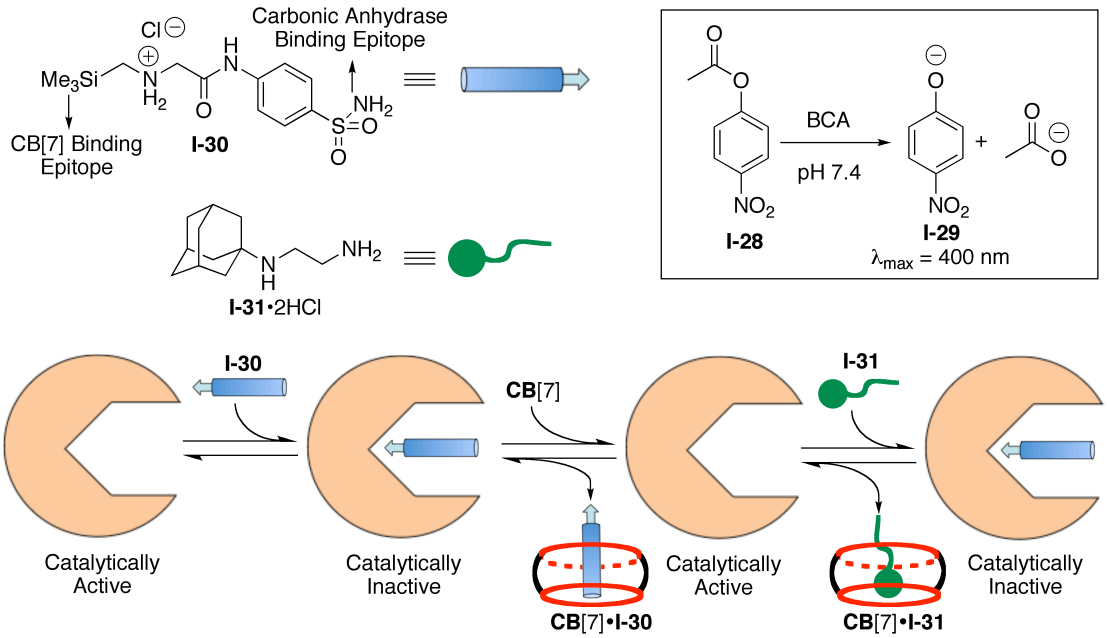

Scheme I-8. The catalytic cycle for activation and inhibition of BCA using CB[7].

1.6.3 Sensing.

Sensing applications accessible through the host-guest interactions of CB[n] macrocycles have accelerated the pursuit of creative solutions for detecting anions and cations, metals, amines, and other molecules of interest.[52-55] Several of these methods have embraced the indicator-displacement assay innovated by Anslyn[56] where an encapsulated dye molecule is displaced, thus freeing the dye from the host cavity and resulting in a change in fluorescence or absorbance. Displacement of the dye is accomplished by introducing a tighter binding analyte or by adding an excess of weaker binding analyte.

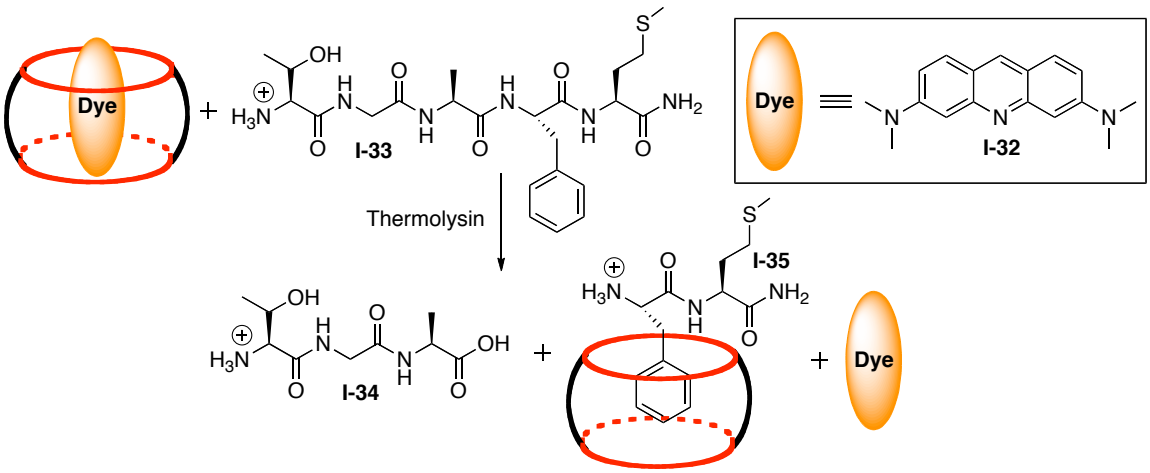

Scheme I-9. Displacement of dye **I-32** from CB[7] by the more tightly binding N-terminal phenylalanine of **I-35**.

A recent example of this methodology was reported by Nau and Urbach in 2011 through the use of CB[7] and peptides containing N-terminal phenylalanine residues.[55] Due to the expense and time consuming nature of protease activity assays that require labeled substrates, it was proposed that CB[7] could be used for its excellent recognition and selective binding to create a label-free protease assay (Scheme I-9). The success of this assay was critically dependent on the choice of acridine orange (**I-32**) as a dye due to its weak fluorescence in aqueous solutions, its strong fluorescence when sequestered in a CB[7] cavity, and it's binding constant of 2.9×10^5 M^{-1} with CB[7]. Several peptides used in this assay including **I-33** measured a binding constant of $K \approx 10^4$ M^{-1}, which is insufficient to displace the more tightly binding dye. However, treatment of the peptide solution containing an enkephalin-based substrate with thermolysin resulted in enzymatic products containing N-terminal phenylalanine residues **I-35** with $K > 10^6$. The terminal phenylalanine is therefore sufficient to displace the more weakly binding dye and produce a decrease in fluorescence.

The methodology presents a robust and elegant solution for monitoring complex enzymatic systems but only provides a proof-of-principle using a small collection of potential peptides. The versatility of the CB[7] macrocycle is remarkable but the implementation of monofunctional CB[n] may provide the customization necessary to investigate a wider range of substrates and create assays that are highly desirable to chemists, biologists, and medical practitioners alike. These custom modifications include the covalent attachment of fluorophores, competitive ligands, and multicavity systems that could revolutionize the use of CB[n] in sensing applications.

1.6.4 Solid Surfaces.

The use of CB[n] in surface chemistry has been explored through both covalent and non-covalent interactions by the groups of Kim,[32,36,37] Scherman,[57] and Zhang.[58] Supramolecular macrocycles affixed to solid surfaces present several advantages in purification by sequestering molecules of interest in the host cavity. However, covalent attachment of CB[n] to solid surfaces has been held back by the limited availability of functionalized derivatives. Consequently, the implementation of CB[n] on solid surfaces has been limited to the use of Kim's perhydroxy CB[n] derivatives.

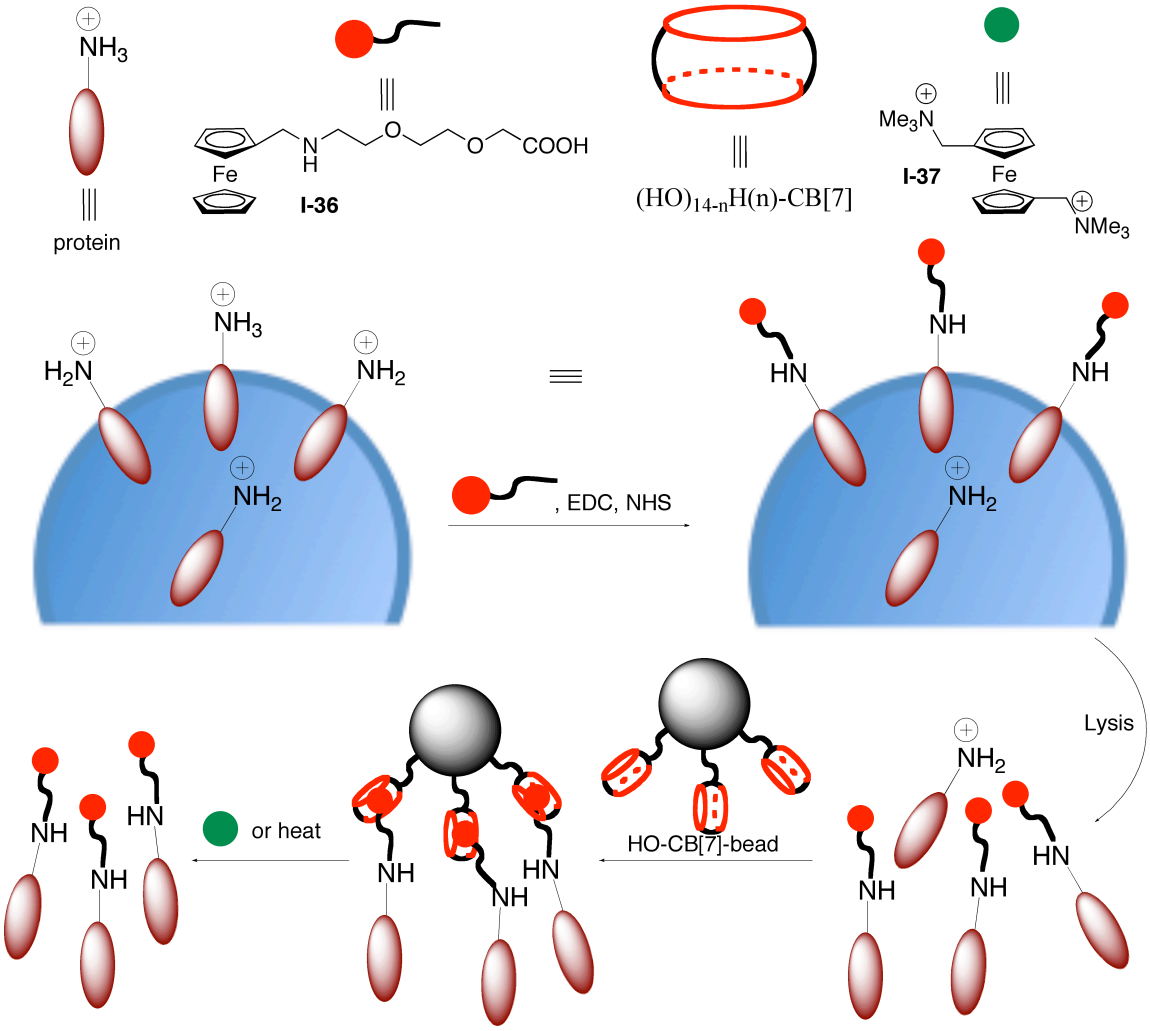

Scheme I-10. Protein "fishing" using CB[7] functionalized beads to bind ferrocene functionalized proteins followed by dissociation of the complex to deliver the free proteins.

An effective use of CB[n] on surfaces as a way of purifying membrane proteins was recently published by Kim in 2011.[36] This method of separating membrane proteins was built as an improvement over previous methods using biotin and streptavidin functionalized beads, which suffered from degradation and purification issues. Alternatively, CB[7] immobilized beads ($(HO)_{14-n}H(n)$-CB[7] beads) were prepared by

treating *N*-hydroxysuccimidyl sepharose beads (NHS beads) with $(HO)_{14-n}H(n)$-CB[7] (Scheme I-10). Functionalization of the membrane proteins in rat fibroblast (Rat-1) cells was accomplished with ferrocene adduct **I-36** and carbodiimide (EDC) as depicted in scheme I-10. After cell lysis, the addition of the $(HO)_{14-n}H(n)$-CB[7] beads took advantage of the extremely high binding affinity of CB[7] towards the ferrocene amine unit of **I-36** ($K_a \approx 10^{12}$ M^{-1}). The functionalized proteins were sequestered in the CB[7] hosts and allowed for their selective separation. The proteins could then be removed from the $(HO)_{14-n}H(n)$-CB[7] beads by heating or by the addition of the tighter binding guest 1,1'-bis(trimethylammoniomethyl)ferrocene ion (**I-37**) ($K_a \approx 10^{15}$ M^{-1}). This method highlights the excellent selectivity of CB[7] and the advanced applications possible through the implimentation of functionalized CB[n] macrocycles.

1.7 Templation of Macrocycles.

The synthesis of macrocycles can be a daunting task for an organic chemist. Many of the large and complex systems presented in the field of supramolecular chemistry have proven to be mechanistically intriguing and useful for a wide variety of applications. For these reasons it is essential that synthetic chemists find simple, elegant, and highly efficient solutions for assembling these molecules. This section examines the use of templates in the assembly and purification to give several macrocycles in a concise and predictable manner. These examples explore the use of kinetic, thermodynamic, positive, and negative templates or a combination of these various classifications as defined in the 1993 review by Anderson and Sanders.[59] In short, a thermodynamic template operates in a reversible reaction by stabilizing a particular product at the

expense of another. A kinetic template promotes product formation by influencing the transition state energies, and as consequence, favors the formation of a single product. Kinetic templates are further classified as positive or negative depending on whether they speed up the product formation or by discouraging the formation of a product, respectively.

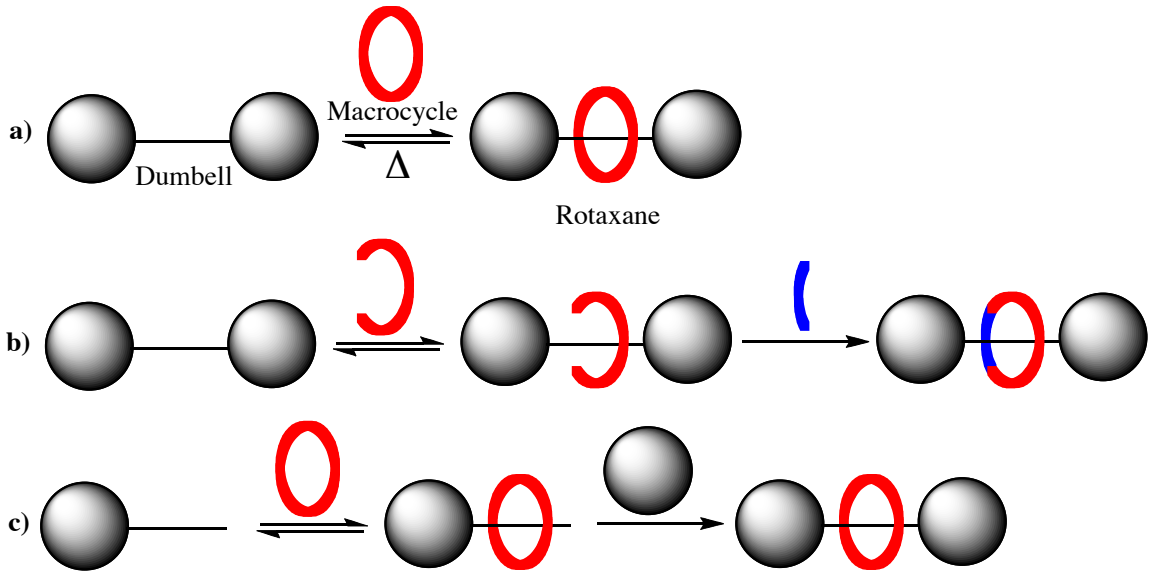

Scheme I-11. Synthesis of rotaxanes by: a) slipping, b) clipping, and c) threading followed by stoppering.

1.7.1 Templation of Rotaxanes.

A rotaxane is a mechanically interlocked molecule consisting of a macrocycle and a dumbbell shaped thread (Scheme I-11). The capped ends (stoppers) on the molecular dumbbell are larger than the internal diameter of the macrocycle, thereby trapping the macrocycle on the dumbbell. The templated synthesis of rotaxanes has been explored by many chemists in the supramolecular field including Leigh,[60] Beer,[61,62] and Stoddart.[63,64]

The synthesis of rotaxanes can proceed following a clipping, slippage, and threading followed by stoppering.[65]

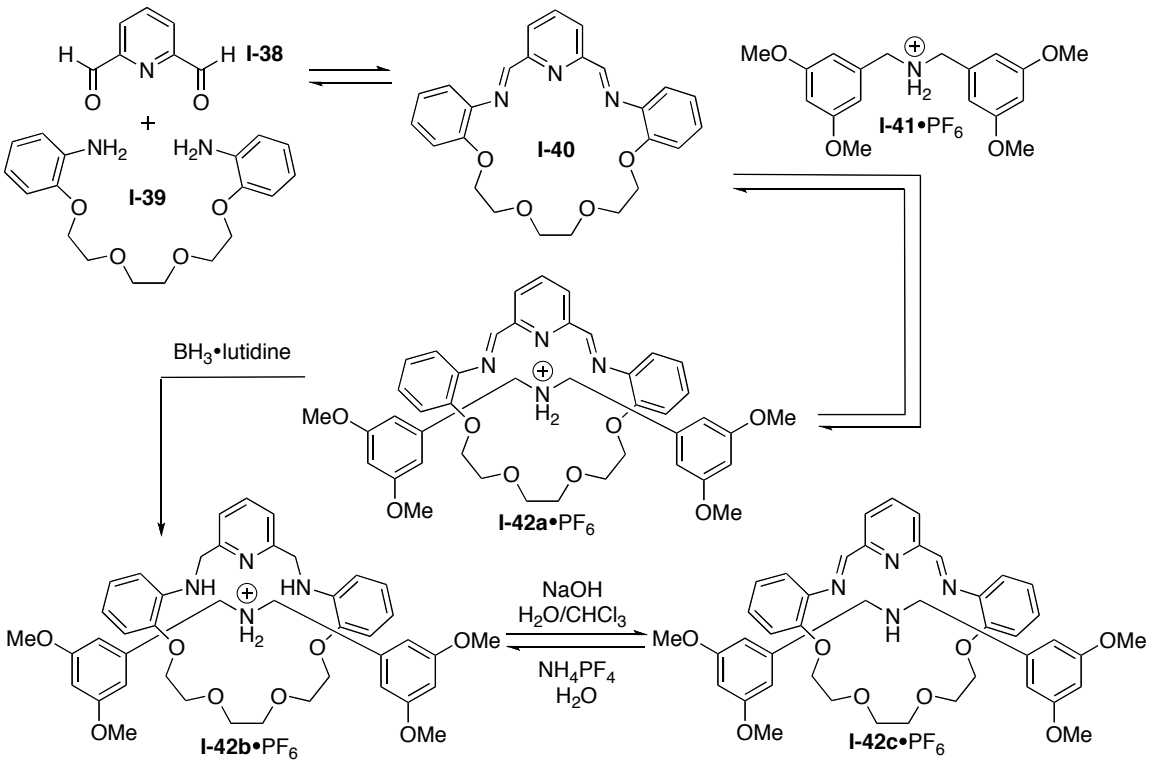

Scheme I-12. Templated synthesis of rotaxane **I-42a-c** using templating thread **I-41**.

An excellent example of rotaxane assembly using a template-directed, clipping mechanism was published by Stoddart in 2001.[64] The 2,6-pyridinedicarboxaldehyde (**I-38**) and tetraethyleneglycol bis(2-aminophenyl)ether (**I-39**) were chosen as suitable macrocycle fragments due to their non-covalent interactions with the dialkylammonium ion of **I-41** (Scheme I-12). The non-covalent interactions serve as a thermodynamic template and induced the cyclization via imine formation around thread **I-41** to give rotaxane **I-42a**. Treatment of rotaxane **I-42a** with BH_3•lutidine reduced the imine bonds

to the more stable amine bond thereby eliminating the reversibility of **I-42a** and delivering rotaxane **I-42b**. Finally, addition of base to reaction deprotonated the dialkylammonium proton to give the free base in rotaxane **I-42c**, demonstrating the 3,5-dimethoxylbenzene stoppers were adequate to prevent dethreading via slippage of the macrocycle.

1.7.2 Templation of Cyclic Oligomers.

An investigation of metalloporphyrin-based oligomerization by Sanders examined the templating effects of selected guests in order to deliver desired products.[66] As shown in Scheme I-13, metalloporphyrin **I-43** treated with DBU and oxygen resulted in disulfide bond formation for oligomer macrocycles **I-43a**, **I-43b**, **I-43c**, and higher oligomers. When this reaction was conducted in the absence of a templating guest the outcome was cyclic porphyrin dimer **I-43a** (87%), trimer **I-43b** (11%), and higher oligomers (3%). However, when DABCO **I-44** was used as a template the reaction gave almost entirely cyclic porphyrin dimer product **I-43a•I-44** (99%). Similar effects were revealed by HPLC for guests **I-45** and **I-46** to generate cyclic oligomers **I-43b•I-45** and **I-43c•I-46**, respectively. Alternatively, use of 4,4'-bipyridine **I-47** as a template resulted in a large mixture of cyclic oligomers and higher oligomers. The example clearly demonstrates the templated control over ring size through crucial involvement of non-covalent interactions, size, and shape of the selected template. By structuring experiments for the synthesis of CB[n] using these templating elements it can be expected that a degree of control can be exhibited over the reaction outcome.

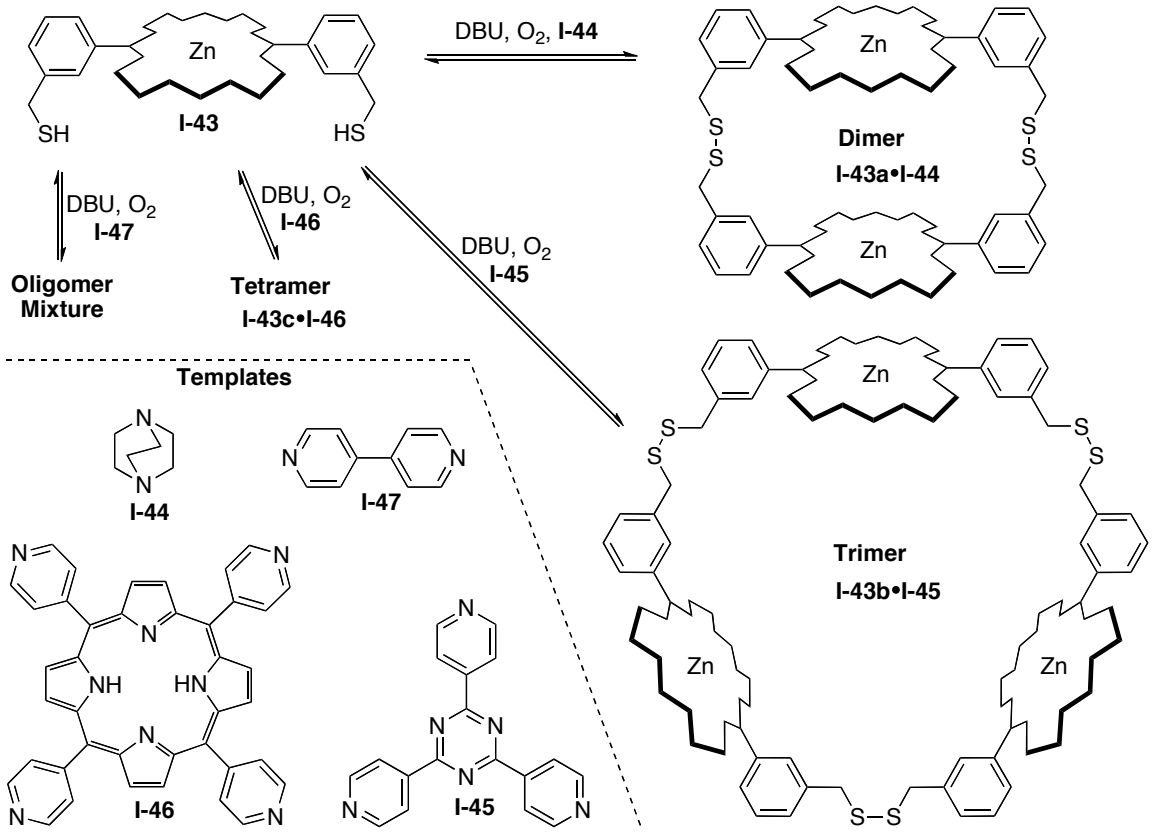

Scheme I-13. Templated synthesis of cyclic porphyrin oligomers.

1.7.3 Implications for Cucurbit[n]uril Templation.

The implications for the use of templation in CB[n] synthesis are apparent. Day and group have been heavily involved in the elucidation of CB[n] mechanism and investigated the effect of templates on CB[n] mixtures.[67] Due to the strong binding interactions between CB[n] and cationic species, Day chose to use alkali metal cations as suitable templates in the CB[n] forming reaction between 1 equivalent of glycoluril (**1**) and 2 equivalents of formaldehyde (Scheme I-14). Two methods of templation were studied, the first included a metal cation in the mixture of **1** and formaldehyde, the second added a metal cation after the reaction had undergone oligomer formation. The latter

experiment is highlighted in this discussion due to the generation of more promising product distributions (Table I-2).

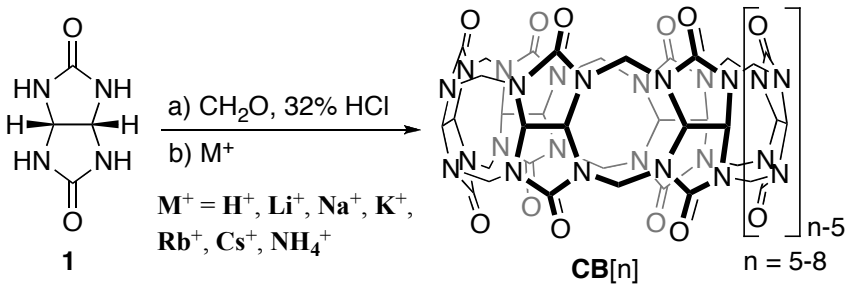

Scheme I-14. The generation of CB[n] using alkali metal cation templates.

M^+	CB[5]	CB[6]	CB[7]	CB[8]
H^+	25	51	20	4
Li^+	40	36	18	5
Na^+	31	41	21	7
K^+	46	38	13	3
Rb^+	33	45	19	3
Cs^+	19	56	19	6
NH_4^+	25	47	21	7

Table I-2. Product distributions of CB[n] generated by cationic templates.

It was expected that larger cationic guests would generate larger CB[n] macrocycles as the glycoluril oligomers assembled around the cation, however, as seen in table I-2 the product distributions do not exhibit recognizable trends. It can be seen that the use of Li, Na^+, K^+, and Rb^+ show a relatively high preference for CB[5] while the larger Cs^+ and NH_4^+ seem to slightly favor CB[6]. The product distribution of CB[7] and CB[8] appears to be uninfluenced by the use of metal cations and show no obvious pattern.

Despite the rigorous experimentation conducted by Day, the templated synthesis of single CB[n] products was not observed. Further studies with alkyl and aryl ammonium ions gave similar product distributions under fixed reaction conditions.[68] However, very few of the controllable experimental variables were examined in these studies including reaction time, solvent effects, reactant concentration, temperature, and equivalents of formaldehyde. These variables are likely to have a significant impact on the reaction outcome as seen for the synthesis of glycoluril oligomers and *nor-seco*-CB[n] by depriving the reaction of formaldehyde. A thorough examination of CB[n] templation that scans the various controllable variables along with a careful selection of templating guests is required for a mechanistic understanding and potentially the templated synthesis of single CB[n] products.

1.8 Building Block Approach to CB[n] Synthesis.

The proper building blocks are needed in the pursuit of efficient synthetic pathways in the construction of new CB[n] derivatives. Glycoluril dimer **2** has been widely used as a building block for the synthesis of new CB[n] analogues,[69] congeners,[70] and derivatives[71-73] due to their high yield and simple purification. It is foreseeable that the understanding gained from these studies will lead to the synthesis of new CB[n] derivatives using a building block method.

1.8.1 CB[n] Analogues, Clips, and Acyclic Congeners.

The intrinsic C-shaped glycoluril provides an interesting scaffold, not only for the CB[n] homologues, but also for the synthesis of analogues,[69] clips,[74] and acyclic

congeners.[70] These molecules benefit from similar non-covalent interactions as CB[n] due to the incorporation or glycoluril units but offer a more straightforward approach to synthesis and purification.

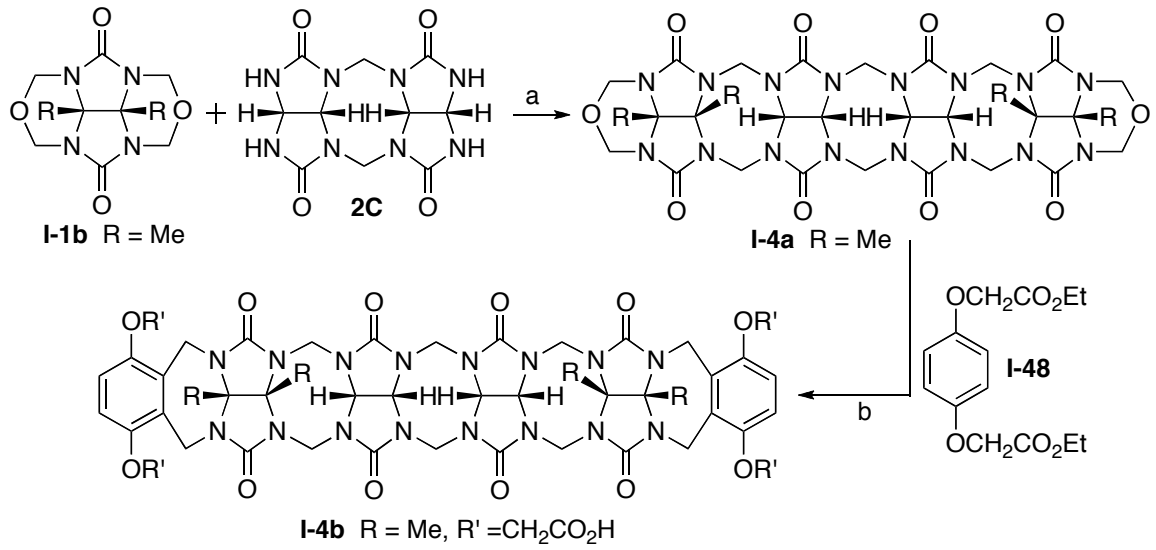

Scheme I-15. The synthesis of CB[n] congener **I-4b** using a building block approach. a) $MeSO_3H$, 50 °C, b) **I-48**, TFA, AC_2O, reflux then LiOH, $MeOH/H_2O$, 70 °C then conc. HCl.

The acyclic CB[n] congeners discovered by Isaacs and group clearly demonstrate that the effective use of glycoluril building blocks can deliver high affinity hosts (Scheme I-15).[70] The use of glycoluril bisether **I-1b** foregoes the use of an external formaldehyde source and promotes the condensation reaction between C-shaped glycoluril dimer **2C** to give C-shaped glycoluril tetramer **I-4a** (35%). The bisether **I-4a** can now undergo addition of two para-substituted xylylene walls via electrophilic aromatic substitution to give glycoluril tetramer **I-4b** (32%). Although **I-4b** only contains four glycoluril units,

the acyclic design demonstrates flexibility and allows for high binding affinities for a large variety of alkyl and aryl ammonium guests. Not surprisingly, the host displays especially high binding affinities towards aromatic guests such as **I-14** and 3,6-diaminoacridine hemisulfate, possibly due to the addition of π-π interactions from the xylylene sidewalls. More interestingly, the acyclic design allows the molecular to expand its cavity size to accommodate bulky guests such as **I-16** and **I-17**. Furthermore, the substituted xylylene walls may allow for further functionalization thus expanding its use in a variety of applications. This example of a building block method highlights its ability to efficiently construct CB[n] type cavities in the preferred C-shaped geometry while maintaining the high affinity binding toward ammonium ions and creating the potential for further host functionalization.

1.8.2 CB[n] Derivatives

Compared to the synthesis of CB[n] analogues and congeners, the synthesis of CB[n] derivatives remains relatively undeveloped except for Kim's perhydroxylation method using preformed macrocycles. Although the building block methods used for constructing CB[n] derivatives to date have been primarily for proof-of-concept, this method may provide an efficient pathway for constructing monofunctionalized CB[n] derivatives in high yields.

Tao and Day discovered that a building block approach could be used to deliver tetramethylCB[6] (Me_4CB[6]).[71] A mixture of dimethylglycoluril bisether (**1b**) and dimer **2C** gives the symmetrical Me_4CB[6] product (30%) after precipitation from HCl

with water (Scheme I-16). The structure was confirmed by ^{1}H-NMR, ESI-MS, and X-ray crystallography and revealed the two opposing dimethyl glycoluril units separated by two glycoluril dimers to form an ellipsoidal CB[6] cavity. The ellipsoidal cavity shape is unusual for a CB[n] macrocycle and suggests that the methylated glycoluril units induce a deformation of the CB[6]. The macrocycle also showed evidence for the free and encapsulated protons of 2,2'-bipyridine by ^{1}H NMR, supporting the presence of a 1:1 (Host : guest) inclusion complex. Although this building block approach to give Me_4CB[6] introduces functionality to the host, the methyl groups do not allow for further functionalization.

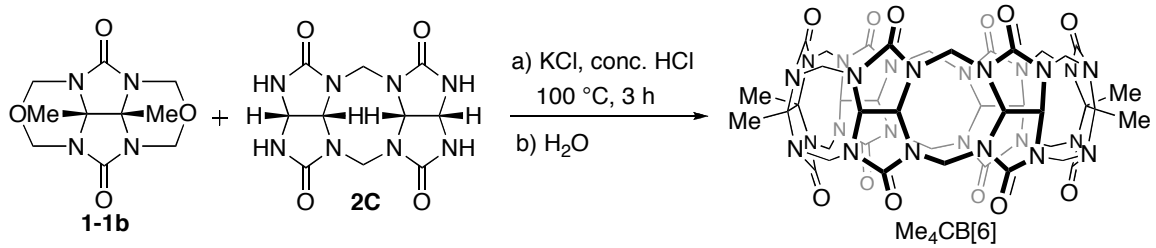

Scheme I-16. Synthesis of Me_4CB[6] using a building block approach.

A study by Isaacs lead to the discovery of another functionalized CB[6] macrocycle that incorporated a xylene ring.[73] The previously isolated *nor-seco*-CB[6] (*ns*-CB[6]) resembles a CB[6] host but lacks one methylene bridge thus exposing the two uridyl NH tips to further reactions. A condensation reaction between *ns*-CB[6] and *o*-xylylenedialdehyde (**I-49**) released one equivalent of water to deliver **I-50** in near quantitative yield (Scheme I-17). Compound **I-50** is unusual because it contains a N-C-O-C-N bridge which differs from the standard N-C-N connectivity. This result

encouraged us to further investigate using dialdehyde **I-49** in reactions with glycoluril and glycoluril oligomers.

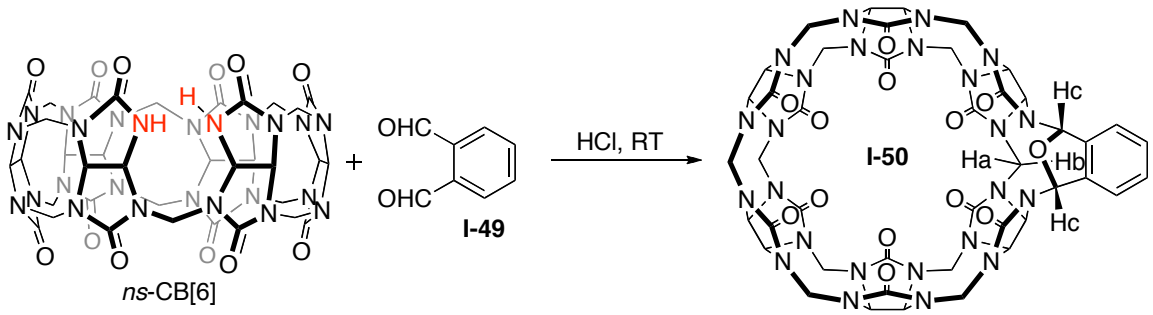

Scheme I-17. Ring closure using *ns*-CB[6] and **I-49** to form macrocycle **I-50**.

A building block strategy using glycoluril dimer **2C** and **I-49** was implemented in the interest of forming new CB[6] derivatives.[24] As shown in Scheme I-18, this reaction does not result in the desired CB[6] product. Instead S-shaped glycoluril tetramer **I-4s1** (37%) was discovered along with tetramers **I-4c1** and **I-4c2** as minor components. Unlike the formation the of N-C-O-C-N bond in macrocycle **I-50**, the condensation of **1b** and **I-49** releases two molecules of water to form two N-C-N bonds. More interestingly, the reaction shows the S-shaped diastereomer as the dominant component of the reaction.

Further experiments investigated the reactions of glycoluril derivatives and **I-49** and confirmed the formation of S-shaped oligomers. The S-shaped oligomers are unable to undergo cyclization due to the improper orientation of the glycoluril units. It is likely that *ns*-CB[6] cyclizes with **I-49** due to its C-shaped preorganization which has direct implications for the orientation of glycoluril building blocks and their use in CB[n] derivative synthesis.

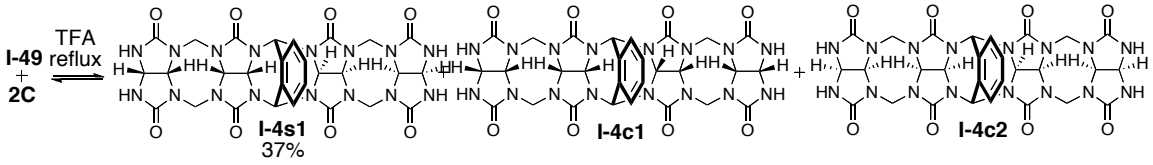

Scheme I-18. Dominant formation of S-shaped tetramer **I-4s1** using **2C** and **I-49**.

1.9 Summary and Conclusions.

Since the initial discovery of CB[6] by Behrend et. al. in 1905, the cucurbituril field has undergone considerable growth to give a family of CB[n] homologues due to the efforts of Mock, Buschmann, Day, Kim, and Isaacs. Today CB[5], CB[6], CB[7], and CB[8] are commercially available and the rapid emergence of new homologues, analogues, congeners, and derivatives have shown the CB[n] family to be a favorable platform in a large number of applications (e.g. drug delivery, biomimetic systems, sensoring, surface chemistry). The exceptionally high binding affinities and selectivities as well as the number of structural variants now available have allowed CB[n] to rival, and in many ways surpass, other supramolecular hosts such as cyclodextrins. Despite the highly desirable properties displayed by CB[n], the difficult purification and limited number of functionalized derivatives have held back their use in advanced applications. The efficient synthesis of mono-functionalized CB[n] is likely to break this barrier and allow the field to further blossom into a number of commercial and advanced applications.

The Isaacs group has been heavily involved in the elucidation of the mechanism of formation for CB[n]. The isolation of oligomers **2C**-**6C** along with other kinetically

controlled intermediates such as *ns*-CB[6], (±)-bis-*ns*-CB[6], and bis-*ns*-CB[10] have provided a great deal of depth to this mechanistic insight. It was also demonstrated that C-shaped oligomers are reactive species that can significantly impact the CB[n] product distribution in condensation reactions with formaldehyde. However, the oligomers **3C**-**6C** have not been pursued as desirable starting materials due to the difficult purification processes required for their purification. The reactivity of easily obtained **2C** has been illustrated by the use of **2C** in the construction of CB[n] derivatives, analogues, and acyclic congeners. The substitution of formaldehyde for dialdehyde **I-49** in reactions with **2C** delivered S-shaped tetramer (**I-4s1**) as the dominant product. The use of the preorganized species, *ns*-CB[6], in the reaction with **I-49** resulted in cyclization to **I-50**. The C-shaped preorganization of glycoluril oligomers is therefore essential to ring closure reactions with **I-49** and implies that the larger **6C**, **7C**, and **8C** gycoluril oligomers may be able to form CB[6], CB[7], and CB[8] derivatives, respectively, under similar reaction conditions.

The synthesis and purification of CB[n] homologues and especially kinetic intermediates **3C**-**6C** has proven to be difficult and low yielding. Several supramolecular groups have investigated the use of templation as a means of controlling the cyclization reaction pathways to deliver desired products. This is accomplished through the templates non-covalent interactions with the host, shape, and size. Although this has been applied to CB[n] reactions by Day through the use of metal cation templates, his results were less than promising and failed to scan several variables know to dramatically influence the outcome of CB[n] forming reactions (e.g. solvent, temperature, time,

equivalents of formaldehyde, and concentration). It is foreseeable that the careful selection of a template along with a thorough scanning of controllable reaction variables can selectively create CB[n] homologues and C-shaped oligomers. The obtainment of these highly desired materials in good yield may provide pathways towards new CB[n] derivatives and further elevate the CB[n] family as the platform of choice in host-guest applications.

II. Chapter 2: Templated Synthesis of Glycoluril Hexamer and Monofunctionalized Cucurbit[6]uril Derivatives.[75]

(This work was recently published in *J. Am. Chem. Soc.* as a full article. Although I am the main contributor to the work, James Wittenberg was responsible for the large scale synthesis of bis-*ns*-CB[10], LiPing Cao was responsible for the synthesis of **II-17**, and Pavel Anzenbacher, Jr. and Tsuyoshi Minami created the fluorescence turn-on assay using **II-19**).

2.1 Introduction.

The cucurbit[n]uril (CB[n]; n = 5, 6, 7, 8, 10) family of molecular container compounds are prepared by the condensation reaction of glycoluril (**1**) and formaldehyde under strongly acidic conditions (Chart II-1).[1,2,7,8,12,20] Interest in CB[n] molecular containers[13,23] has surged in recent years, in large part due to the high affinity (K_a up to 10^{15} M^{-1}) and highly selective (K_{rel} up to 10^8 for closely related guests) binding processes that occur inside the CB[n] cavity.[3,17,76-78] These large differences in binding free energy amount to a potent driving force that can be used to drive switching processes in biological and technological applications. For example, CB[n]•guest complexes have been used in applications ranging from stimuli responsive molecular machines,[79] supramolecular polymers,[80-88] sensing ensembles,[89-91,53-55] and in biomimetic systems.[22,35,48-51] Still other application areas include drug delivery,[33,34,42-45,92-97] gas purification,[98-104] and supramolecular catalysis.[105-113] Despite the wide range of applications to which the parent unfunctionalized CB[n] compounds may be applied there

is real need for versatile synthetic methods for the preparation of CB[n] derivatives that contain reactive functional groups that are amenable to further functionalization reactions for incorporation into more complex systems. To date, the most versatile method for the functionalization of CB[n] compounds is the (per)hydroxylation of CB[n] developed by the Kim group,[32,114] who have used the (per)hydroxylated CB[n] compounds for several applications including membrane protein fishing and stimuli responsive polymer nanocapsules for drug delivery.[33,34,36,115,116] Despite these advances, the preparation of monofunctionalized CB[n] compounds containing reactive functional groups remains unknown.

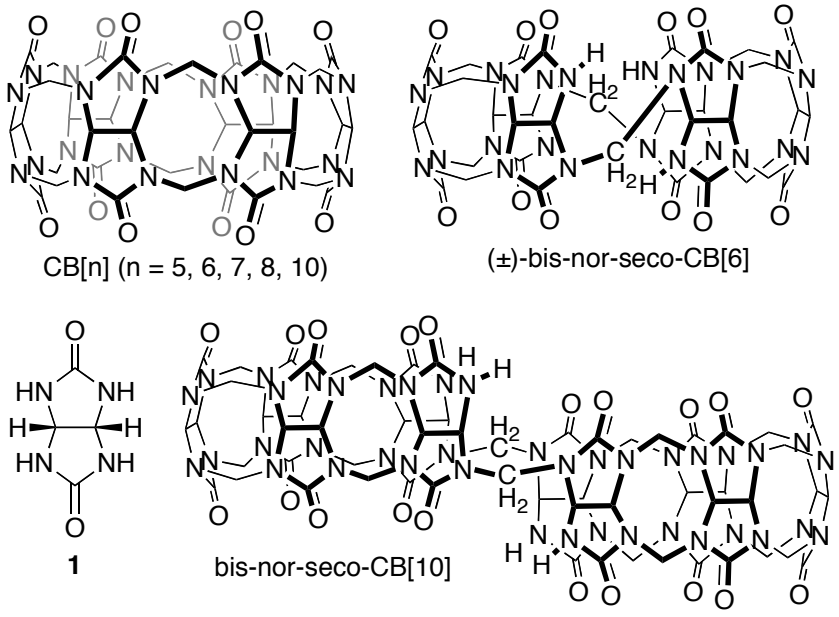

Chart II-1. Structures of glycoluril (**1**), CB[n], (±)-bis-nor-seco-CB[6], and bis-nor-seco-CB[10].

For many years, our group has been interested in understanding the mechanism of CB[n] formation (Scheme II-1) as a means to prepare new CB[n]-type receptors with the goal of endowing the synthesized CB[n] compounds with exciting new functions.[21,22] This line of inquiry has led us to prepare CB[n] analogues,[69,117,118] inverted CB[n],[27,119] and *nor*-*seco*-CB[n] containers[25,26,50,73,120,121] (Chart II-1) which were demonstrated to function in applications including UV/Vis and fluorescence sensing, chiral recognition, size-dependent homotropic allostery, and foldamer reconfiguration. In the course of these studies, we have garnered mechanistic information that suggested to us that templated synthesis of CB[n] type compounds would be possible. For example, we established the presence of an equilibrium between S-shaped and C-shaped glycoluril oligomers (e.g. **2C** – **8C**)[11] that greatly favors the C-shaped form required for the formation of CB[n] type receptors.[122] We also showed that the macrocyclization reaction to give CB[n]-type receptors glycoluril oligomers occurs by a combination of chain growth and step growth processes.[10,11,123] Previously, Day and co-workers studied the influence of potential templating compounds (e.g. metal ions or ammonium ions) on the product distribution of the CB[n] forming reaction.[67,124,125] Although the presence of templates does effect the ratio of CB[n] formed, the effects are generally modest and the underlying mechanistic reasons for those effects remain unclear. In this paper we explore the templated synthesis of methylene bridged glycoluril hexamer (**6C**), the transformation of **6C** into monofunctionalized CB[6] derivatives by reaction with (substituted) phthalaldehydes in the presence of templates, and demonstrate unique sensing abilities of a CB[6] derivative covalently functionalized with a naphthalene fluorophore.

2.2 Results and Discussion.

This results and discussion section is subdivided into several subsections detailing the template synthesis of glycoluril hexamer **6C** and bis-*ns*-CB[10], the transformation of **6C** into CB[6] derivatives, exploration of the basic recognition properties of these CB[6] derivatives, and their use in creating a turn-on fluorescence sensor for biologically important histamine.

2.2.1 Mechanism of CB[n] Formation.

First, we review the state-of-the-art understanding of the mechanism of CB[n] formation (Scheme II-1) which is required to understand our hypothesis that *templated formation of CB[n]-type receptors will be possible when the reactions are conducted with fewer than two equivalents of formaldehyde.* In brief, the condensation of two molecules of glycoluril (**1**) with two molecules of formaldehyde delivers a mixture of C-shaped **2C** and its S-shaped diastereomer **2S**. Previous model system studies have shown that the C-shaped diastereomer is more stable that the S-shaped form by > 1.55 kcal mol^{-1} so isomerization to the more stable **2C** occurs readily under the reaction conditions.[10] Dimer **2C** can undergo chain growth by the stepwise addition of glycoluril (**1**) to deliver trimer – octamer (**3C** – **8C**); at each step along the way isomerization from the less stable S-shaped to the more stable C-shaped forms occur. At this stage, two mechanistic pathways may occur. In the first pathway two molecules of oligomer (e.g. pentamer **5C**) may condense with two molecules of formaldehyde via intermediates (±)-**II-9** (n=5) and (±)-**II-10** (n=5) which leads to bis-*nor-seco*-CB[10] by a step growth process. Similar

step growth processes lead to (±)-bis-*nor-seco*-CB[6] and an acyclic glycoluril decamer that we have studied previously.[25,50] A second pathway involves the condensation of **6C** with formaldehyde to initially deliver (±)-**II-9**(n=6) followed by macrocyclization to give nor-seco-CB[6]. Based on the results of model system studies and product resubmission experiments we depict all of these fundamental steps with *reversible equilibrium arrows*.[11,24] Finally, the reaction of *nor-seco*-CB[n] with formaldehyde delivers CB[n]. Within the CB[n] product manifold, resubmission experiments conducted by Day establish that CB[8] undergoes contraction to the smaller CB[n] (n = 5, 6, 7) but that CB[5], CB[6] and CB[7] are stable to the reaction conditions.[20] This result implies that the final ring closing transformation of nor-seco-CB[n] to CB[n] is *irreversible under the reaction conditions*. Based on this analysis it is perhaps unsurprising that previous attempts to use ammonium ions that are good guests for CB[n] as *thermodynamic templates* have not been particularly successful. The key hypothesis explored in this paper is whether substituted ammonium ions (e.g. *p*-xylylenediammonium ion **II-11**) are suitable templates for nor-seco-CB[n] forming reactions conducted between one equivalent of glycoluril and less than two equivalents of formaldehyde. Under these formaldehyde deficient reaction conditions irreversible cyclization to CB[n] is suppressed[11] allowing thermodynamic effects to become enhanced.

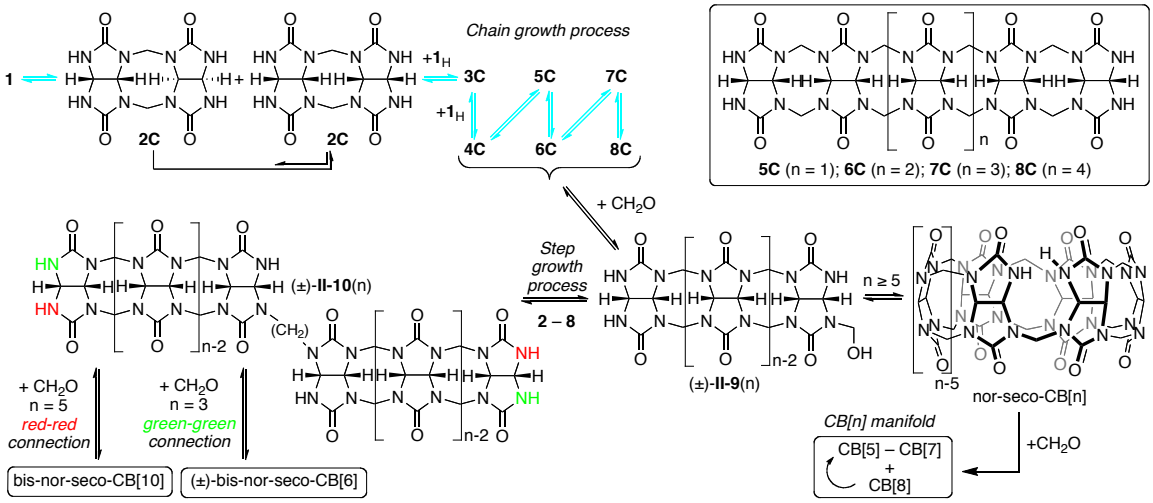

Scheme II-1. Mechanism of CB[n] formation. Color code: reversible equilibria, green arrows; irreversible reactions, red arrows.

2.2.2 Classification of Templates

Classification of the different types of template effects that may occur in covalent bond forming reactions has been beautifully reviewed by Anderson and Sanders and is therefore only briefly described here.[59] Template molecules promote the formation of a specific product by either kinetic or thermodynamic means. Thermodynamic templates enhance the yield of reactions under thermodynamic control by stabilizing one product at the expense of others. Kinetic templates influence the yield of a particular product by changing the various transition state energies and therefore the rate of product formation. Kinetic templates may be further classified as positive or negative based on whether they speed up or slow down the rate of formation of a particular product, respectively. Finally, because kinetic templates – which influence transition state energies – typically bind to reaction intermediates or products they commonly also exert thermodynamic influences on the reaction.

2.3 Templated Synthesis of Hexamer 6C and Bis-nor-seco-CB[10].

2.3.1 Selection of paraXylylenediammonium Ion as Template and ^{1}H NMR Probe Guest.

Based on the hypothesis described above, we decided to conduct reactions between one equivalent of glycoluril (**1**) and less than two equivalents of formaldehyde in the presence of an ammonium ion as template. As the template ammonium ion we selected *p*-xylylenediammonium ion (**II-11**) for several reasons (Figure II-1). First, **II-11** is known to form well defined host-guest complexes with CB[6], CB[7], CB[8], i-CB[6], i-CB[7], **6C**, bis-nor-seco-CB[10], (±)-bis-nor-seco-CB[6], and nor-seco-CB[6] which means that **II-11** could conceivably act as a stabilizing template for many different CB[n]-type receptors. Second, because the kinetics of exchange for complexes of **II-11** with each of these containers is slow on the NMR time scale each different container•**II-11** complex gives a diagnostic pattern of resonances in the ^{1}H NMR spectrum (Figure II-1). For example, for highly symmetric hosts (CB[6], CB[7], i-CB[6], i-CB[7], and **6C**) the ^{1}H NMR resonance for the Ar-H atoms of **II-11** appears as a sharp singlet in the relatively open 6-7 ppm region of the ^{1}H NMR spectrum (Figure II-1 and Supporting Information). Conversely, for less symmetric bis-nor-seco-CB[10]•**II-11**$_2$ and nor-seco-CB[6]•**II-11** complexes the Ar-H (H_a and H_b) atoms are non-equivalent and appear as a pair of doublets. Finally, for (±)-bis-ns-CB[6]•**II-11** the Ar-H (H_a and H_b) atoms are equivalent and appear as a singlet but the CH_2-groups of guest **II-11** are diastereotopic (H_c and $H_{c'}$) and appear as a pair of doublets in the upfield region of the spectrum. Third, we find that using **II-11** as guest tends to result in good dispersion of the host resonances for the less symmetrical host•**II-11** complexes. For these reasons it was particularly

efficacious to use **II-11** as template and simultaneously as an *in situ* probe for analysis of the content of CB[n] reaction mixtures.

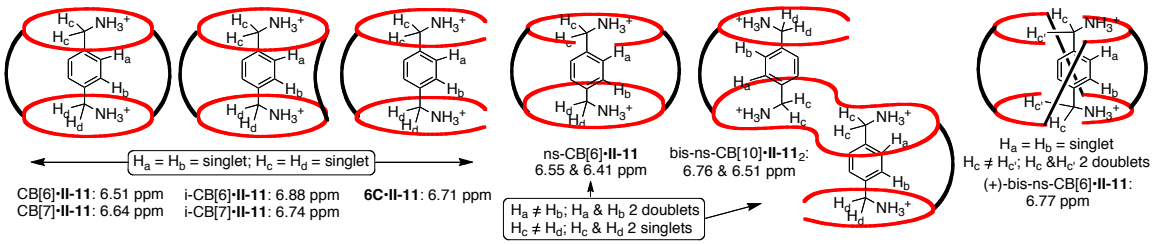

Figure II-1. Illustration of the use of **II-11** as a probe of CB[n] reaction mixtures by ^{1}H NMR spectroscopy.

2.3.2 Discovery of Templated Synthesis of Hexamer 6C.

After much experimentation we discovered that heating a mixture of **II-1** (7.1 g, 1 equiv., 5 M), paraformaldehyde (1.67 equiv.), and **II-11** (0.1 equiv.) in concentrated HCl at 58 ˚C for 3-5 days delivers a thick off-white precipitate that can be isolated by centrifugation. Analysis of the ^{1}H NMR spectrum of the crude solid indicates that it contains mainly (≈ 89%) the **6C•II-11** complex. We also analyzed the content of the soluble portion of the reaction mixture by ^{1}H NMR after precipitating the supernatant by addition to MeOH. The soluble portion of the reaction mixture contains 11% **6C**, 10% bis-ns-CB[10], 5% nor-seco-CB[6], and 5% CB[6]. To obtain free **6C**, we dissolved the crude solid in water, centrifuged away insoluble materials, and then added 5M aq. NaOH which resulted in the precipitation of **6C**. Hexamer **6C** is obtained as a white powder (0.901 g, 10% yield). Our hypothesis is that the presence of **II-11** as template served at least two purposes: 1) to bind to **6C** and therefore thermodynamically stabilize it, and 2)

to cause precipitation which also thermodynamically stabilizes **6C** toward further transformation. In an attempt to further optimize this reaction we changed some key variables (e.g. temperature, acid concentration, equivalents of **II-11**, equivalents of formaldehyde) but were unable to further improve the process.

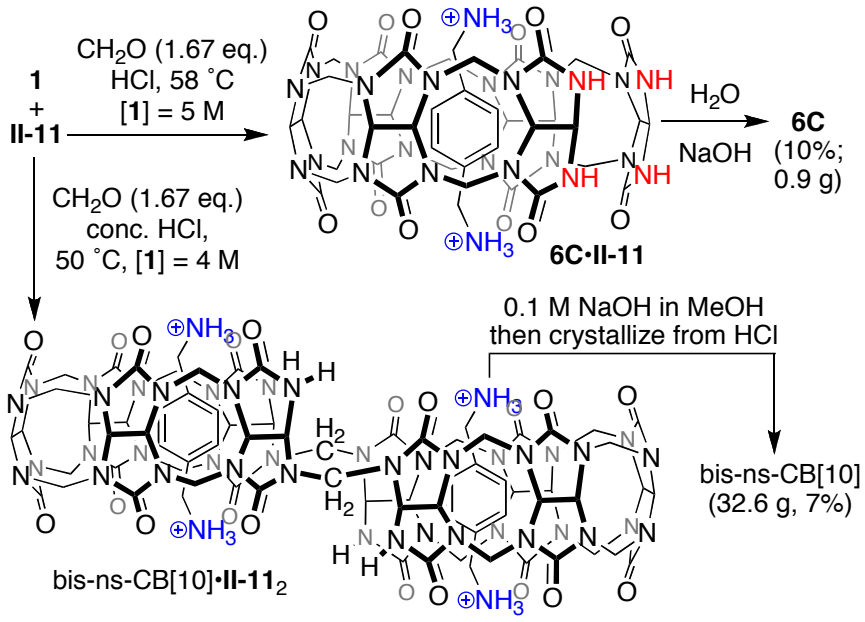

Scheme II-2. Templated synthesis of **6C** and bis-*nor-seco*-CB[10].

2.3.3 Templated Synthesis of Bis-*nor-seco*-CB[10].

Previously, we have reported that the reaction of **1** (1.42 g, 1 equiv., 2.5 M) and paraformaldehyde (1.67 equiv.) in conc. HCl at 50 ˚C delivers bis-*nor-seco*-CB[10] as an insoluble precipitate (0.238 g, 15%). We found that this reaction is very sensitive to many variables including the initial mixing of the solid reagents with the HCl solvent, the nature of the reaction vessel (20 mL scintillation vial preferred), and the nature of the vessel closure (14/20 Suba-Seal attached with copper wire preferred). Given the high

sensitivity of this reaction it is perhaps unsurprising that we have been unable to scale-up this reaction to the 10 g or 100 g levels; reactions on this scale typically deliver large amounts of CB[6] as product. Since the CB[n] forming reaction is a cyclo-oligomerization reaction[11] whose fundamental condensation steps respond to changes in concentration over the mM to M range[24] we reasoned that it would be worthwhile to perform the **II-11** templated reaction at higher concentrations of **1**. For example, when [**1**] = 4 M, the reaction mixture remains homogenous and ^{1}H NMR analysis of the crude reaction mixture reveals the presence of bis-*ns*-CB[10] (11%), **6C** (6%), ns-CB[6] (5%), and CB[6] (13%). The more soluble compounds **6C**, CB[6], and *ns*-CB[6] were removed by washing with H_2O. Decomplexation of bis-*nor*-*seco*-CB[10]•**II-11**$_2$ by washing with 0.1 M NaOH in MeOH followed by recrystallization from HCl delivered bis-*ns*-CB[10] (32.6 g, 7% yield). The observation of the enhanced formation of bis-*nor*-*seco*-CB[10] (derived from two units of pentamer **5C**) at lower concentrations and hexamer **6C** at higher concentrations of **1** is consistent with our description of the mechanism of CB[n] formation as a co-polymerization process between **1** and formaldehyde which is expected to deliver longer oligomers at higher concentrations according to Le Chatelier's principle.

2.3.4 The Role of Template II-11 in CB[n] Forming Reactions.

There are many possible roles for template **II-11** in these reactions (e.g. thermodynamic, kinetic, positive, negative). First, it is known from the literature that **II-11** binds to **5C** ($K_a = 1.2 \times 10^6$ M^{-1}) and **6C** ($K_a = 2.2 \times 10^7$ M^{-1}) substantially stronger than it does to either CB[6] ($K_a = 550$ M^{-1}) or a tetramethyl derivative of **II-4** ($K_a = 5.6 \times 10^3$ M^{-1}).[123] This information suggests that the formation of the **6C•II-11** and bis-*nor*-

seco-CB[10]•**II-11**$_2$ complexes thermodynamically stabilize these oligomers. Second, the precipitation of the **6C•II-11** complex suggests that complexation of **6C** with **II-11** changes the maximal solubility of the **6C•II-11** complex (relative to **6C**) which in turn results in precipitation when that solubility limit is exceeded. Third, Figure II-2 shows an MMFF minimized model of the **6C•II-11** complex. An examination of this complex shows that the presence of guest **II-11** enforces a geometry in which the reactive NH tips of **6C** are held apart from each other. As shown in Figure II-2, the geometry of **6C** in the **6C•II-11** complex increases the distance between the two top and two bottom NH tips (4.018 Å and 3.475 Å, respectively) compared to the distance observed in the CB[6]•**II-11** complex (2.419 Å). This geometrical feature might kinetically disfavor transformation of **6C•II-11** into CB[6]•**II-11**.

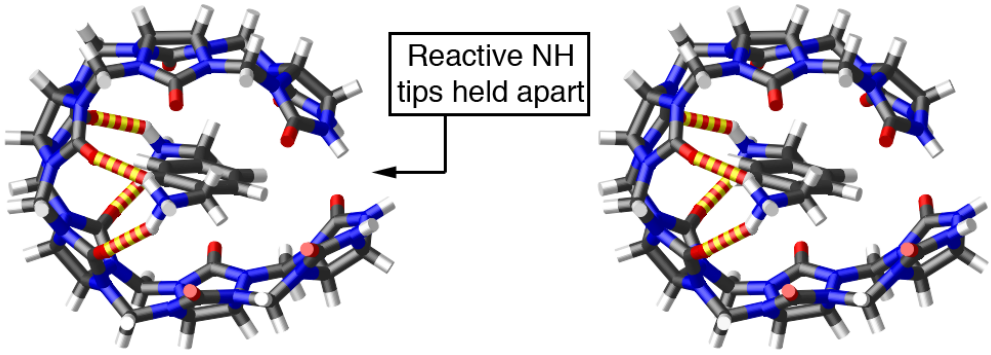

Figure II-2. Stereoview of an MMFF minimized model of the **6C•II-11** complex.

Given access to gram-scale quantities of **6C** we decided to study the kinetics of the transformation of **6C** and paraformaldehyde into CB[6] in the absence or presence of **II-11** as template as a means to assess the importance of kinetic stabilization of the **6C•II-11** complex on the reaction. We conducted the reactions in conc. HCl at room

temperature with [**6C**] = 200 mM. Figure II-3 shows plots of the mole fraction of CB[6] determined by integration of the ^{1}H NMR spectra recorded versus time. After only 102 min. the untemplated reaction is complete whereas in the presence of **II-11** as template the reaction is only 2% complete. Clearly the presence of **II-11** as template substantially slows down the macrocyclization reaction between **6C** and formaldehyde to deliver CB[6] as product.

Accordingly, it appears that **II-11** as template serves several roles in influencing the outcome of CB[n] forming reactions. These roles include differential thermodynamic stabilization due to complex formation, controlling the solubility of various components of the reaction mixture through complexation, and finally in influencing the kinetics of the macrocyclization step of the CB[n] forming reaction. Because of the complexity of the analysis of such reaction mixtures using templates other than **II-11** we have not yet been able to expand our study to the full range of potential templates.

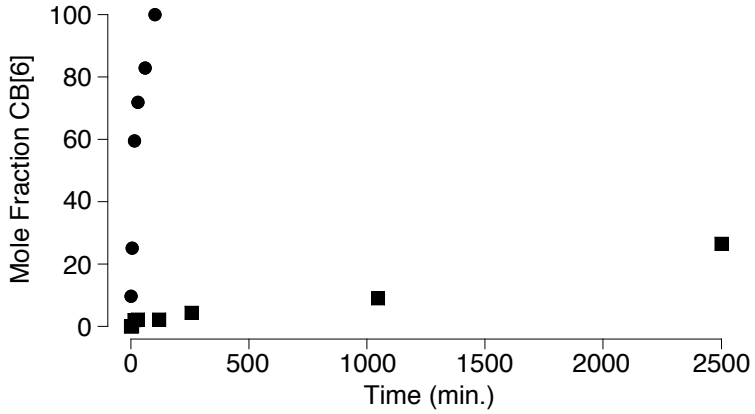

Figure II-3. Plot of mole fraction of CB[6] versus time for reactions between **6C** and paraformaldehyde in the absence (•) or presence (▪) of **II-11** as template.

2.4 Transformation of 6C into Monofunctionalized CB[6] Derivatives.

Previously, we have studied the reaction between 2 equivalents of N,N'-dimethylglycoluril with *o*-phthaldehyde (**II-12**) under acidic conditions and observed the dominant formation of S-shaped products.[24] However, we reasoned that the reaction between **6C** and **II-12** might be successful because **6C** is preorganized to form the C-shaped macrocyclic product (Scheme II-3). In the event, we allowed **6C** (1 g) to react with **II-12** in 9 M H_2SO_4 at room temperature for 36 h. Purification of the crude reaction mixture was easily achieved by a combination of precipitation and washing steps to deliver CB[6] derivative **II-13** in 72% yield (792 mg). Compound **II-13** is C_{2v}-symmetric and that is reflected in the simplicity of its ^{1}H NMR spectrum recorded as its **II-13•II-11** complex (Figure II-4a). The most diagnostic resonances in the ^{1}H NMR spectra are those for host protons H_n (6.89 ppm) as well as H_o and H_p (4.93 and 5.12 ppm) which are upfield shifted due to their proximity to the fused aromatic *o*-xylylene ring. Similar reactions were conducted between **6C** and carboxylic acid or nitro-substituted phthalaldehydes **II-14**[126] and **II-15**[127] which delivered monofunctionalized CB[6] derivatives **II-16** and **II-17** in 56% (641 mg) and 58% (65 mg), respectively. Figure II-4c-d shows their ^{1}H NMR spectra recorded as their complexes with **II-11** which reflects the lower C_s-symmetry of these CB[6] derivatives. Finally, we conducted the reaction between **6C** (1 g) and 2,3-napthalenedialdehyde **II-18**[128] in conc. HCl at room temperature and obtained **II-19** as a precipitate. Simple washing with MeOH delivered **II-19** in pure form (83%, 0.951 g). Unfortunately, we have not been able to obtain crystals of **II-13**, **II-16**, **II-17**, or **II-19** that are suitable for x-ray crystallographic

structure determination. To provide some structural information, we minimized the structure of **II-13** by MMFF calculations (Figure II-5). As is readily apparent, the fusion of the *o*-xylylene ring to the methylene bridges of the CB[6] skeleton result in an overall ellipsoidal deformation of the cavity along the plane defined by the *o*-xylylene ring. Similar deformations have been observed for CB[6] derivatives prepared from substituted glycolurils[71] and for certain CB[6]•guest complexes.[129,130] Since the main reason to prepare CB[6] derivatives is to use their host•guest binding properties to enable advanced applications, it is critical that the CB[6] derivatives maintain the high affinity and high selectivity binding interactions typical of the CB[n] family. Given the ellipsoidal deformation described above we decided that it was necessary to experimentally determine the binding constant of these new CB[6] derivatives toward common guests.

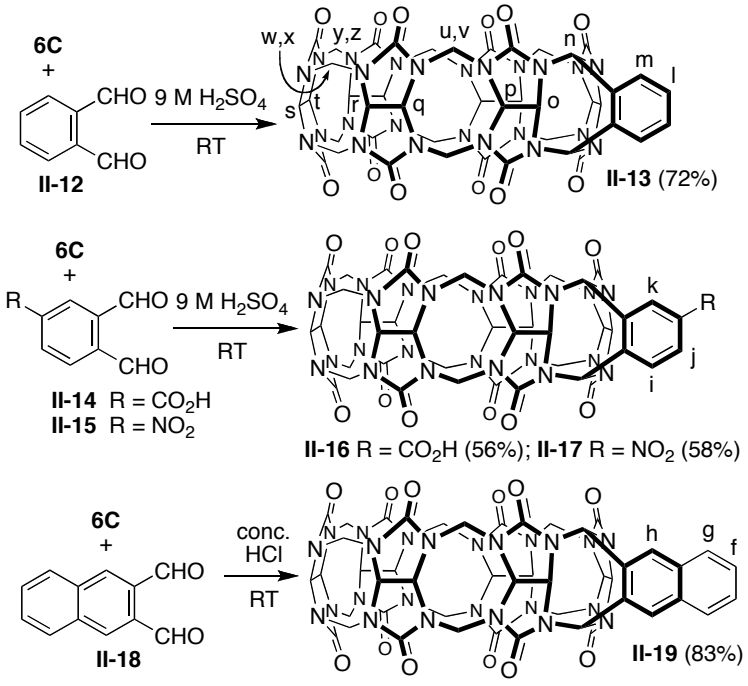

Scheme II-3. Synthesis of CB[6] derivatives **II-13**, **II-16**, **II-17**, and **II-19**.

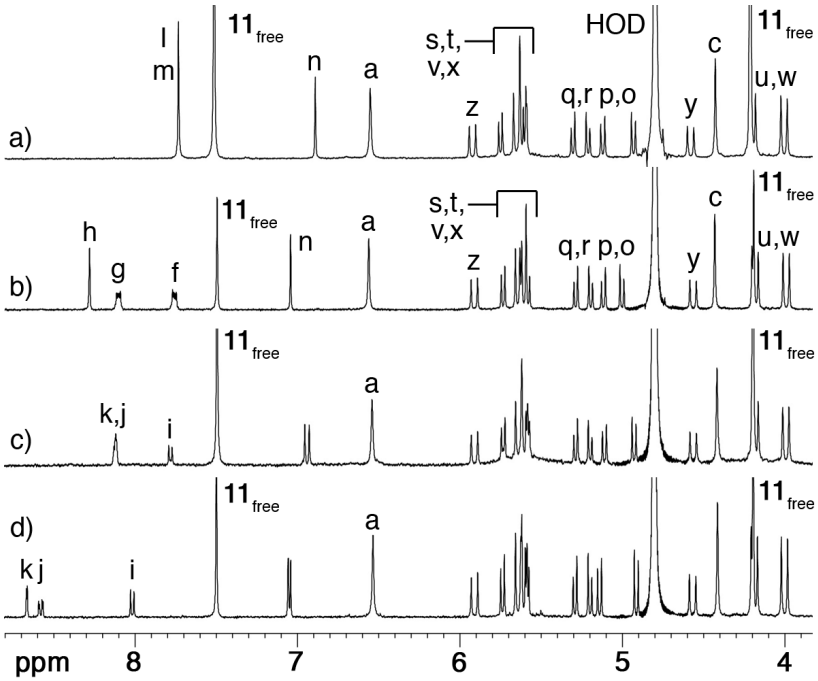

Figure II-4. ^{1}H NMR spectra recorded (400 MHz, D_2O, RT) for: a) **II-13•II-11**, b) **II-19•II-11**, c) **II-16•II-11**, and d) **II-17•II-11**. Only partial assignments are given in c) and d) because the lower symmetry of **II-16** and **II-17** complicated the assignments.

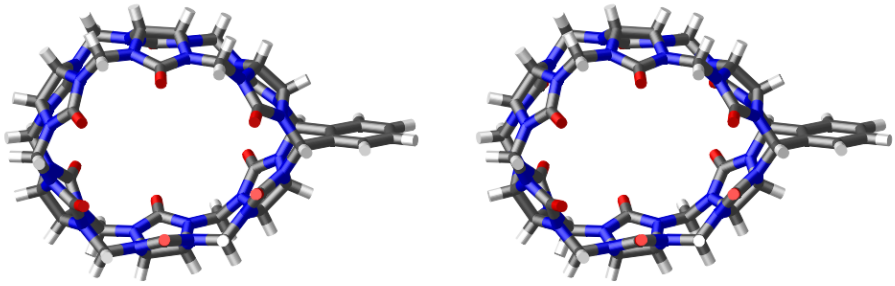

Figure II-5. Stereoview of the MMFF minimized structure of **II-13**.

2.4.1 Template Effects Also Operate During the Reactions Between 6C and II-12.

The observation of intermediates by ^{1}H NMR during the reactions between **6C** and **II-12** shown in Scheme II-3 suggested to us that it might be possible to observe the influence of templates on the reaction between **6C** and **II-12**. First, we monitored the kinetics of the reaction between **6C** and **II-12** in the absence of any template (Figure II-6a, •) and observed that the reaction delivered **II-13** over 240 min. Similarly, when NH_4^+ – which can bind to the ureidyl C=O portals but not the hydrophobic cavities of CB[6] compounds – is used as template we observe comparable reaction kinetics as the untemplated reaction. The situation is very different when larger diammonium ions **II-20** and **II-11** are used as templates. For example, when **6C** reacts with **II-12** in the presence of **II-20** as template (9 M H_2SO_4, RT), the reaction very rapidly (< 1 min.) gives an intermediate ((±)-**II-21**) which very slowly transforms (over several weeks) into **II-13•II-20** (Figure II-6b, • = (±)-**II-21**; o = **II-13•II-20)**. However, when the reaction between **6C** and **12** were conducted (9 M H_2SO_4, RT) in the presence of **II-11** as template (Figure II-6b, ■ = (±)-**II-21**; □= **13•II-11**) the reaction again rapidly delivers intermediate ((±)-**II-21**) that is kinetically stable over the course of several weeks. Attempts to stop either of these templated reactions at the intermediate stage, remove template, and purify by Dowex ion exchange chromatography were uniformly unsuccessful for the reason detailed below. Fortunately, a sample containing predominantly (±)-**II-21** could be obtained when the reaction between **6C** and **II-12** was conducted in CF_3CO_2H as solvent. We characterized (±)-**II-21** as its (±)-**II-21•II-11** complex. The electrospray ionization mass spectrum showed a peak at *m/z* = 613.15 amu which can be rationalized as arising

from the reaction between **6C** (972 amu), **II-12** (134 amu) and **II-11**$^{2+}$ (138 amu) with expulsion of one molecule of H_2O. The 600 MHz ^{1}H NMR spectrum of the complex (Figure II-7a) provided key clues which allowed us to determine the structure as (±)-**II-21•II-11** (Figure II-7b). For example, the singlet at 6.59 ppm corresponds to the four symmetry equivalent Ar-H protons (H_a) of guest **II-11** which establishes that the two ureidyl C=O portals of (±)-**II-21** are symmetry equivalent (See Figure II-1, CB[n], i-CB[n], **6C**, (±)-bis-*nor*-*seco*-CB[6]). The upfield region of the ^{1}H NMR spectrum shows a pair of coupled doublets at 4.08 and 4.01 ppm which correspond to the diastereotopic CH_2-group (H_c, H_c') of guest **II-11** which indicates that (±)-**II-21** is chiral and racemic (See Figure II-1, (±)-bis-*nor*-*seco*-CB[6]). Based on the combined inference of the ESI-MS and diagnostic ^{1}H NMR resonances, we formulate the structure of (±)-**II-21•II-11** as shown in Figure II-7b. This structure features a top-bottom connection between the two ends of the hexamer unit of (±)-**II-21** enforced by an NCOCN-bridge which contains two stereogenic centers. The availability of free (±)-**II-21** allowed us to understand the difficulties that we encountered during the attempted purification of (±)-**II-21** during Dowex ion exchange chromatography. When (±)-**II-21** was dissolved in H_2O we observed hydrolysis of the NCOCN-bridge over the course of 4 days to deliver starting material **6C** (Supporting Information, Figure II-S14).

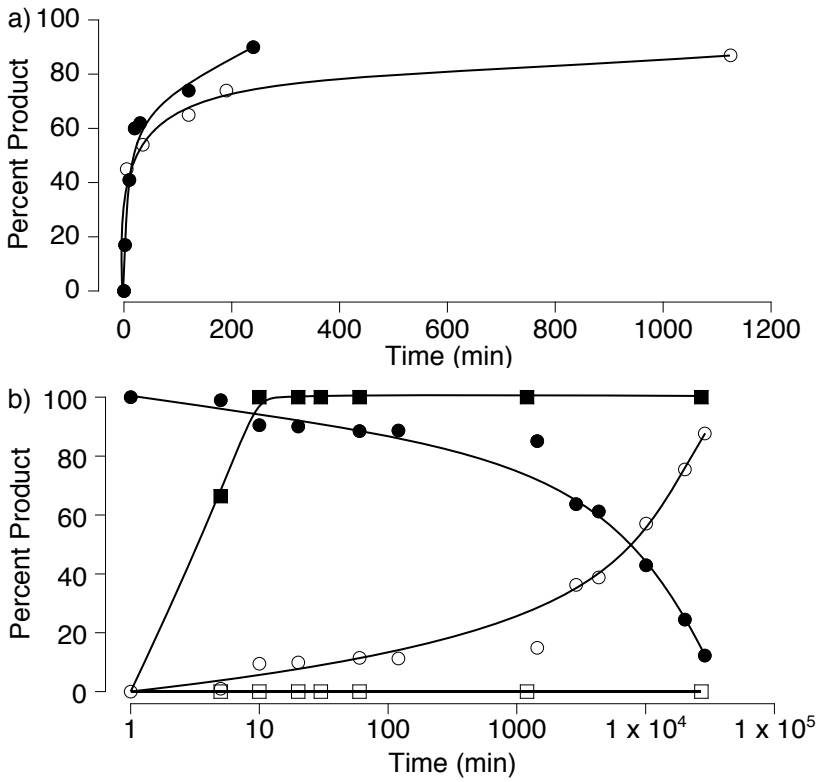

Figure II-6. Plot of percent product **II-13** and (±)-**II-21** versus time for the reaction of **6C** with **II-12** (9 M H_2SO_4, RT): a) percent **II-13** in the absence of template (•) or with NH_4Cl as template (o), and b) in the presence of **II-20** as template (• = percent (±)-**II-21**; o = percent **II-13**) or **II-11** as template (■ = percent (±)-**II-21**; □= percent **II-13**).

The observation of (±)-**II-21•11** as the sole product in the reaction between **6C** and **II-12** in the presence of **II-11** is significant for several reasons. First, it represents the first clear-cut example of a high fidelity template effect operating in CB[n] chemistry.[131] We believe that the reaction stops at the stage of (±)-**II-21•II-11** because this larger cavity is better able to accommodate guest **II-11** whose affinity toward CB[6] sized cavities is rather weak. Second, the observed hydrolytic lability of (±)-**II-21** provides further evidence of the reversibility of the macrocyclization upon which the

success of this thermodynamic template effect is based. Third, the observation of (±)-**II-21•II-20** as an intermediate along the pathway to **II-13•II-20** suggests that size of the guest (e.g. differential affinity toward (±)-**II-21** and **II-13**) might be used in related reactions to template the formation of other, more spacious CB[n]-type containers.

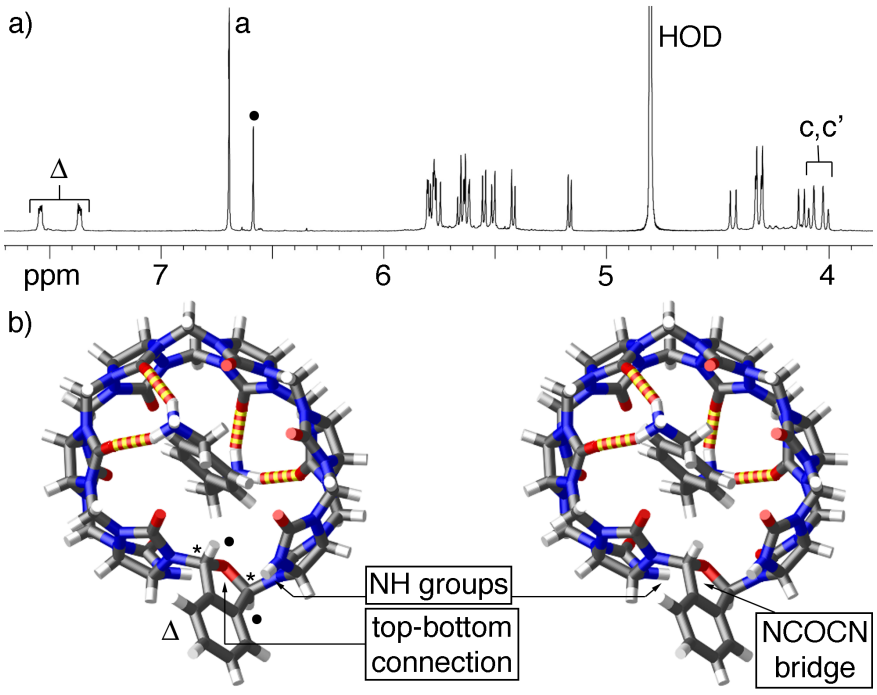

Figure II-7. a) ^{1}H NMR spectrum recorded for (±)-**II-21•II-11** (600 MHz, D_2O, RT). b) MMFF minimized models of one diastereomer of (±)-**II-21•II-11**. * = stereogenic center.

2.4.2 Derivatives Are Capable of Self-Association.

Before undertaking the study of any new host system it is wise to perform ^{1}H NMR dilution experiments to exclude the possibility of self-association interfering with the host-guest complexation events. We found that diluting a sample of **II-13** (20 mM $NaCO_2CD_3$ buffer, pD 4.74) from 2 mM down to 0.06 mM results in a downfield shift of

H_l and H_m, and an upfield shift for H_o (Supporting Information). These shifts are consistent with self association by insertion of the *o*-xylylene ring of **II-13** into the cavity of another molecule of **II-13** which positions H_l and H_m in the cavity of the other molecule of **II-13** and H_o at the deshielding ureidyl C=O portal. We fitted the data to a two-fold self-association model and obtain $K_{self} = 1.2 \pm 0.1 \times 10^3$ M^{-1} (Supporting Information). Similar dilution experiments performed with **II-16**, **II-17**, and **II-19** did not reveal any changes in chemical shift which indicates that they do not undergo self-association processes (Supporting Information). Even though **II-19** does not self-associate it does form a complex with CB[7] – namely CB[7]•**II-19** – whose ^{1}H NMR resonances change little down to 100 mM (Supporting Information). The upfield shifts observed for the naphthalene ring of **II-19** indicates it is sequestered in the cavity of CB[7]. These results highlight the potential of CB[6] derivatives to undergo complexation with themselves or other species and suggests that care must be taken in designing CB[6] derivatives for use in advanced applications.

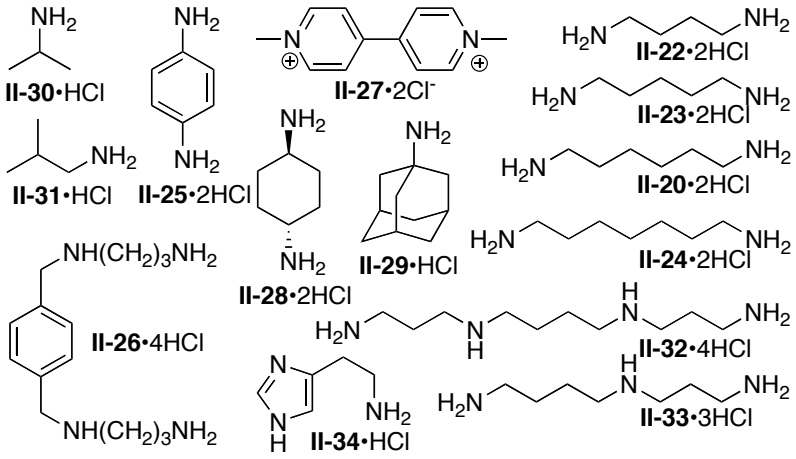

Chart II-2. Chemical structure of guests used in this study.

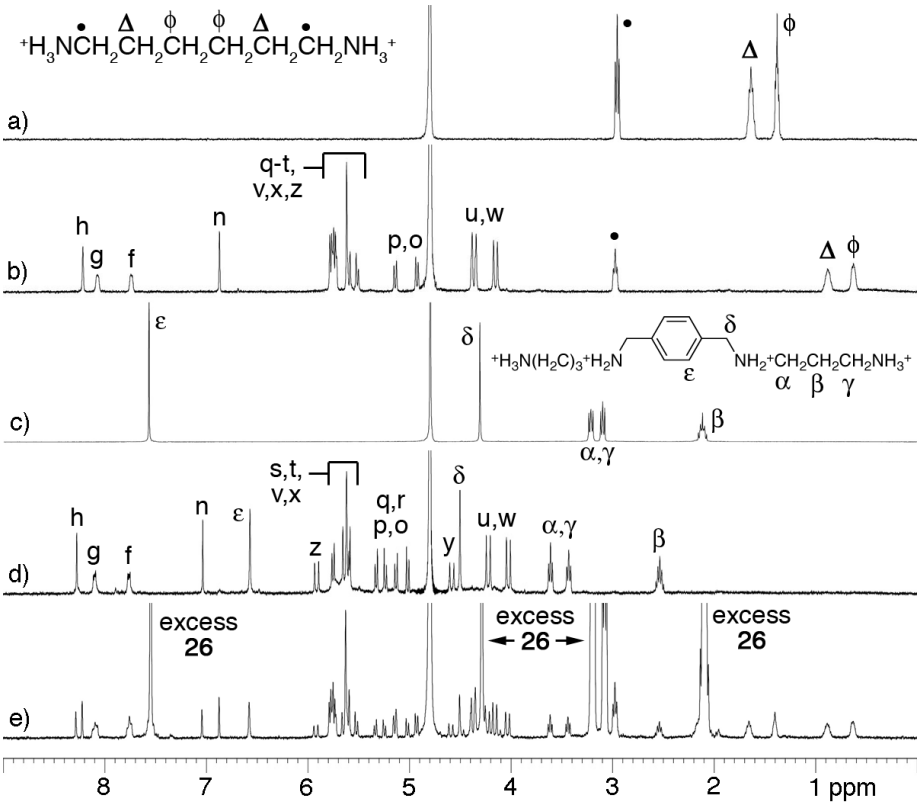

Figure II-8. ^{1}H NMR spectra recorded (400 MHz, 20 mM NaO_2CCD_3, buffered D_2O, pD 4.74, RT) for: a) **II-20**, b) **II-19•II-20**, c) **II-26**, d) **II-19•II-26**, and e) a mixture of **II-19** (0.5 mM), **II-20** (0.5 mM), and **II-26** (5.0 mM).

2.4.3 Host•Guest Complexes and Determination of Binding Constants

Given the observed self-association of **II-13** and the top-bottom dissymmetry of **II-16** and **II-17** we decided to focus our efforts on elucidating the host-guest recognition properties of **II-19**. Chart II-2 shows the structures of guests **II-20** and **II-22** – **II-34** that were studied. Initially, we measured the ^{1}H NMR spectra for 1:1 and 1:2 mixtures of host **II-19** and guests **II-11**, **II-20**, and **II-22** – **II-34** (Supporting Information). As expected the majority of these guests formed **II-19•**guest inclusion complexes that display slow kinetics of exchange on the ^{1}H NMR timescale; guests **II-27**, **II-30**, and **II-**

34 show fast kinetics of exchange. Just like CB[6], **II-19** does not form inclusion an inclusion complex with adamantane amine **II-29**. Unlike CB[6], **II-19** forms the **II-19•II-27** inclusion complex which suggests that the observed ellipsoidal deformation (Figure II-5) of **II-19** allows it to bind wider guests like **II-27**. Figure II-8a-d shows the ^{1}H NMR spectra recorded for **II-20**, **II-19•II-20**, **II-26**, and **II-19•II-26**. The observed upfield shifts of the hexylene and *p*-xylylene regions of guests **II-20** and **II-26** confirm their inclusion inside the cavity of **II-19** as expected. Interestingly, all three CH_2-groups of the $^+H_2N(CH_2)_3NH_3^+$ arms of **II-26** shift downfield in the **II-19•II-26** complex which confirms that these groups are in the deshielding region nearby the ureidyl C=O portals of **II-19**. Overall, the recognition properties of **II-19** are qualitatively quite similar to those known for CB[6].

Next, we decided to quantify the **II-19•**guest binding constants to ascertain whether the ellipsoidal deformation induced by the *o*-xylylene ring (Figure II-5) significantly influences values of K_a. First, we measured the value of K_a of **II-19** toward **II-30** – which undergoes fast kinetics of exchange on the NMR time scale – by a standard NMR titration in which the concentration of guest **II-30** was fixed (0.125 mM) and the concentration of **II-19** was changed (0 → 1.83 mM) (Supporting Information, Figure II-S51). Figure II-S52 shows a plot of the chemical shift of the CH_3-groups of **II-30** as a function of [**II-19**] and the non-linear least squares fitting to a 1:1 binding model (Table II-1, $K_a = 852 \pm 114\ M^{-1}$). Subsequently, we used the ^{1}H NMR competition methodology – involving competition of an excess of a mixture of two guests for a limiting amount of **II-19** – originally developed by Mock[3] and used extensively by our group[17,123] to

determine K_a values for **II-19**•guest complexes of increasing stability in a stepwise manner. For example, Figure II-8e shows the ^{1}H NMR spectra used to calculate the relative K_{rel} values for the competition between **II-19** (0.5 mM), **II-20** (0.5 mM), and **II-26** (5.0 mM); we use the integrals for H_n (**II-19•II-20**: 6.88 ppm and **II-19•II-26**: 7.05 ppm) for this purpose. Table II-1 reports the values of K_a obtained for nine **II-19**•guest complexes obtained similarly. The measured values of K_a range from $\approx 10^3$ M^{-1} up to 10^8 M^{-1} in 20 mM NaOAc buffered D_2O at pD 4.74. Table II-1 also presents the values of K_a measured previously by Mock and co-workers in 1:1 HCO_2H:H_2O toward many of these guests. As expected, the values of K_a measured for **II-19** are larger (up to 50-fold) than the corresponding values measured for CB[6] because of the effect of the more strongly competitive (1:1 HCO_2H:H_2O) solvent. Similar to CB[6], **II-19** exhibits a length dependent selectivity toward alkanediammonium ions **II-20** and **II-22**-**II-24** with highest affinity toward pentane and hexanediammonium ions **II-23** and **II-20**.[3] Tetracationic spermine **II-34** – which is an outstanding guest for CB[6][97] – binds very tightly to **II-19** ($K_a = 1.0 \pm 0.2 \times 10^8$ M^{-1}) which will enable the use of derivatives of **II-19** in a variety of application areas. Overall, the recognition properties of **II-19** closely parallels those known for unsubstituted CB[6].

Table II-1. Binding constants (K_a, M^{-1}) measured for the host-guest complexes of **II-19** and compared to literature values for CB[6][a].

Guest	Host **II-19**	CB[6][b]
II-11	$2.7 \pm 0.5 \times 10^3$	550 ± 30[c]
II-22	$4.9 \pm 1.2 \times 10^5$	1.5×10^5
II-23	$5.7 \pm 1.4 \times 10^6$	2.4×10^6
II-20	$1.4 \pm 0.3 \times 10^7$	2.8×10^6
II-24	$2.6 \pm 1.4 \times 10^6$	4.3×10^4
II-26	$4.7 \pm 1.0 \times 10^5$	n.d.[d]
II-30	852 ± 114	n.d.[d]
II-31	$3.0 \pm 0.6 \times 10^4$	2.1×10^4
II-32	$1.0 \pm 0.2 \times 10^8$	1.3×10^7

a) Conditions: 20 mM NaO_2CCD_3, buffer, D_2O, pD 4.74, RT. b) Taken from Mock and Shih[3]; c) Taken from Isaacs and co-workers.[17] d) n.d. = not determined.

2.5 Host II-19 as a Turn-On Fluorescence Sensor for Amines.

CB[n] containers have been used previously to construct a variety of sensing ensembles, most notably those prepared by Urbach and Nau that are used to sense the presence of peptides and even proteins.[91,52,132] All these assays are based on the indicator displacement assay[56] in which guest competes with chromophore or fluorophore for binding inside the CB[n] cavity. We envisioned that CB[6] derivative **II-19** with its covalently attached 2,3-dialkylnaphthalene fluorophore, its metal binding[133-135] ureidyl C=O portals, and its hydrophobic cavity[78] could form the basis for a new type of fluorescence based CB[n] sensing system. The concept is illustrated in Scheme II-4. Briefly, we anticipated that the 2,3-dialkylnaphthalene fluorophore of **II-19** would undergo fluorescence quenching in the presence of certain metal ions due to the heavy-metal effect and/or paramagnetic quenching induced by the binding of the metal ions at

the ureidyl C=O portals of **II-19**. Finally, we expected that addition of a competing guest that occupies the ureidyl C=O portals and the hydrophobic cavity of **II-19** would force the release of the metal ion and result in an increase in the fluorescence intensity that would signal the presence and concentration of competing guest.

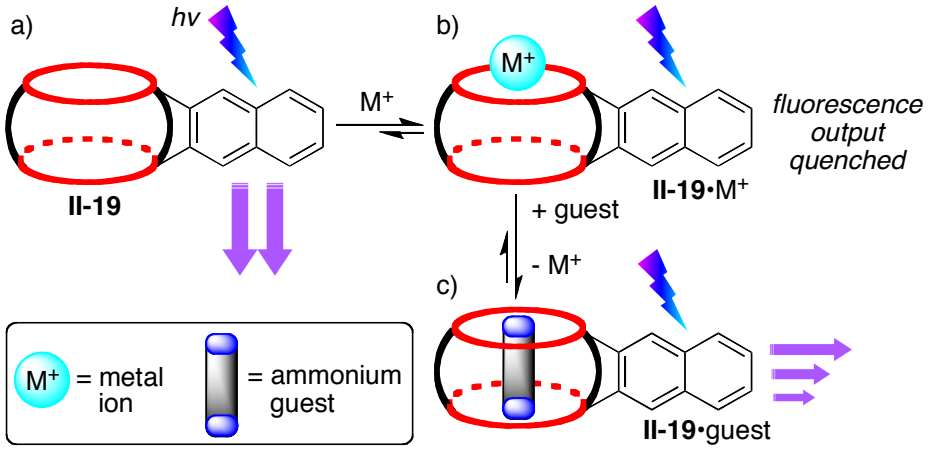

Scheme II-4. Concept of fluorescence assay based on flurescent CB[6]-derivative **II-19**. a) Host **II-19** is excited by UV light and emits fluorescence in response; b) In the prescence of a quenching metal ion the fluorescence is quenched due to an intra-complex resonance energy transfer from naphthalene to metal; c) the addition of a guest leads to displacement of the quenching metal ion.

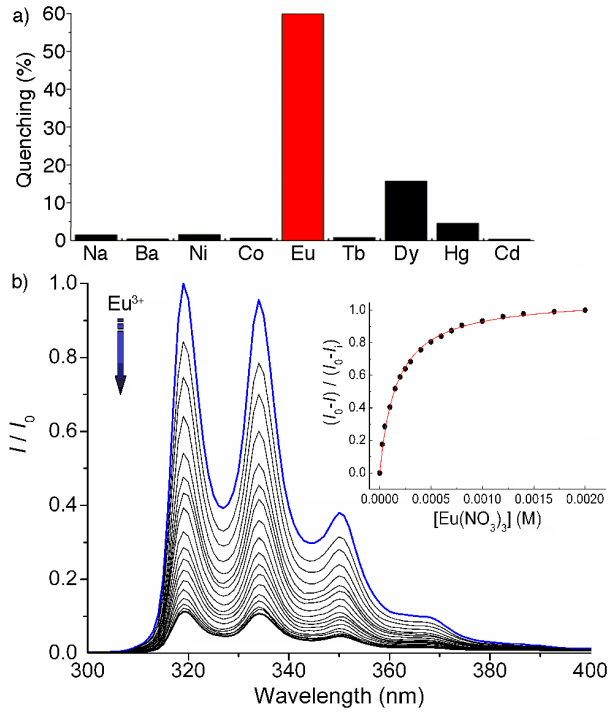

Figure II-9. a) Fluorescence quenching at 319 nm of **II-19** (3 μM) by various metal ions (300 μM). The measurements were carried out in water at pH 7, λ_{ex} = 266 nm. b) Fluorescence spectra of **II-19** (3 μM) upon the addition of an incremental amounts of Eu^{3+} in water at pH 7. λ_{ex} = 266 nm. Inset: Normalized titration isotherm corresponding to the Eu^{3+}-induced quenching process.

2.5.1 The Quencher.

First, we investigated the ability of a variety of metal ions to quench the fluorescence of **II-19**. Figure II-9a shows the percent quenching observed when **II-19** (3 mM) was treated individually with 300 mM of nine different metal ions. We chose these metal ions because they form stable hydrated ions at pH 7. Qualitatively it is easy to see that only Eu^{3+} and Dy^{3+} exhibit significant amounts of fluorescence quenching. We believe that Eu^{3+} coordinates to the ureidyl C=O portals of **II-19** and quenches the

naphthalene fluorescence by an intra-complex resonance energy transfer from naphthalene to Eu^{3+}. We selected Eu^{3+} which is able to quench approximately 60% of naphthalene fluorescence under these conditions for our further studies. First, we observed the changes in the fluorescence spectrum as a solution of **II-19** was titrated with Eu^{3+} (Figure II-9b). The inset to Figure II-9b shows the non-linear least squares best fit of the data to a standard 1:1 binding model with $K_a = 6.16 \times 10^3\ M^{-1}$. The magnitude of this K_a value dictates that we must use Eu^{3+} at concentrations at or above a concentration of $1/K_a$ ($1/6160\ M^{-1} = 162$ mM) for efficient quenching in the competition experiments described below.

2.5.2 Use of the Ensemble Comprising II-19 and Eu^{3+} to Sense II-20 and the Biogenic Amine Histamine (II-34).

We next decided to explore the use of the ensemble comprising **II-19** and Eu^{3+} as a chemical sensor that exhibits a turn-on fluorescence response. For this purpose, we selected **II-20** as a prototypical guest for CB[n] type receptors, and histamine **II-34** which is a biogenic amine that is involved in a variety of biological processes. For example, **II-34** triggers the inflammatory response, plays an important role in the immune response to pathogens, regulates physiological function in the gut, and acts as a neurotransmitter.[154] Figure II-10a shows the fluorescence spectra recorded for a mixture of **II-19** and Eu^{3+} upon titration with a solution of **2II-0**. As expected based on the design shown in Scheme II-4, we observe an increase in fluorescence intensity which is consistent with **II-20** acting as a competitor for Eu^{3+} binding toward **II-19** which results in the formation of **II-19•II-20**. The analysis of the fluorescence data is shown in the inset to Figure II-10a

which shows a breakpoint type-titration at 3 mM concentration which corresponds to the 1:1 **II-19•II-20** complex. Because the titration at this concentration of **II-19** (3 mM) consists of essentially two linear segments it is not possible to fit this curve to obtain a K_a value for the **II-19•II-20** complex under these conditions. Figure II-10b shows the fluorescence spectra obtained when a solution of **II-19** (3 mM) and Eu^{3+} (300 mM) was titrated with **II-34**. Similar to the observation for **II-20**, the fluorescence intensity increases as **II-34** competes with Eu^{3+} for binding to the ureidyl C=O portals of **II-19**. We feel that the observation of significant fluorescence recovery in the case of **II-34** – which is a monoammonium ion – is significant. Monoammonium **II-34** would be expected to occupy the hydrophobic cavity and one ureidyl C=O portal of **II-19** which might leave the other ureidyl C=O portal available for binding to Eu^{3+}. The observation of the significant fluorescence recovery means that ammonium ions with a sufficiently large alkyl or aryl residue is sufficient to sterically block the other ureidyl C=O portal from Eu^{3+} binding. The inset to Figure II-10b shows the best non-linear fitting of the fluorescence intensity as a function of [**II-34**] to a 1:1 binding model with $K_a = 1.66 \times 10^4$ M^{-1}. The present system responds to **II-34** in the 20–200 mM range, in accord with the measured K_a value for **II-19•II-34**. We expect that this system – based on the highly selective host **II-19** and its moderate affinity toward **II-34** – has significant potential for use in sensor development especially as a component of sensor arrays.

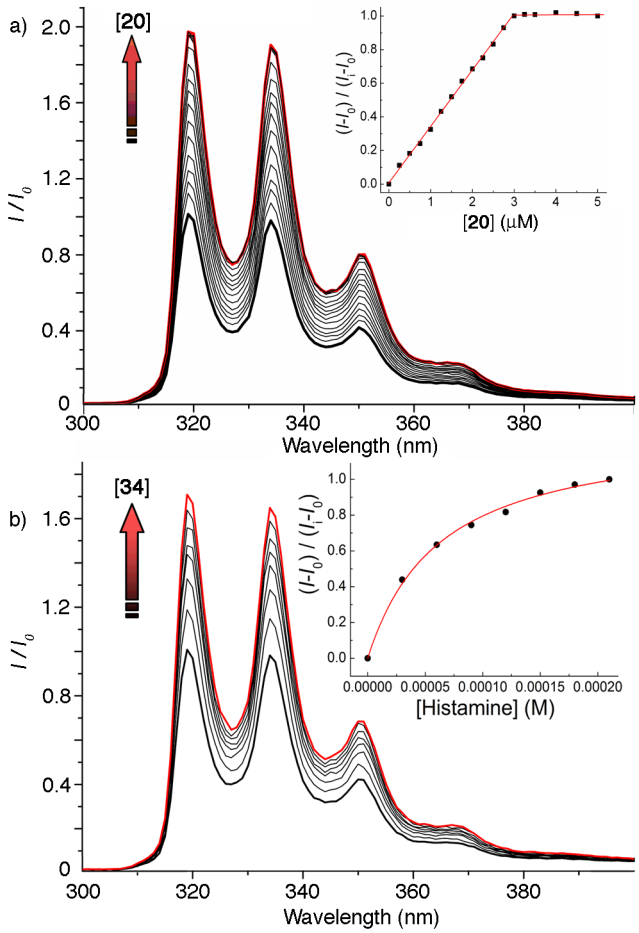

Figure II-10. Fluorescence spectra of **II-19** (3 μM) and Eu^{3+} (300 μM) in water (pH 7) upon addition of incremental amounts of: a) **II-20** and b) **II-34**. λ_{ex} = 266 nm. Insets: Normalized titration isotherm corresponding to the amine-induced fluorescence recovery.

2.6 Conclusions.

In summary, we have reported that the CB[n] forming reaction conducted between glycoluril (**1**) and less than two equivalents of formaldehyde in the presence of *p*-xylylenediammonium ion (**II-11**) as template have a reduced tendency to undergo irreversible formation of CB[n] products which enables the straighforward isolation of **6C** and bis-*ns*-CB[10] in multi-gram quantities. Template **II-11** influences the reaction

by both kinetic and thermodynamic means: 1) by thermodynamically stabilizing **6C** and bis-*ns*-CB[10] by host-guest binding, 2) by slowing down the rate of transformation of **6C** into CB[6], and 3) by causing precipitation of the **6C•II-11** complex. Hexamer **6C** can be transformed into monofunctionalized CB[6] derivatives **II-13**, **II-16**, **II-17**, and **II-19** in very good yields on gram scale without the need for chromatographic purification. Host **II-13** – but not **II-16**, **II-17**, or **II-19** – undergoes self-association processes which highlights the need to be vigilant in the molecular design of CB[6] derivatives for advanced applications. We studied the **II-19•**guest complexes by ^{1}H NMR methods and observed that the recognition properties of **II-19** are comparable to that of CB[6] in terms of slow exchange kinetics on the NMR time scale and values of K_a. Finally, we demonstrated that **II-19** – with its covalently attached naphthalene chromophore and its ureidyl C=O portals and hydrophobic cavity binding sites – undergoes fluorescence quenching in the presence of Eu^{3+} which forms the basis for fluorescence turn-on assays for suitable CB[n] guests like **II-20** and histamine **II-34**.

We believe the results of this paper have implications that will strongly impact the future development of the synthesis and applications of functionalized CB[n] molecular containers. First, the ready availability of **6C** on gram scale and its high yielding transformation into monofunctionalized CB[6] derivatives will allow their incorporation into more complex solution or surface bound architectures for advanced technological or biomimetic applications. Second, the demonstration that both the CB[n] forming reaction and the macrocyclization of glycoluril oligomer **6C** with phthalaldehydes is subject to template effects delivers an unprecedented level of control over the formation of CB[n]

type receptors. For example, it is straightforward to predict that the use of larger templates might deliver the currently unknown glycoluril heptamer **7C** and octamer **8C** as building blocks for CB[7] or CB[8] derivatives and that chiral templates may lead to chiral and enantiomerically pure CB[n] type receptors for chiral recognition. Third, the demonstration of **II-11** and derivatives as a diagnostic probe for ^{1}H NMR monitoring of CB[n] type reactions promises to impact all synthetic studies in the CB[n] area. Finally, the ability to prepare monofunctionalized CB[n] derivatives tailor-made with reactive functional groups (e.g. NO_2, CO_2H) or synergistic structural elements (e.g. fluorophores) has the potential to enlarge the utility of CB[n] type receptors as components of more complex systems including sensor arrays and for fluorescence imaging applications.

III. Chapter 3: Recognition Properties of Acyclic Glycoluril Oligomers.[123]

3.1 Introduction.

Cucurbit[n]uril molecular containers are prepared by the condensation of glycoluril (**1**) with formaldehyde (**III-2**) under acidic conditions.[2,12,20] Interest in the cucurbit[n]uril (CB[n]) family of molecular containers[13,23,78] has surged in recent years due to the availability of a homologous series (n = 5, 6, 7, 8, 10) of hosts that display high affinity and high selectivity toward cationic guests in aqueous solution.[3,17,76,136] These high affinity and high selectivity CB[n]•guest interactions have been used to create a number of functional CB[n] systems including molecular machines,[79,137,138] biomimetic systems,[42,48,51,132,139] supramolecular catalysts,[105-109,140-142] sensing ensembles,[53-55,143] stimuli responsive polymers,[144-147] and drug delivery systems.[33,44,45,148,149] Our research group has developed an in-depth knowledge of the mechanism of CB[n] formation[10,11,24,117,119] and used these insights to prepare macrocyclic CB[n] type receptors lacking one or more bridging CH_2-groups known as nor-seco-CB[n] which display interesting recognition properties such as size dependent homotropic allostery, chiral recognition, and control over guest folding.[25,26,50,73] In this paper we continue this line of inquiry by comparing and contrasting the recognition properties of acyclic glycoluril oligomers **III-4-6C** (Figure III-1) with those of their macrocyclic counterparts CB[6] and CB[7]. We delineate some key factors governing the recognition properties of CB[n]-type receptors (e.g., preorganization and macrocyclic effect).

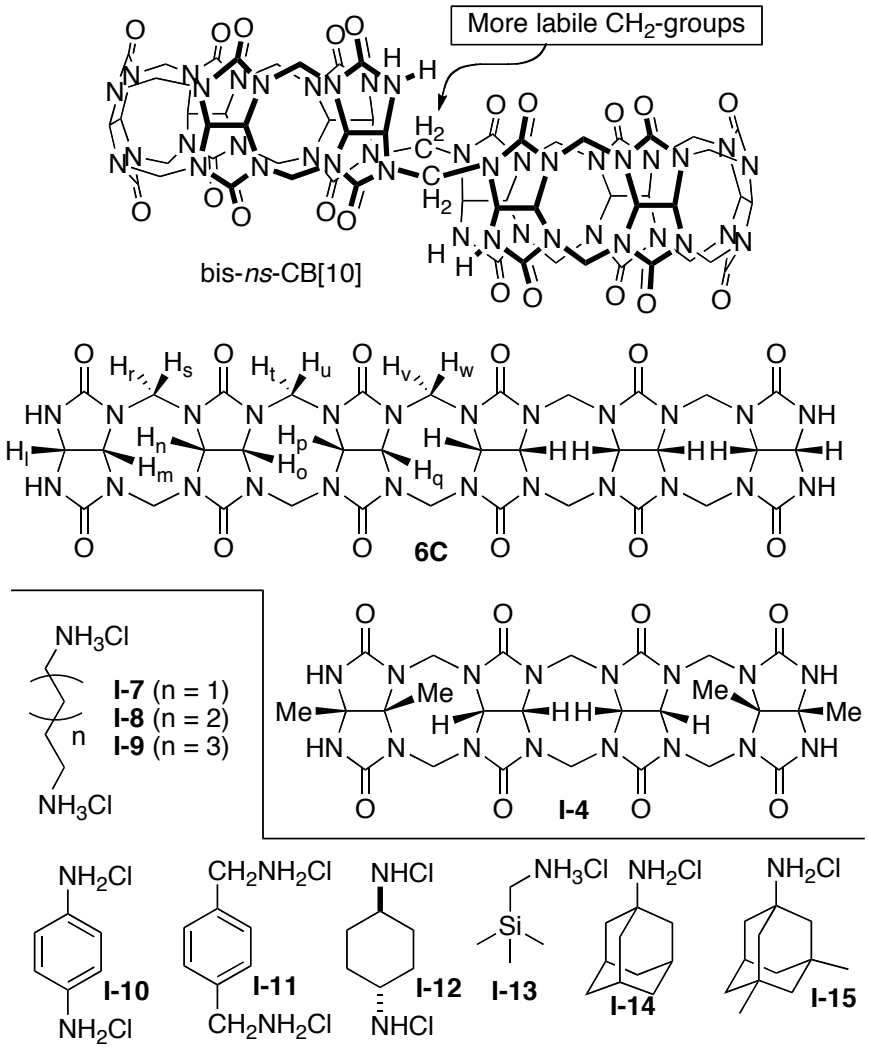

Figure III-1. Hosts and guests used in this study.

3.2 Synthesis of Glycoluril Pentamer 5C.

We have previously reported the synthesis of methylene bridged glycoluril pentamer **5C** and hexamer **6C** and their purification by time-consuming DOWEX ion-exchange chromatography.[11] In order to streamline the synthesis and purification of **5C** we considered the use of bis-*ns*-CB[10] as a readily available starting material (Figure III-1).[26] Bis-*ns*-CB[10] is a macrocycle composed of 10 glycoluril rings and 18 CH_2-

bridges whose connectivity features two glycoluril pentamer fragments connected by a single CH_2-bridge. We envisioned that these single CH_2-bridges would be more susceptible to cleavage than the remaining double CH_2-bridges. In practice, we found that heating bis-*ns*-CB[10] with 3,5-dimethylphenol (**III-3**) as a formaldehyde scavenger at 50 °C in HCl delivers **5C** in 81% yield (Scheme III-1). Next, we decided to investigate the recognition properties of **5C** and **6C** toward cationic guests in aqueous solution.

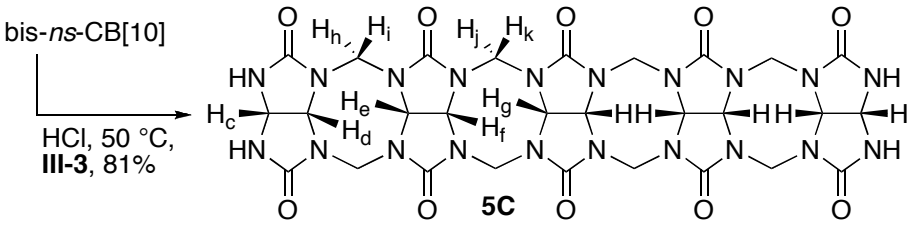

Scheme III-1. Synthesis of glycoluril pentamer **5C**.

3.3 Recognition Properties of Acyclic Glycoluril Oligomers.

Before studying the recognition properties of any new host it is wise to perform dilution experiments to determine whether the host undergoes self-association. We performed ^{1}H NMR dilution experiments for **5C** (maximum solubility = 1 to 0.1 mM) and **6C** (maximum solubility = 2.57 to 0.1 mM) and did not observe any changes in chemical shift that would be indicative of self-association (Supporting Information). Therefore, we decided to investigate the binding of **5C** and **6C** toward guests **III-7** to **III-15** which are typical guests for CB[n]-type receptors by ^{1}H NMR spectroscopy (Supporting Information). All guests show upfield shifts in their NMR spectra upon binding which indicates guest binding within the cavity of hosts **5C** and **6C** as expected. In contrast to what is commonly observed with CB[n] hosts, only a few of the guests investigated

displayed slow kinetics of guest exchange (Host **5C**: **III-11**; Host **6C**: **III-11**, **III-9**, **III-12**) on the chemical shift time scale.[3,17] For illustration, Figure III-2 shows the ^{1}H NMR spectra recorded for mixtures of host **5C** or host **6C** in the presence of 1 or 2 equiv of guest **III-11**. Overall, these studies suggest that **5C** and **6C** retain the essential binding features typical of the CB[n] family but do so with faster kinetics of exchange. Because **5C** and **6C** are acyclic they should not display the constrictive binding generally observed for CB[n] hosts[18,150] which decreases the association and dissociation rate constants due to steric effects in the transition state. This is an essential difference between the recognition behavior of **5C** and **6C** relative to CB[n].

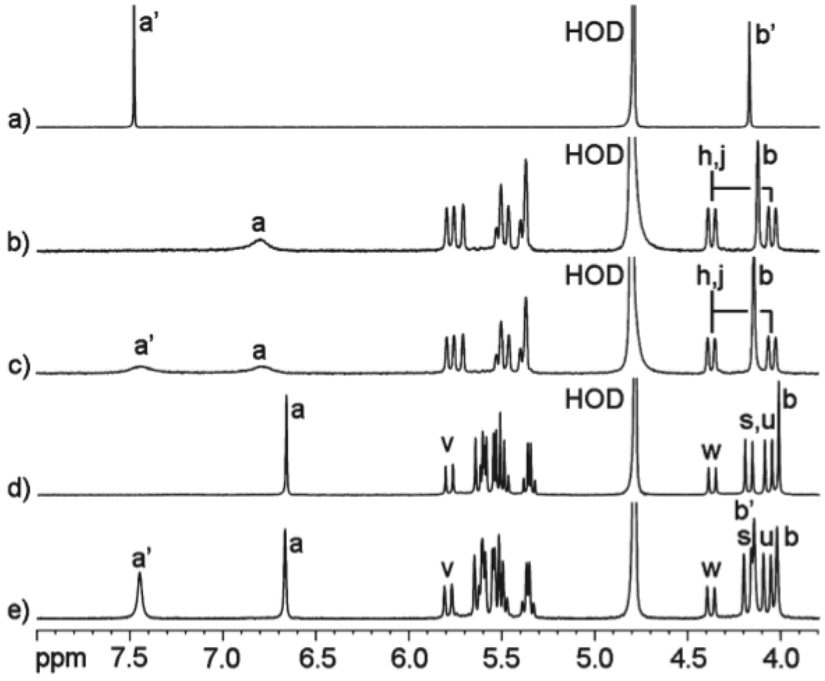

Figure III-2. ^{1}H NMR spectra recorded (D2O, 400 MHz, RT) for (a) **III-11** (1 mM), (b) a mixture of **5C** (1 mM) and **III-11** (1 mM), (c) a mixture of **5C** (1 mM) and **III-11** (2 mM), (d) a mixture of **6C** (1 mM) and **III-11** (1 mM), and (e) a mixture of **6C** (1 mM) and **III-11** (2 mM).

Table III-1. Binding Constants (K_a, M^{-1}) Measured for Host•Guest Complexes between Hosts **III-4**, **5C**, **6C**, CB[6], and CB[7] and Guests **III-7** to **III-15**.

Guest	**Host III-4**[a]	**Host 5C**	**Host 6C**
III-7	-	$(4.7 \pm 0.5) \times 10^4$	$(5.0 \pm 0.3) \times 10^4$
III-8	-	$(1.4 \pm 0.1) \times 10^5$	$(1.6 \pm 0.3) \times 10^6$
III-9	$(5.6 \pm 0.4) \times 10^3$	$(1.0 \pm 0.2) \times 10^6$	$(2.2 \pm 0.4) \times 10^6$
III-10	-	$(1.0 \pm 0.1) \times 10^4$	$(4.9 \pm 0.6) \times 10^4$
III-11	$(1.5 \pm 0.1) \times 10^4$	$(1.2 \pm 0.1) \times 10^6$	$(2.2 \pm 0.4) \times 10^7$
III-12	-	$(2.7 \pm 0.4) \times 10^4$	$(6.8 \pm 1.4) \times 10^5$
III-13	-	nb[e]	$(2.6 \pm 0.3) \times 10^4$
III-14	-	$(1.1 \pm 0.2) \times 10^6$	$(1.8 \pm 0.4) \times 10^7$
III-15	-	$(6.1 \pm 0.9) \times 10^5$	$(6.0 \pm 1.3) \times 10^6$
Guest	**Host CB[6]**	**Host CB[7]**	
III-7	$(2.0 \pm 0.2) \times 10^7$ [c]	-	
III-8	$(1.5 \pm 0.1) \times 10^8$ [c]	-	
III-9	$(4.5 \pm 0.8) \times 10^8$ [b] $(2.9 \pm 0.2) \times 10^8$ [c]	$(9.0 \pm 1.4) \times 10^7$ [b]	
III-10	$(1.9 \pm 0.1) \times 10^3$ [b]	$(2.1 \pm 0.3) \times 10^6$ [b]	
III-11	550 ± 30[b]	$(1.8 \pm 0.3) \times 10^9$ [b]	
III-12	1.4×10^4 [d]	$(2.3 \pm 0.4) \times 10^7$ [b]	
III-13	nb	$(8.9 \pm 1.4) \times 10^8$ [b]	
III-14	-	$(4.2 \pm 1.0) \times 10^{12}$ [b]	
III-15	-	$(2.5 \pm 0.4) \times 10^4$ [b]	

a) K_a values taken from ref 70. b) K_a values taken from ref 17. c) K_a values taken from ref 136. d) K_a values taken from ref 18. e) nb = no binding.

We next decided to measure the binding constants for **5C** and **6C** toward guests **III-7** to **III-15**. For this purpose we first performed the direct ^{1}H NMR titration of *p*-phenylenediammonium ion **III-10** with **5C** and of trimethylsilylmethylammonium ion **III-13** with **6C** (Table III-1; Supporting Information). For example, Figure III-3a shows a plot of chemical shift of H_a of guest **III-10** as a function of [**5C**] and the best fit of the data to a 1:1 binding model with $K_a = (1.0 \pm 0.1) \times 10^4\ M^{-1}$.

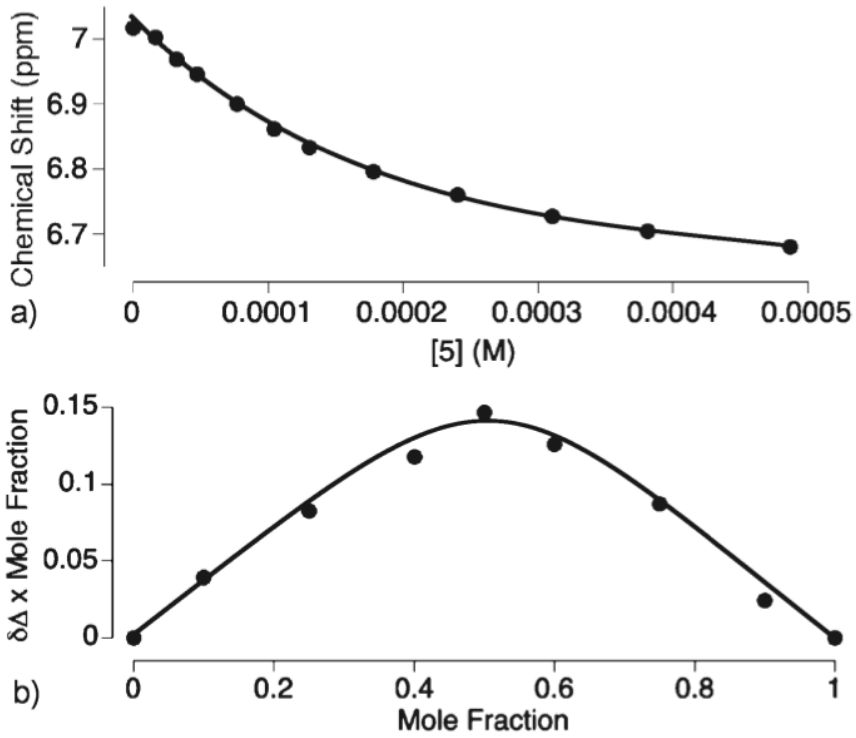

Figure III-3. (a) A plot of chemical shift of **III-10** obtained in the direct NMR titration (298 K, 20 mM NaO_2CCD_3, pD 4.74) with 5 (0-487 μM) and (b) Job plot for **5C•III-10** ([**5C**] + [**III-10**] = 0.5 mM).

Figure III-3b shows a Job plot prepared for mixtures of **5C** and **III-10** ([**5C**] + [**III-10**] = 0.5 mM) which confirms the 1:1 nature of the **5C•III-10** complex. Next, we

performed ^{1}H NMR competition experiments between **5C•III-10** and guests **III-7**, **III-8**, and **III-12** and between **6C•III-13** and guests **III-7** and **III-10** by monitoring the chemical shift of guests **III-10** (for **5C•III-10**) and **III-13** (for **6C•III-13**) which undergo fast exchange on the chemical shift time scale and fit the data to a standard competitive binding model (Supporting Information) to determine K_a values (Table III-1). To determine the remaining values of K_a we performed ^{1}H NMR competition experiments between **5C•III-11** (or **6C•III-11**) and guests by monitoring the integrals for the free and binding guest **III-11** which exhibits slow exchange on the chemical shift time scale (Table III-1). Table III-1 also presents the K_a values measured previously for hosts **III-4**, CB[6], and CB[7] for purposes of comparison.

The binding constant data presented in Table III-1 allows us to tease out some features of the recognition behavior across the series of glycoluril oligomers to macrocyclic CB[n]. First, consider the binding constants of guests **III-9** and **III-11** toward oligomers **III-4** to **6C** of increasing length. Progression from **III-4** to **5C** results in an ~100-fold increase in K_a whereas the lengthening to **6C** results in more modest increases (2−18-fold) in K_a. We believe these differences reflect the fact that tetramer **III-4** is a clip-like receptor whereas **5C** and **6C**, by virtue of the additional glycolurils, possess a more well-defined hydrophobic cavity. The smaller increases in K_a from **5C** to **6C** reflect the increase in the hydrophobic surface area and volume of the cavity of the oligomer and also the more fully formed electrostatically negative ureidyl C=O portals which may provide increased ion−dipole interaction driving force for complexation. Second, we can compare the binding constants of **6C** and its macrocyclic counterpart

CB[6] to gauge the influence of cyclization on binding strength and selectivity. For example, **III-9** binds to **6C** 205-fold less tightly than to CB[6]; similar trends hold for **III-8** (94-fold) and **III-7** (400-fold). For guests that do not exceed the capacity of CB[6] (e.g., **III-7** to **III-9**) macrocyclization of **6C** results in an ~100-fold increase in affinity probably due to increased preorganization, higher energy solvating H_2O molecules inside CB[6], and increased negative electrostatic potential at the C=O portals. For guests like **III-11** (**III-10**) that are slightly too large to fit comfortably inside CB[6], a 40 000-fold (26-fold) decrease in K_a is observed. For even larger guests **III-12** to **III-14** the more appropriate comparison is between hosts **6C** and CB[7]. In these cases the CB[7]•guest complexes are more stable by 34-fold to 3.4×10^5-fold which reflects both the presence of an additional glycoluril unit and macrocyclization. The high selectivity[3,17] observed for macrocyclic CB[n] is due in part to the relative rigidity of the host which disfavors inappro- priately sized or shaped guests. Third, for both **5C** and **6C**, adamantane derivatives **III-14** and **III-15** are among the guests with the highest K_a values. This is surprising for two main reasons: (a) guests **III-14** and **III-15** are too large to form inclusion complexes with CB[5] or CB[6], and (b) guests **III-14** and **III-15** are monoammonium ions whereas the tightest binding guest for **5C** and **6C** is **III-11** which is a diammonium ion. It is known from CB[n] binding studies that an additional NH_3^+ group increases the binding affinity by factors of 10^1-10^5.[78] Figure III-4 shows MMFF minimized models of **6C•III-9**, **6C•III-12**, and **6C•III-14**. As the guest gets larger the glycoluril oligomer backbones of **5C** and **6C** are able to undergo conformational changes (e.g., flex like a hand) to accommodate larger guests (e.g., **III-14** and **III-15**).[26,70,151] The fact that guest **III-15**, which is slightly too large for CB[7], binds better to **6C** suggests

that **6C** is able to expand its cavity size beyond that of CB[7] toward CB[8]. We believe that the excellent size and shape match of hydrophobic adamantane derivatives documented for CB[7] plays an important role in the strong binding affinity of **III-14** and **III-15** toward **5C** and **6C**.[17,78,152]

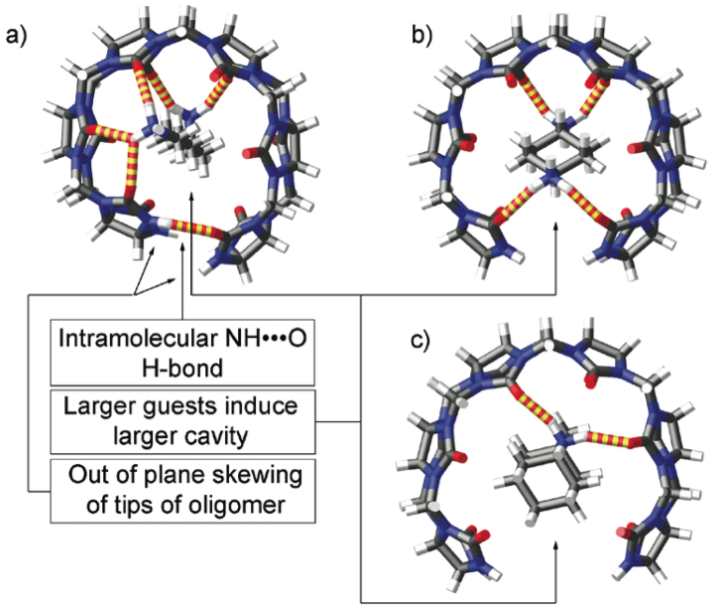

Figure III-4. MMFF94s minimized models of (a) **6C•III-9**, (b) **6C•III-12**, and (c) **6C•III-14**. Color code: C, gray; H, white; N, blue; O, red; H-bonds, red-yellow striped.

3.4 Summary and Conclusions.

In summary, we have reported a directed synthesis of glycoluril pentamer **5C** by the fragmentation reaction of bis-*ns*-CB[10] under acidic conditions in the presence of **III-3** as a formaldehyde scavenging reagent. The recognition properties of pentamer **5C** and hexamer **6C** toward a series of ammonium ions (**III-7** to **III-15**) in water were investigated. Acyclic glycoluril oligomers **5C** and **6C** preserve the ability of the CB[n] family to bind to cationic species in water but do so with lower affinity, lower selectivity,

and faster kinetics of exchange than their macrocyclic counterparts. Particularly interesting trends in binding affinity are seen: (a) across the tetramer **III-4**-hexamer **6C** series where an increasing number of glycolurils increases binding affinity by ~10^3 overall; (b) between K_a values of hexamer **6C** or CB[6] toward a common guest (e.g., **III-7** to **III-9**) where macrocyclization increases affinity by ~100-fold; and (c) for K_a values of adamantane derivatives **III-14** and **III-15** toward **5C** or **6C** where high affinity is observed and attributed to the hydrophobicity of the adamantane group and the good shape match with the cavity of **5C** and **6C**. We believe the work described here has broader significance. Because **5C** and **6C** are acyclic, are structurally responsive to guest size, and preserve many of the binding properties of CB[n] but do so with faster kinetics of exchange, they may be particularly well suited for certain classes of applications. For example, we envision that acyclic CB[n]-type hosts would be useful for the preparation of stimuli responsive molecular machines with fast response times, for the derivatization of polymeric materials by direct clipping onto linear polymer backbones, and as a component of sensor arrays with broad analyte affinity for chemically and biologically important amines. As such we believe that acyclic glycoluril oligomers promise to enrich the scope of CB[n] supramolecular chemistry.

IV. Chapter 4: Summary and Future Work.

5.1 Summary.

In summary, the ongoing development of the CB[n] field has expanded their use in drug delivery, biomimetic system, molecular sensor, and applications based on covalent attachment to solid surfaces (e.g. chromatography, sensors). The search for improved synthetic pathways toward CB[n] and their derivatives has lead our group to perform a thorough investigation of their mechanism of formation and the isolation of glycoluril oligomers **2C**-**6C**. Chapter 2 describes the synthesis of **6C** on the gram scale using a *p*-xylylenediamine template in a one step reaction. The access to large quantities of **6C** in allowed for its use as a building block in the synthesis of monofunctionalized CB[6] derivatives **II-13**, **II-16**, **II-17**, **II-19**, and (±)-**II-21** which show similar binding properties as CB[6]. Futhermore, the use of alkaneammonium guests strongly influenced the ring closures of **6C** to form CB[6] and CB[6] derivatives. The fluorescence exhibited by host **II-19** allowed for the detection of ammonium guests through the binding and displacement of an ionic quencher, Eu^{3+}. Chapter 3 describes the synthesis of oligomer **5C** via the 3,5-dimethylphenol induced fragmentation of bis-*ns*-CB[10] under acid conditions. The acyclic structure **5C** and **6C** allowed for guest dependent flexibility demonstrated by the high binding affinities for larger guests such as adamantaneamine hydrochloride and dimethyladamantaneamine hydrochloride.

5.2 Future Work.

The templated synthesis of **6C** and its use to create monofunctionalized derivatives will have a broad impact on the accessibility of new CB[6] derivatives. Preliminary evidence for the conversion of carboxylic acid CB[6] derivative **II-16** into the methyl ester **IV-1** (Scheme IV-1a) may allow **IV-1** to undergo nucleophilic attack by hydrazine (Scheme IV-2). The isolation of hydrazide derivative **IV-4** provides a useful functional scaffold that will undergo hydrozone forming reactions with aldehydes to deliver CB[6] acyl hydrazide derivatives. For example, as shown in Scheme IV-2, a reaction between **IV-4** and dimethylaminobenzaldehyde (**IV-5**) may deliver azo-dye **IV-4a** which should emit a bright yellow color. Alternatively, a fluorophore could be directly attached to the CB[6] by using chromosome red (**IV-6**) to give **IV-4b** which could be useful for fluorescene imaging. Preliminary evidence also suggests that a reaction between **6C** and anthracenedialdehyde **IV-2**[128] can deliver anthracene functionalized CB[6] **IV-3**. CB[n] hosts with covalently attached fluorophores show promise as chemical sensors and for detection during intracellular transport in biological applications .

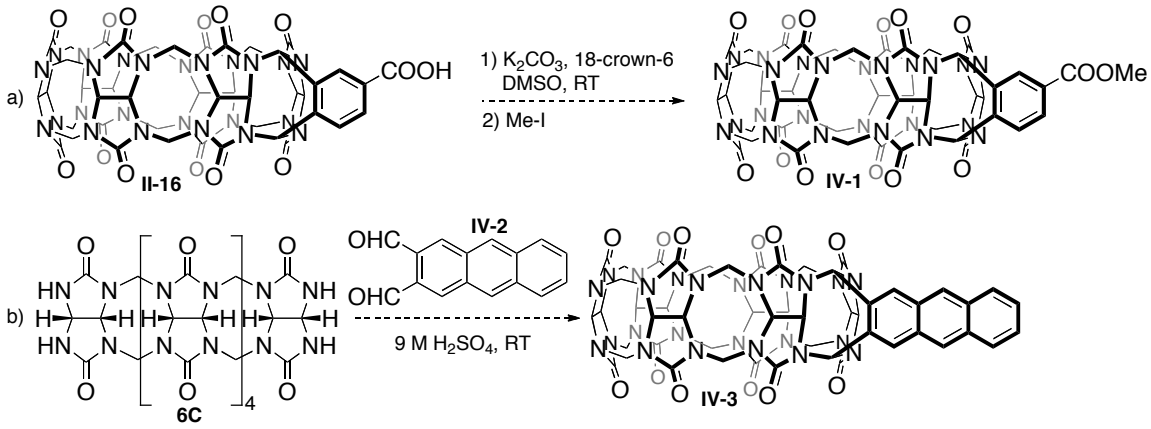

Scheme IV-1. Preliminary evidence for CB[6] derivatives **IV-1** and **IV-3**.

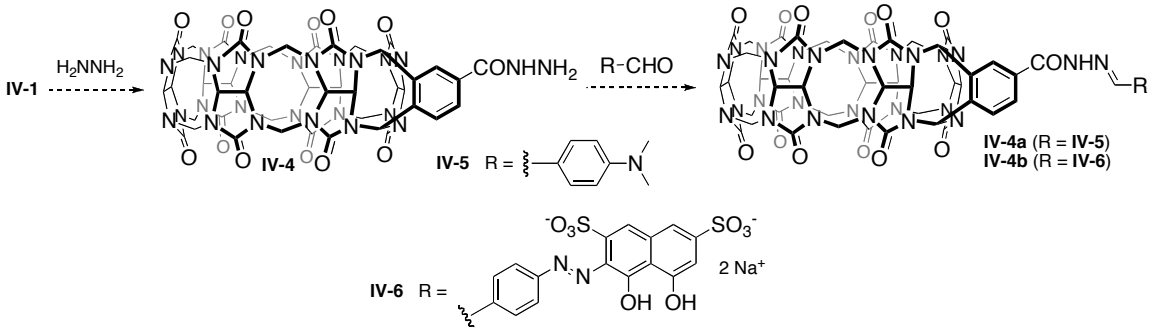

Scheme IV-2. Synthesis of hydrazide derivative **IV-4** and its reactions with aldehydes to give acyl hydrazides derivatives.

The placement of single reactive groups on CB[n] will provide access to a number of potential applications by limiting the attachment to one molecule of interest (Scheme IV-3). The covalent attachment of fluorophores will serve in fluorescence imaging during intracellular transport in drug delivery appications or other specialized sensor assays. Targeting ligands will also be attached providing targeted transport of the container while leaving the cavity available for non-covalent interactions with drugs and other molecules of interest. Supramolecular polymers will be attainable through the

attachment of alkaneammonium groups thereby creating the potential for the self-assembly of supramolecular oligomers and discrete complexes. Furthermore, the attachment of CB[n] to solid surfaces may provide access to advanced technological or biomimetic applications.

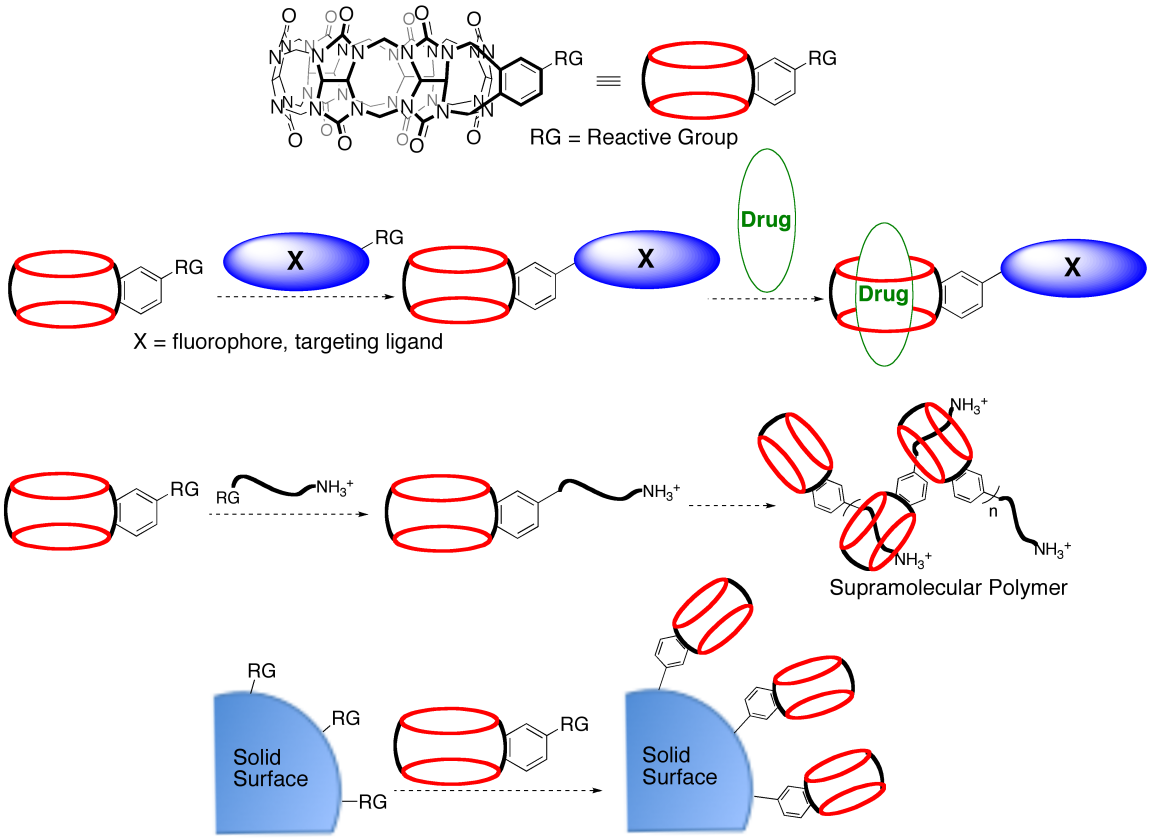

Scheme IV-3. Future applications of monofunctionalized CB[n].

Appendices

Templated Synthesis of Glycoluril Hexamer and Monofunctionalized Cucurbit[6]uril Derivatives

Supporting Information

by Derick Lucas,[†] Tsuyoshi Minami,[‡] Greg Iannuzzi,[†] Liping Cao,[†] James B. Wittenberg,[†] Pavel Anzenbacher, Jr.,[,‡] and Lyle Isaacs*[,†]*

[†]Department of Chemistry and Biochemistry, University of Maryland, College Park, MD 20742 and [‡]Department of Chemistry and Center for Photochemical Sciences, Bowling Green State University, Bowling Green, OH, 43403

Table of Contents **Pages**

General Experimental Details. Starting materials were purchased from commercial suppliers were used without further purification. Compounds **II-14**, **II-15**, and **II-18** were prepared according to the literature procedures.[126,127,128] Melting points were measured on a Meltemp apparatus in open capillary tubes and are uncorrected. TLC analysis was performed using pre-coated plastic plates from Merck. IR spectra were recorded on a JASCO FT/IR 4100 spectrometer and are reported in cm^{-1}. NMR spectra were measured on a spectrometers operating at 400, 500, or 600 MHz for ^{1}H and 100, 125, and 150 MHz for ^{13}C NMR spectra. Mass spectrometry was performed using a JEOL AccuTOF electrospray instrument (ESI). Absorption spectra were recorded using a Hitachi U-3010 spectrophotometer. Fluorescence measurements were performed on a single photon counting spectrofluorimeter from Edinburgh Analytical Instruments (FL/FS 920). Optically dilute solutions used for all photophysical experiments were prepared using nanopure water in quartz cuvettes. For titration experiments the samples were excited at the isosbestic point of the lowest energy. Solutions of **II-19** were excited at 266 nm. Fluorescence emission spectra were recorded between 300 and 400 nm. Titration isotherms were constructed from changes in the fluorescence maximum at 319 nm. Data analysis and curve fitting was performed according to previously published methods.[153]

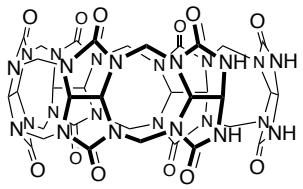

Synthetic Procedures and Characterization Data

***Compound* 6C.** A mixture of **1** (7.100 g, 49.96 mmol), paraformaldehyde (2.500 g, 83.43 mmol), and *p*-xylylenediamine (0.680 g, 4.996 mmol) was added to a 25 mL round bottom flask equipped with a stir bar. The solids were mixed by shaking the flask by hand for 2

minutes. Concentrated HCl (10 mL) was quickly added to the powdered mixture. The vial was capped with a SubaSeal 14/20 septum and then vigorously shaken for 30 seconds to expose all reagents to solvent. The septum was then securely attached using a copper wire. The slurry was then heated at 58 °C for 3-5 d, at which point an off-white precipitate was generally observed. The heterogenous reaction mixture was poured into a centrifuge tube and centrifuged at 7600 rpm for 5 min at RT. The clear yellow supernatant was decanted and set aside. The crude solid was then dried in the centrifuge tube under high vacuum for 24 h (1.213 g, 1.092 mmol). The estimated purity of the crude **6C•11** complex was determined by ^{1}H NMR. Integration of the **6C•II-11** Ar-H hydrogens of **II-11** at 6.71 ppm (s, 4H) versus that of the methylene/methine C-H hydrogens of **6C** between 3.95-4.45 ppm (m, 10H) and 5.35-5.85 ppm (m, 22H) allowed us to calculate that **6C•II-11** comprised 89% of the crude solid. ^{1}H NMR (400 MHz, D_2O): 6.71 (s, 4H), 5.82 (d, J = 15.6, 2H), 5.70-5.50 (m, 16H), 5.41 (d, J = 8.8, 2H), 5.38 (d, J = 8.8, 2H), 4.41 (d, J = 15.6, 2H), 4.22 (d, J = 15.6, 4H), 4.12 (d, J = 15.6, 4H), 3.99 (s, 4H). The crude **6C•II-11** complex (1.213 g, 1.092 mmol) was mixed with H_2O (17 mL). The heterogeneous mixture was then sonicated in a 50 mL centrifuge tube for 10 min and was allowed to cool to RT. The resulting white, heterogenous mixture was centrifuged at 7200 rpm for 10 min and the supernatant was decanted into another, pre-weighed centrifuge tube. A solution of 5 M aq. NaOH (1.65 mL, 8.22 mmol) was added to the supernatant which resulted in the precipitation of a white solid. The white, heterogenous mixture was then sonicated for 30 min and was allowed to cool to RT before centrifuging at 7200 rpm for 10 min. The supernatant was decanted and the white precipitate (**6C**) was washed with a solution of 0.1 M NaOH in MeOH (40 mL) followed

by centrifugation at 7200 rpm for 5 min. Finally, the supernatant was decanted and the precipitate was washed with MeOH (40 mL) followed by centrifugation at 7200 rpm for 5 min. After the supernatant was decanted and set aside, the precipitate was dried under high vacuum to give **6C** as a white powder (0.901 g, 0.926 mmol, 10% yield). M.p. > 300 ˚C. ^{1}H NMR (400 MHz, D_2O): 5.82 (d, J = 15.6, 2H), 5.70-5.50 (m, 16H), 5.41 (d, J = 8.8, 2H), 5.38 (d, J = 8.8, 2H), 4.41 (d, J = 15.6, 2H), 4.22 (d, J = 15.6, 4H), 4.12 (d, J = 15.6, 4H). The ^{1}H NMR data matches that reported in the literature.[11,26]

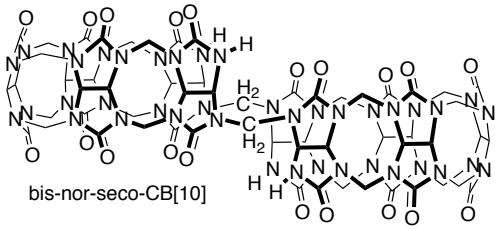

Bis-nor-seco-CB[10]. Glycoluril (400 g, 2.81 mol), paraformaldehyde prills (141 g, 4.69 mol), and *p*-xylenediamine (38.3 g, 0.281 mol) were mixed together in a 2.5 L reaction vessel equipped with an airtight cap. Conc. HCl (702 mL) was added quickly to the mixture and shaken vigorously to obtain a consistent mixture then sealed with the cap. The mixture was heated at 50 °C for 7 d. After the reaction cooled to RT it was slowly poured into MeOH (5 L) to precipitate the crude mixture and stirred overnight then collected by filtration and dried at high vacuum. ^{1}H NMR analysis of the crude material using **II-11** as probe allowed us to estimate the crude content as approximately 11% bis-nor-seco-CB[10], 6% **6C**, 5% *ns*-CB[6], and 13% CB[6]. The crude solid (630 g) was stirred with H_2O (6 L) overnight, the remaining solid was isolated by filtration and dried at high vacuum. The remaining solid (170 g) was then washed in 0.1 M NaOH soln. in MeOH (2 × 1.7 L) to remove *p*-xylenediamine from the host, then filtered and dried under high vacuum. A final H_2O wash (1 L) was carried out on the solid (164 g) leaving 121 g of

crude material after filtration and drying at high vacuum. Final purification was accomplished by recrystallization from 5 M HCl (360 mL) to leave bis-nor-seco-CB[10] as a white solid (32.6 g, 0.020 mol, 7%). The spectroscopic data matches the literature.[5]

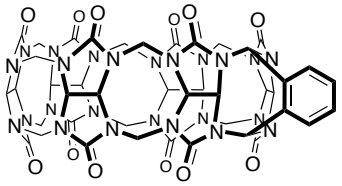

***Compound* II-*13*.** A mixture of **6C** (1.000 g, 1.028 mmol) and **12** (0.152 g, 1.131 mmol) was treated with aq. 9 M H_2SO_4 (10 mL) and stirred at RT for 36 h. The reaction solution was slowly poured into a vigorously stirred solution of MeOH (100 mL) which resulted in a white precipitate. After 30 min, the slurry was centrifuged at 7200 rpm for 5 min. The supernatant was decanted and the precipitate was dried under high vacuum to give an off-white crude solid (1.078 g). The crude solid was then stirred in water (50 mL) for 30 min. The resulting slurry was poured into a centrifuge tube and centrifuged at 7200 rpm for 5 min. The supernatant was decanted into a round bottom flask and the precipitate was discarded. Solvent was removed from the supernatant by rotary evaporation resulting in a yellow solid that was dried under high vacuum. The yellow solid was then washed with MeOH (40 mL) and centrifuged at 7200 rpm for 5 min. The supernatant was decanted and the precipitate was dried under high vacuum to give compound **II-13** as a white powder (0.792 g, 0.740 mmol, 72%). M.p. > 300 °C. IR (ATR, cm^{-1}): 1710s, 1457m, 1231m, 1182s, 961m, 792m, 756m. ^{1}H NMR (400 MHz, D_2O, >1 equiv. **II-11**): 7.74 (m, 4H), 7.50 (s, unbound **II-11**), 6.89 (s, 2H), 6.55 (s, 4H), 5.92 (d, J = 16.0, 2H), 5.80-5.59 (m, 12H), 5.30 (d, J = 8.8, 2H), 5.21 (d, J = 8.8, 2H), 5.12 (d, J = 9.6, 2H), 4.93 (d, J = 9.6, 2H), 4.58 (d, J = 16.0, 2H), 4.43 (s, 4H), 4.18 (s, unbound **II-11**), 4.17 (d, J = 15.6, 4H), 4.00 (d, J = 15.2, 4H). ^{13}C NMR (100 MHz,

D_2O, dioxane as internal reference, 1 equiv. **II-11**): δ 156.9, 156.4, 155.7, 132.9, 132.1, 130.8, 129.9, 123.9, 71.6, 70.7, 70.0, 69.8, 65.6, 64.5, 53.1, 51.5, 50.9, 41.6 (only 18 of the 19 resonances expected were observed). ESI-MS: *m/z* 604.2 ([**II-13•II-11**]$^{2+}$, $C_{42}H_{38}N_{24}O_{12}$•$C_8H_{14}N_2^{2+}$, calcd. 604.21)

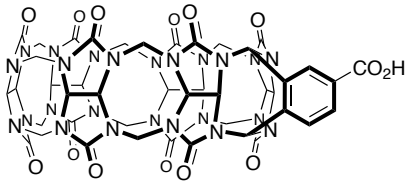

Compound* II-*16. A mixture of **6C** (1.000 g, 1.028 mmol) and **II-14**[126] (0.201 g, 1.131 mmol) was treated with aq. 9 M H_2SO_4 (10 mL) and mixed at RT for 48 h. The reaction solution was slowly poured into a vigorously stirred solution of MeOH (100 mL) which resulted in a white precipitate. After mixing for 30 min., the slurry was centrifuged at 7200 rpm for 5 min. The supernatant was decanted and the precipitate was dried under high vacuum to give a crude brown solid (1.105 g). The crude solid was dissolved in a solution of 88% formic acid/0.8 M HCl (1:1, v:v) (2 mL). The solution containing the crude solid was loaded onto a column (4 cm diameter) containing 20 cm Dowex 50WX2 ion-exchange resin pretreated with 88% formic acid/0.8 M HCl (1:1, v:v). The column was eluted with 88% formic acid/0.8 M HCl (1:1, v:v). The fraction purity was assessed by ^{1}H NMR using **II-11** as a probe. The appropriate factions were combined and solvent was removed by rotary evaporation and dried under high vacuum. The yellow solid was then washed with MeOH (40 mL) and centrifuged at 7200 rpm for 5 min. The supernatant was decanted and the precipitate was dried under high vacuum to give compound **II-16** as a white powder (0.641 g, 0.5749 mmol, 56%). M.p. > 300 °C. IR (ATR, cm^{-1}): 3390br, 1710s, 1457m, 1230m, 1182m, 961m, 791m, 755m. ^{1}H NMR (400 MHz, D_2O, >1 equiv. **II-11**): 8.34 (s, 1H), 8.32 (d, *J* = 7.8, 1H), 7.87 (d, *J* = 7.8,

1H), 7.50 (s, unbound **II-11**), 6.99 (s, 1H), 6.98 (s, 1H), 6.55 (s, 4H), 5.91 (d, *J* = 15.8, 2H), 5.80-5.55 (m, 12H), 5.29 (d, *J* = 9.1, 2H), 5.20 (d, *J* = 9.1, 2H), 5.13 (d, *J* = 9.8, 2H), 4.92 (d, *J* = 9.8, 2H), 4.60 (d, *J* = 15.8, 2H), 4.42 (s, 4H), 4.20 (s, unbound **II-11**), 4.19 (d, *J* = 15.6, 4H), 4.00 (d, *J* = 15.6, 4H). ^{13}C NMR (125 MHz, D_2O, dioxane as internal reference, > 1 equiv. **II-11**): δ 169.4, 156.9, 156.4, 155.6, 135.4, 135.0, 134.4, 133.1, 133.0, 131.3,130.7, 130.5, 129.5 (unbound **II-11**), 123.9, 71.6, 70.7, 70.0, 69.8, 69.7, 65.5, 64.4, 64.2, 53.1, 51.5, 51.0, 42.7 (unbound **II-11**), 41.6 (only 27 of the 36 expected resonances were observed. ESI-MS: *m/z* 626.3 ([**II-16•II-11**]$^{2+}$, $C_{43}H_{38}N_{24}O_{14}$•$C_8H_{14}N_2$, calc. 626.21).

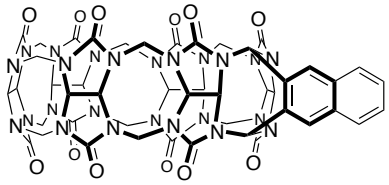

Compound* II-*19. A mixture of **6C** (1.000 g, 1.028 mmol) and **II-18**[128] (0.208 g, 1.131 mmol) was treated with concentrated HCl (5 mL) and stirred at RT for 24 h. The yellow, heterogeneous mixture was then poured into a centrifuge tube and centrifuged at 7200 rpm for 5 min. The supernatant was decanted and the precipitate was washed with MeOH (40 mL) and centrifuged at 7200 rpm for 5 min. The precipitate was then dried under high vacuum to give **II-19** as a white powder (0.951 g, 0.849 mmol, 83%). M.p. > 300 °C. IR (ATR, cm^{-1}): 1712s, 1464m, 1232m, 1182m, 961m, 795m, 758m. ^{1}H NMR (400 MHz, D_2O, >1 equiv. **II-11**): 8.27 (s, 2H), 8.10 (m, 2H), 7.75 (m, 2H), 7.49 (s, unbound **II-11**), 7.04 (s, 2H), 6.56 (s, 4H), 5.91 (d, *J* = 16.0, 2H), 5.75-5.55 (m, 12H), 5.28 (d, *J* = 8.8, 2H), 5.19 (d, *J* = 8.8, 2H), 5.12 (d, *J* = 9.6, 2H), 5.00 (d, *J* = 9.6, 2H), 4.57 (d, *J* = 16.0, 2H), 4.43 (s, 4H), 4.18 (d, *J* = 15.2, 4H), 4.19 (s, unbound **II-11**), 4.00 (d, *J* = 15.6, 4H). ^{13}C NMR (150 MHz, D_2O, dioxane as internal reference, >1

equiv. **II-11**): δ 156.9, 156.4, 155.7, 133.6 (unbound **II-11**), 133.5, 133.0, 130.3, 129.6 (unbound **II-11**), 128.5, 127.3, 123.9, 71.6, 70.7, 70.0, 69.9, 69.8, 65.7, 64.7, 53.1, 51.5, 51.0, 42.7 (unbound **II-11**), 41.6 (only 23 of the 24 expected resonances were observed). ESI-MS: *m/z* 629.1 ([**II-19•II-11**]$^{2+}$, $C_{46}H_{40}N_{24}O_{12}$•$C_8H_{14}N_2$, calcd. 629.22)

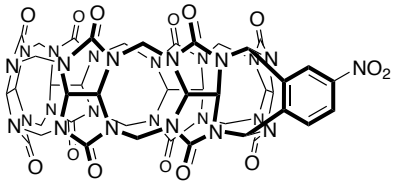

Compound* II-*17. A mixture of **6C** (0.097 g, 0.100 mmol) and **II-15**[127] (0.022 g, 0.120 mmol) was treated with 9M aq. H_2SO_4 (1 mL) and mixed at room temperature for 3 d. The reaction solution was poured into MeOH (20 mL) which resulted in a white precipitate. The mixture was centrifuged at 7200 rpm for 5 min and the supernatant was decanted. The precipitate was washed with 10 mM aq. **II-11** (2 mL) and centrifuged at 7200 rpm for 5 min. The supernatant was decanted and the precipitate was washed with H_2O (1 mL) and then centrifuged at 7200 rpm for 5 min. The supernatant was decanted and the precipitate was dried under high vacuum. The precipitate was then recrystallized from TFA (1 mL). The recrystallized solid was dried under high vacuum to give compound **II-19** as a white powder (0.065 g, 0.058 mmol, 58%). Mp > 300 °C. IR (cm^{-1}): 3521s, 3400s, 1730s, 1630m, 1526m, 1460s, 1417m, 1373m, 1321s, 1291m, 1256s, 11239s, 1182s, 965m. ^{1}H NMR (400 MHz, D_2O, >1 equiv. **II-11**): 8.66 (s, 1H), 8.57 (d, *J* = 8.4 Hz, 1H), 8.01 (d, *J* = 8.4 Hz, 1H), 7.49 (s, unbound **II-11**), 7.05 (s, 1H), 7.04 (s, 1H), 6.53 (s, 4H), 5.90 (d, *J* = 15.6 Hz, 2H), 5.76 (d, *J* = 8.8 Hz, 2H), 5.75-5.55 (m, 10H), 5.28 (d, *J* = 9.2 Hz, 2H), 5.19 (d, *J* = 9.2 Hz, 2H), 5.13 (d, *J* = 9.6 Hz, 2H), 4.90 (d, *J* = 9.6 Hz, 2H), 4.56 (d, *J* = 15.6 Hz, 2H), 4.41 (s, 4H), 4.18 (d, *J* = 15.6 Hz, 4H), 4.19 (s, unbound **II-11**), 4.00 (d, *J* = 15.6 Hz, 4H). ^{13}C NMR (125 MHz,

D_2O, dioxane as internal reference, >1 equiv. **II-11**): 156.9, 156.3, 155.5, 149.4, 137.1, 132.9, 132.6, 131.7, 129.5 (unbound **II-11**), 127.1, 125.2, 123.8, 71.5, 70.6, 70.0, 70.0, 69.7, 65.3, 64.0, 63.9, 53.1, 51.4, 50.9, 42.7 (unbound **II-11**), 41.5 (only 25 of the 35 expected resonances were observed. ESI-MS: *m/z* 626.6 ([**II-19•II-11**]$^{2+}$, calcd. $C_{42}H_{37}N_{25}O_{14}•C_8H_{14}N_2$, 626.70).

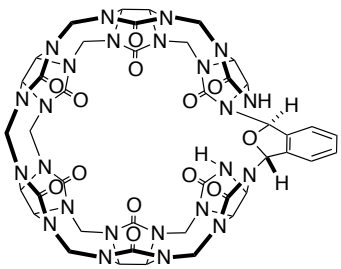

Compound (±)-II-21. A mixture of **6C** (0.100 g, 0.103 mmol) and **II-12** (0.015 g, 0.113 mmol) was treated with TFA (1 mL) and mixed at RT for 24 h. The reaction solution was slowly poured into a vigorously stirred solution of MeOH (10 mL) which resulted in an off-white precipitate. After 10 min., the slurry was centrifuged at 7200 rpm for 5 min. The supernatant was decanted and the precipitate was dried under high vacuum to give (±)-**II-21** as a pale yellow crude solid (0.102 g, 0.0937 mmol, 91%). M.p. > 220 °C (dec.). ^{1}H NMR (600 MHz, D_2O, 1 equiv. **II-11**): 7.54 (m, 2H), 7.36 (m, 2H), 6.70 (s, 4H), 6.59 (s, 2H), 5.80-5.60 (m, 14H), 5.55 (d, *J* = 9.0, 2H), 5.51 (d, *J* = 9.0, 2H), 5.42 (d, *J* = 9.0, 2H), 5.16 (d, *J* = 9.0, 2H), 4.44 (d, *J* = 15.6, 2H), 4.32 (d, *J* = 15.6, 2H), 4.31 (d, *J* = 15.6, 4H), 4.12 (d, *J* = 15.6, 2H), 4.08 (d, *J* = 13.8, 2H), 4.01 (d, *J* = 13.8, 2H). ^{13}C NMR (125 MHz, D_2O, dioxane as internal reference, 1 equiv. **II-11**): 159.8, 157.1, 156.7, 156.6, 156.5, 156.3, 135.4, 133.2, 130.6, 127.6, 123.5, 85.4, 72.6, 71.2, 70.9, 70.6, 70.5, 61.9, 52.6, 52.1, 52.0, 51.3, 51.1, 42.6 (all 24 expected resonances were observed). ESI-MS: *m/z* 613.2 ([(±)-**II-21•II-11**]$^{2+}$, calcd. for $C_{42}H_{40}N_{24}O_{13}•C_8H_{14}N_2$, 613.22).

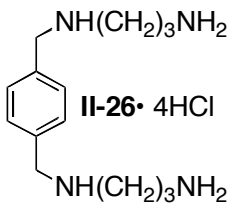

Compound* II-*26. 1,4-Bis(bromomethyl)benzene (1.32 g, 5.00 mmol) was slowly added to a solution of propane-1,3-diamine (3.70 g, 49.9 mmol) in EtOH (20 mL) over 5 h. The mixture was stirred for 12 h under reflux. The solvent and excess propane-1,3-diamine were removed by rotary evaporation and the resulting oil was dried under high vacuum. The resulting oil was dissolved in MeOH (20 mL) and then KOH (0.56 g, 10.0 mmol) was added to the solution. Diethyl ether was added to the solution until a white precipitate was formed which was removed by filtration. The filtrate was concentrated by rotary evaporation to give a yellow oil. The oil was dissolved in THF (20 mL) and conc. HCl was added dropwise to the solution (40 mL) until a white precipitate was formed. The precipitate was then filtered and dried under high vacuum to give **II-26** as a white powder (1.81 g, 4.60 mmol, 92%). Mp > 300 °C (dec.). IR (cm^{-1}): 3421s, 2943s, 2786s, 1586w, 1473w, 1443m, 1386m, 1078m, 1042m. ^{1}H NMR (400 MHz, D_2O): 7.57 (s, 4H), 4.31 (s, 4H), 3.21 (t, J = 8.0 Hz, 4H), 3.10 (t, J = 8.0 Hz, 4H), 2.11 (m, 4H). ^{13}C NMR (100 MHz, D_2O, DMSO-d_6 as internal reference): 131.0, 129.7, 49.8, 43.3, 35.6, 22.8. $C_{14}H_{26}N_4$ ESI-MS): m/z 251.2 ($[M + H]^+$, calcd. for $C_{14}H_{27}N_4$, 251.22).

References

(126) Haris, S. P.; Zhang, Y.; Bourdonnee, B. L.; McCurdy, C. R.; Portoghese, P. S. *J. Med. Chem*. **2007**, 50, 3392-3396.

(128) Miao, Q.; Lefenfeld, M.; Nguyen, T.-Q.; Siegrist, T.; Kloc, C.; Nuckolls, C. *Adv. Mater*. **2005**, *17*, 407-412.

(127) Zhu, P. C.; Wang, D-H.; Lu, K.; Mani, N. *Sci. China Ser. B-Chem.* **2007**, 50, 249.

(153) Lakowicz, J. R. *Principles of Fluorescence Spectroscopy*, Springer, New York, 3rd Ed., 2006.

(11) Huang, W-H.; Zavalij, P. Y.; Isaacs, L. *J. Am. Chem. Soc.* **2008**, *130*, 8446-8454.

(26) Huang, W.; Liu, S.; Zavalij, P. Y.; Isaacs, L. *J. Am. Chem. Soc.* **2006**, *128*, 14744-14745.

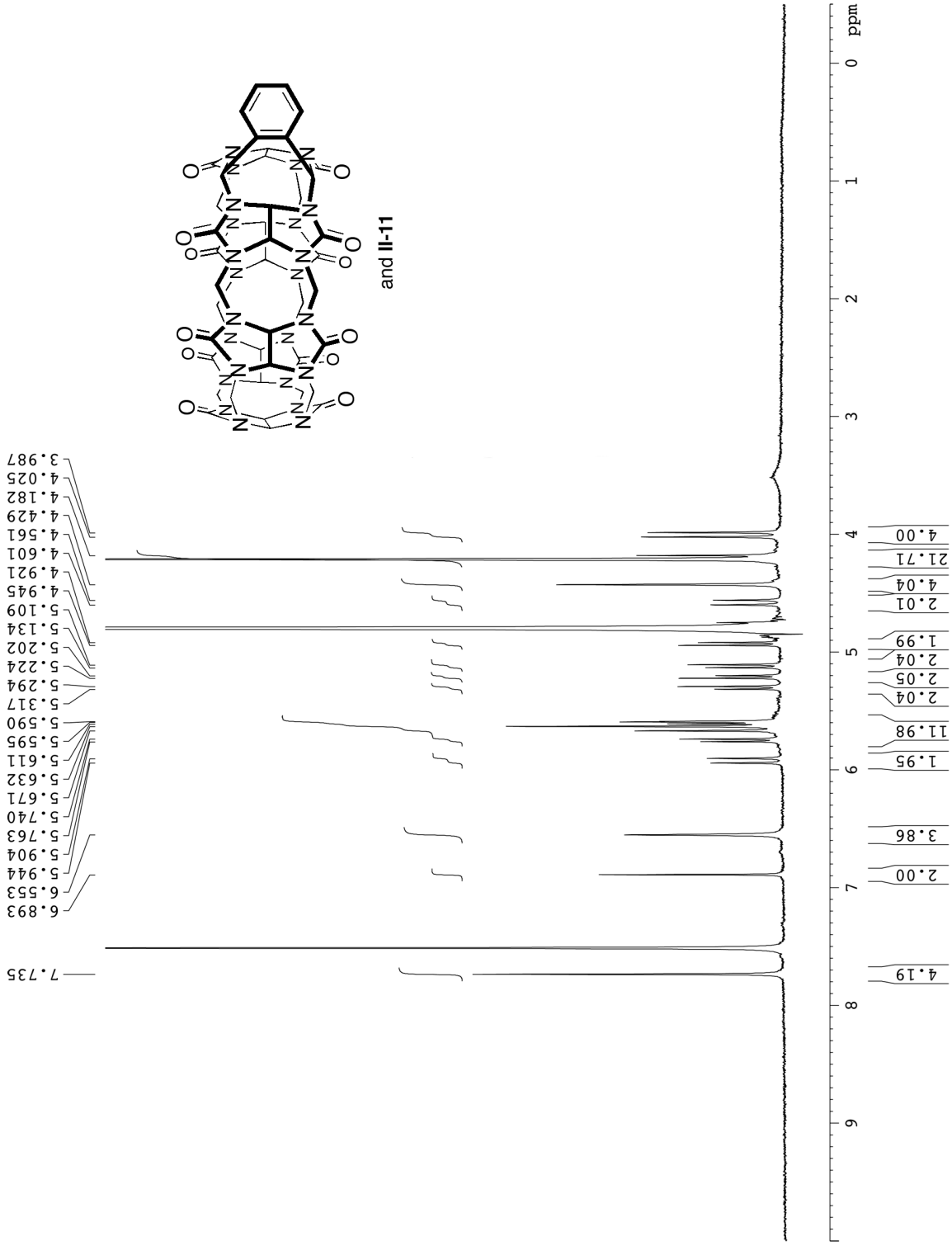

Figure II-S1. ^{1}H NMR spectrum recorded (400 MHz, D_2O, RT) for a mixture of **II-13** and **II-11**.

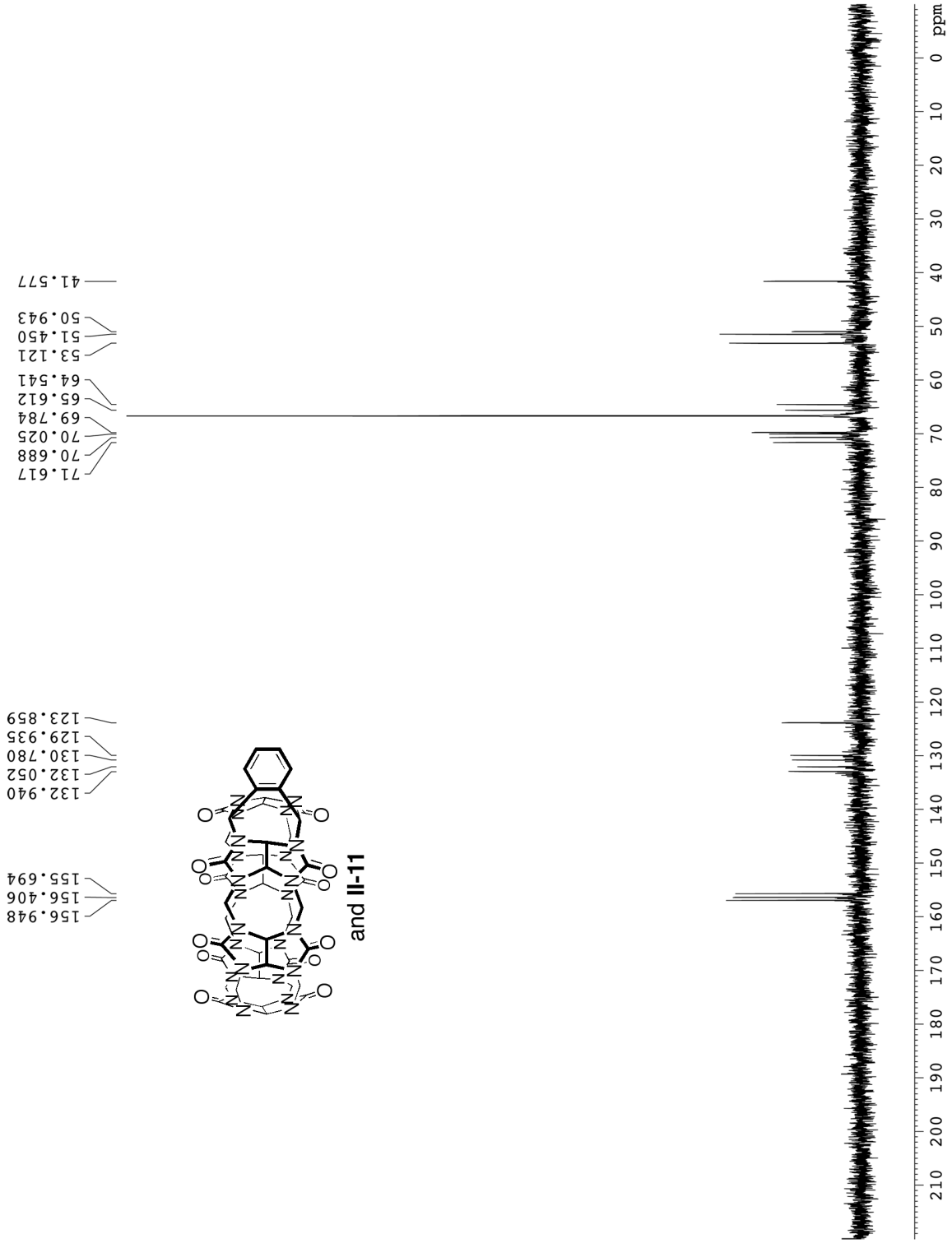

Figure II-S2. ^{13}C NMR spectrum recorded (100 MHz, D_2O, dioxane as internal reference, RT) for a mixture of **II-13** and **II-11**.

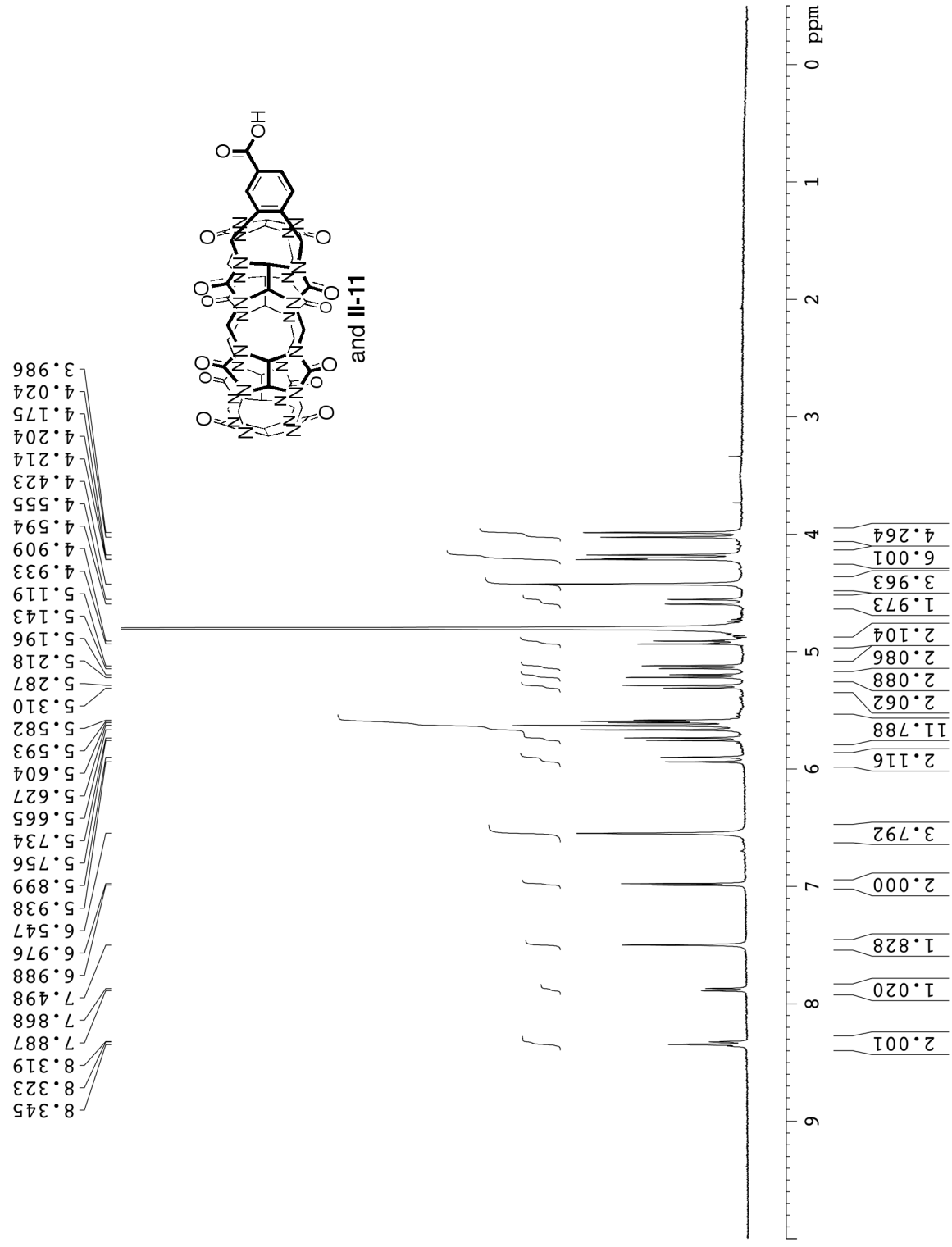

Figure II-S3. ^{1}H NMR spectrum recorded (400 MHz, D_2O, RT) for a mixture of **II-16** and **II-11**.

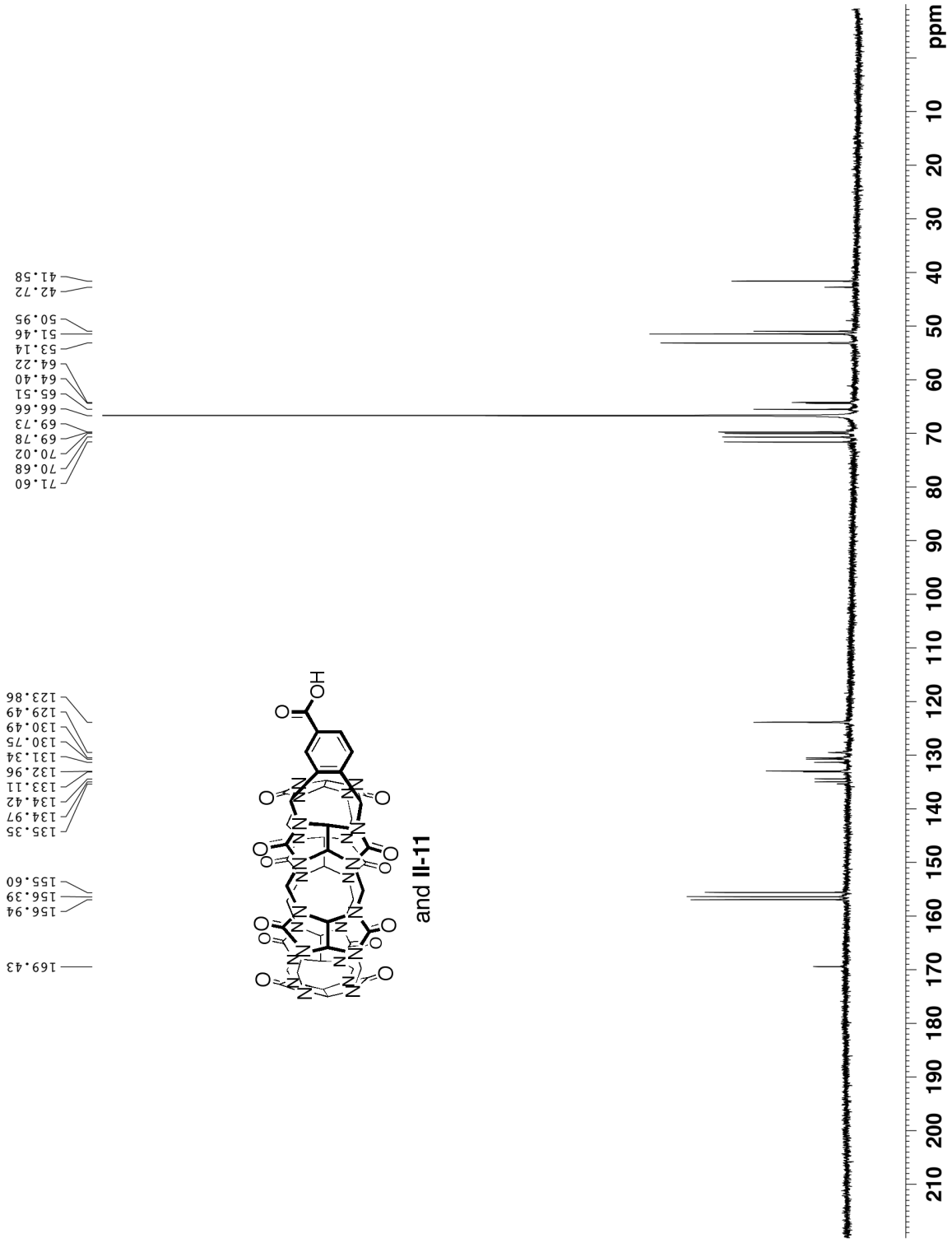

Figure II-S4. ^{13}C NMR spectrum recorded (125 MHz, D_2O, dioxane as internal reference, RT) for a mixture of **II-16** and **II-11**.

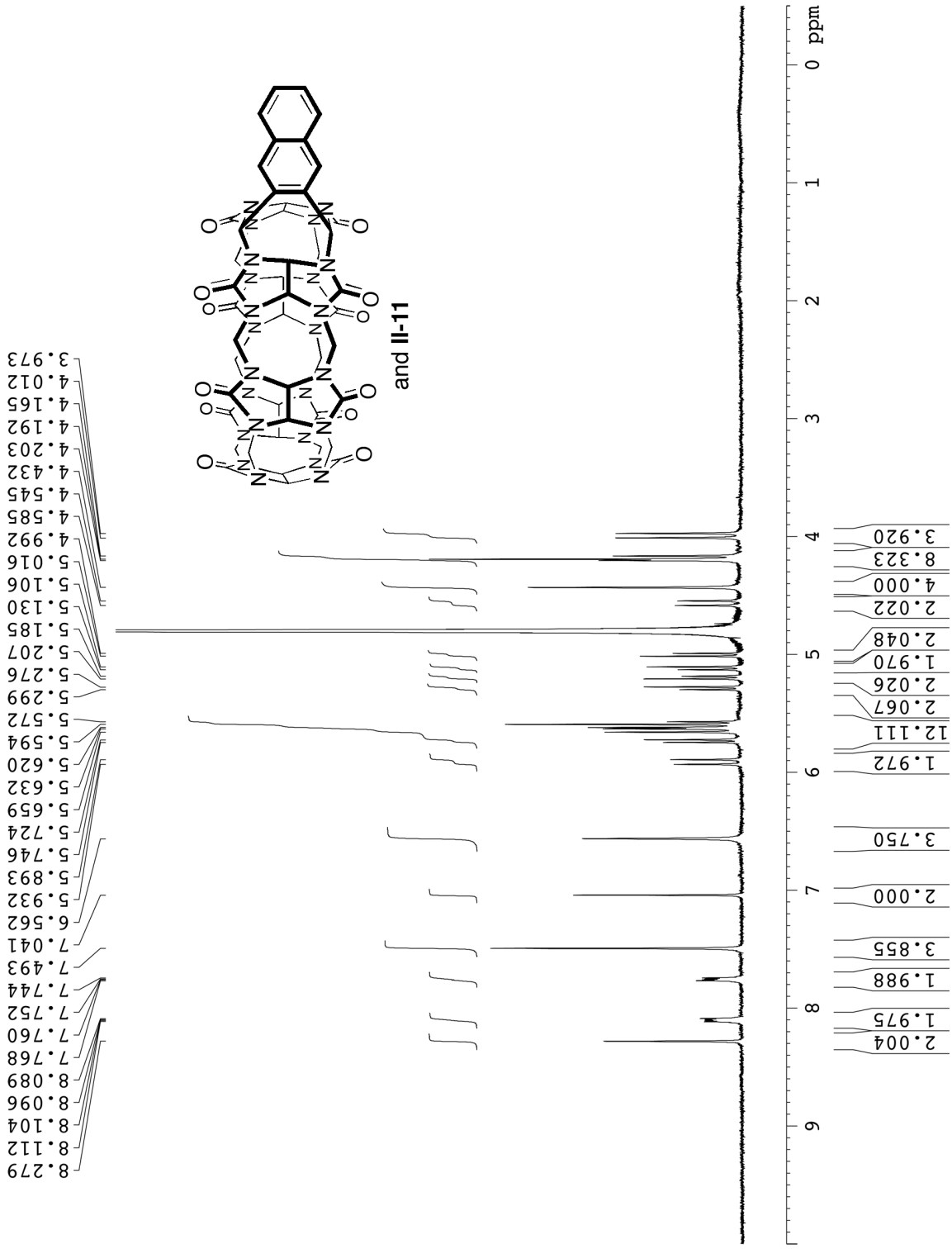

Figure II-S5. ^{1}H NMR spectrum recorded (400 MHz, D_2O, RT) for a mixture of **II-19** and **II-11**.

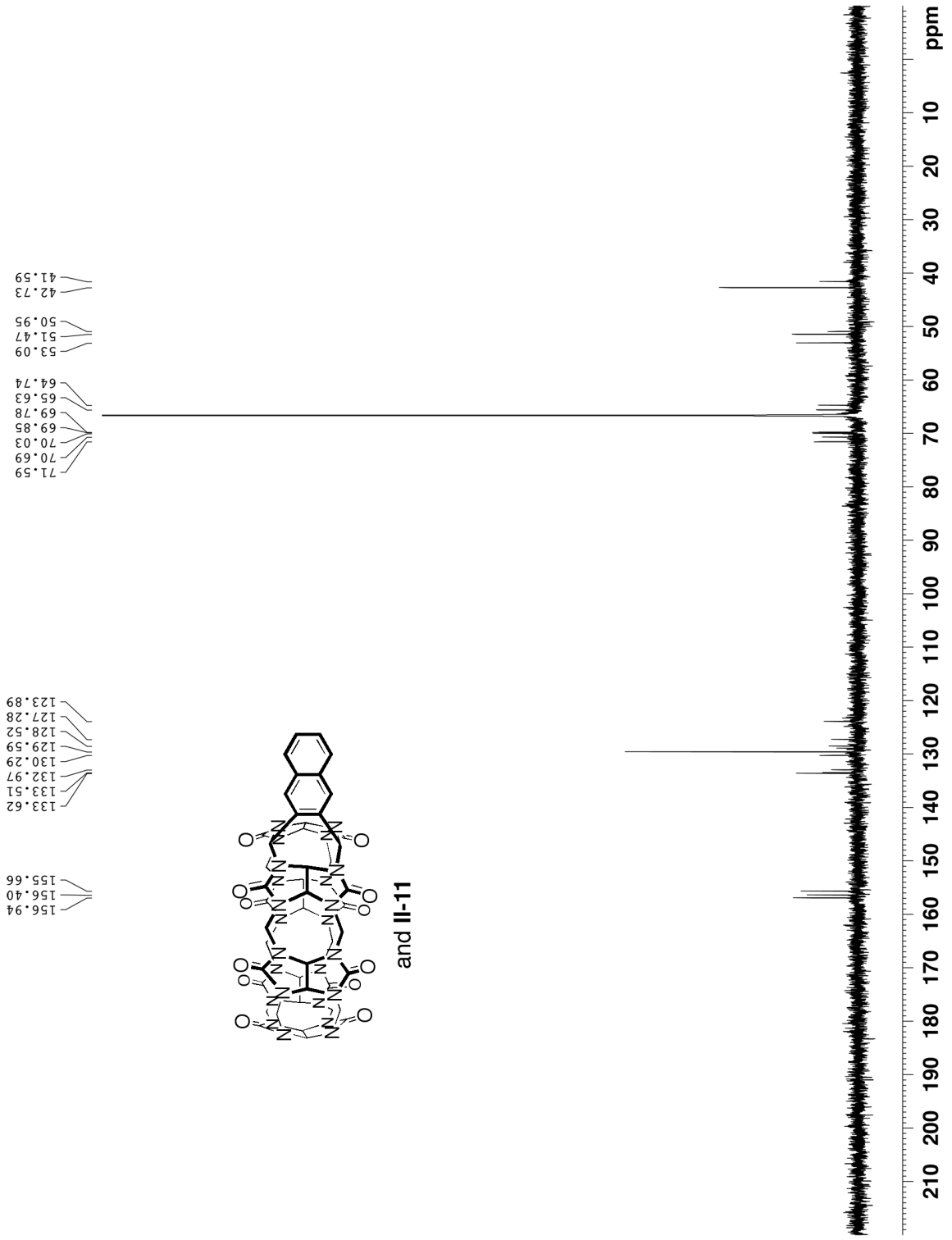

Figure II-S6. ^{13}C NMR spectrum recorded (150 MHz, D_2O, dioxane as internal reference, RT) for a mixture of **II-19** and **II-11**.

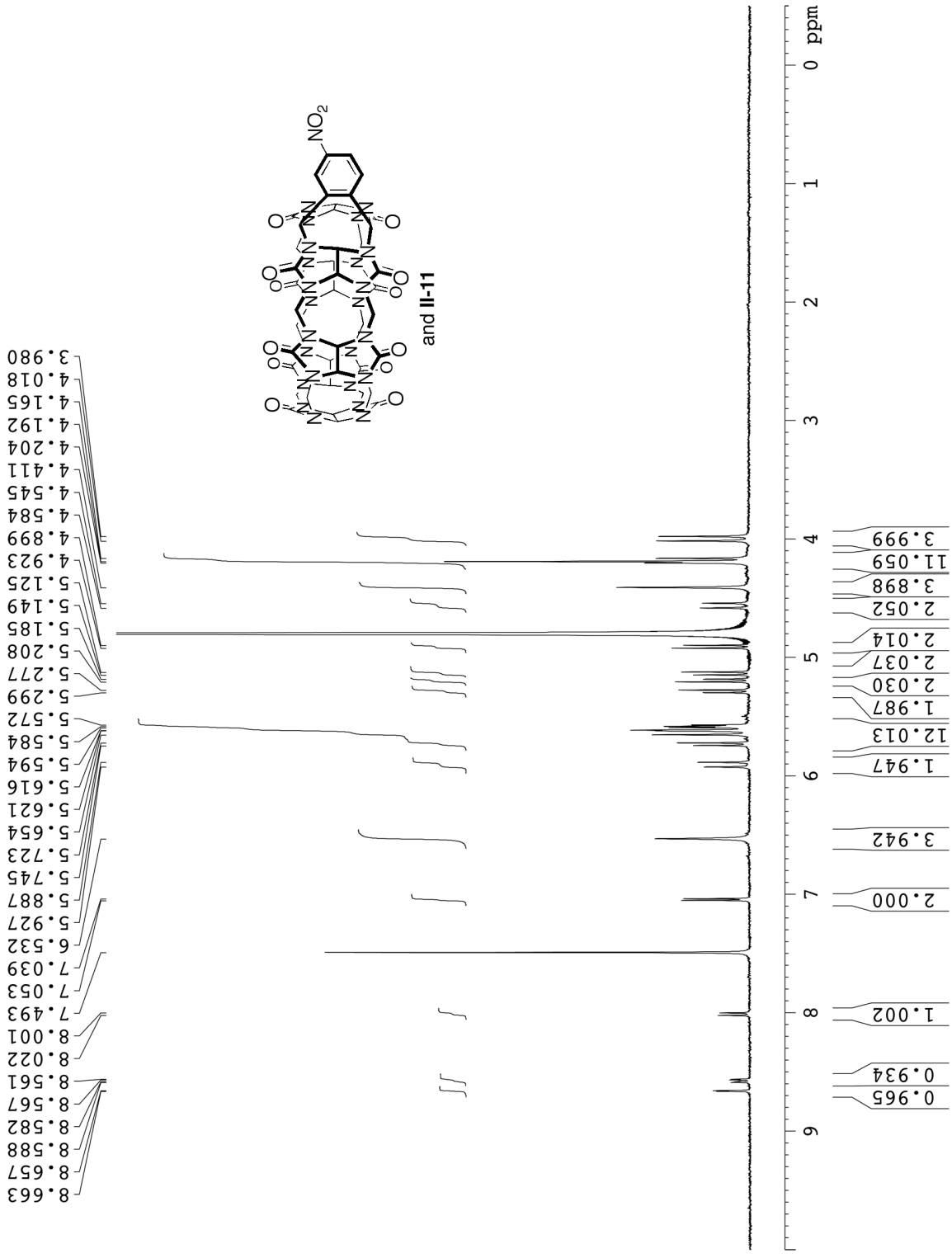

Figure II-S7. ^{1}H NMR spectrum recorded (400 MHz, D_2O, RT) for a mixture of **II-17** and **II-11**.

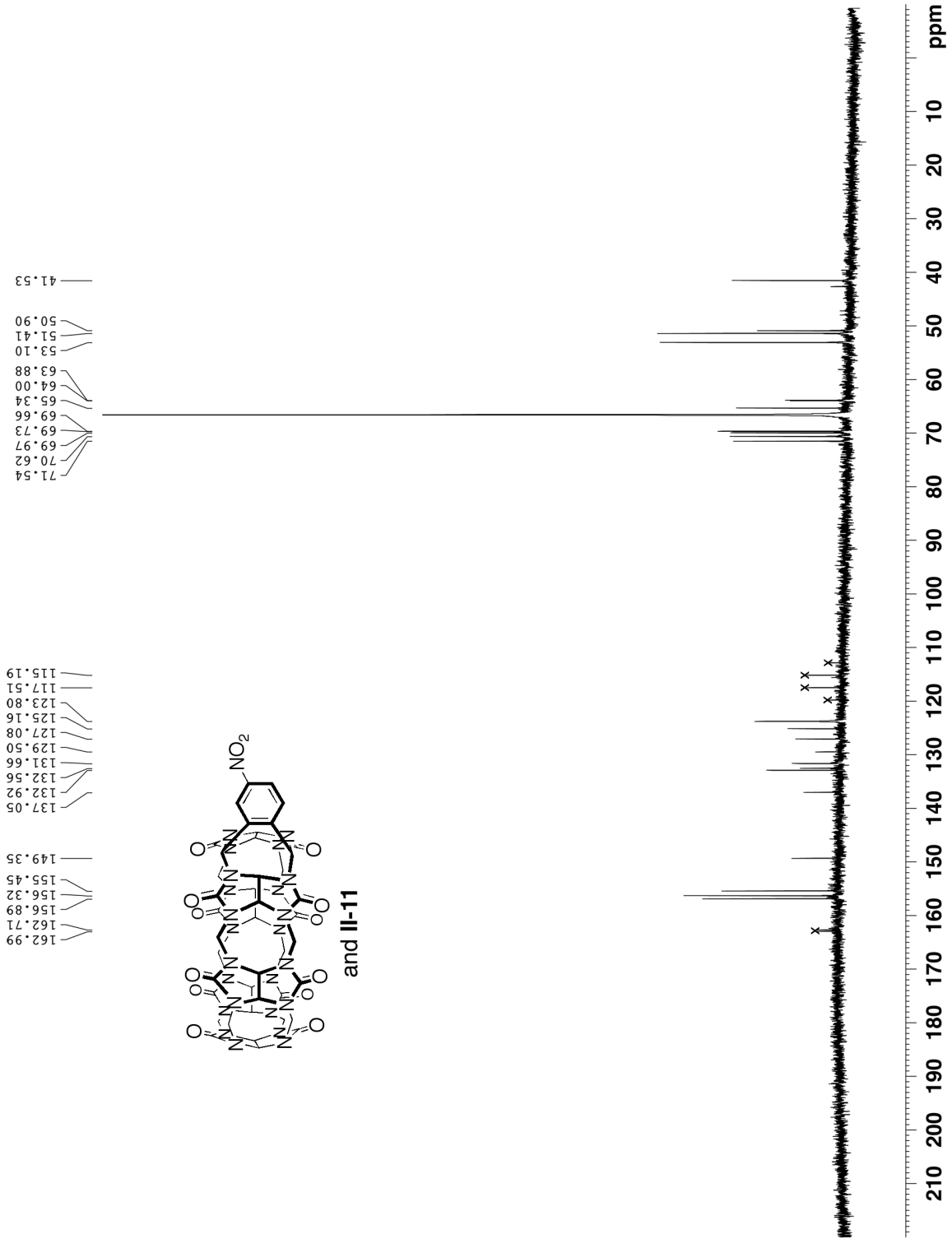

Figure II-S8. ^{13}C NMR spectrum recorded (125 MHz, D_2O, dioxane as internal reference, RT) for a mixture of **II-17** and **II-11**. X = TFA.

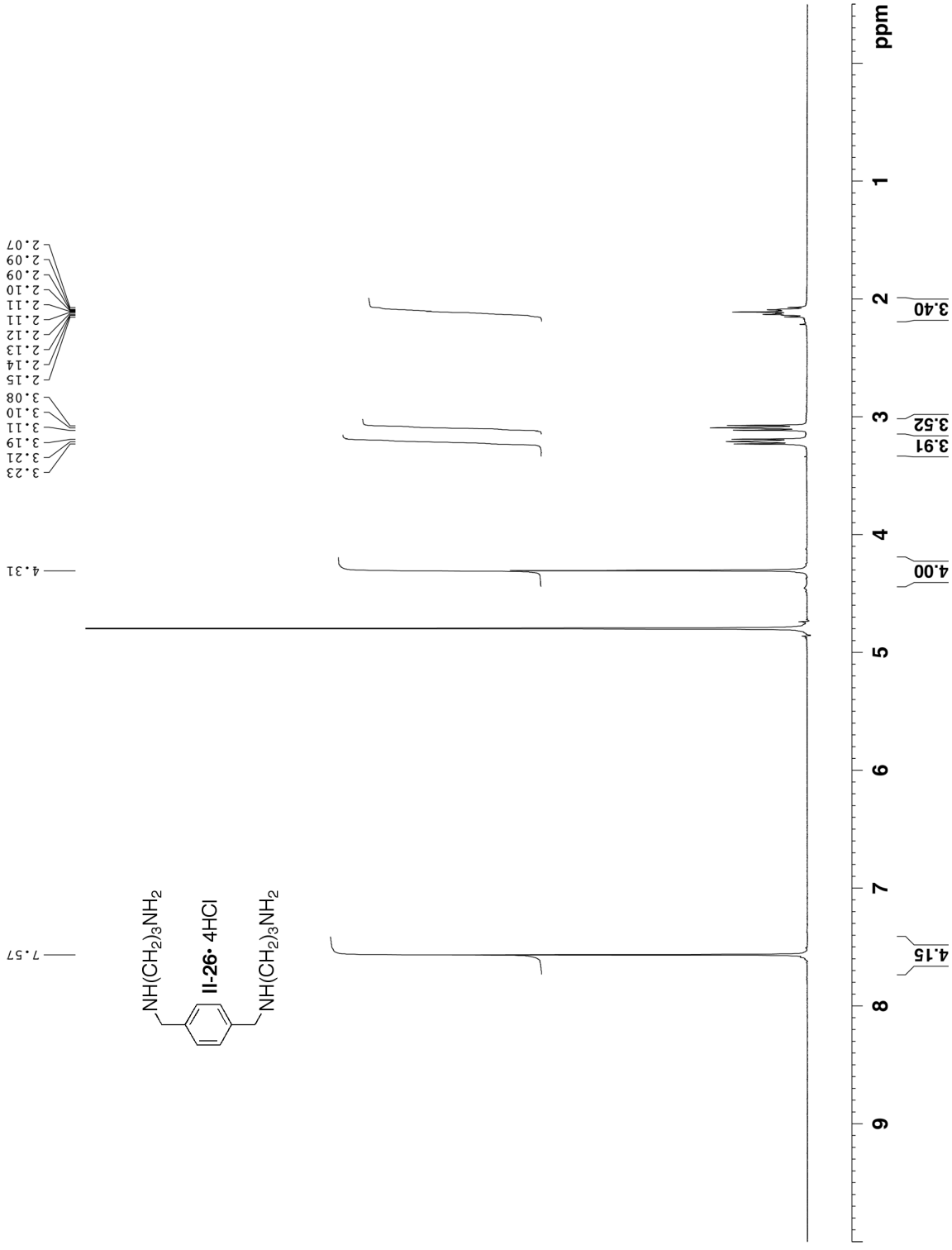

Figure II-S9. ^{1}H NMR spectrum recorded (400 MHz, D_2O, RT) for **II-26**.

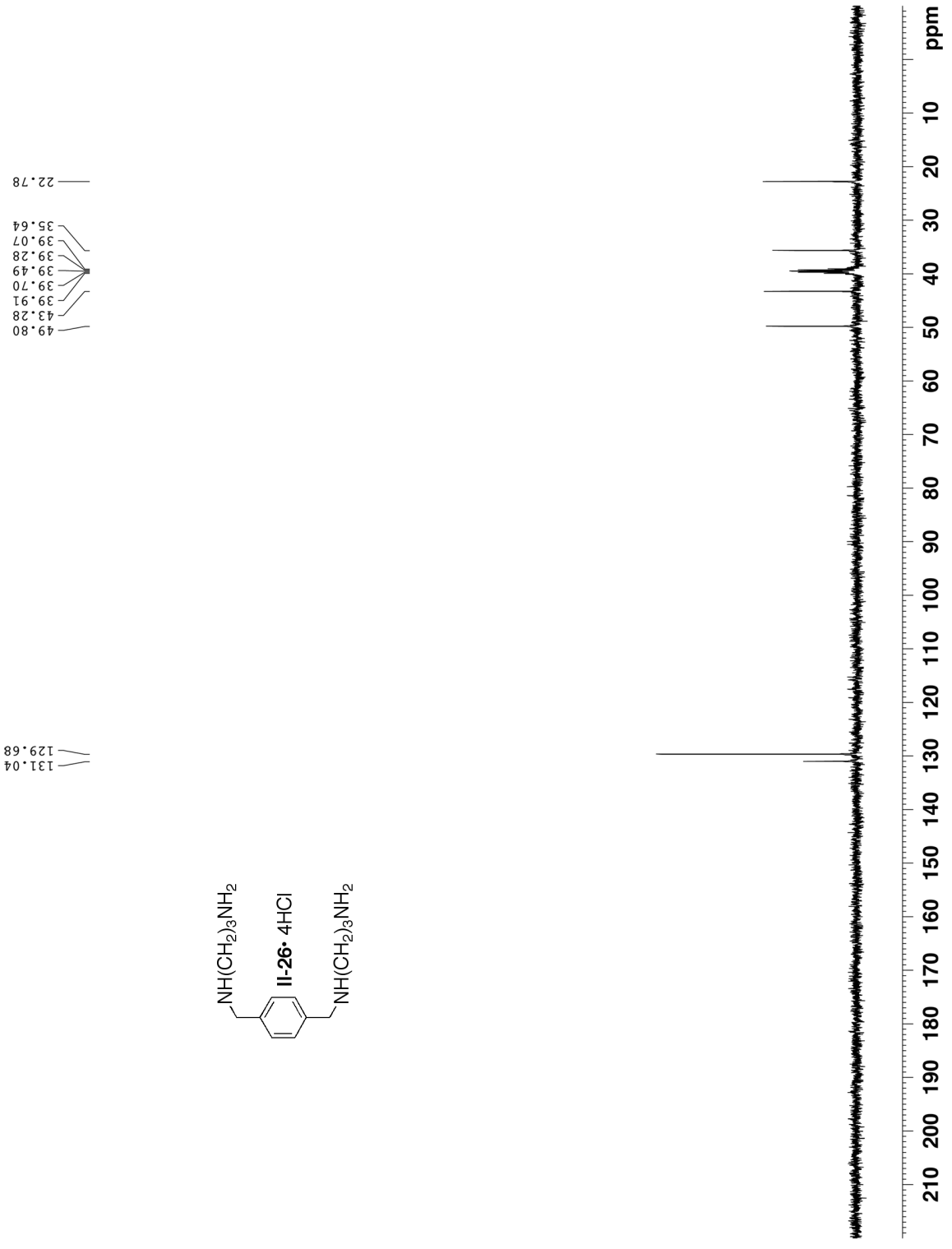

Figure II-S10. ^{13}C NMR spectrum recorded (100 MHz, D_2O, DMSO as reference, RT) for **II-26**.

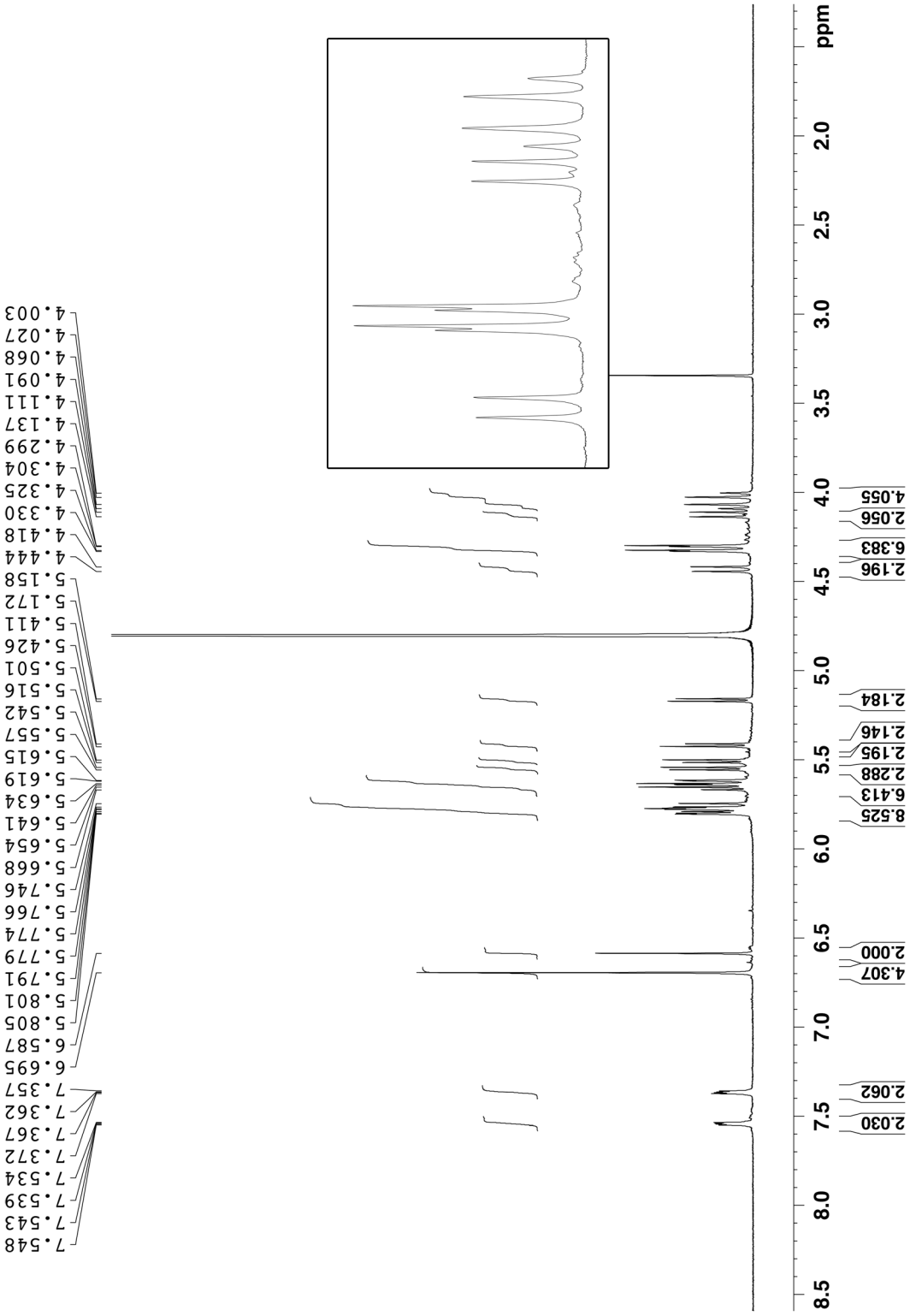

Figure II-S11. ^{1}H NMR spectrum recorded (600 MHz, D_2O, RT) for a mixture of (±)-**II-21** and **II-11**.

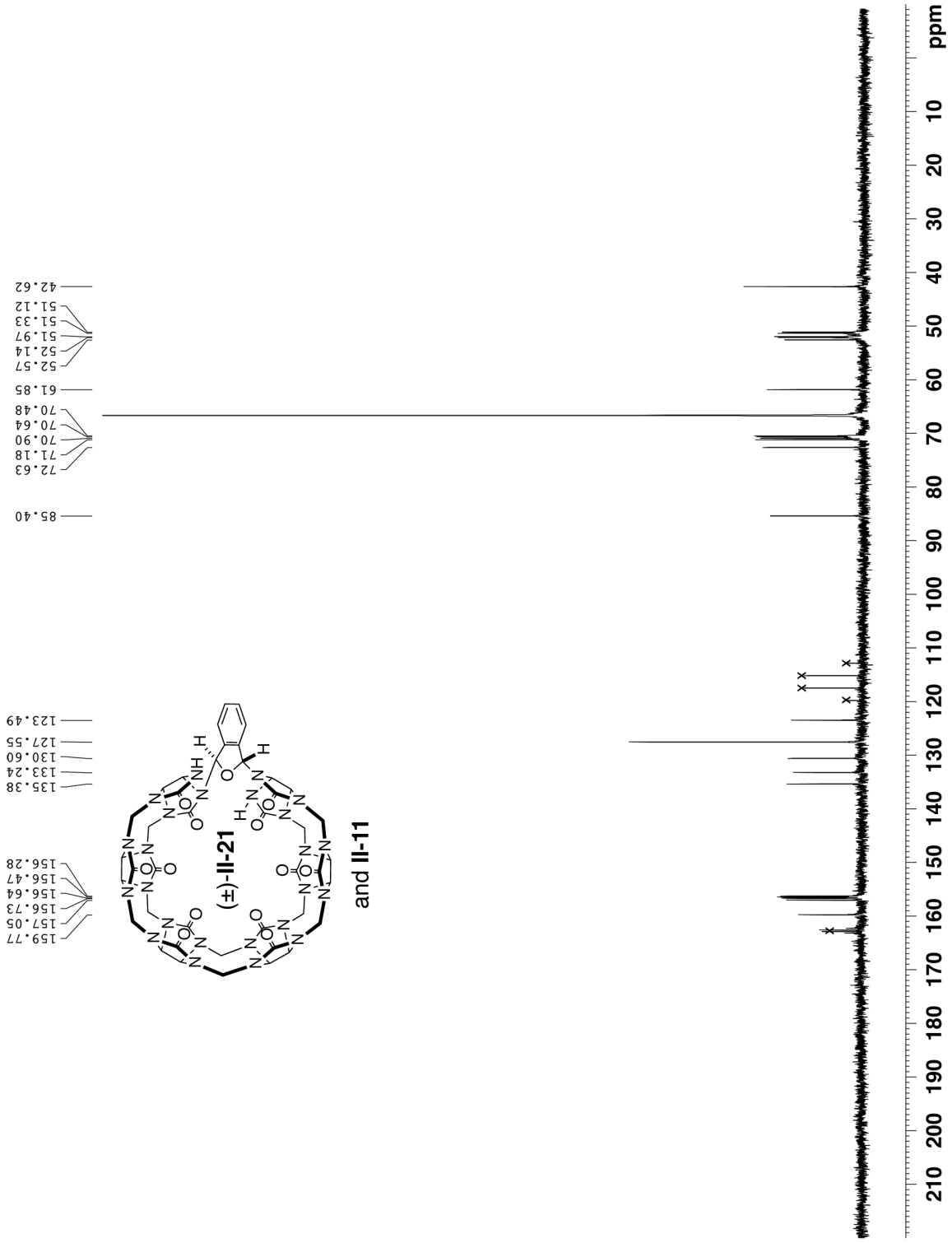

Figure II-S12. ^{13}C NMR spectrum recorded (125 MHz, D_2O, dioxane as internal reference RT) for a mixture of (±)-**II-21** and **II-11**.

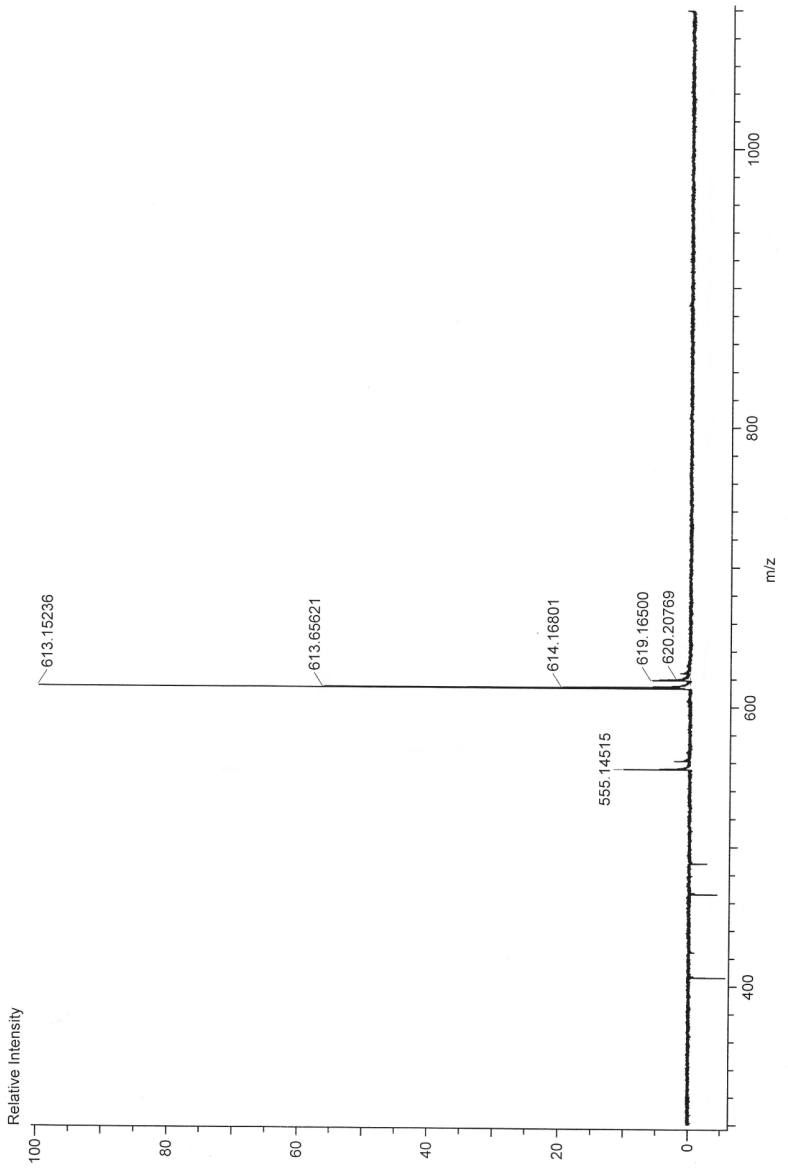

Figure II-S13. ESI-MS spectrum recorded (H_2O, Ionization mode: ESI^+) for a mixture of (±)-**II-21** and **II-11**.

Procedure for the decomposition of (±)-**II-21**. H_2O (1 mL) was added to a vial containing (±)-**II-21** (0.010 g, 0.009 mmol) with stirring at room temperature. The reaction was monitored at appropriate time points by adding an aliquot (2 drops) of the reaction to a centrifuge tube containing MeOH (5 mL). The resulting precipitate was centrifuged at 7200 rpm for 5 min. The supernatant was decanted and the precipitate was dried under high vacuum. The percentage of (±)-**II-21** was calculated by analyzing the precipitate by ^{1}H NMR in D_2O using **II-11** as probe. The integrations of the Ar-H resonance of (±)-**II-21•II-11** at 7.38 ppm and the C-H resonance at 5.17 were compared to the integration of the region between 5.17 and 5.81 ppm which allows calculation of the percentage of (±)-**II-21** in the mixture.

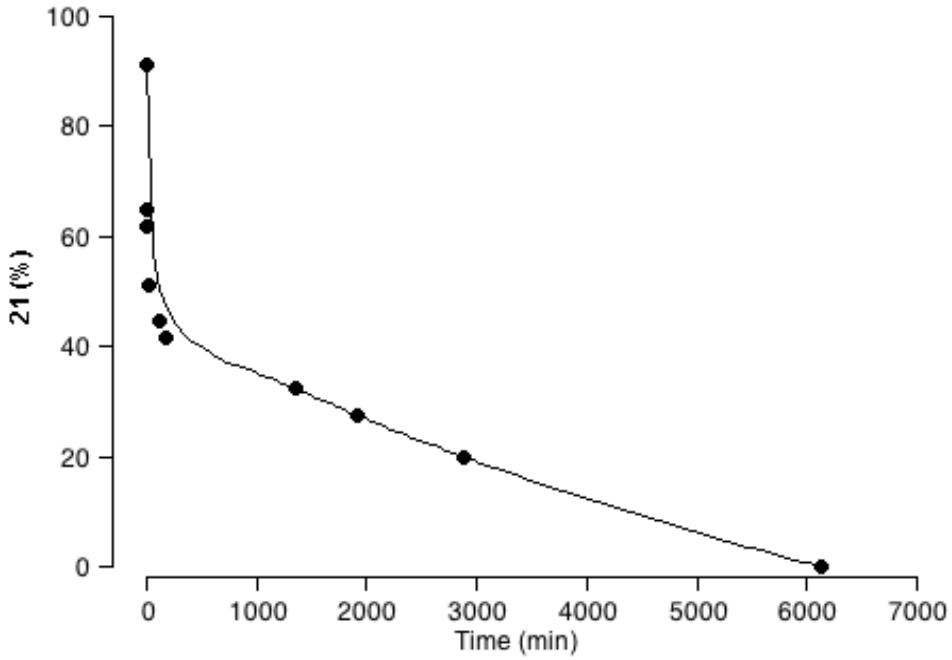

Figure II-S14. Kinetic trace for the decomposition of (±)-**II-21** into **6C** in D_2O at RT over 6140 min.

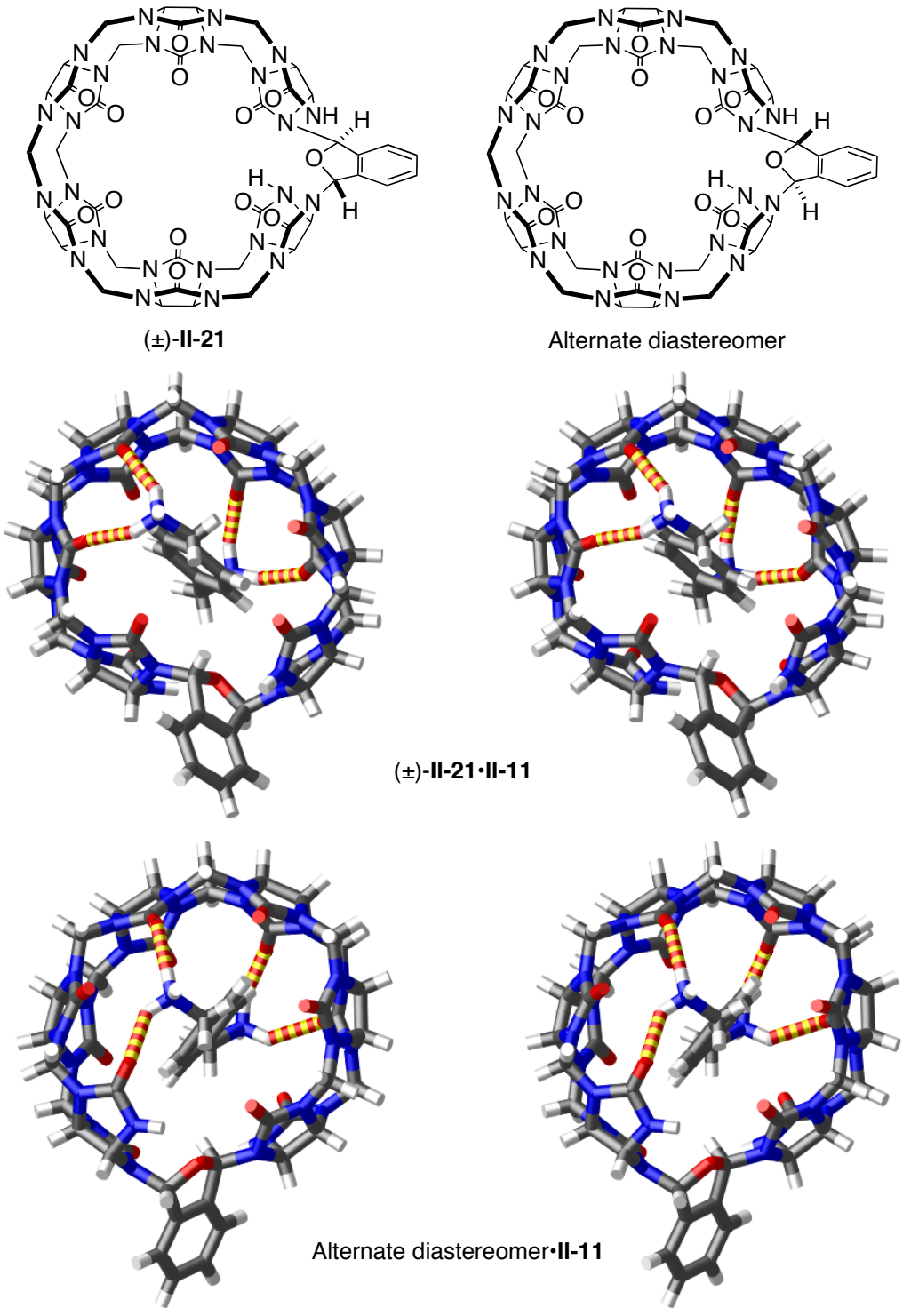

Figure II-S15. Chemical structures of (±)-**II-21** and its diastereomer along with cross eyed stereoviews of MMFF minimized models of their complexes with **II-11**.

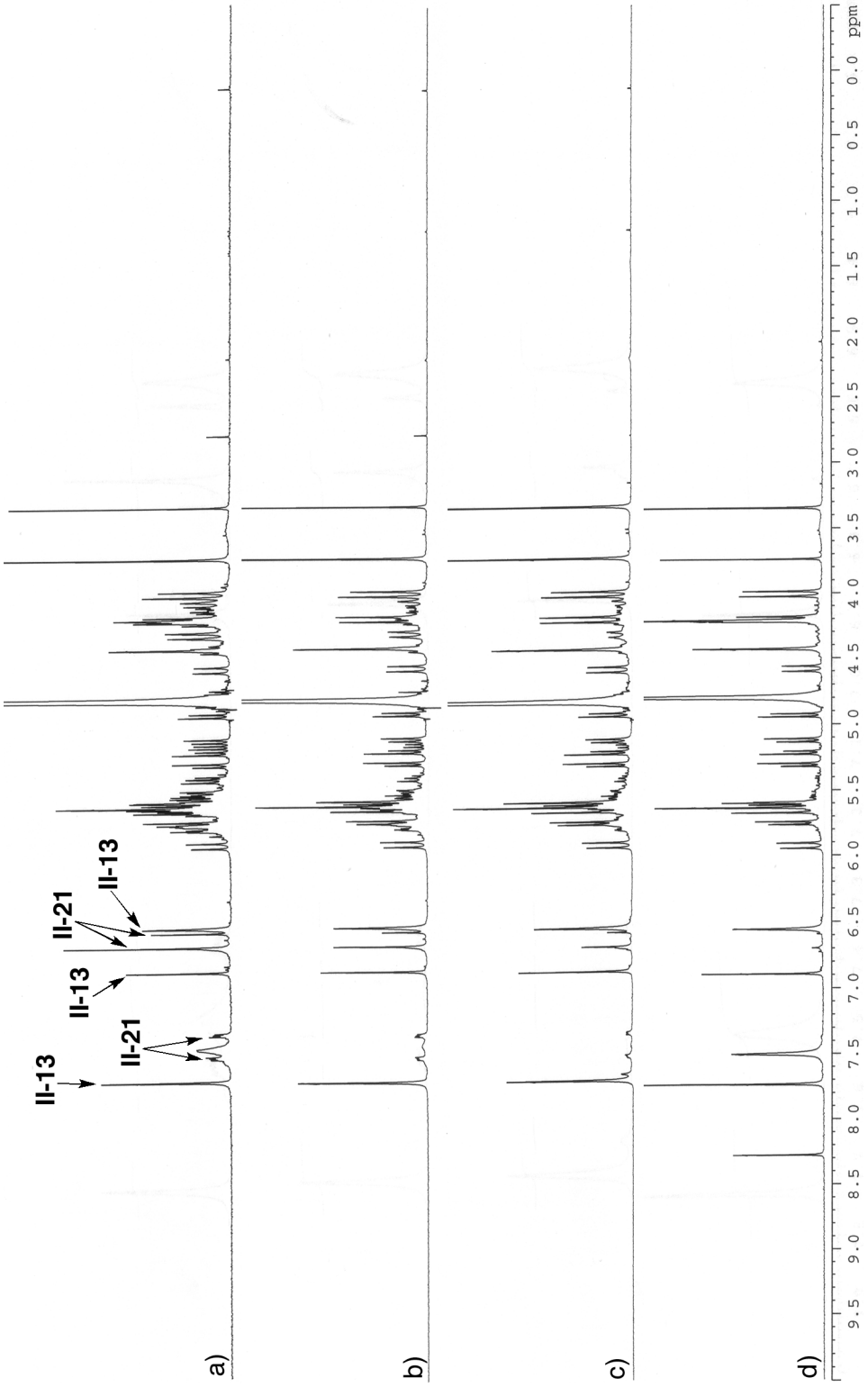

Figure II-S16. ^{1}H NMR spectra recorded for the reaction between **6C** and **II-12** in 9 M H_2SO_4 as a function of time. a) 1 min., b) 20 min., c) 60 min., d) 120 min.

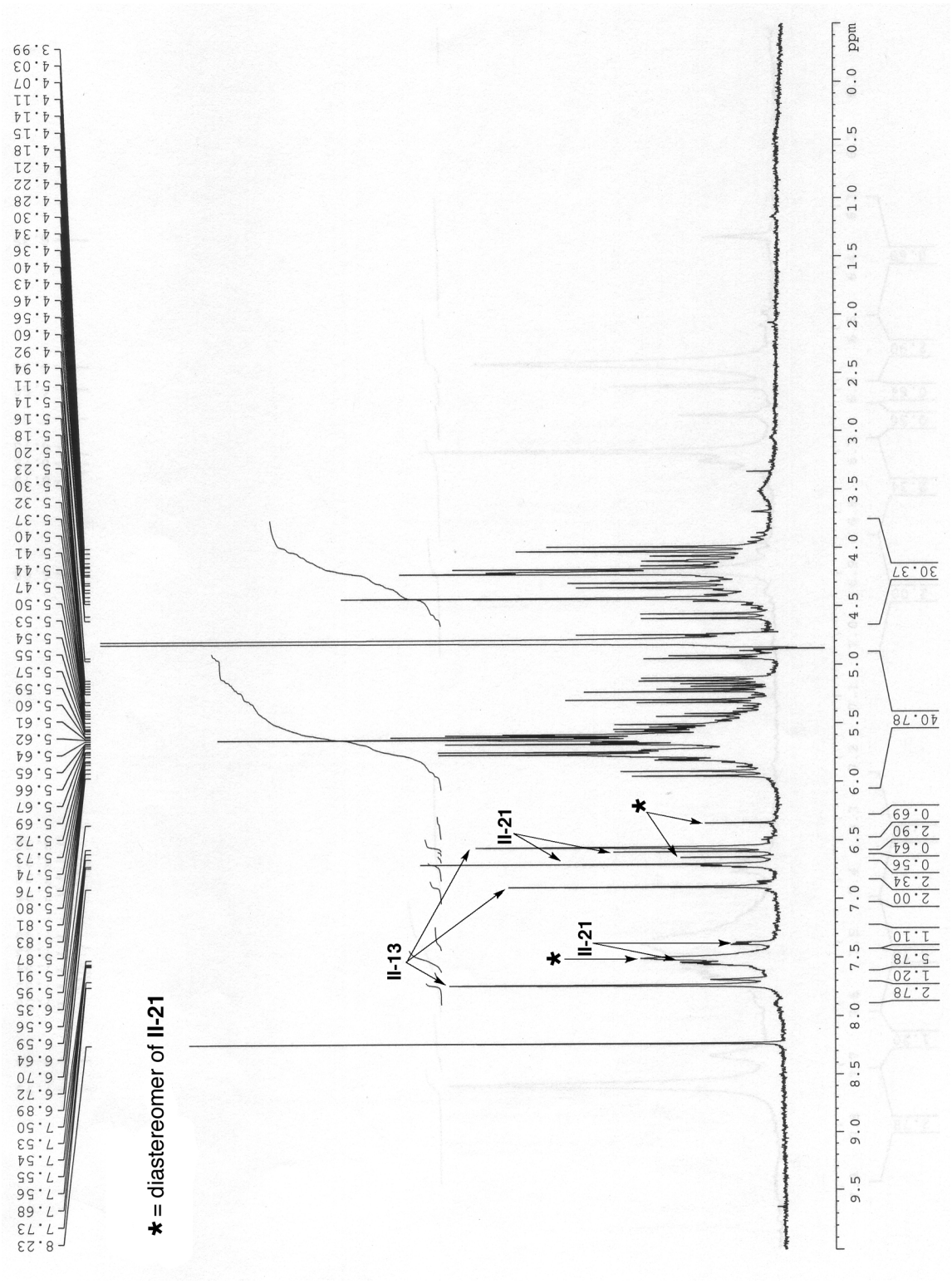

Figure II-S17. ^{1}H NMR spectra recorded for the reaction between **6C** and **II-12** in conc. HCl after 20 h that shows the presence of a mixture of **II-13** and (±)-**II-21** and its diastereomer.

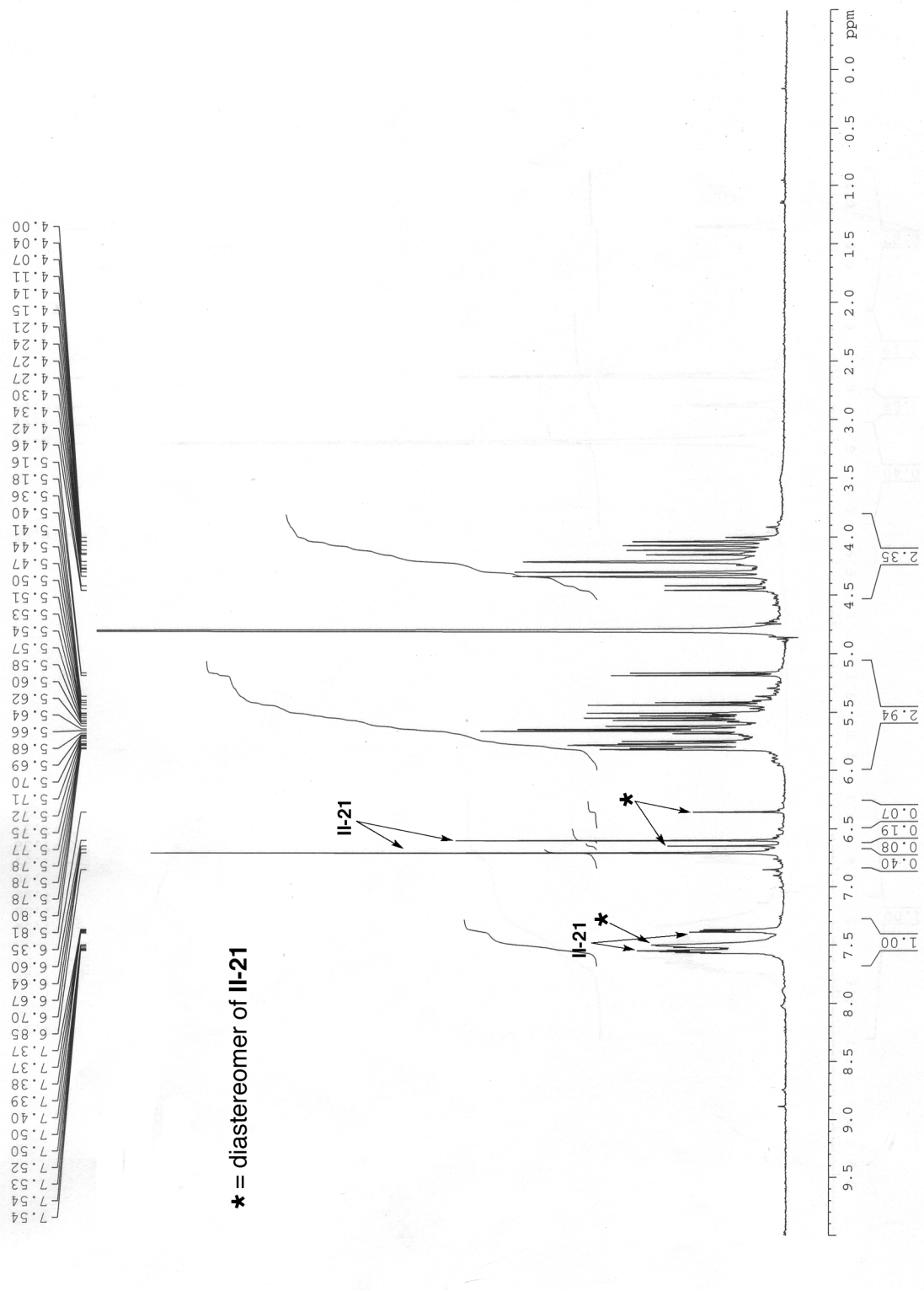

Figure II-S18. ^{1}H NMR spectra recorded for the reaction between **6C** and **II-12** in TFA which shows the presence of (±)-**II-21** and its diastereomer.

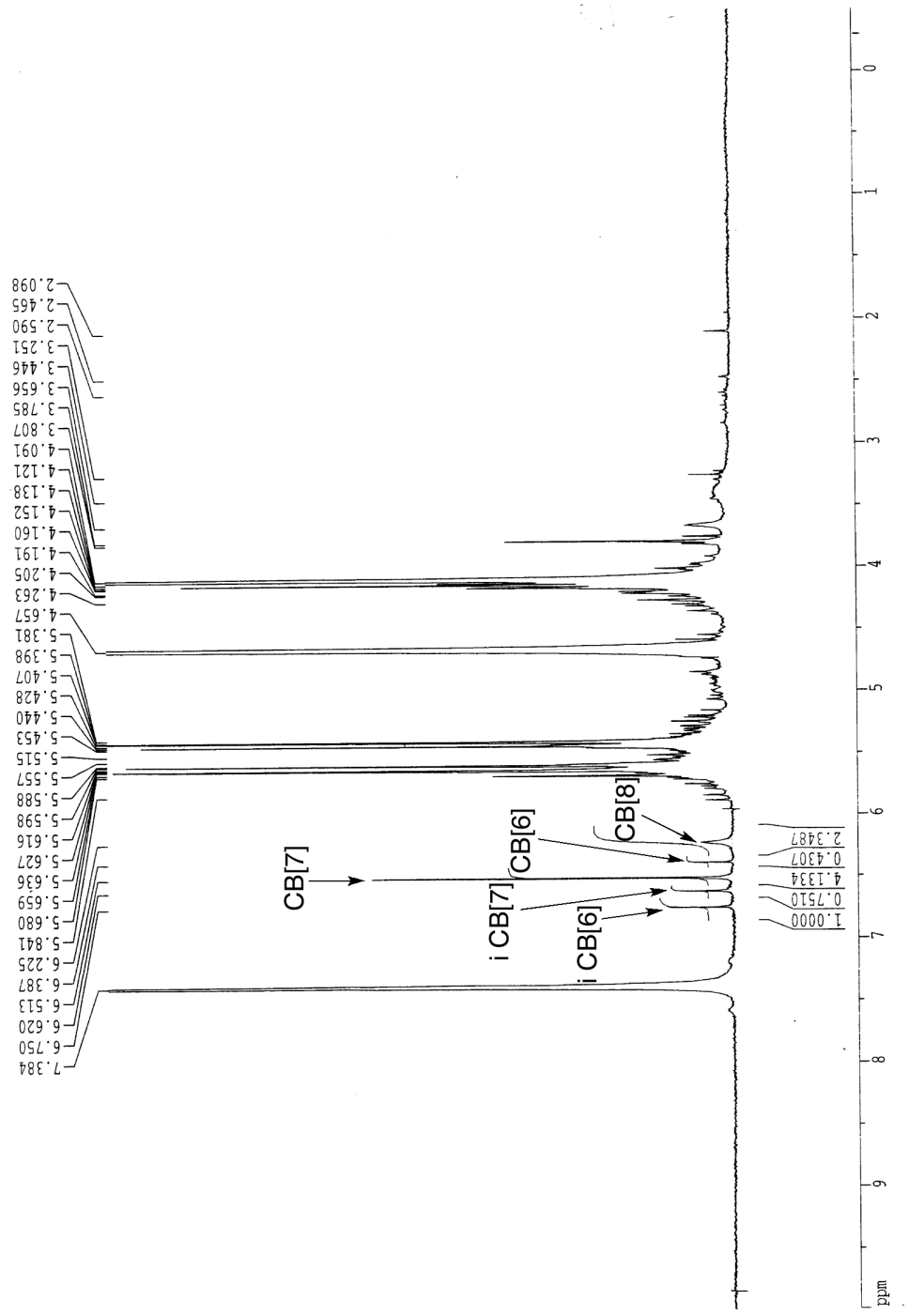

Figure II-S19. ^{1}H NMR spectrum recorded (400 MHz, D_2O, RT) for a mixture of CB[6], CB[7], CB[8], iCB[6], iCB[7], and **II-11**.

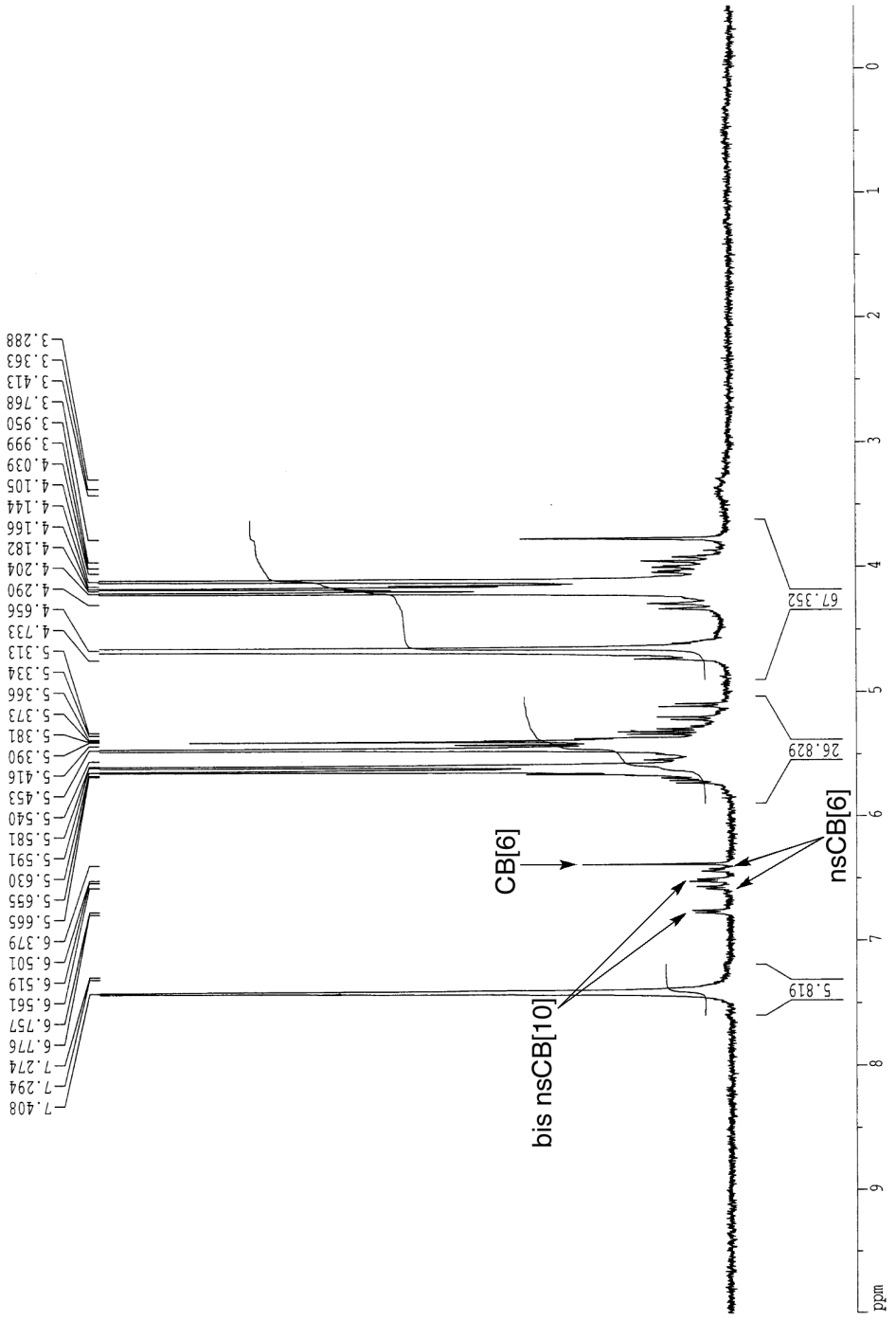

Figure II-S20. ^{1}H NMR spectrum recorded (400 MHz, D_2O, RT) for a mixture of CB[6], nor-seco-CB[6], bis-nor-seco-CB[10], and **II-11**.

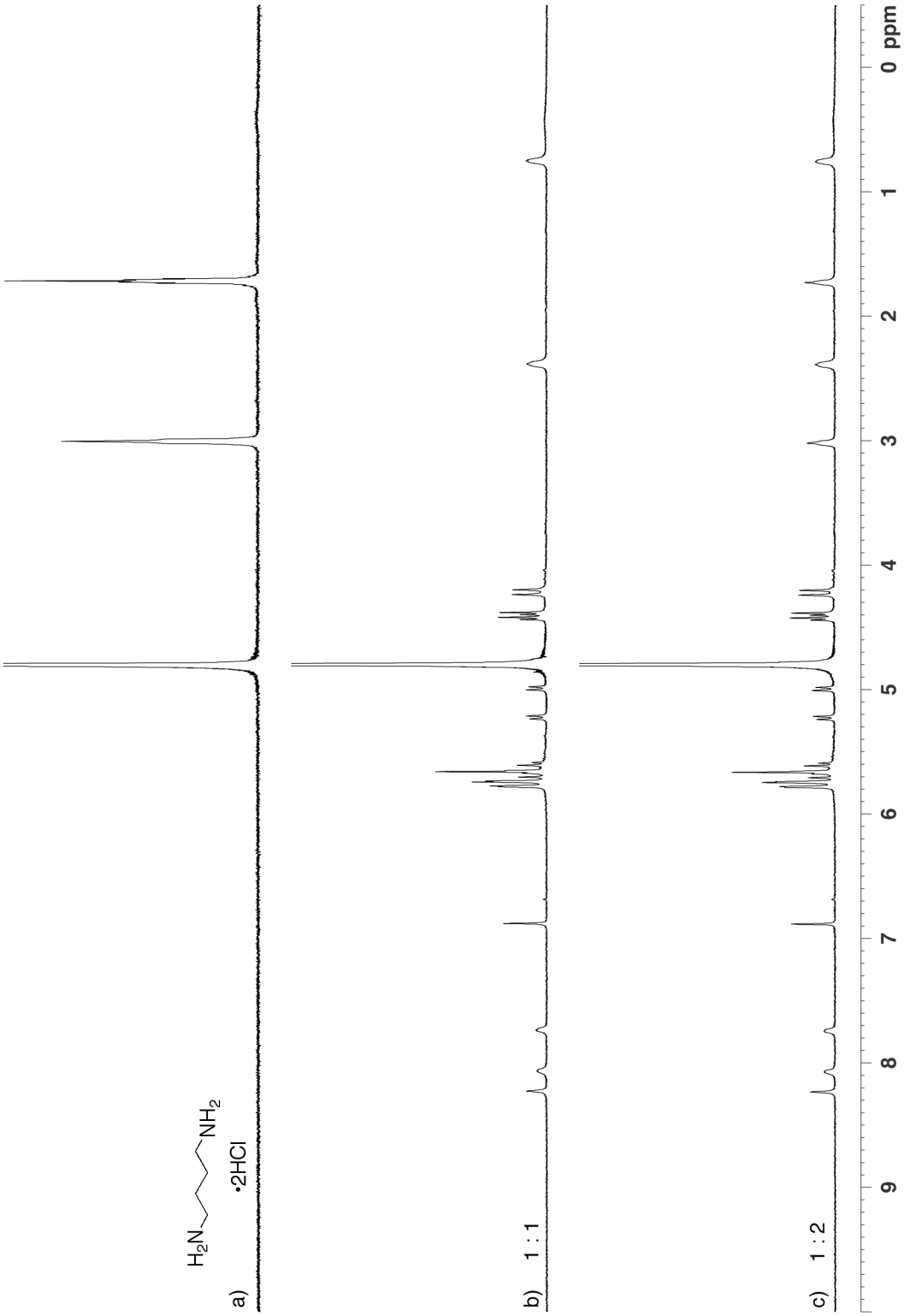

Figure II-S21. ^{1}H NMR spectra recorded (D_2O, 400 MHz, RT) for: a) **II-22** (0.5 mM), b) a mixture of **II-19** (0.5 mM) and **II-22** (0.5 mM), and c) a mixture of **II-19** (0.5 mM) and **II-22** (1 mM).

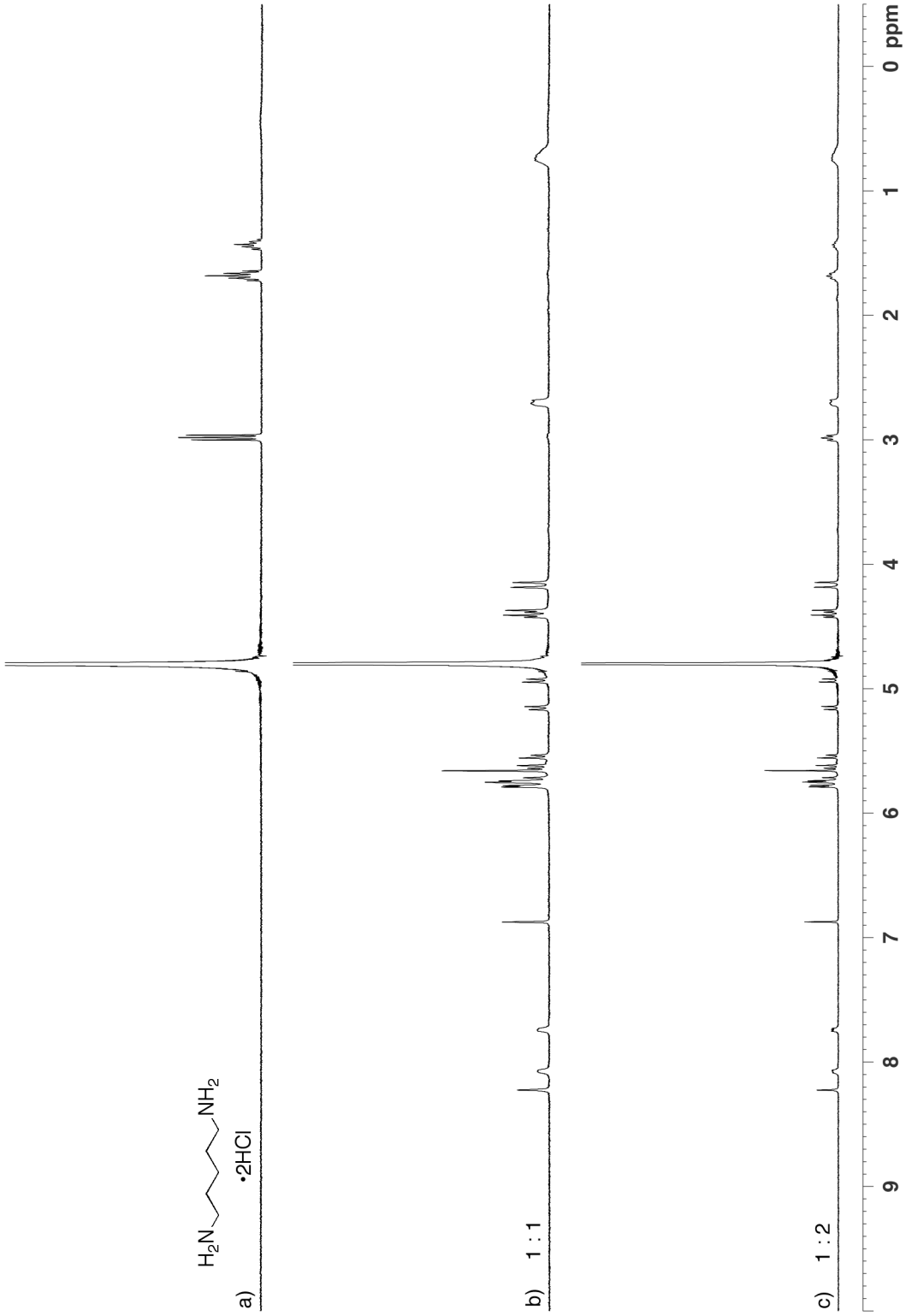

Figure II-S22. ^{1}H NMR spectra recorded (D_2O, 400 MHz, RT) for: a) **II-23** (0.5 mM), b) a mixture of **II-19** (0.5 mM) and **II-23** (0.5 mM), and c) a mixture of **II-19** (0.5 mM) and **II-23** (1 mM).

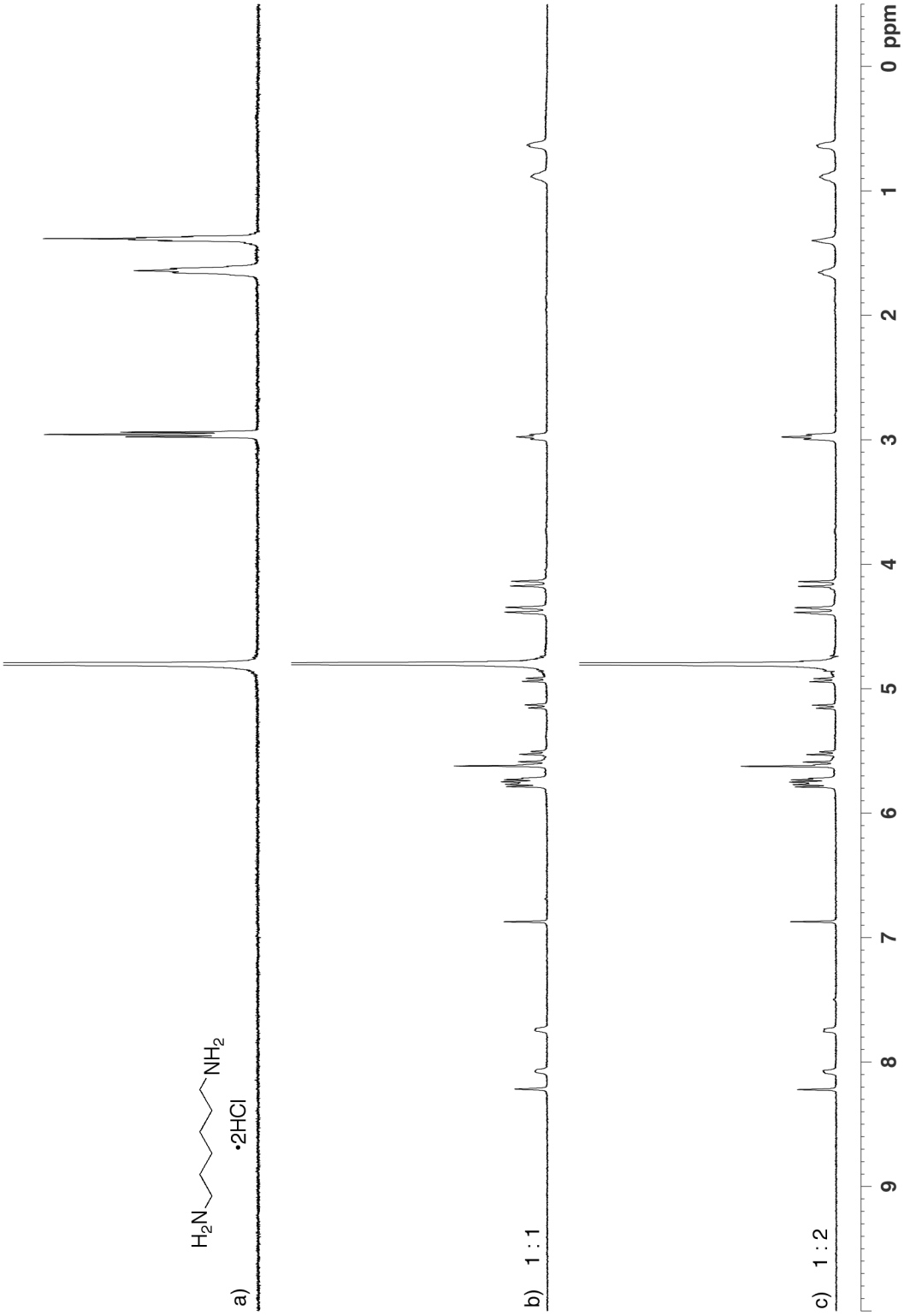

Figure II-S23. ^{1}H NMR spectra recorded (D_2O, 400 MHz, RT) for: a) **II-20** (0.5 mM), b) a mixture of **II-19** (0.5 mM) and **II-20** (0.5 mM), and c) a mixture of **II-19** (0.5 mM) and **II-20** (1 mM).

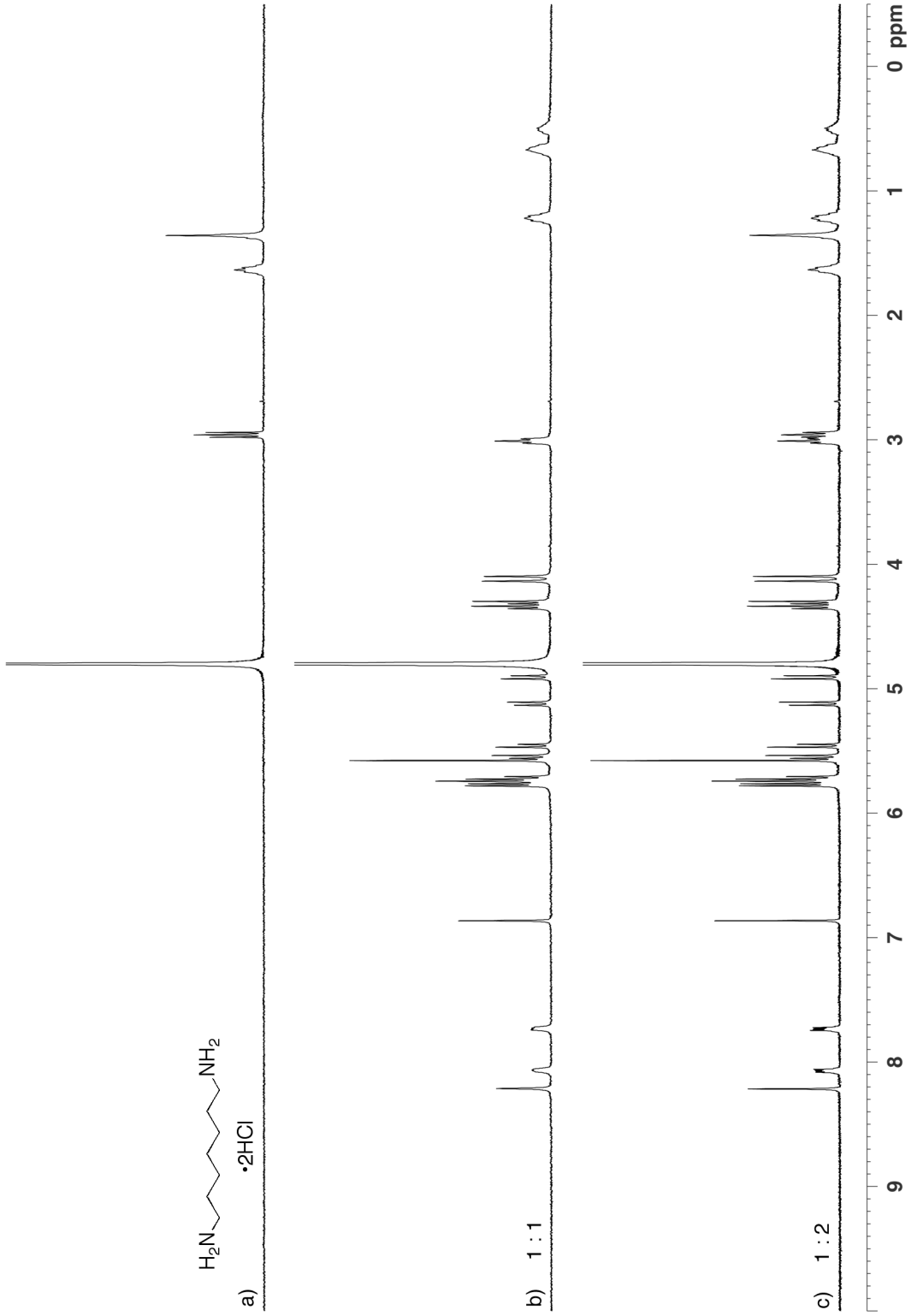

Figure II-S24. ^{1}H NMR spectra recorded (D_2O, 400 MHz, RT) for: a) **II-24** (0.5 mM), b) a mixture of **II-19** (0.5 mM) and **II-24** (0.5 mM), and c) a mixture of **II-19** (0.5 mM) and **II-24** (1 mM).

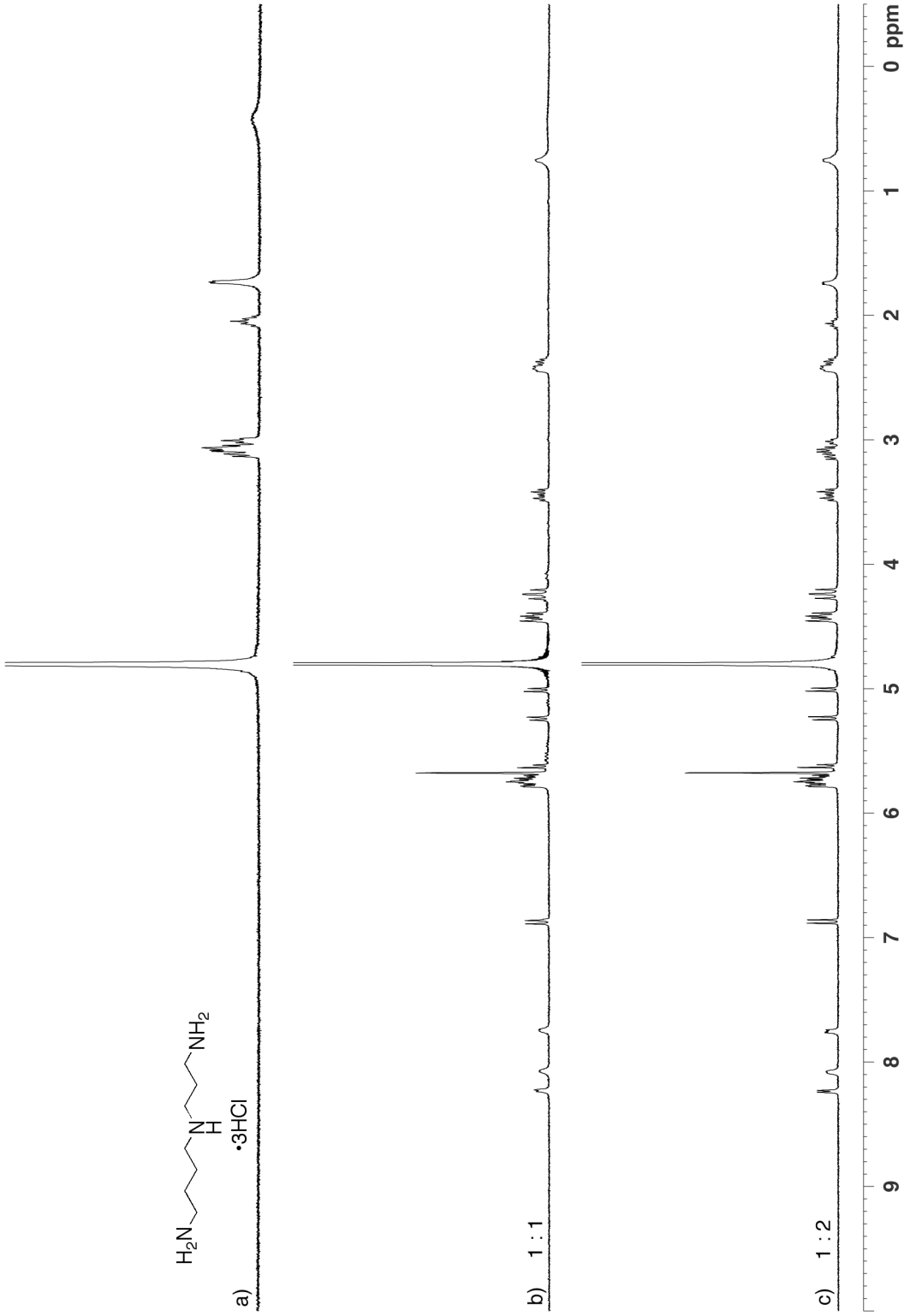

Figure II-S25. ^{1}H NMR spectra recorded (D_2O, 400 MHz, RT) for: a) **II-33** (0.5 mM), b) a mixture of **II-19** (0.5 mM) and **II-33** (0.5 mM), and c) a mixture of **II-19** (0.5 mM) and **II-33** (1 mM).

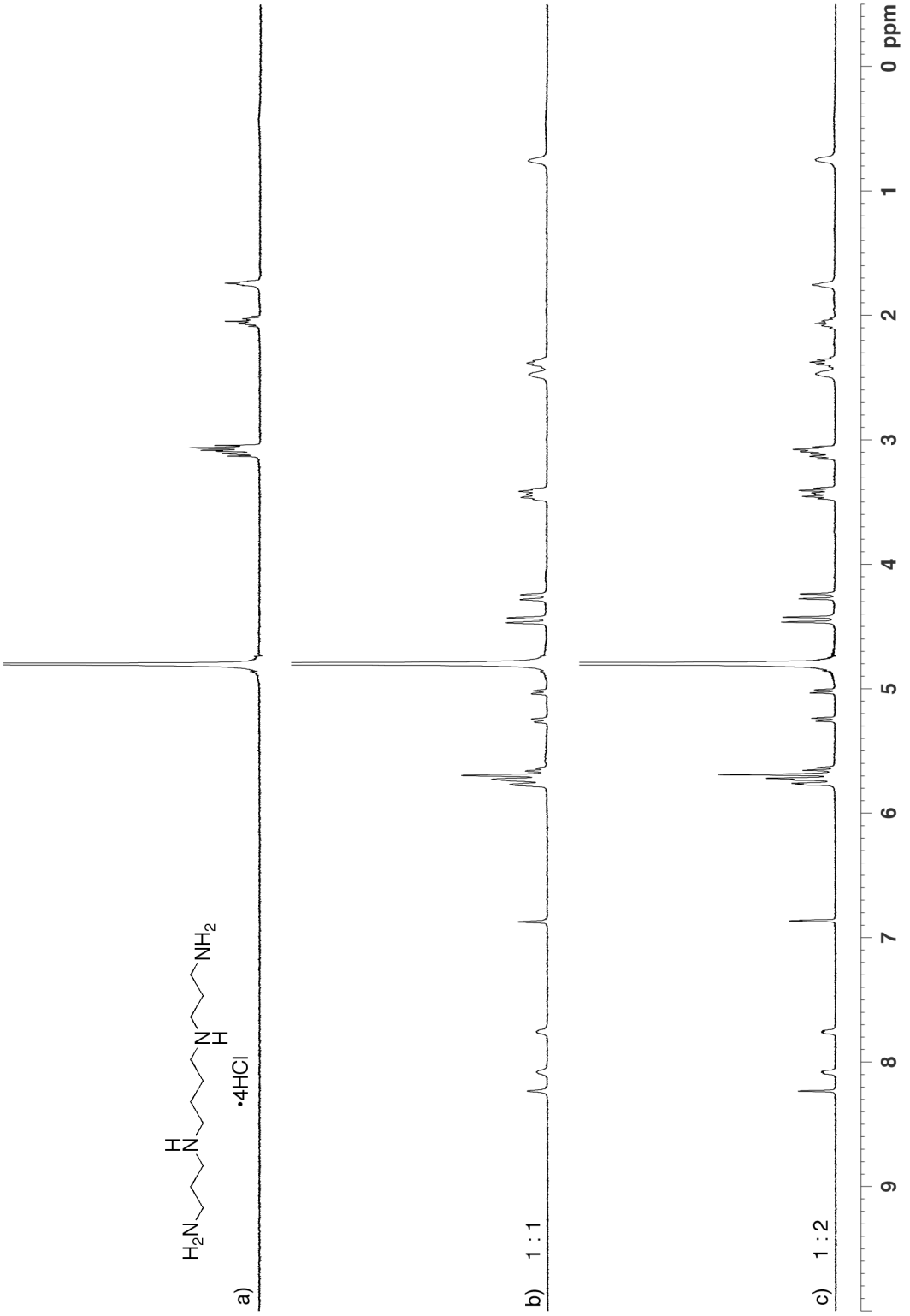

Figure II-S26. ^{1}H NMR spectra recorded (D_2O, 400 MHz, RT) for: a) **II-32** (0.5 mM), b) a mixture of **II-19** (0.5 mM) and **II-32** (0.5 mM), and c) a mixture of **II-19** (0.5 mM) and **II-32** (1 mM).

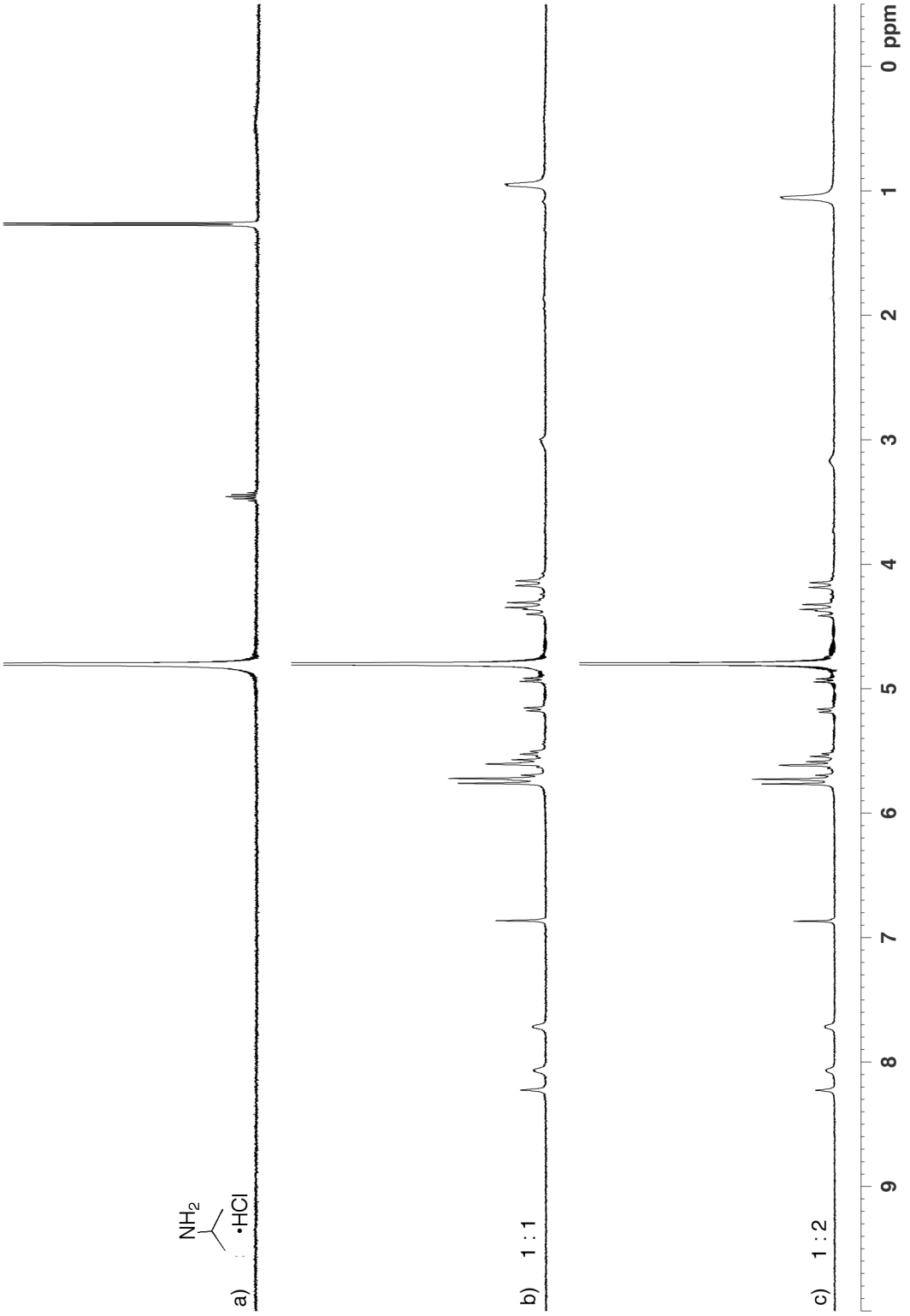

Figure II-S27. ^{1}H NMR spectra recorded (D_2O, 400 MHz, RT) for: a) **II-30** (0.5 mM), b) a mixture of **II-19** (0.5 mM) and **II-30** (0.5 mM), and c) a mixture of **II-19** (0.5 mM) and **II-30** (1 mM).

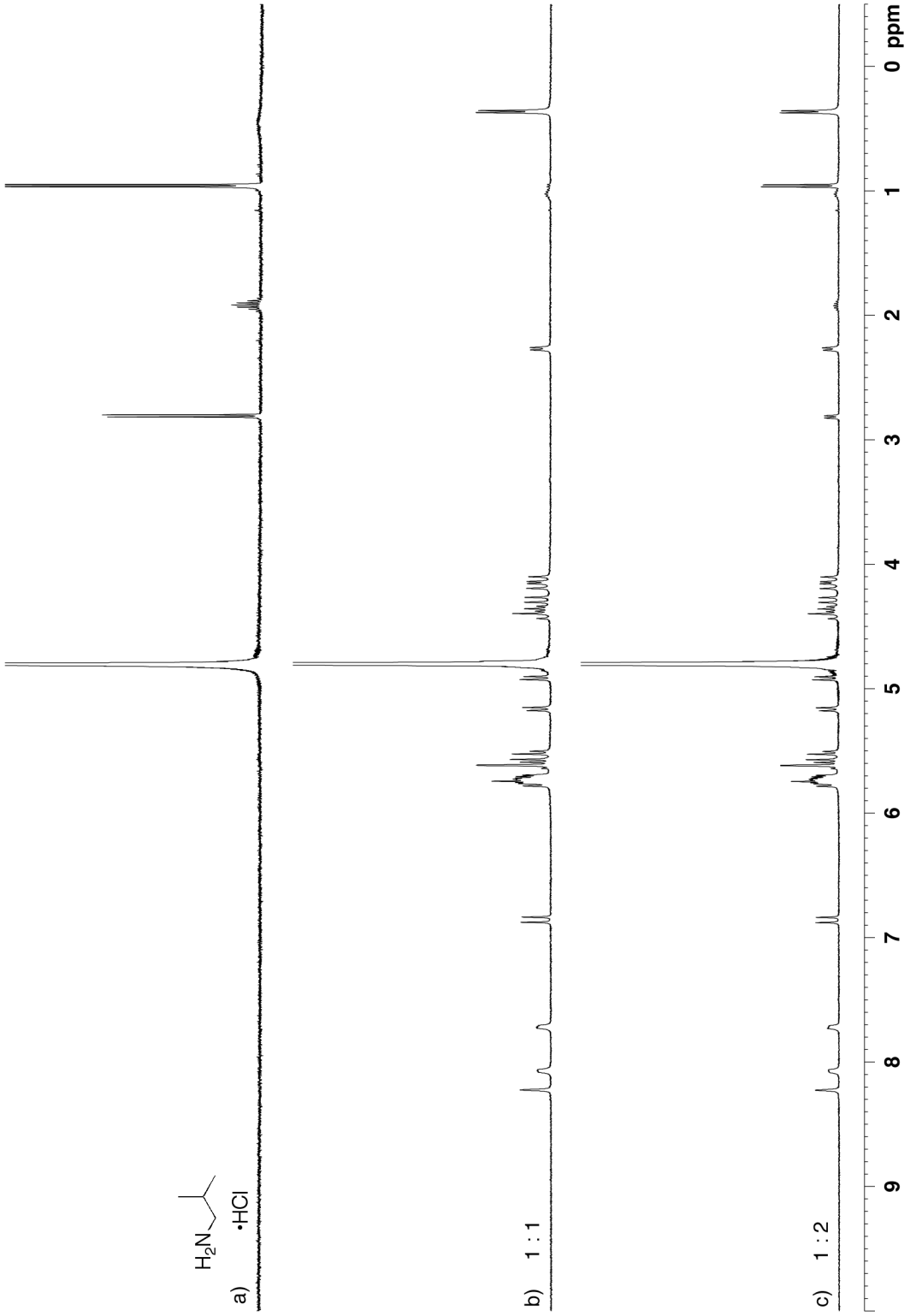

Figure II-S28. ^{1}H NMR spectra recorded (D_2O, 400 MHz, RT) for: a) **II-31** (0.5 mM), b) a mixture of **II-19** (0.5 mM) and **II-31** (0.5 mM), and c) a mixture of **II-19** (0.5 mM) and **II-31** (1 mM).

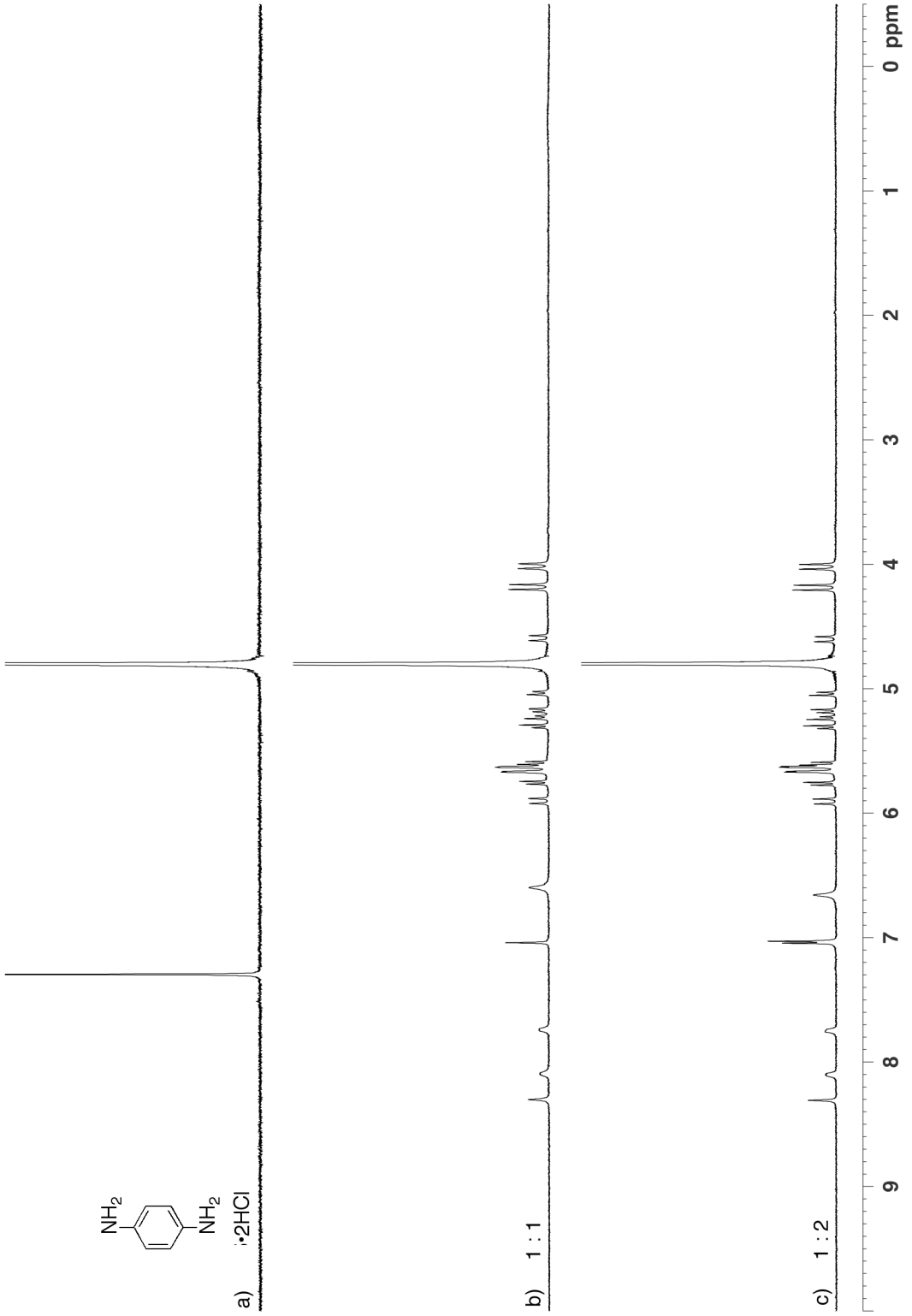

Figure II-S29. ^{1}H NMR spectra recorded (D_2O, 400 MHz, RT) for: a) **II-25** (0.5 mM), b) a mixture of **II-19** (0.5 mM) and **II-25** (0.5 mM), and c) a mixture of **II-19** (0.5 mM) and **II-25** (1 mM).

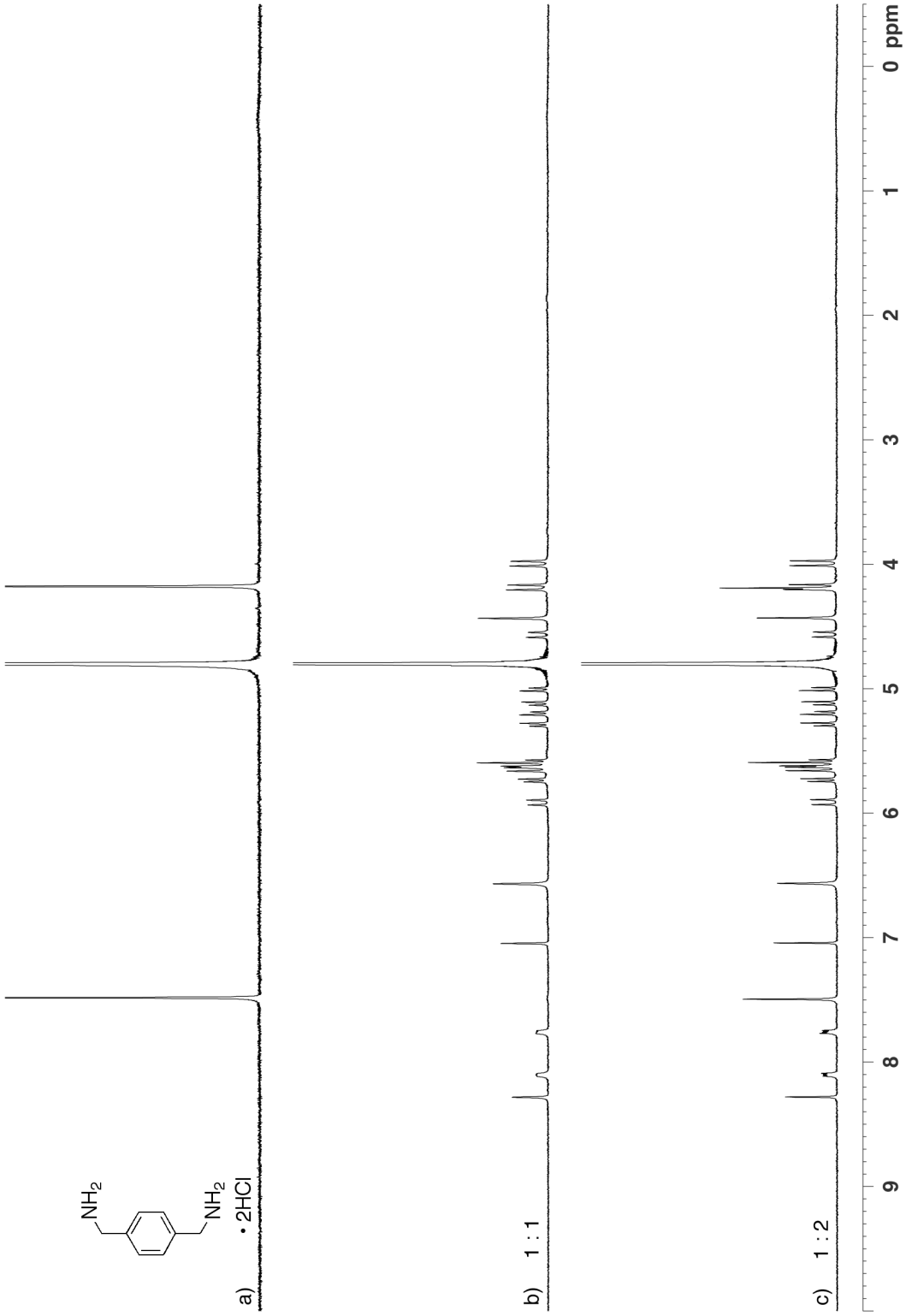

Figure II-S30. ^{1}H NMR spectra recorded (D_2O, 400 MHz, RT) for: a) **II-11** (0.5 mM), b) a mixture of **II-19** (0.5 mM) and **II-11** (0.5 mM), and c) a mixture of **II-19** (0.5 mM) and **II-11** (1 mM).

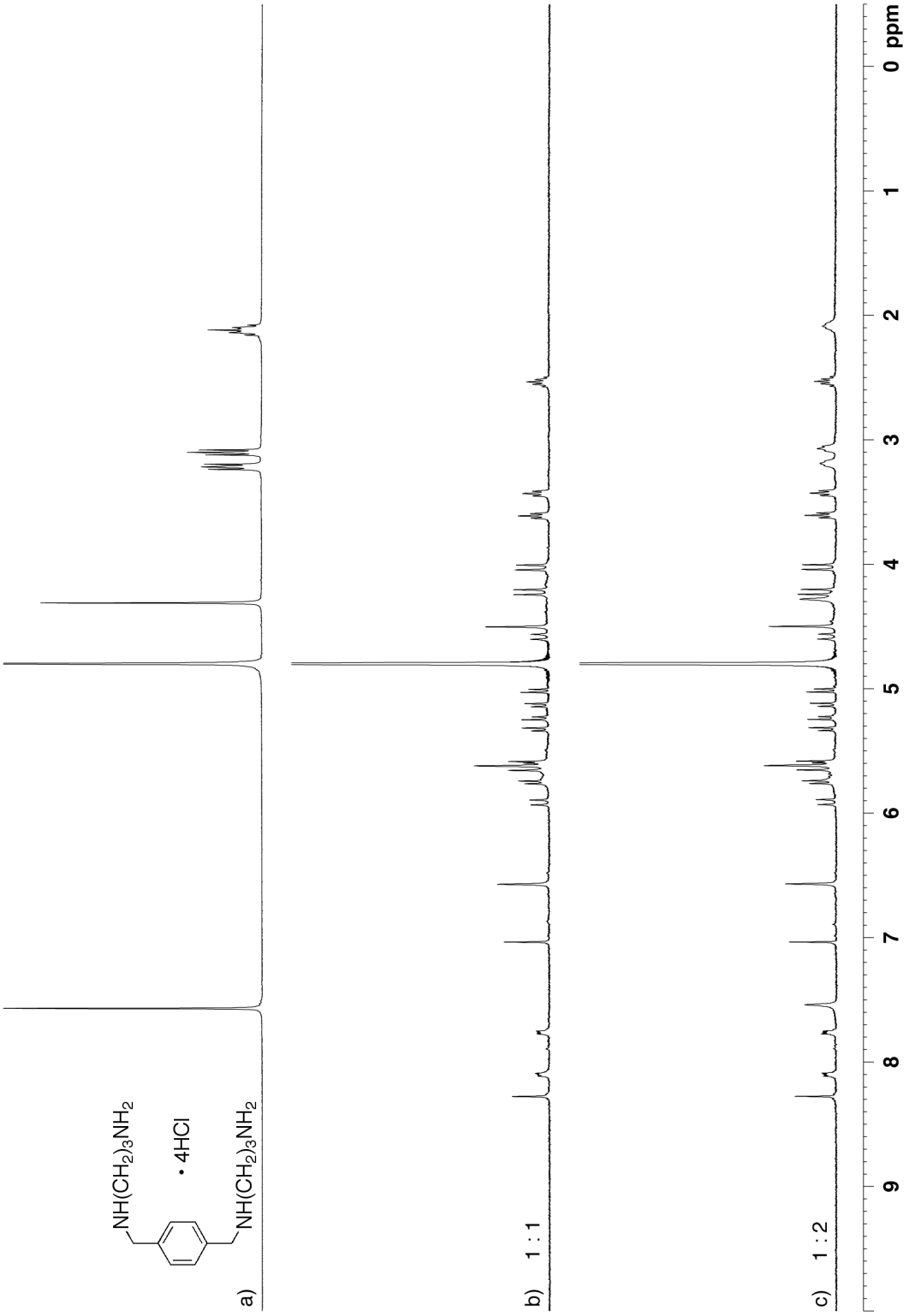

Figure II-S31. ^{1}H NMR spectra recorded (D_2O, 400 MHz, RT) for: a) **II-26** (0.5 mM), b) a mixture of **II-19** (0.5 mM) and **II-26** (0.5 mM), and c) a mixture of **II-19** (0.5 mM) and **II-26** (1 mM).

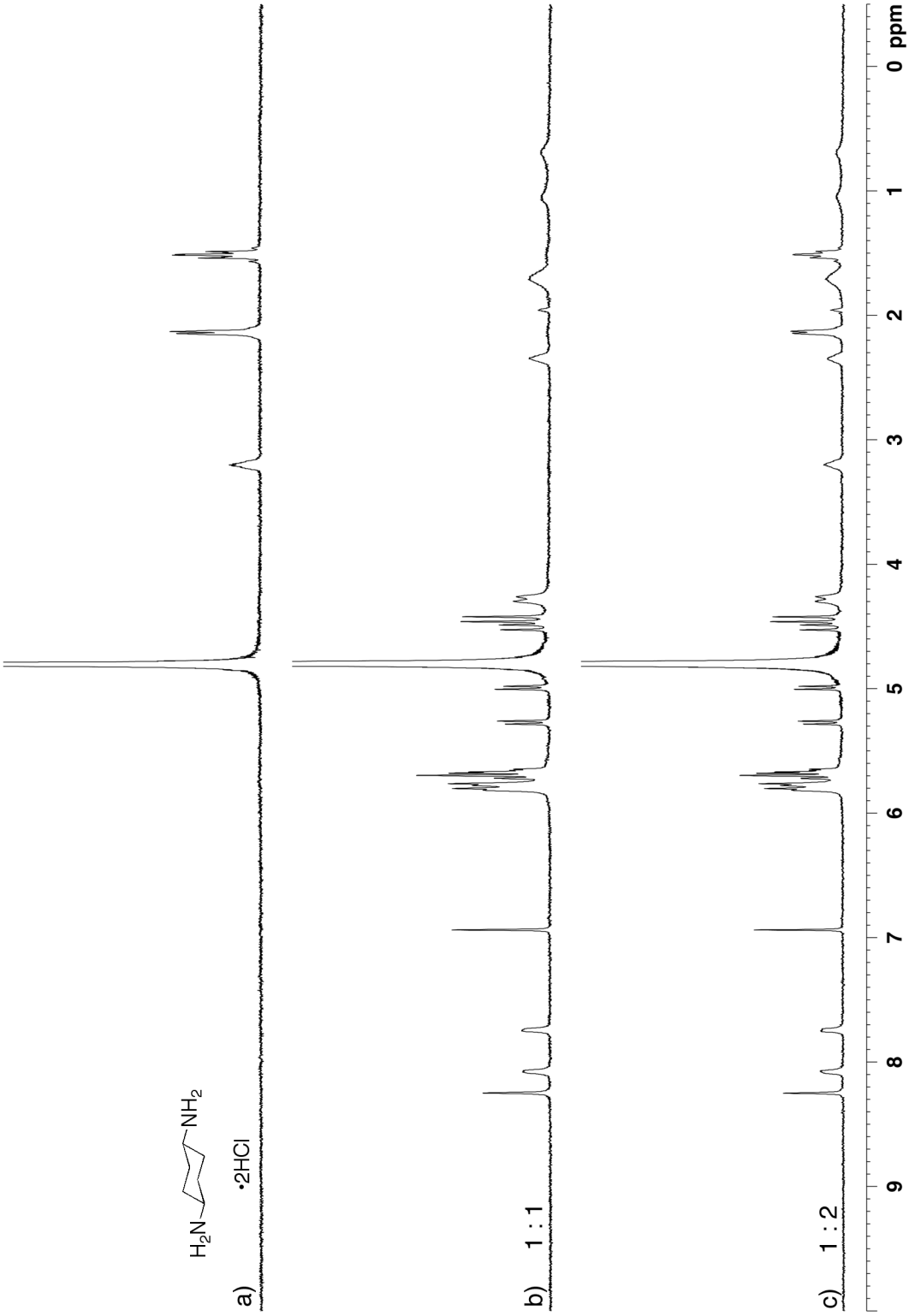

Figure II-S32. ^{1}H NMR spectra recorded (D_2O, 400 MHz, RT) for: a) **II-28** (0.5 mM), b) a mixture of **II-19** (0.5 mM) and **II-28** (0.5 mM), and c) a mixture of **II-19** (0.5 mM) and **II-28** (1 mM).

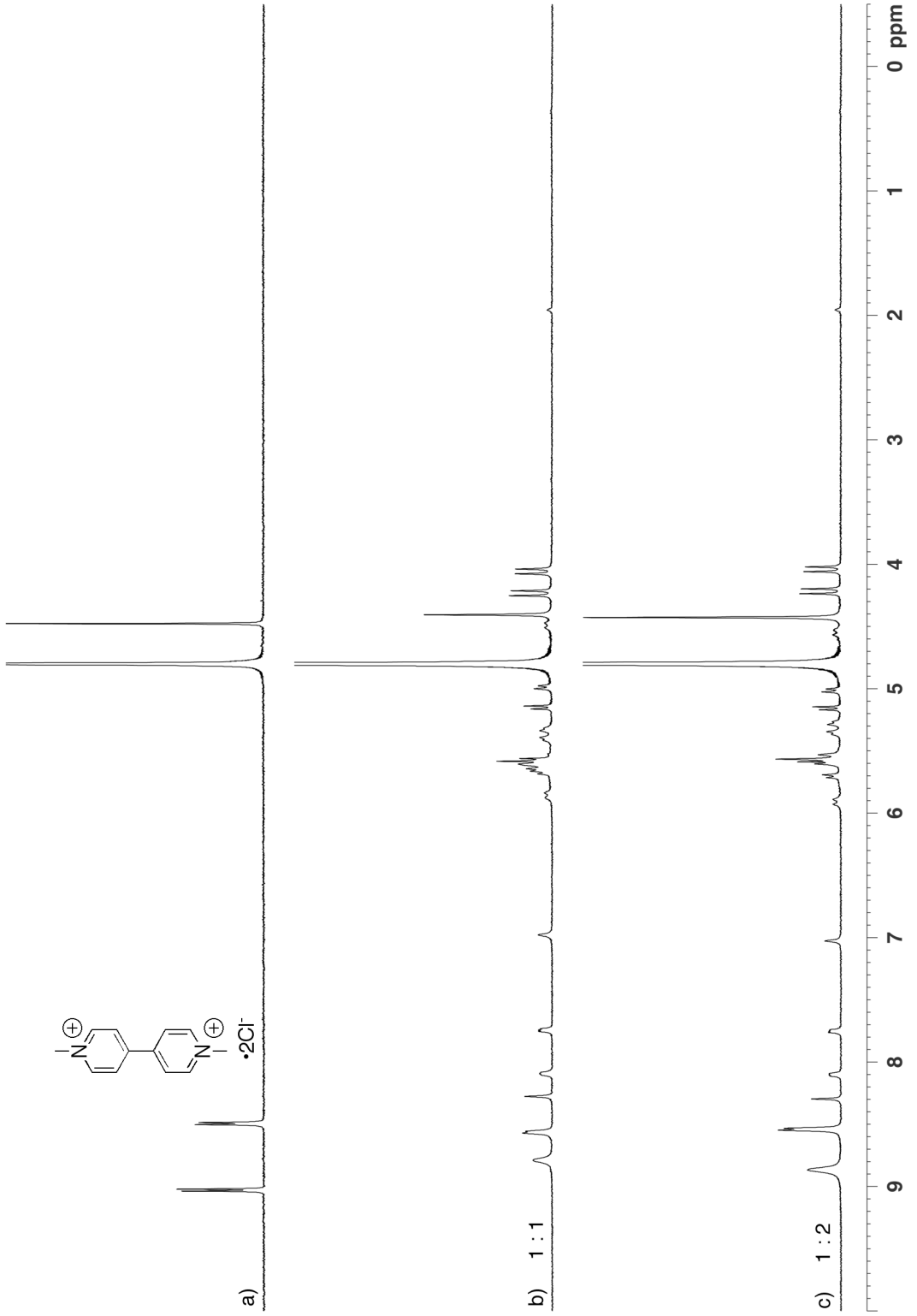

Figure II-S33. ^{1}H NMR spectra recorded (D_2O, 400 MHz, RT) for: a) **II-27** (0.5 mM), b) a mixture of **II-19** (0.5 mM) and **II-27** (0.5 mM), and c) a mixture of **II-19** (0.5 mM) and **II-27** (1 mM).

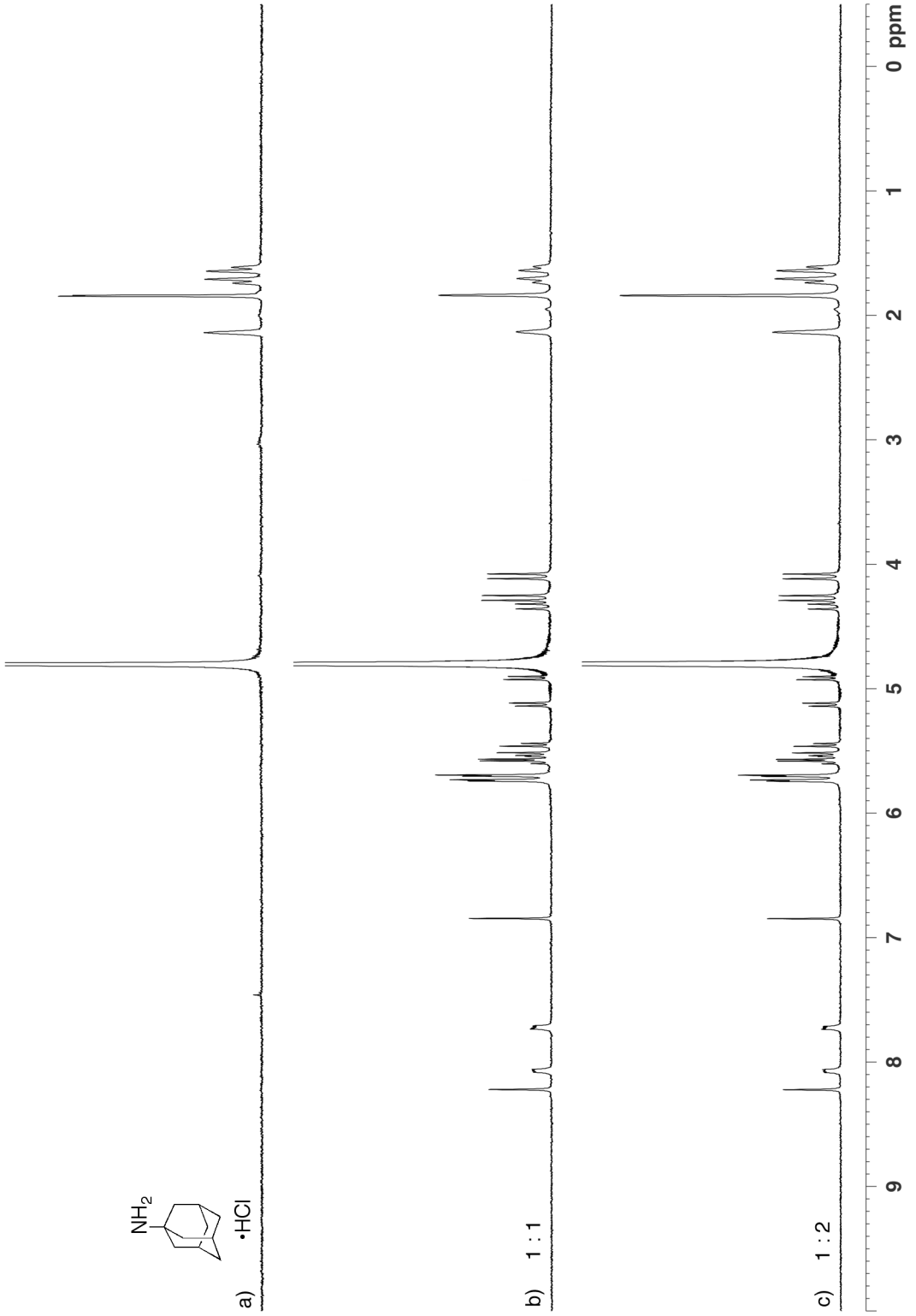

Figure II-S34. ^{1}H NMR spectra recorded (D_2O, 400 MHz, RT) for: a) **II-29** (0.5 mM), b) a mixture of **II-19** (0.5 mM) and **II-29** (0.5 mM), and c) a mixture of **II-19** (0.5 mM) and **II-29** (1 mM). Adamantane ammmonium ion **II-29** does not form an inclusion complex with **II-19**.

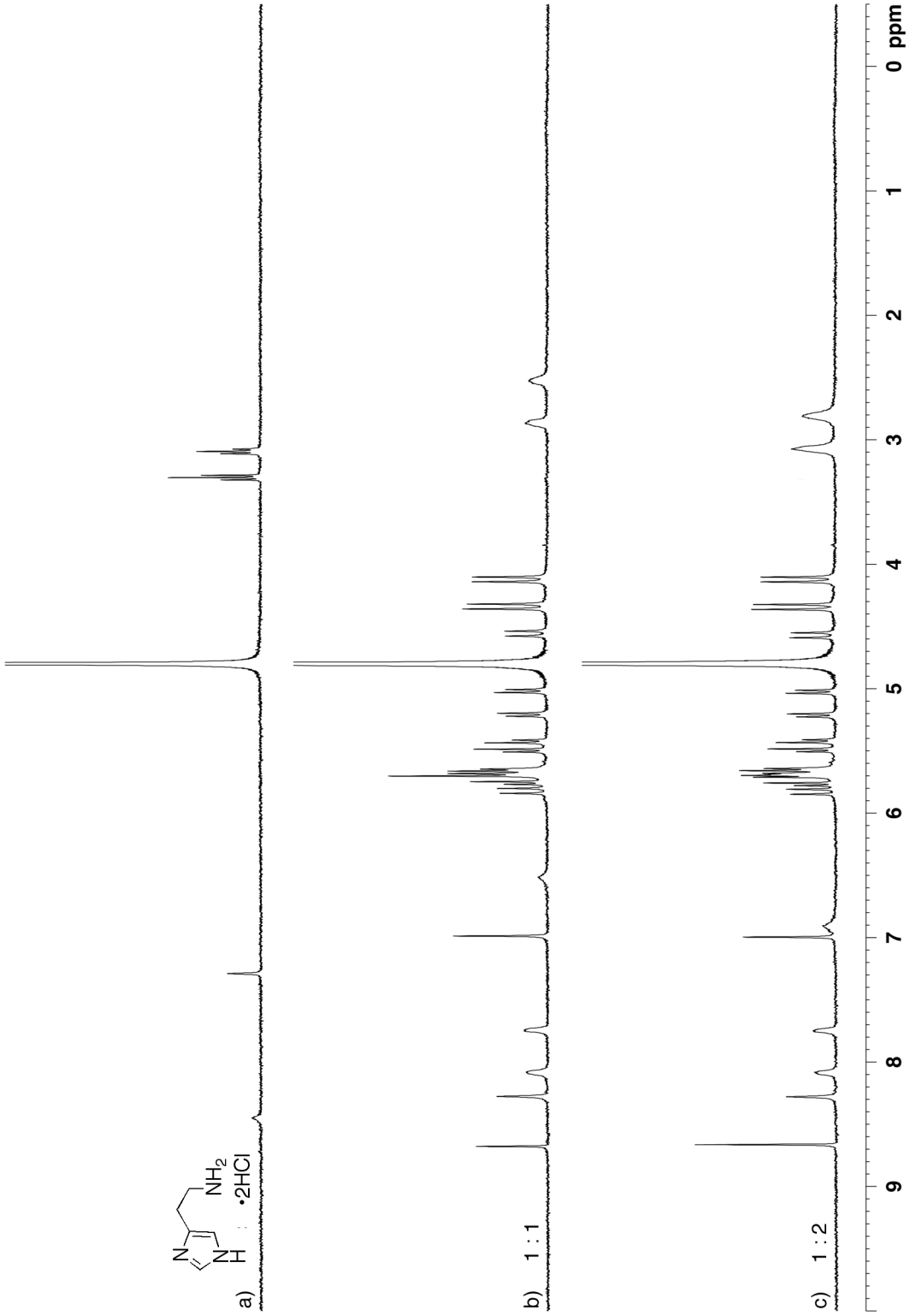

Figure II-S35. ^{1}H NMR spectra recorded (D_2O, 400 MHz, RT) for: a) **II-34** (0.5 mM), b) a mixture of **II-19** (0.5 mM) and **II-34** (0.5 mM), and c) a mixture of **II-19** (0.5 mM) and **II-34** (1 mM).

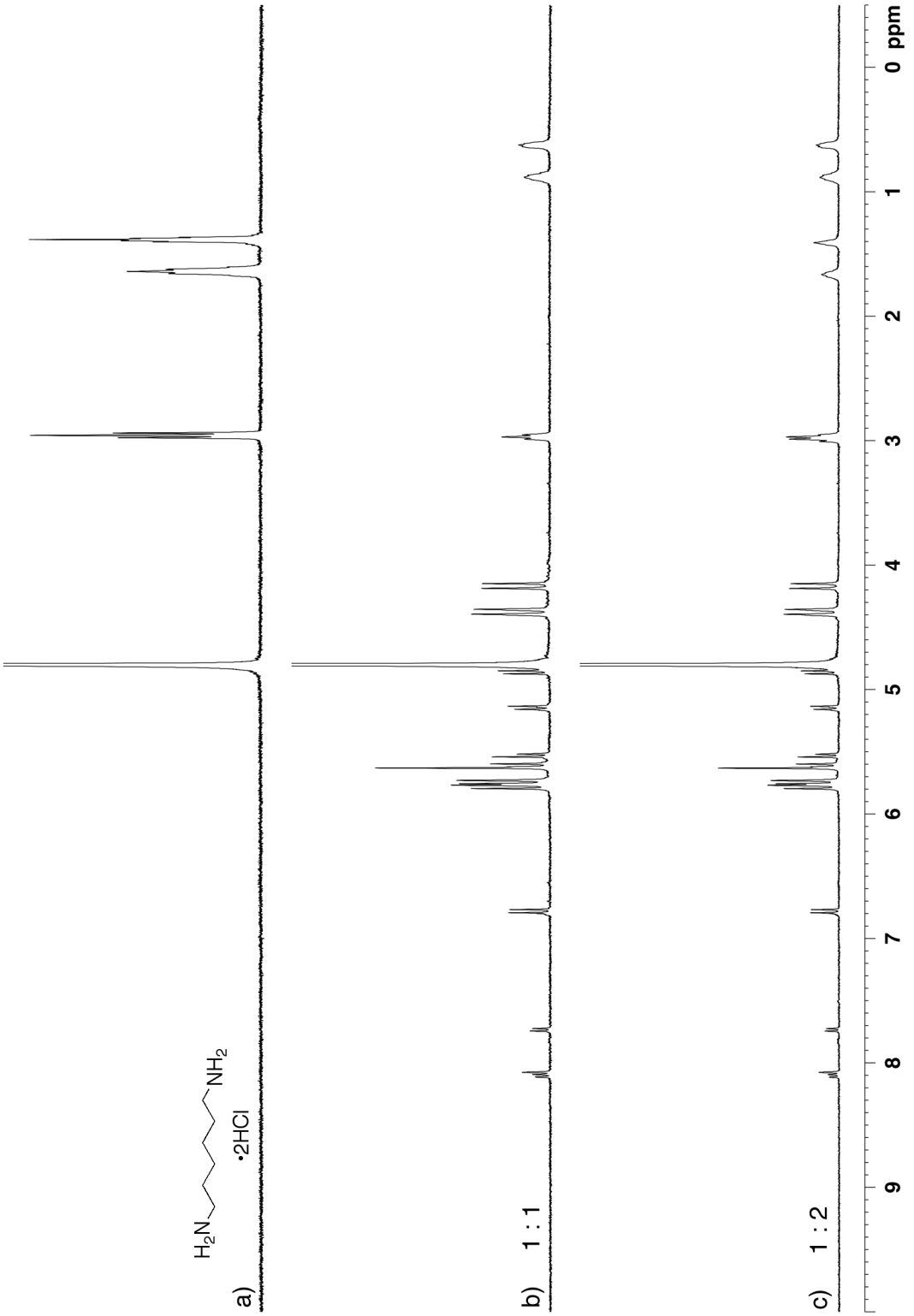

Figure II-S36. ^{1}H NMR spectra recorded (D_2O, 400 MHz, RT) for: a) **II-20** (0.5 mM), b) a mixture of **II-16** (0.5 mM) and **II-20** (0.5 mM), and c) a mixture of **II-16** (0.5 mM) and **II-20** (1 mM).

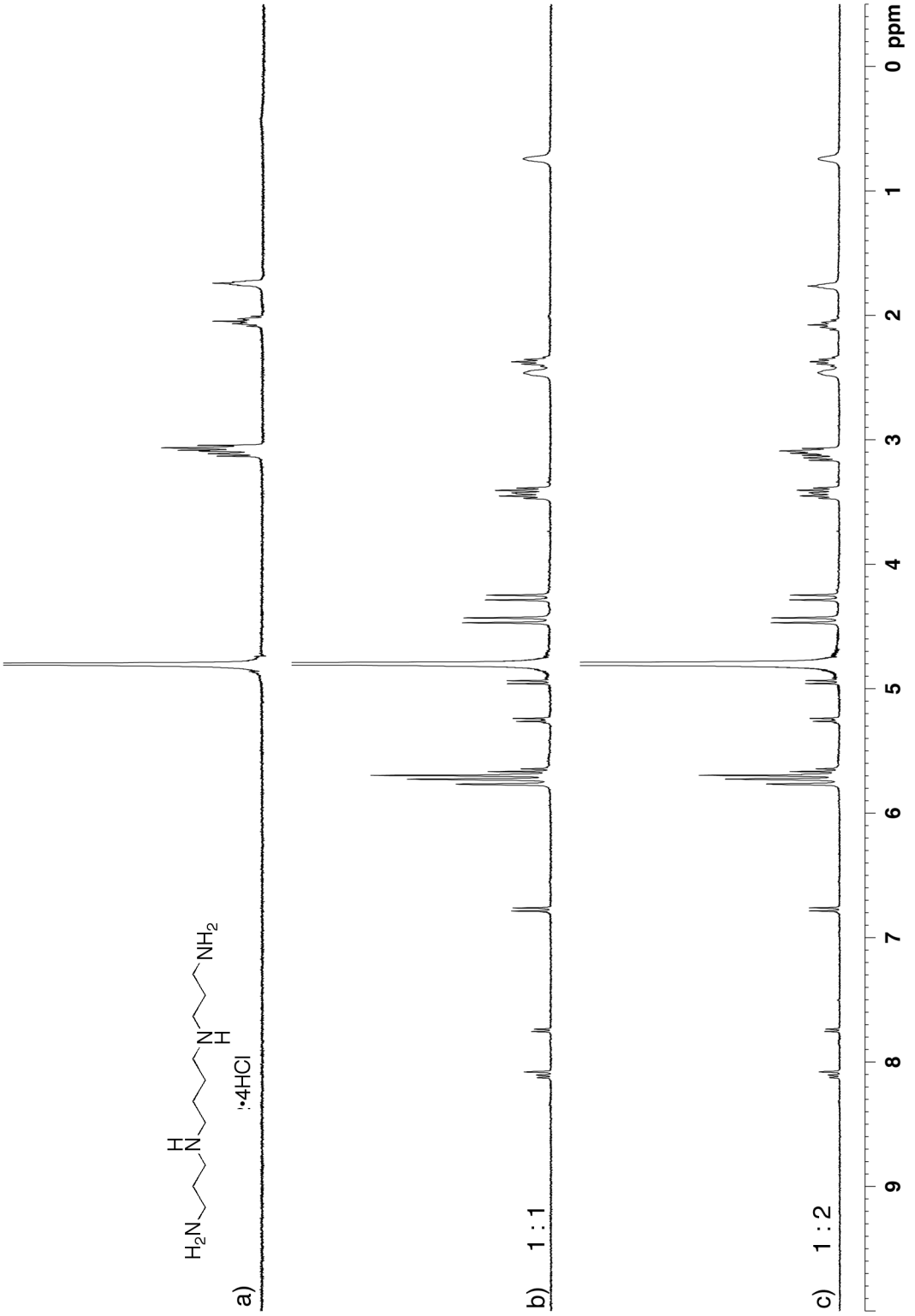

Figure II-S37. ^{1}H NMR spectra recorded (D_2O, 400 MHz, RT) for: a) **II-32** (0.5 mM), b) a mixture of **II-16** (0.5 mM) and **II-32** (0.5 mM), and c) a mixture of **II-16** (0.5 mM) and **II-32** (1 mM).

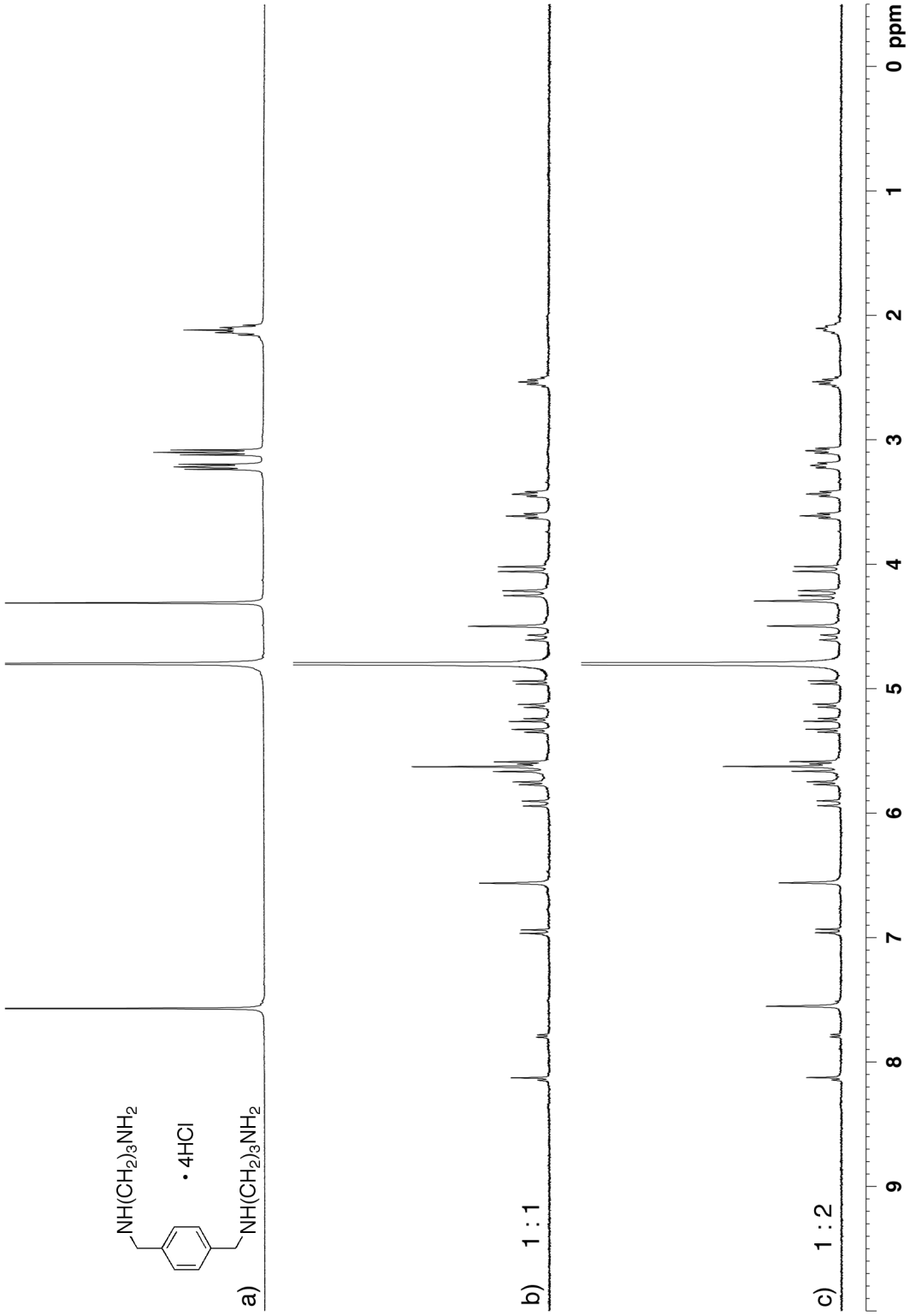

Figure II-S38. ^{1}H NMR spectra recorded (D_2O, 400 MHz, RT) for: a) **II-26** (0.5 mM), b) a mixture of **II-16** (0.5 mM) and **II-26** (0.5 mM), and c) a mixture of **II-16** (0.5 mM) and **II-26** (1 mM).

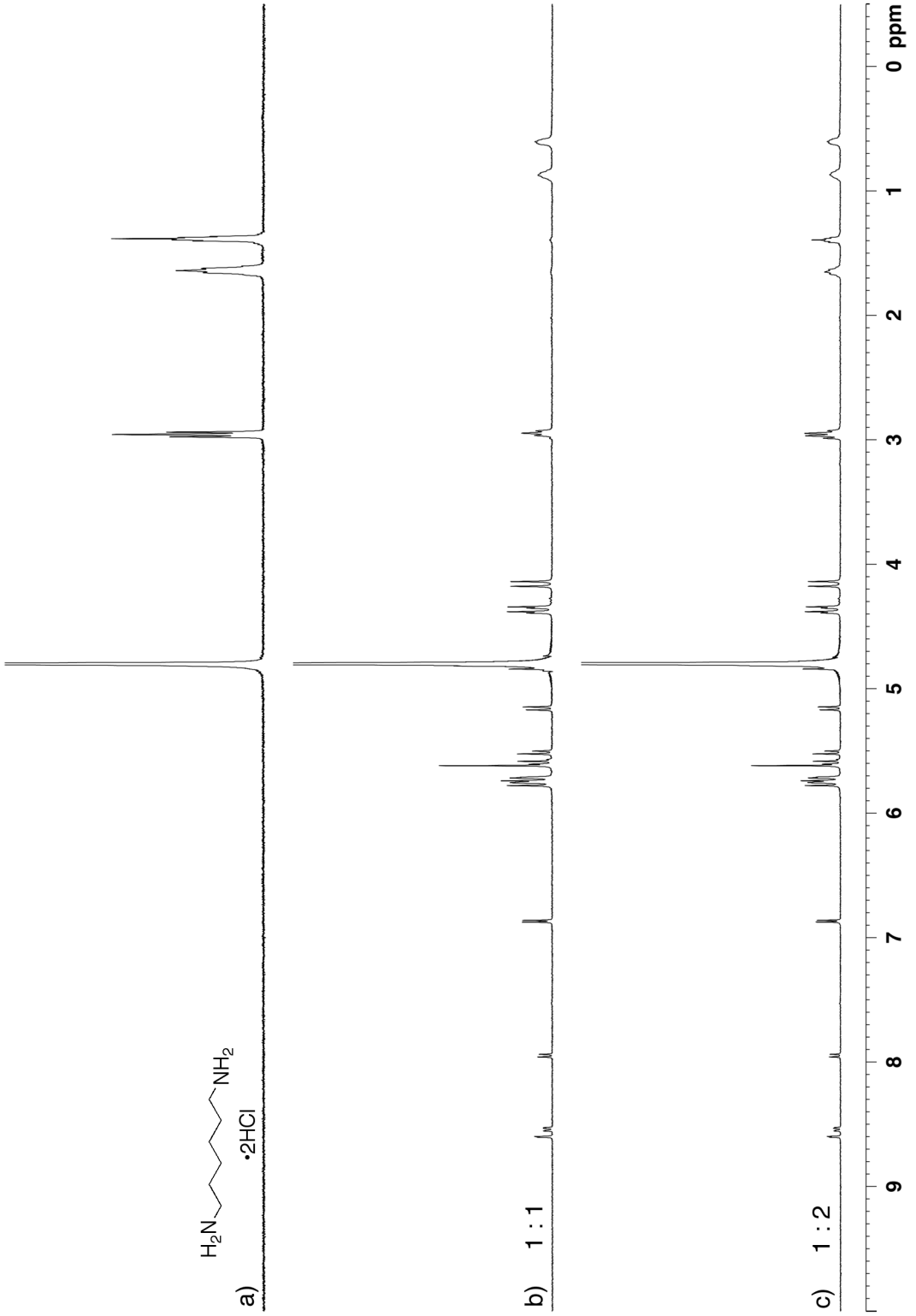

Figure II-S39. ^{1}H NMR spectra recorded (D_2O, 400 MHz, RT) for: a) **II-20** (0.5 mM), b) a mixture of **II-17** (0.5 mM) and **II-20** (0.5 mM), and c) a mixture of **II-17** (0.5 mM) and **II-20** (1 mM).

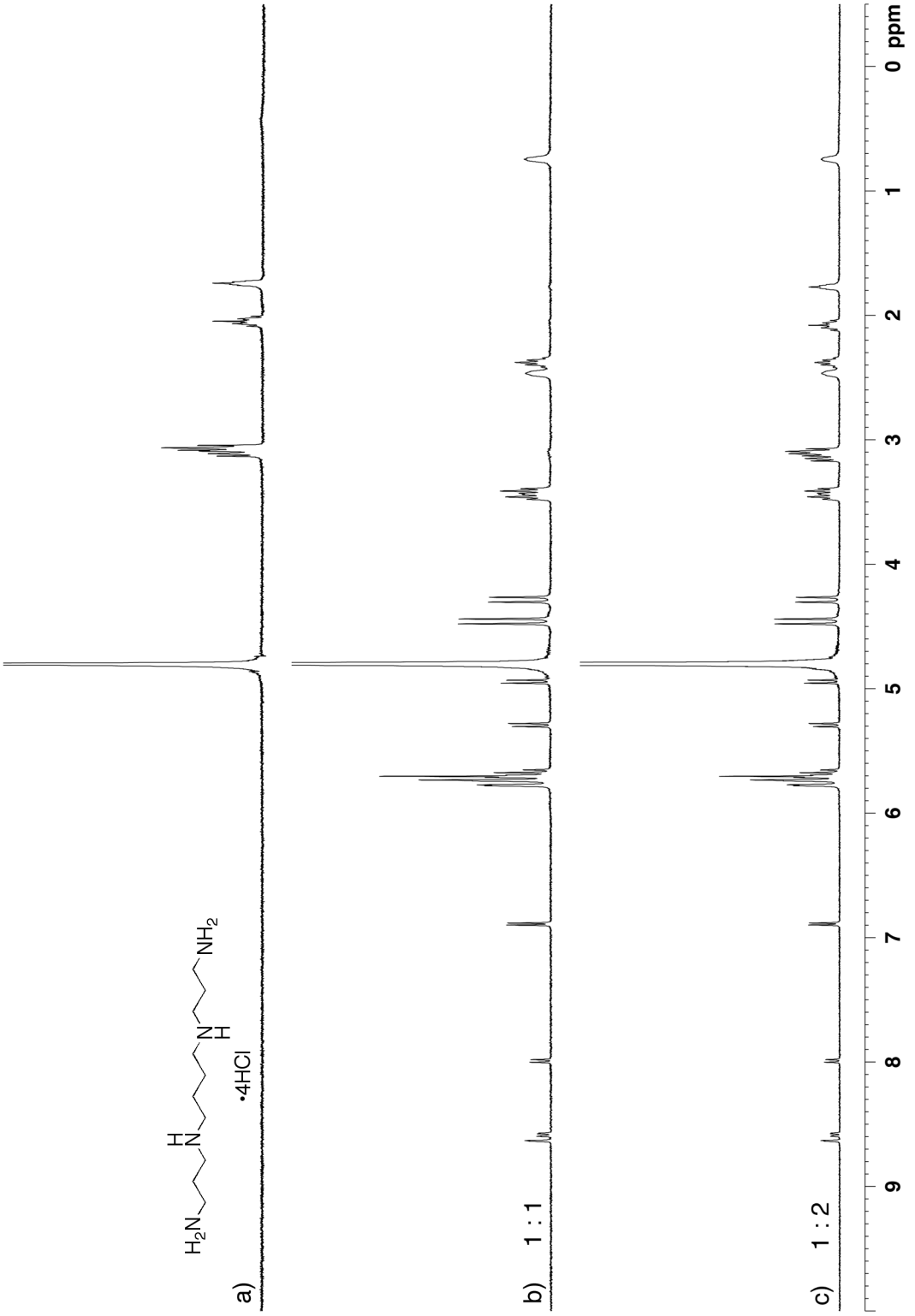

Figure II-S40. ^{1}H NMR spectra recorded (D_2O, 400 MHz, RT) for: a) **II-32** (0.5 mM), b) a mixture of **II-17** (0.5 mM) and **II-32** (0.5 mM), and c) a mixture of **II-17** (0.5 mM) and **II-32** (1 mM).

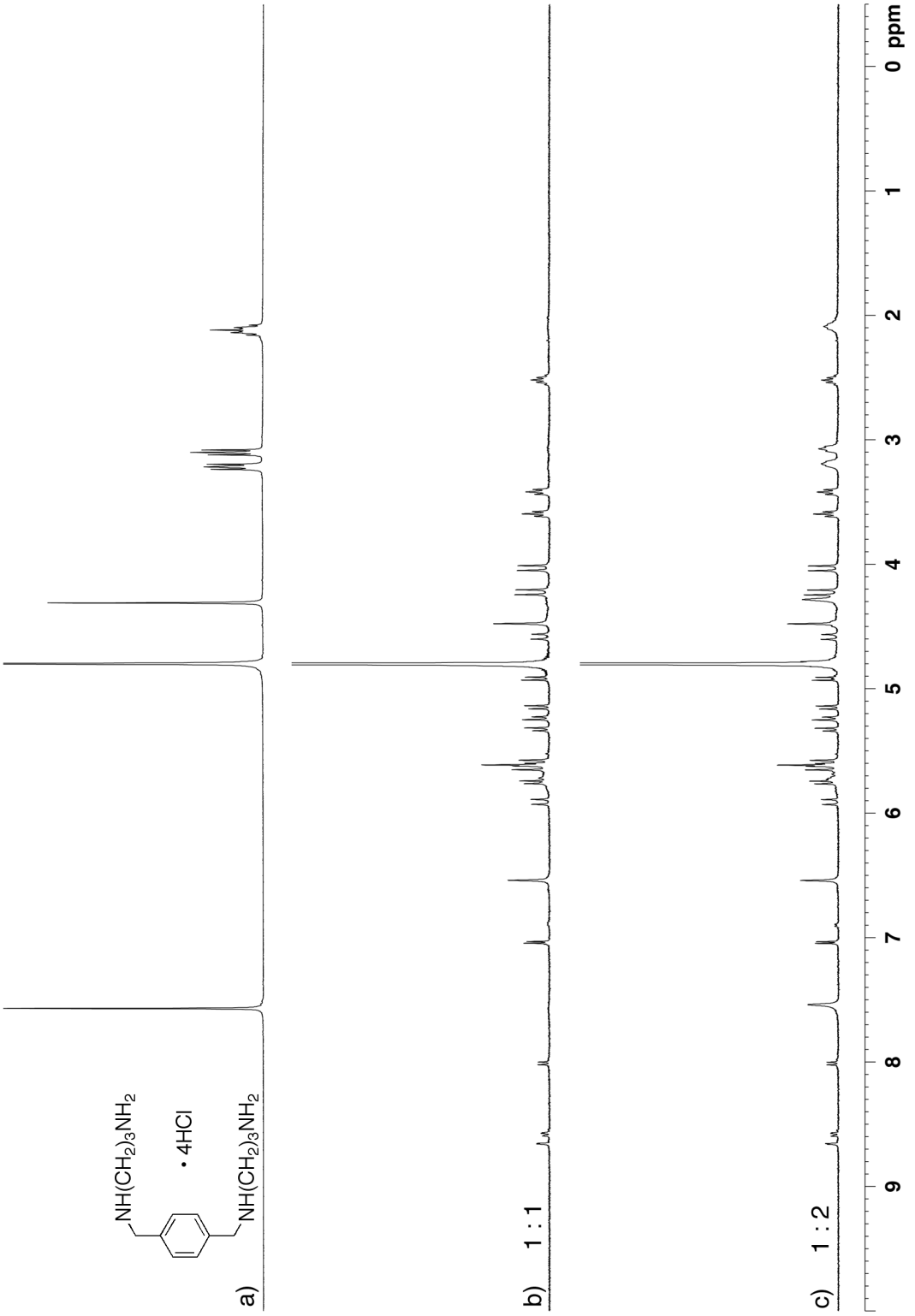

Figure II-S41. ^{1}H NMR spectra recorded (D_2O, 400 MHz, RT) for: a) **II-26** (0.5 mM), b) a mixture of **II-17** (0.5 mM) and **II-26** (0.5 mM), and c) a mixture of **II-17** (0.5 mM) and **II-26** (1 mM).

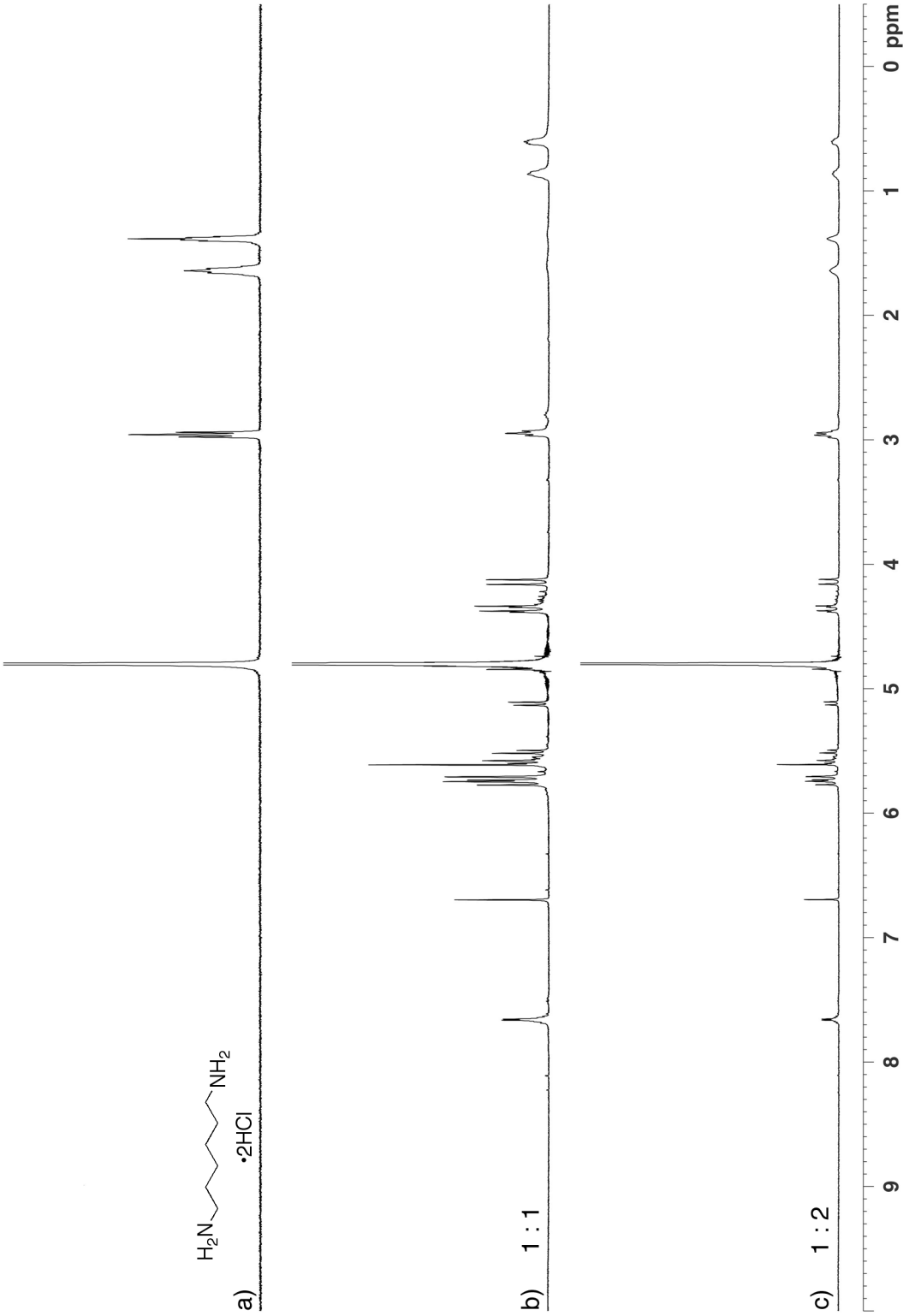

Figure II-S42. ^{1}H NMR spectra recorded (D_2O, 400 MHz, RT) for: a) **II-20** (0.5 mM), b) a mixture of **II-13** (0.5 mM) and **II-20** (0.5 mM), and c) a mixture of **II-13** (0.5 mM) and **II-20** (1 mM).

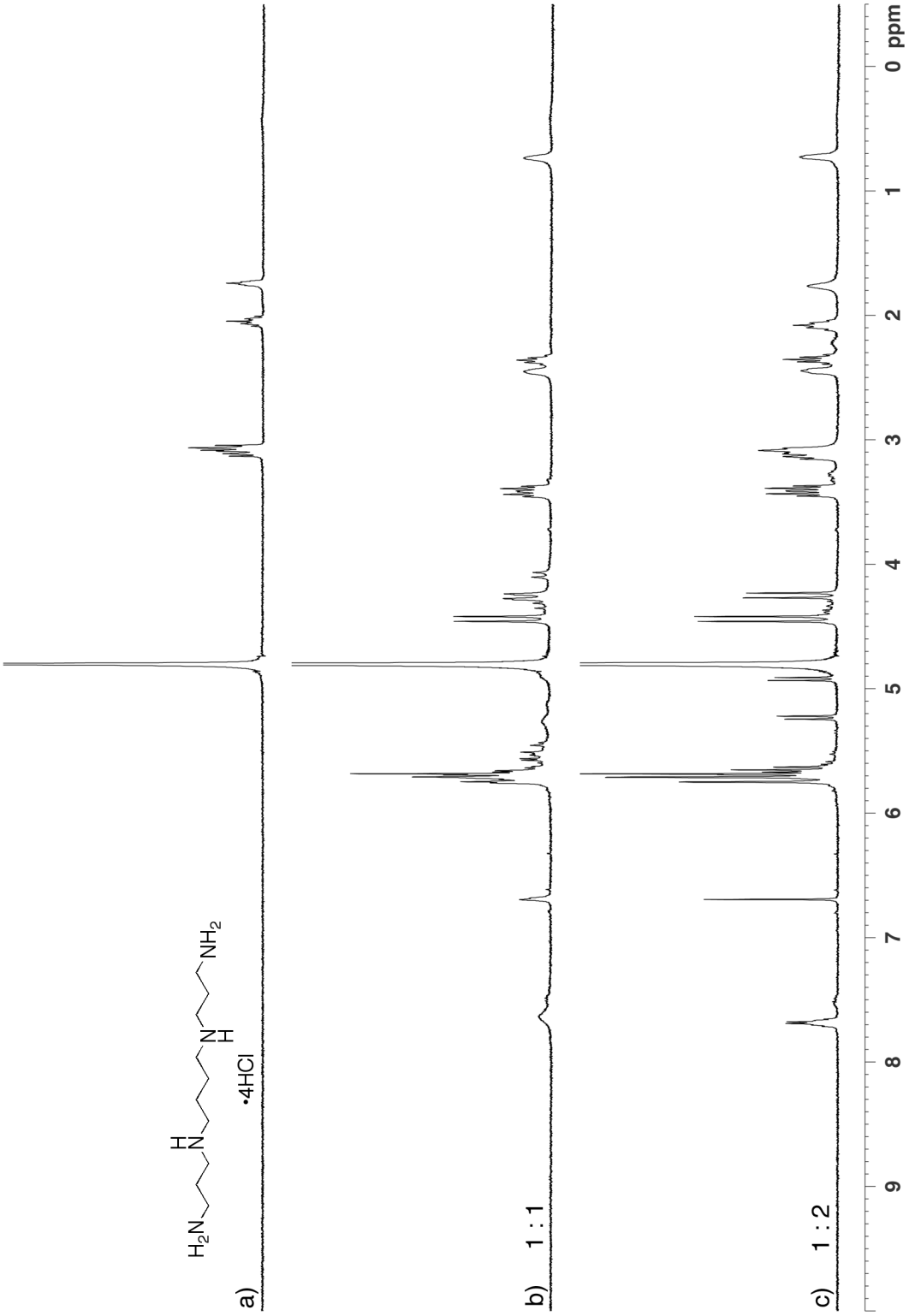

Figure II-S43. ^{1}H NMR spectra recorded (D_2O, 400 MHz, RT) for: a) **II-32** (0.5 mM), b) a mixture of **II-13** (0.5 mM) and **II-32** (0.5 mM), and c) a mixture of **II-13** (0.5 mM) and **II-32** (1 mM).

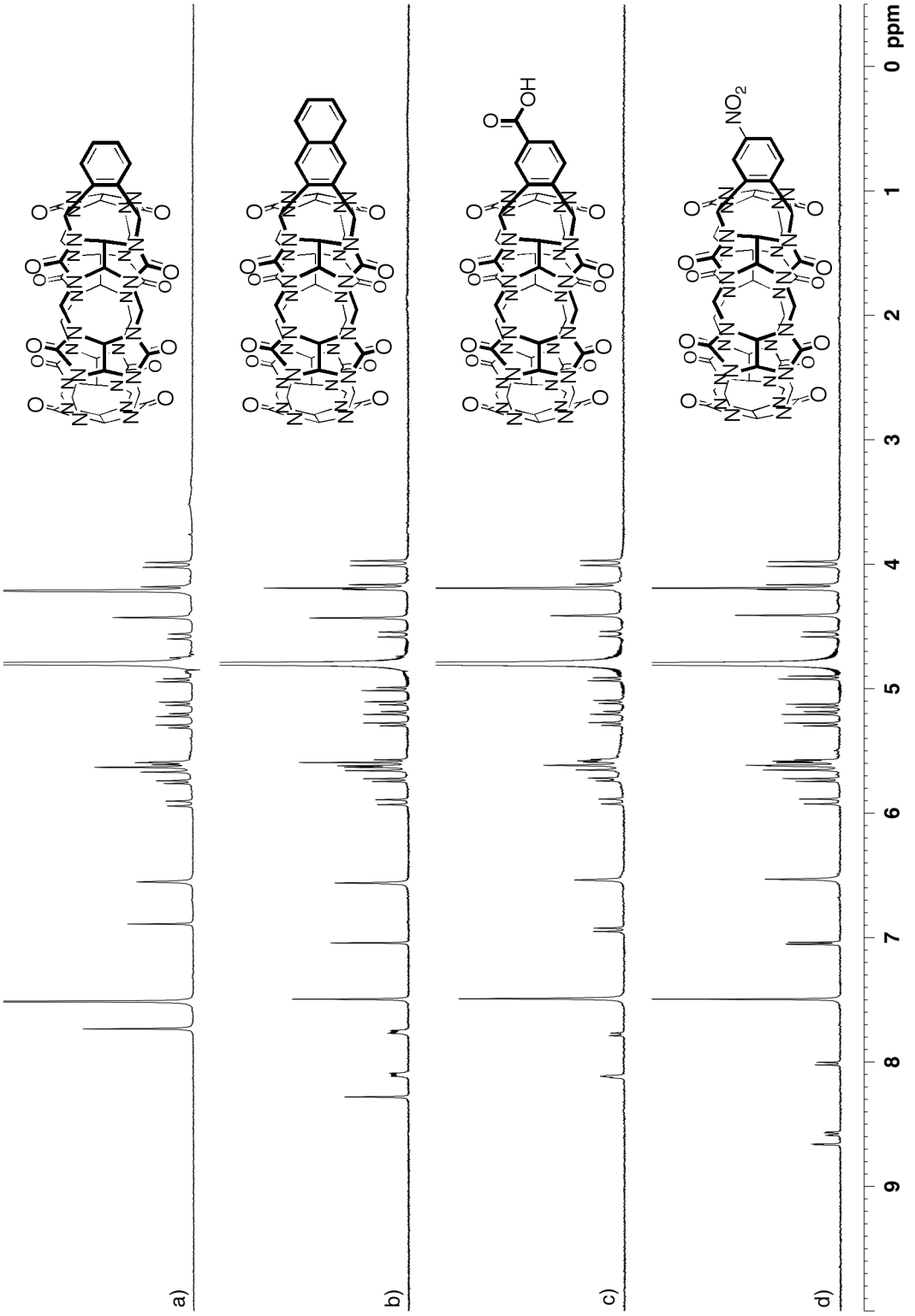

Figure II-S44. ^{1}H NMR spectra recorded (D_2O, 400 MHz, RT) for hosts as Host•**II-11** complexes: a) **II-13**, b) **II-19**, c) **II-16**, and d) **II-17.**

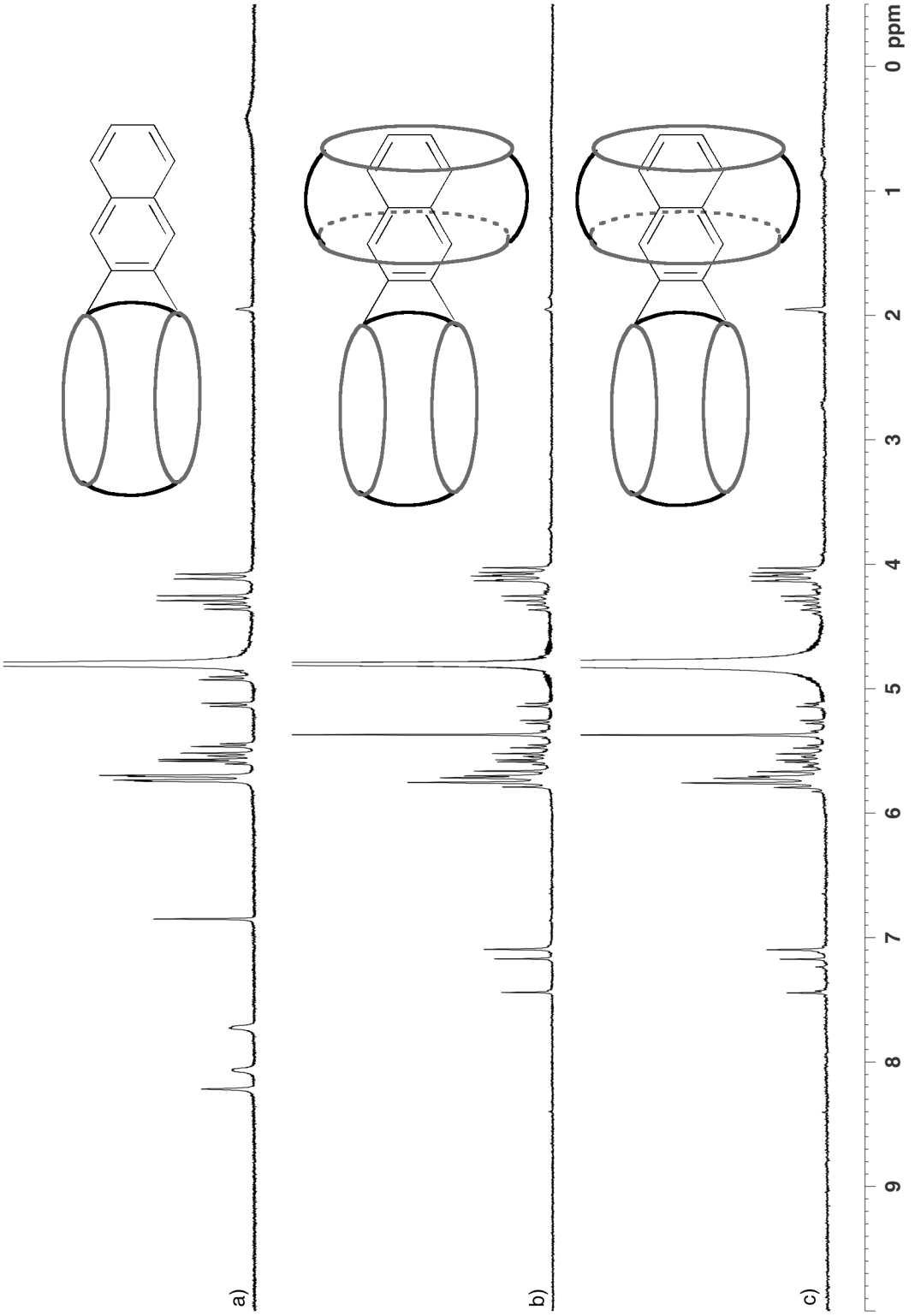

Figure II-S45. ^{1}H NMR spectra recorded (400 MHz, 20 mM $NaCO_2CD_3$ buffer, pD = 4.74, RT) for: a) **II-19** (0.5 mM), b) a mixture of **II-19** (0.5 mM) and CB[7] (0.5 mM), and c) a mixture of **II-19** (0.1 mM) and CB[7] (0.1 mM).

Determination of self-association:
Self-association Model Used in Scientist.
All calculations were performed on a personal computer running Scientist.

Model used to calculate the self-association of **II-13** using NMR titration.

```
// Micromath Scientist Model File
// self-association model for NMR
IndVars: conctot
DepVars: Deltaobs
Params: Ka, Deltasat, Deltazero
Ka = concBound/(concFree*concFree)
concTot=concFree + concBound/2
Deltaobs = Deltazero + (Deltasat - Deltazero) * (1/2*concBound/concTot)
//Constraints
0 < Ka
0 < concFree < concTot
0 < concBound < concTot
***
```

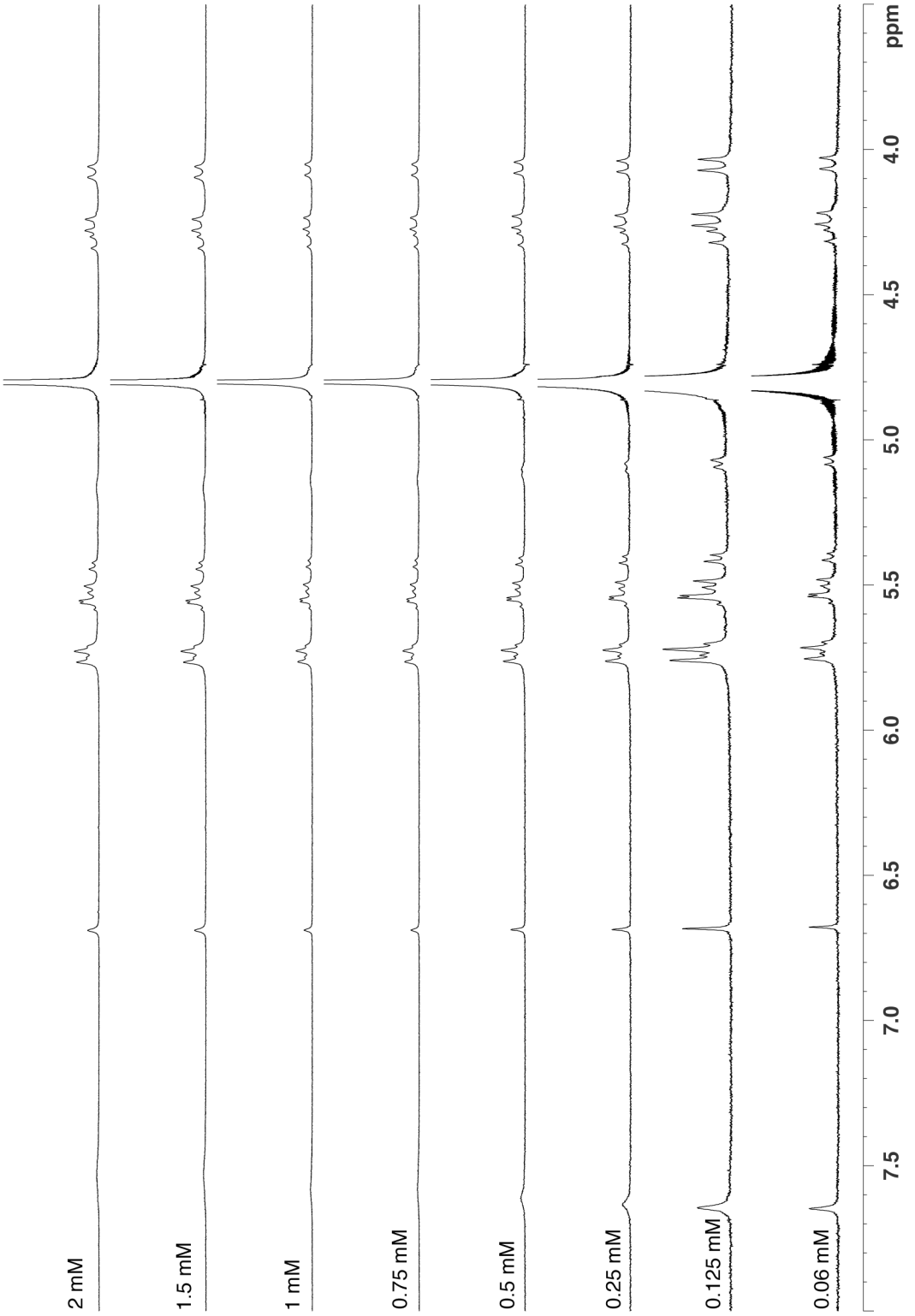

Figure II-S46. ^{1}H NMR spectra (400 MHz, 20 mM $NaCO_2CD_3$ buffer, pD = 4.74, RT) recorded for the self-association of [**II-13**] (2.0 mM – 0.06 mM).

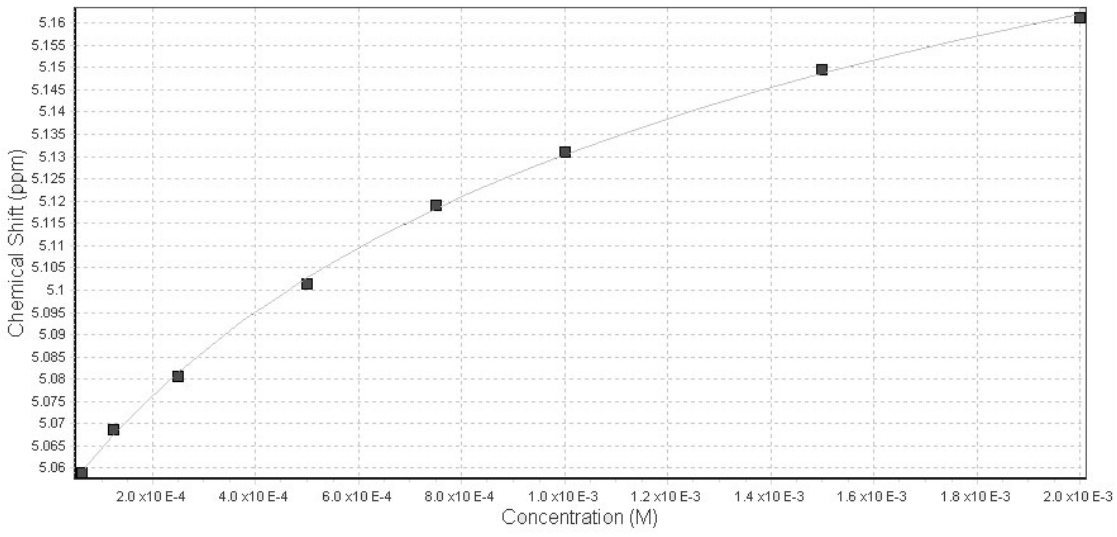

Figure II-S47. Plot of chemical shift versus [**II-13**] created using the data from a ^{1}H NMR dilution experiment (20 mM $NaCO_2CD_3$ buffer, pD = 4.7) of a solution containing **II-13** (0.06-2.00 mM). The solid line is the best non-linear fitting to a 2-fold self association model implemented with Scientist^{TM}. K_a was evaluated as $1.2 \pm 0.1 \times 10^3$ M^{-1}.

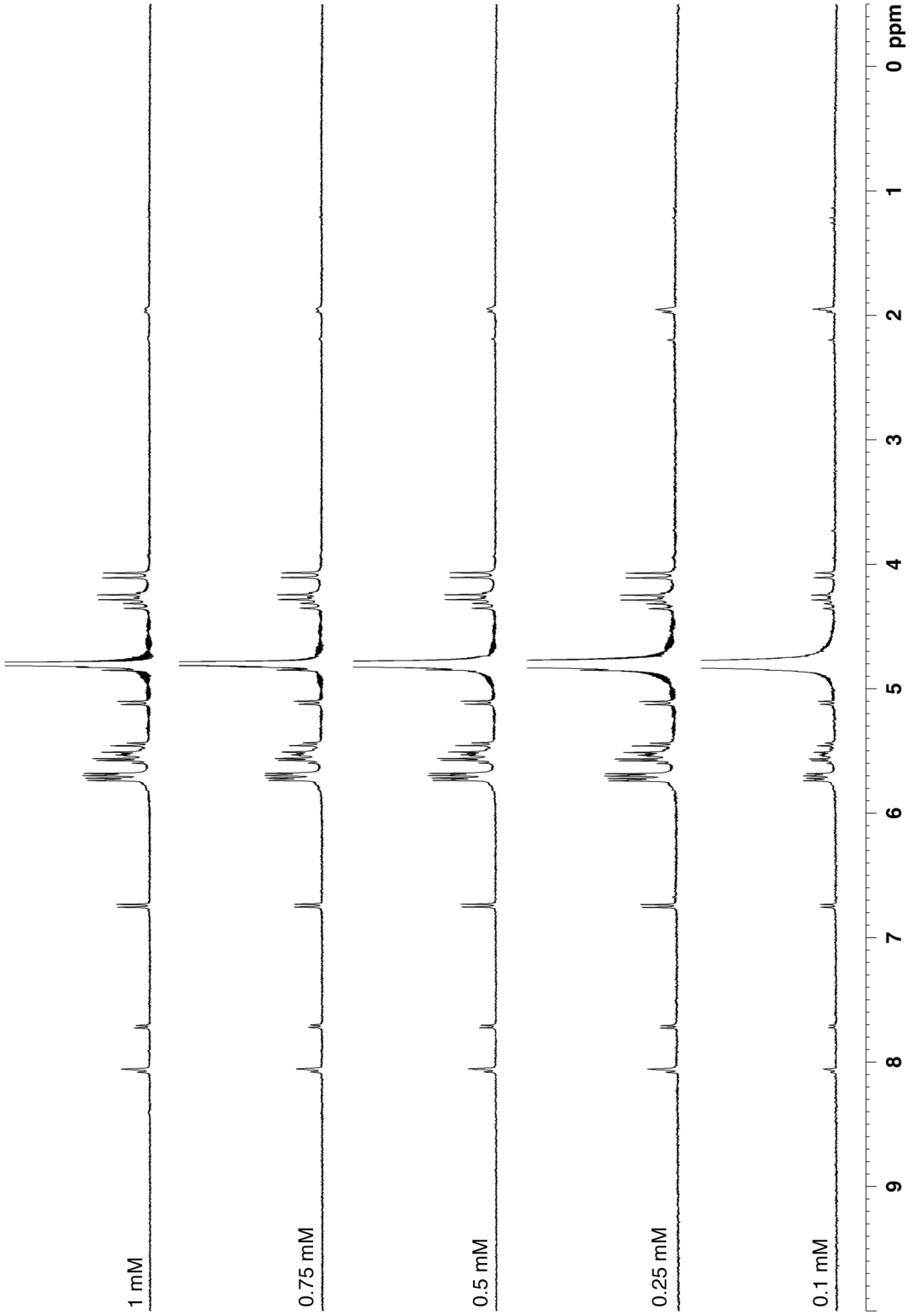

Figure II-S48. ^{1}H NMR spectra (400 MHz, 20 mM $NaCO_2CD_3$ buffer, pD = 4.74, RT) recorded for the dilution of [**II-16**] (1.0 mM – 0.1 mM).

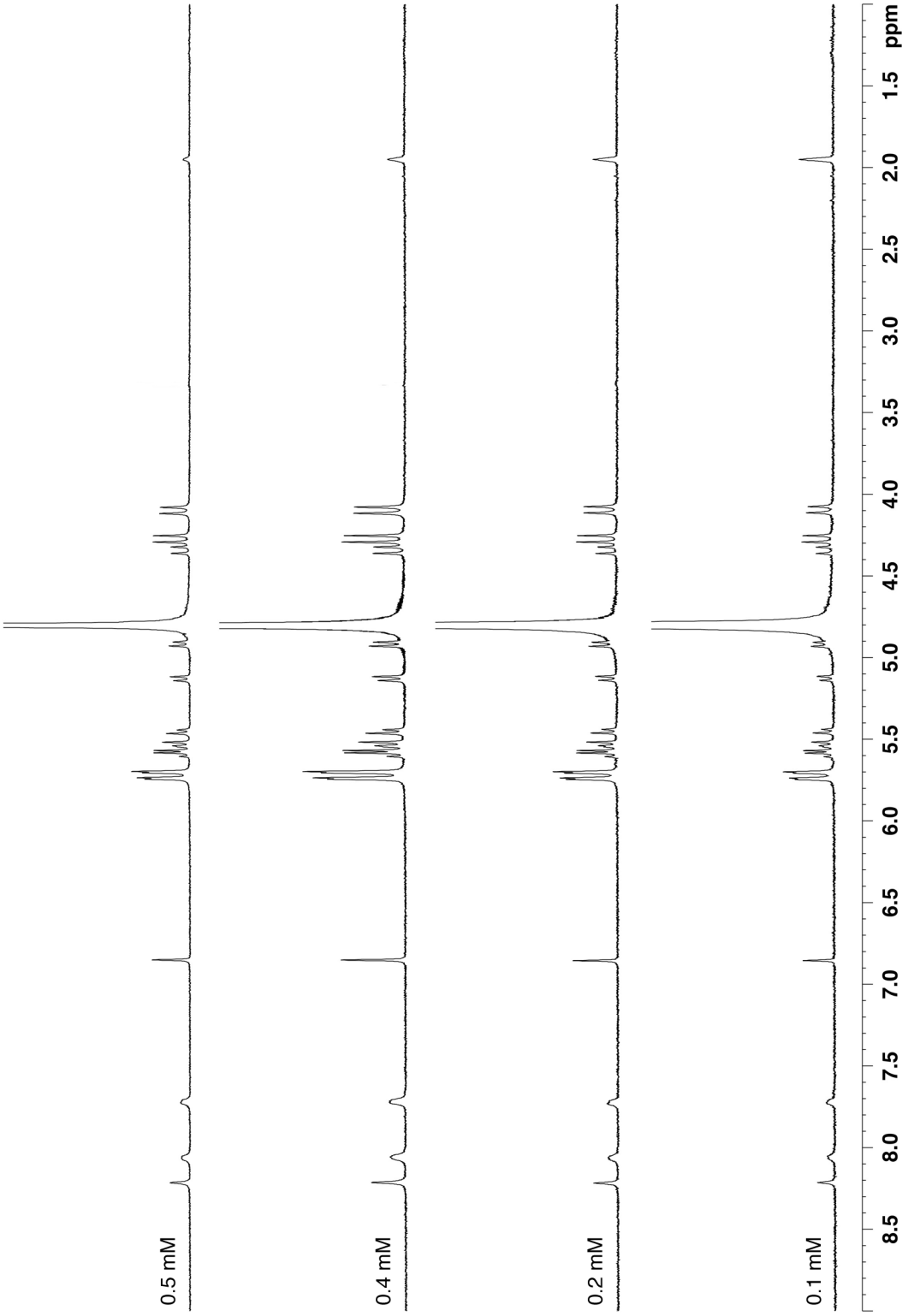

Figure II-S49. ^{1}H NMR spectra (400 MHz, 20 mM $NaCO_2CD_3$ buffer, pD = 4.74, RT) recorded for the dilution of [**II-19**] (0.5 mM – 0.1 mM).

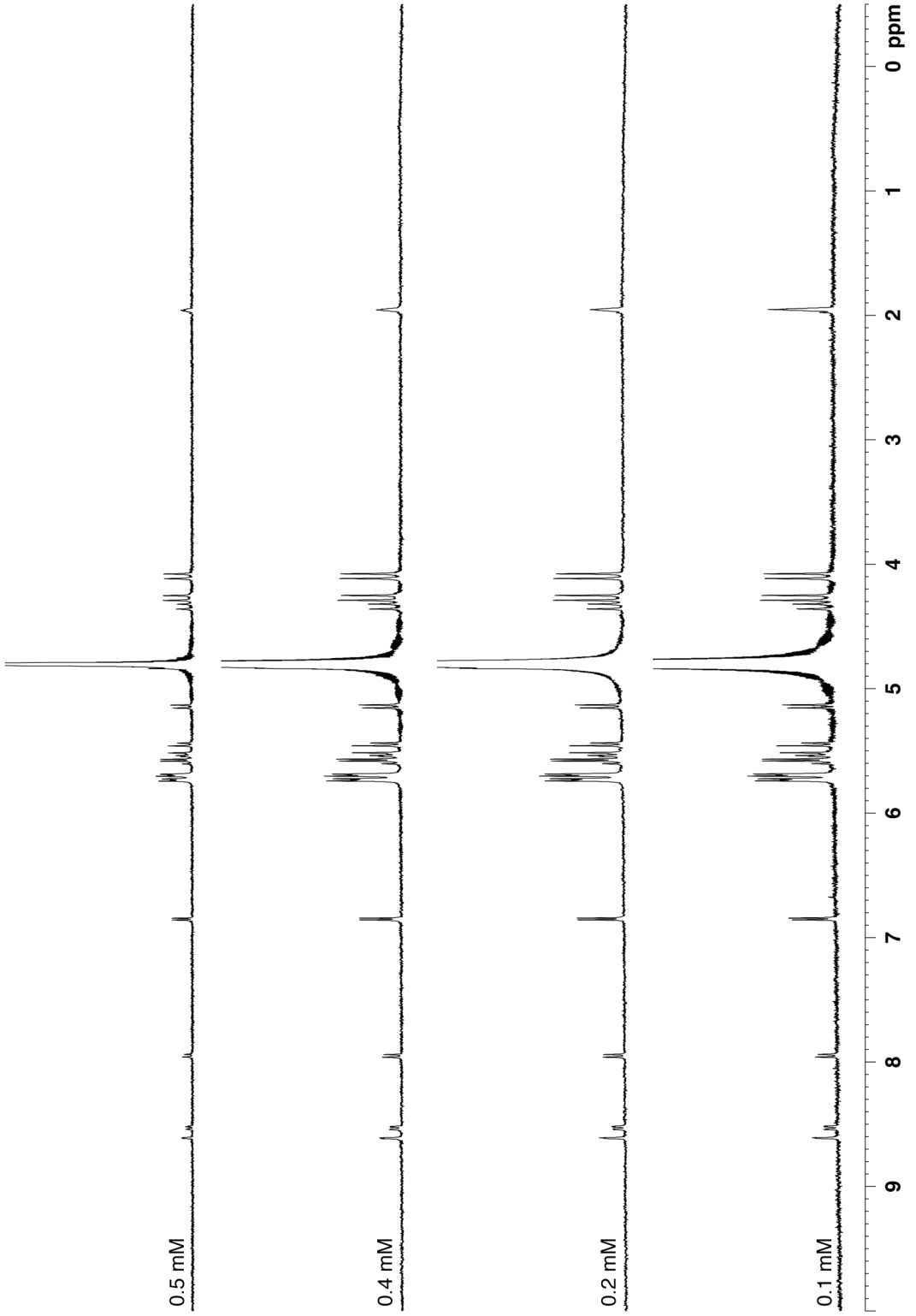

Figure II-S50. ^{1}H NMR spectra (400 MHz, 20 mM $NaCO_2CD_3$ buffer, pD = 4.74, RT) recorded for the dilution of [**II-17**] (0.5 mM – 0.1 mM).

Determination of binding constants:
1:1 Binding Model Used in Scientist.
All calculations were performed on a personal computer running Scientist.

Model used to calculate the binding constant of **II-19•II-30** using NMR titration.

// Micromath Scientist Model File
// 1:1 Host:Guest binding model for NMR
//This model assumes the guest concentration is fixed and host concentration is varied
IndVars: ConcHostTot
DepVars: Deltaobs
Params: Ka, ConcGuestTot, Deltasat, Deltazero
Ka = ConcHostGuest/(ConcHostFree*ConcGuestFree)
ConcHostTot=ConcHostFree + ConcHostGuest
ConcGuestTot=ConcGuestFree + ConcHostGuest
Deltaobs = Deltazero + (Deltasat - Deltazero) * (ConcHostGuest/ConcGuestTot)
//Constraints
0 < ConcHostFree < ConcHostTot
0 < Ka
0 < ConcGuestFree < ConcGuestTot
0 < ConcHostGuest < ConcHostTot
***

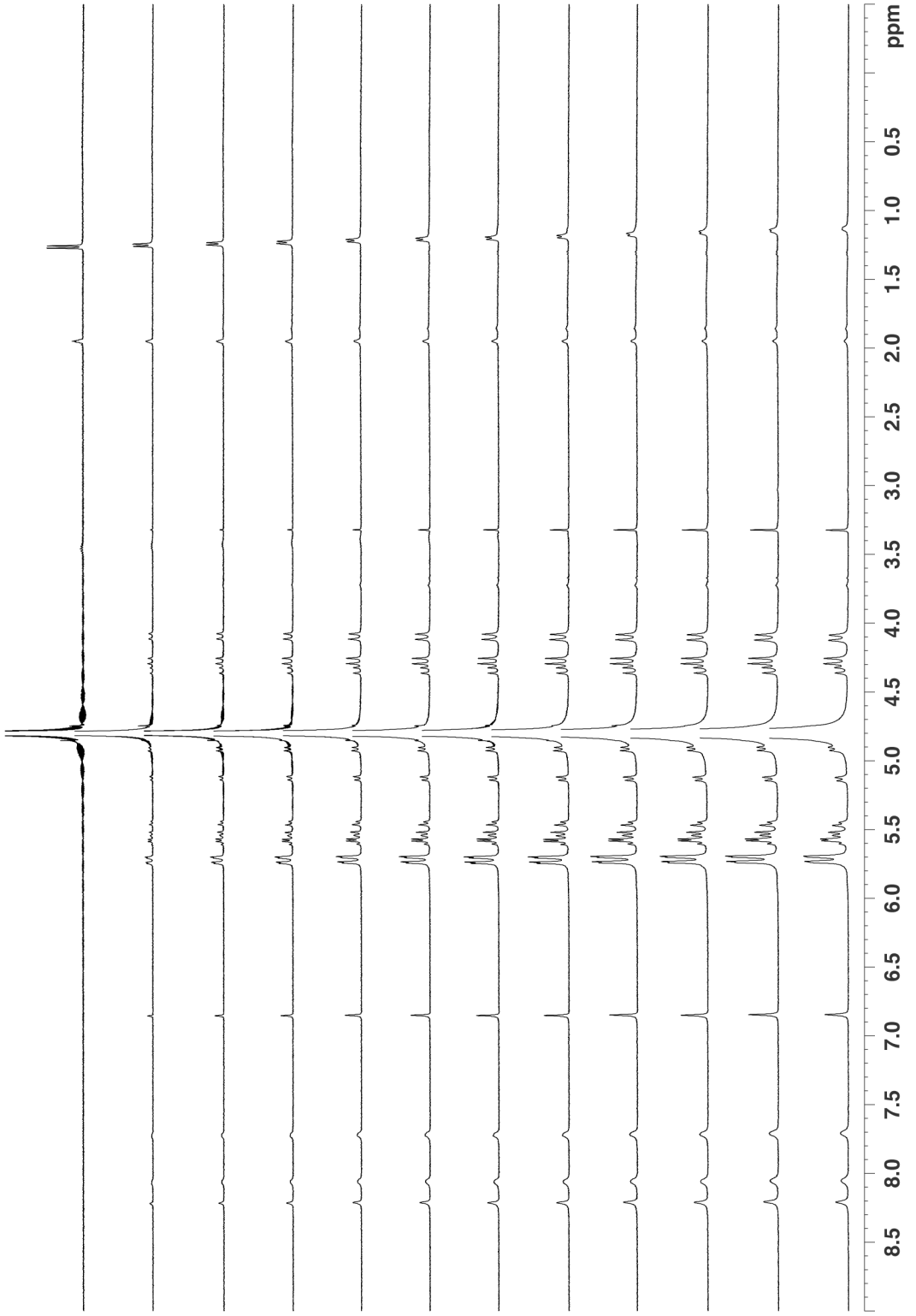

Figure II-S51. ^{1}H NMR spectra (400 MHz, 20 mM $NaCO_2CD_3$ buffer, pD = 4.7, RT) recorded during the titration of a solution of **II-30** (0.125 mM) with **II-19** (0 – 1.83 mM).

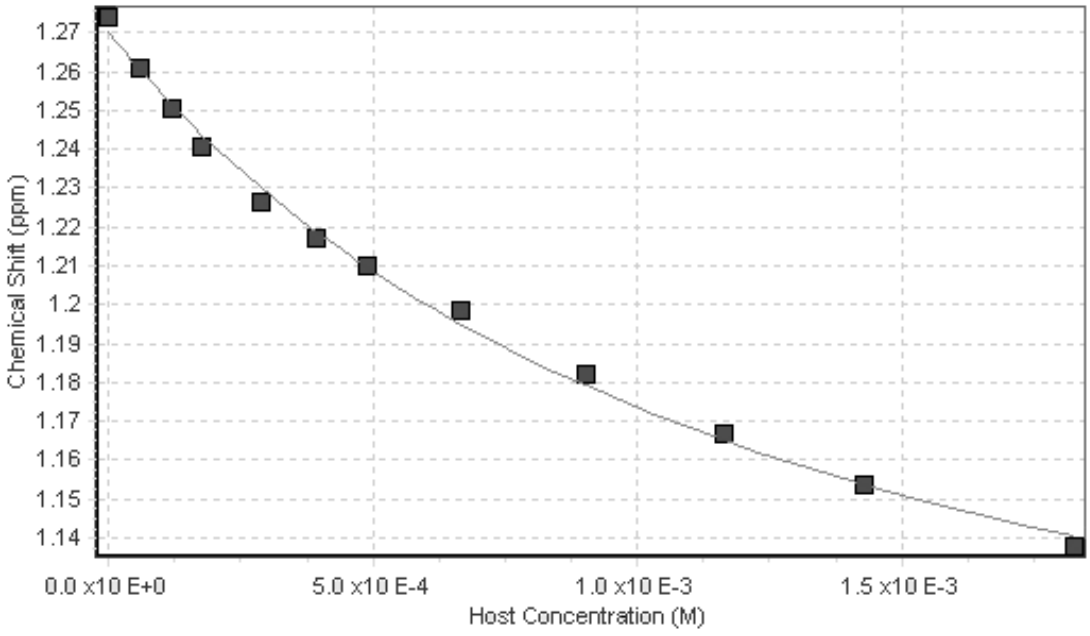

Figure II-S52. Plot of the chemical shift of the CH_3 group of **II-30** as a function of [**II-19**]. The solid line represents the best non-linear fitting of the data to a 1:1 binding model (K_a = 852 ± 114 M^{-1}).

Sample Determination of K_{rel} for the Competition Between II-11 and II-31 for II-19. We use equation 1 to determine K_{rel} for the interaction of **II-11** and **II-31** for **II-19**. For this purpose, we prepared a solution containing **II-19** (0.5 mM), **II-31** (0.5 mM), **II-11** (5.0 mM) and allowed it to reach equilibrium (Figure II-S54). Next, we determined the relative concentration of **II-19•II-11** and **II-19•II-31** by integration of the appropriate resonances in the ^{1}H NMR spectrum (Figure II-S54: **II-19•II-11**: 7.03 ppm; **II-19•II-31**: 6.85 ppm). Using the concentration and the mass balance expression (equation 2) allowed us to calculate [**II-11**]$_{free}$ = 4.703 mM and [**II-19•II-11**] = 0.2967 mM. Equation 3 is then used to calculate [**II-19•II-31**] (0.2033 mM) using the known value of **II-19•II-11**. Lastly, equation 4 is used to calculate [**II-31**]$_{free}$ (0.2967 mM) using the known value of [**19•31**].

K_{rel} = ([**II-19•II-31**][**II-11**]$_{free}$) / ([**II-19•II-11**][**II-31**]$_{free}$) (1)
[**II-11**]$_{Total}$ = 5.0 mM = [**II-11**]$_{free}$ + [**II-19•II-11**] (2)
[**II-13**]$_{Total}$ = 0.5 mM = [**II-19•II-11**] + [**II-19•II-31**] (3)
[**II-31**]$_{Total}$ = 0.5 mM = [**II-31**]$_{free}$ + [**II-19•II-31**] (4)

Substitution of the values of [**II-19•II-11**], [**II-11**]$_{free}$, [**II-19•II-31**], and [**II-31**]$_{free}$ into equation 1 gave K_{rel} = 10.86. These determinations were done in triplicate from independently prepared stock solutions and the average values were used in the calculations of K_a and the error analysis shown below.

Sample Error Analysis Calculation for II-19•II-11. Since the binding constants in this paper are determined by several levels of ^{1}H NMR competition experiments referenced to an absolute K_a measured for **II-19•II-30** measured by ^{1}H NMR titration, a proper error analysis is critical. In this section we give a sample calculation of the error analysis used to determine the uncertainty associated with the K_a value for **II-19•II-11**.

Step 1 – Estimation of the accuracy of ^{1}H NMR methods for the determination of guest and host•guest concentrations. We used ^{1}H NMR to repeatedly determine the concentration of samples of known concentration of guest and host•guest complex by monitoring guest resonances. The ^{1}H NMR based method was accurate with a standard deviation of ± 3%.

Step 2 – Determination of the Uncertainty Associated with a Single Level of Competition (K_{rel}). We propagated the above uncertainty associated with the NMR determination of concentrations (e.g. $\{(\sigma_{[CB[n]\bullet guest]})/[CB[n]\bullet guest]\}$ = 0.03 and $\{(\sigma_{[Guest]})/[Guest]\}$ = 0.03) of using equations 5 and equations 6 – 7 (Bevington, P. R., Robinson, K. D. *Data Reduction and Error Analysis for the Physical Sciences*, 2nd. ed. McGraw-Hill: New York, 1992, pg. 61–62. eq. 4-11). Equation 6 delivers the uncertainty associated with the weighted product (x) of two values (u and v) (e.g. x = ±a u v). Similarly, equation 7 delivers the uncertainty for dividing two numbers (e.g. x = ±(a u) / v). We make the assumption that the fluctuations in u and v are not correlated (σ_{uv} = 0) which when substituted into equations 6 and 7 delivers equation 8. Rearranging slightly yields equation 9 which allows us to directly use the 3% uncertainty determined for our NMR method.

$$K_{rel} = ([CB[n]\bullet G2][G1]) / ([CB[n]\bullet G1][G2]) \quad (5)$$

$$\frac{\sigma_x^2}{x^2} = \frac{\sigma_u^2}{u^2} + \frac{\sigma_v^2}{v^2} + 2\frac{\sigma_{uv}^2}{uv} \quad (6) \qquad \frac{\sigma_x^2}{x^2} = \frac{\sigma_u^2}{u^2} + \frac{\sigma_v^2}{v^2} - 2\frac{\sigma_{uv}^2}{uv} \quad (7)$$

$$\frac{\sigma_x^2}{x^2} = \frac{\sigma_u^2}{u^2} + \frac{\sigma_v^2}{v^2} \quad (8) \qquad \left(\frac{\sigma_x}{x}\right)^2 = \left(\frac{\sigma_u}{u}\right)^2 + \left(\frac{\sigma_v}{v}\right)^2 \quad (9)$$

We break the uncertainty determination in K_{rel} (equation 1) into three steps: 1) Multiplying [CB[n]•G2][G1], 2) multiplying [CB[n]•G1][G2], and 3) dividing the two results. Substituting (σ[CB[n]•G2] / [CB[n]•G2]) = 0.03 and (σ[G1]/[G1]) = 0.03 into equation 9 gives equation 10 and an uncertainty of 4.24% for [CB[n]•G2][G1] (equation 11). Similarly, the uncertainty of [CB[n]•G1][G2] is 4.24%.

$$\left(\frac{\sigma_{[CB[n]\bullet G2][G1]}}{[CB[n]\bullet G2][G1]}\right)^2 = (0.03)^2 + (0.03)^2 \quad (10) \qquad \left(\frac{\sigma_{[CB[n]\bullet G2][G1]}}{[CB[n]\bullet G2][G1]}\right) = 0.0424 \quad (11)$$

With the two values of the uncertainties of [CB[n]•G2][G1] and [CB[n]•G1][G2] (4.24%) in hand we next substituted these values into equation 9 to give the uncertainty in K_{rel} (eq. 12–13) of 6%.

$$\left(\frac{\sigma_{K_{rel}}}{K_{rel}}\right)^2 = \left(\frac{\sigma\frac{[CB[n]\bullet G2][G1]}{[CB[n]\bullet G2][G1]}}{\frac{[CB[n]\bullet G2][G1]}{[CB[n]\bullet G2][G1]}}\right)^2 = (0.0424)^2 + (0.0424)^2 \quad (12) \qquad \frac{\sigma_{K_{rel}}}{K_{rel}} = 0.06 \quad (13)$$

Step 3 – Determination of the Uncertainty in the K_a value for II-19•II-30. We obtained an uncertainty in the value of K_a for **II-19•II-30** ($K_a = 852 \pm 114\ M^{-1}$) (13.38 %) from the non-linear least squares fit of the ^{1}H NMR titration data to a 1:1 binding model (Figure II-S52).

Step 4 – Determination of K_a for II-19•II-11 by competition of II-11 and II-30 for a limiting quantity of II-19. We used ^{1}H NMR competition experiments to determine K_{rel} = 3.22 for these two guests (Figure II-S53). Substitution of $K_{\mathbf{II\text{-}19\cdot II\text{-}30}} = 852 \pm 114\ M^{-1}$ and K_{rel} into equation 14 gave $K_{\mathbf{II\text{-}19\cdot II\text{-}11}} = 2.74 \times 10^3\ M^{-1}$ (equation 15). The uncertainty in $K_{\mathbf{II\text{-}19\cdot II\text{-}11}}$ can be determined using equation 16. Substituting $\sigma(K_{\mathbf{19\cdot 30}})/ K_{\mathbf{19\cdot 30}} = 0.1338$ and $\sigma(K_{rel})/ K_{rel} = 0.10$ [Note that we are using the even more conservative 10% error in this analysis] gives the percent error in $K_{\mathbf{II\text{-}19\cdot II\text{-}11}}$ (equation 17). Substituting eq. 15 into eq. 17 gives $\sigma(K_{\mathbf{II\text{-}19\cdot II\text{-}11}})$ (equation 18) which can be combined with eq. 15 to give a final value for $K_{\mathbf{II\text{-}19\cdot II\text{-}11}}$ (equation 19).

$$K_{G2} = (K_{G1})(K_{rel}) \quad (14)$$

$$K_{\mathbf{II\text{-}19 \cdot II\text{-}11}} = 2.74 \times 10^3\ M^{-1} \quad (15)$$

$$\left(\frac{\sigma K_{\mathbf{II\text{-}19 \bullet II\text{-}11}}}{K_{\mathbf{II\text{-}19 \bullet II\text{-}11}}}\right)^2 = \left(\frac{\sigma K_{\mathbf{II\text{-}19 \bullet II\text{-}30}}}{K_{\mathbf{II\text{-}19 \bullet II\text{-}30}}}\right)^2 + \left(\frac{\sigma K_{rel}}{K_{rel}}\right)^2 \quad (16)$$

$$\frac{\sigma K_{\mathbf{II\text{-}9 \bullet II\text{-}11}}}{K_{\mathbf{II\text{-}19 \bullet II\text{-}11}}} = 0.1670 \ (16.70\ \%) \quad (17)$$

$$\sigma K_{\mathbf{II\text{-}19 \bullet II\text{-}11}} = (0.1670)(2.74 \times 10^3\ M^{-1}) = 458\ M^{-1} \quad (18)$$

$$K_{\mathbf{II\text{-}19 \cdot II\text{-}11}} = 2.74 \pm 0.46 \times 10^6\ M^{-1} \quad (19)$$

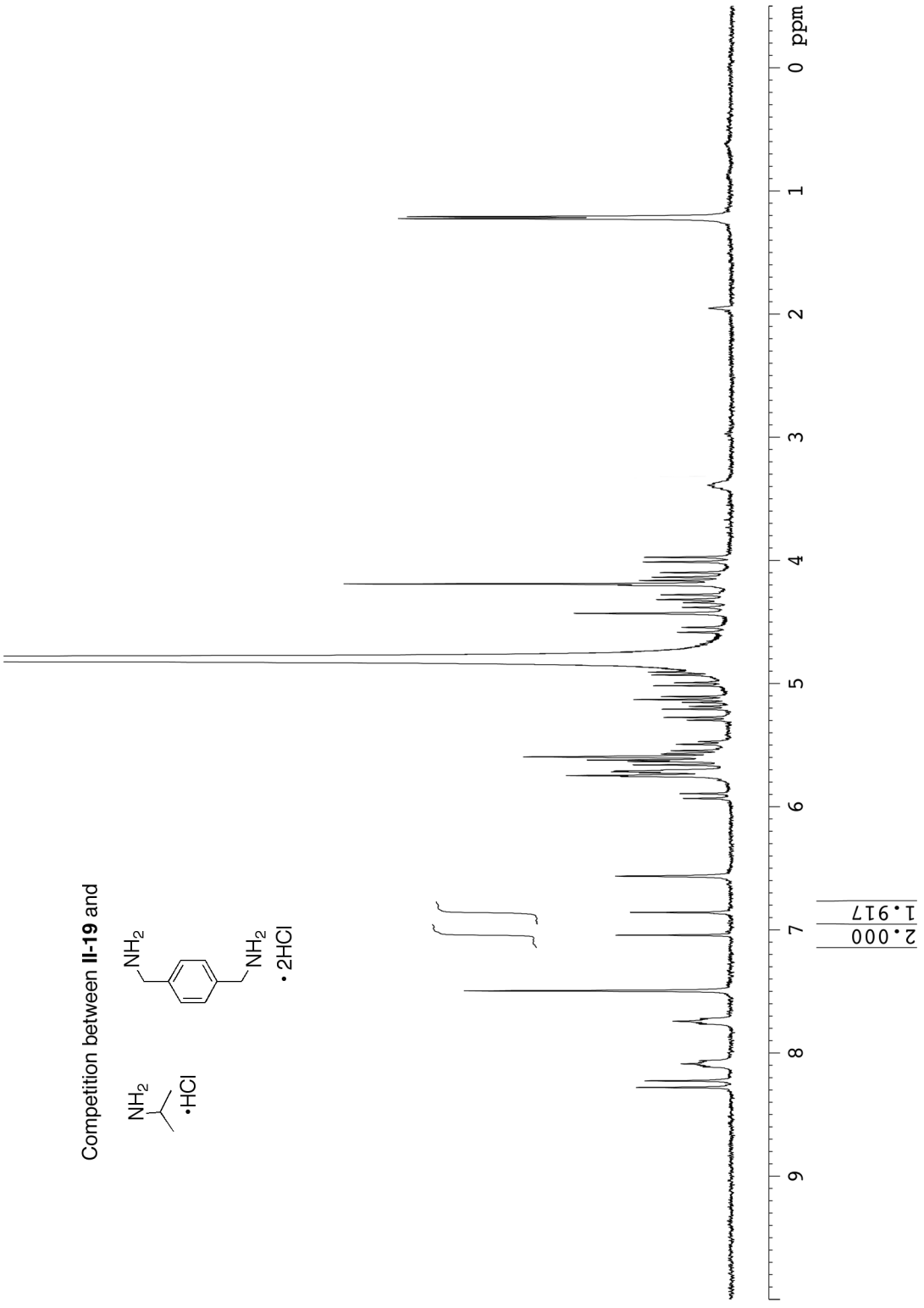

Figure II-S53. One of the ^{1}H NMR spectra (400 MHz, 20 mM $NaCO_2CD_3$ buffer, pD = 4.7, RT) used in the determination of K_{rel} for **II-19•II-30** and **II-19•II-11**. Conditions: **II-19** (0.5 mM), **II-11** (0.5 mM), and **II-30** (1 mM).

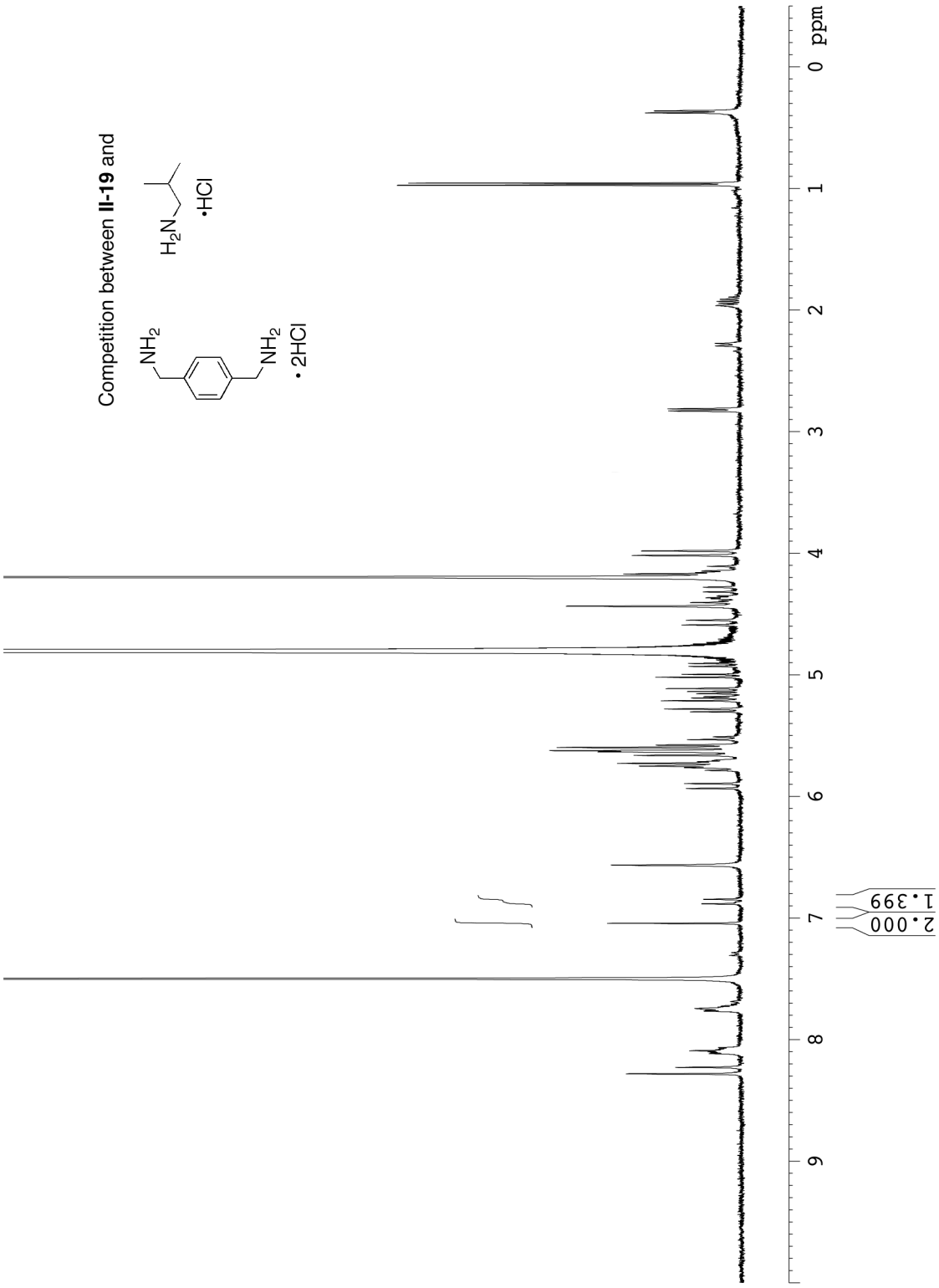

Figure II-S54. One of the ^{1}H NMR spectra (400 MHz, 20 mM $NaCO_2CD_3$ buffer, pD = 4.7, RT) used in the determination of K_{rel} for **II-19•II-11** and **II-19•II-31**. Conditions: **II-19** (0.5 mM), **II-31** (0.5 mM), and **II-11** (5.0 mM).

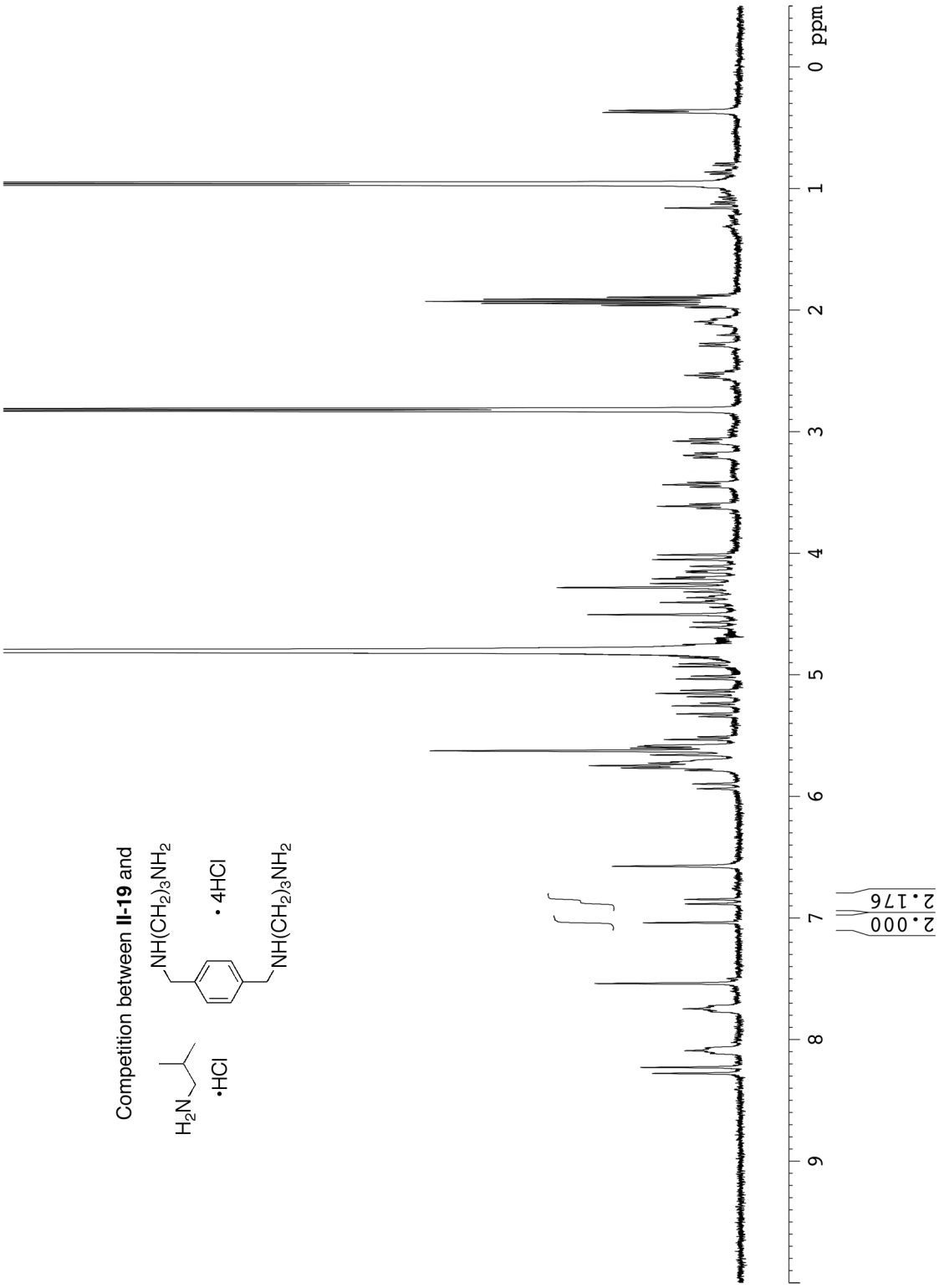

Figure II-S55. One of the ^{1}H NMR spectra (400 MHz, 20 mM $NaCO_2CD_3$ buffer, pD = 4.7, RT) used in the determination of K_{rel} for **II-19•II-31** and **II-19•II-26**. Conditions: **II-19** (0.5 mM), **II-26** (0.5 mM), and **II-31** (5.0 mM).

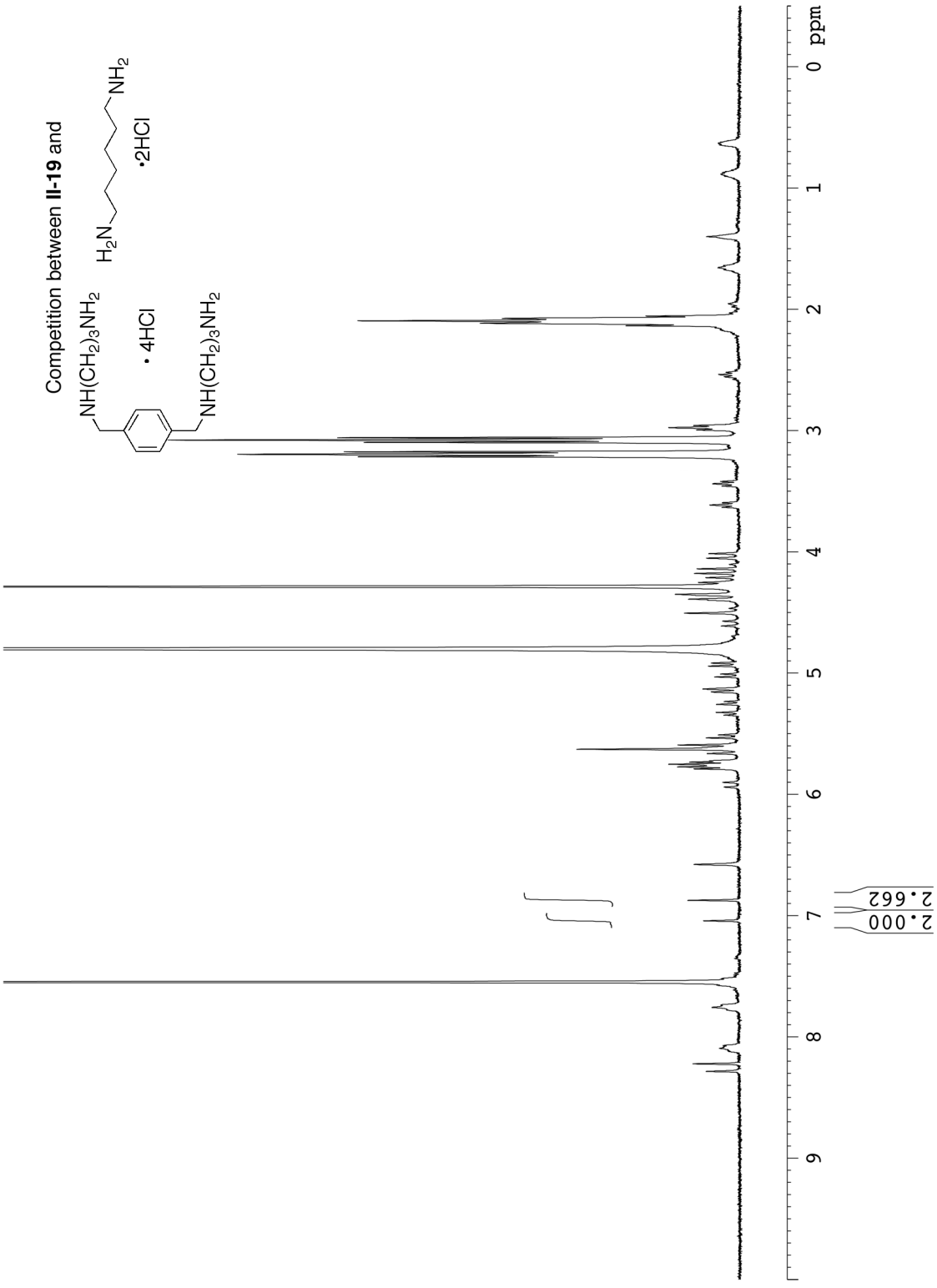

Figure II-S56. One of the ^{1}H NMR spectra (400 MHz, 20 mM $NaCO_2CD_3$ buffer, pD = 4.7, RT) used in the determination of K_{rel} for **II-19•II-26** and **II-19•II-20**. Conditions: **II-19** (0.5 mM), **II-20** (0.5 mM), and **II-26** (5.0 mM).

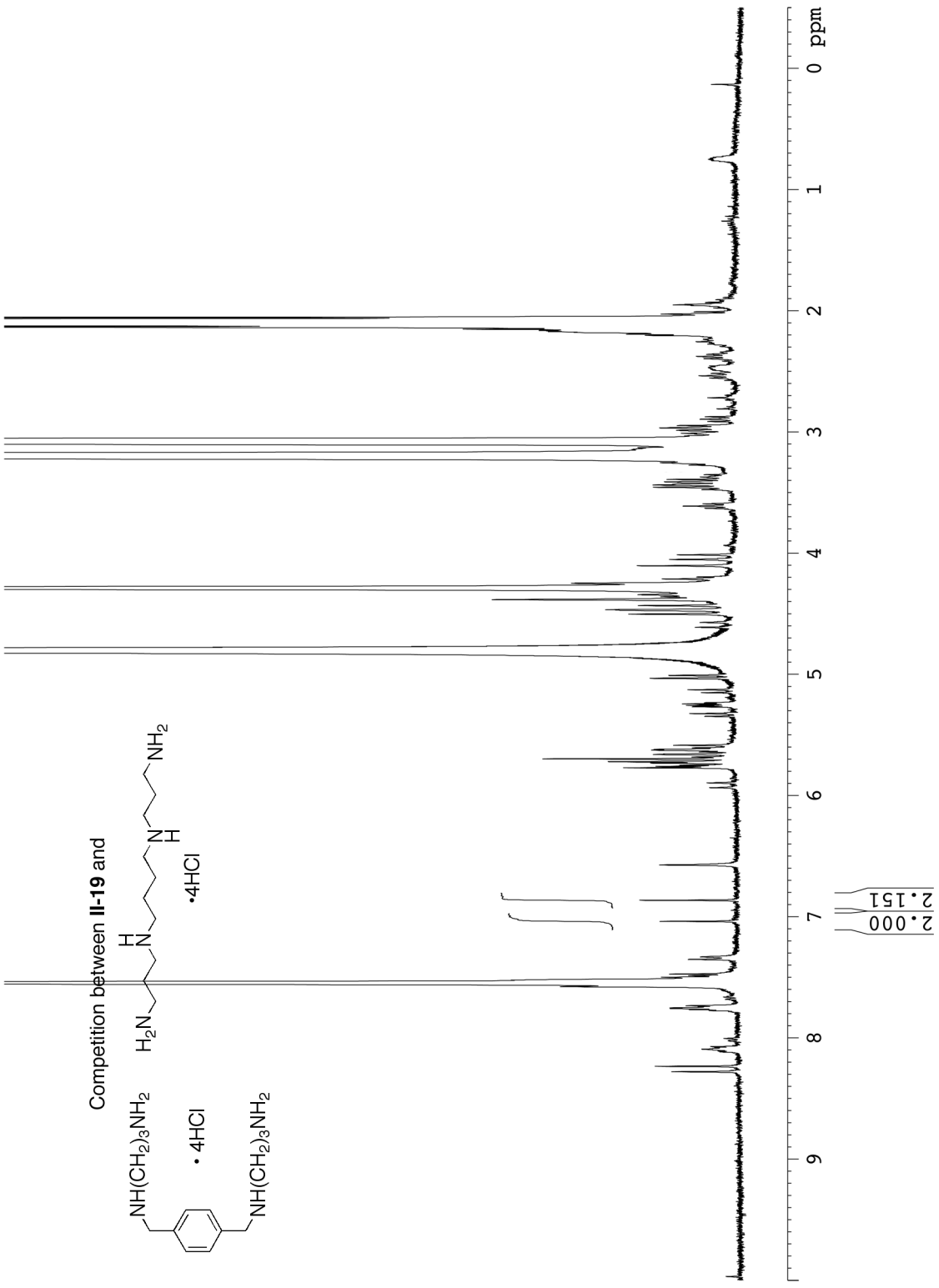

Figure II-S57. One of the ^{1}H NMR spectra (400 MHz, 20 mM $NaCO_2CD_3$ buffer, pD = 4.7, RT) used in the determination of K_{rel} for **II-19•II-26** and **II-19•II-32**. Conditions: **II-19** (0.1 mM), **II-32** (0.1 mM), and **II-26** (10.0 mM).

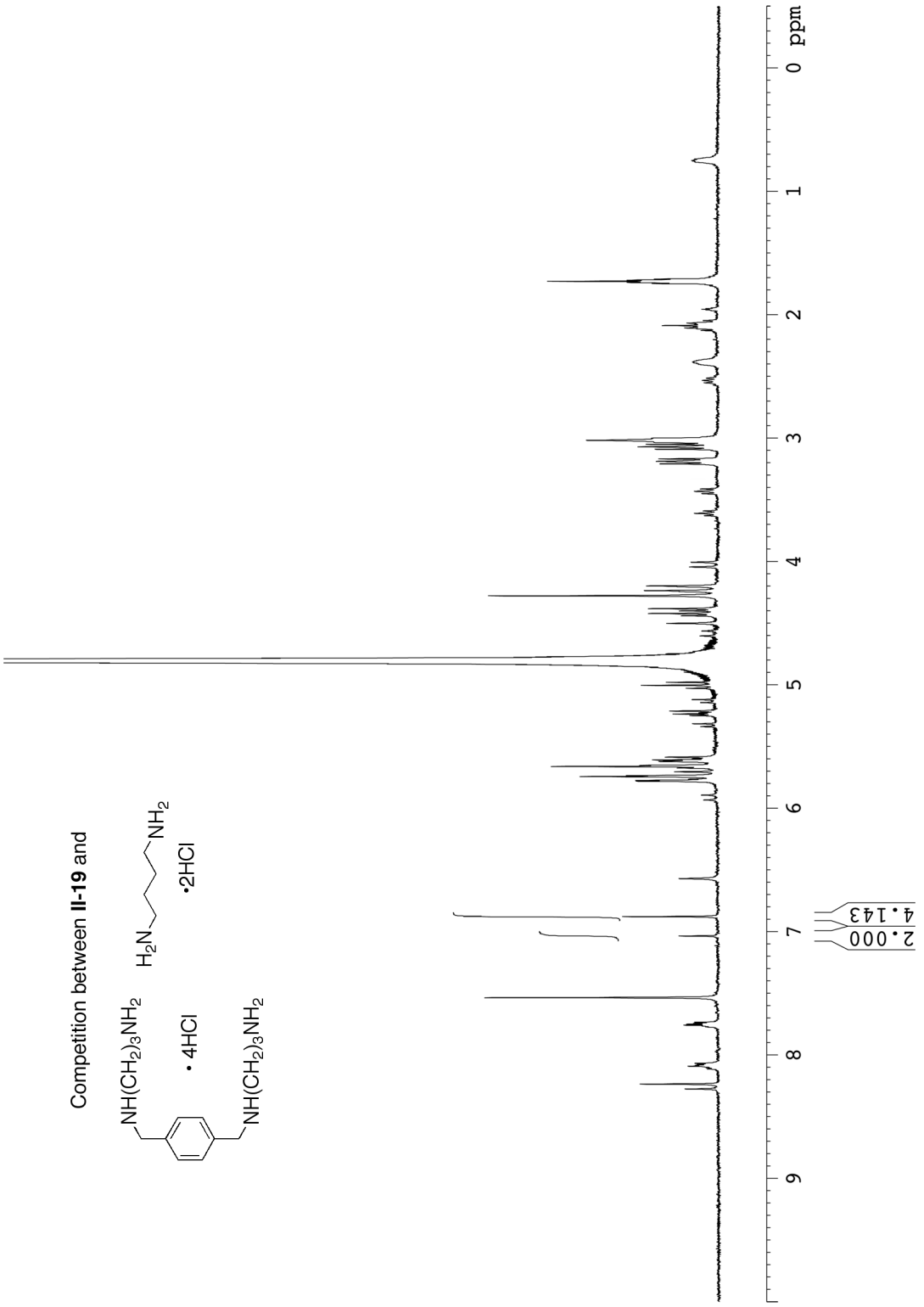

Figure II-S58. One of the ^{1}H NMR spectra (400 MHz, 20 mM $NaCO_2CD_3$ buffer, pD = 4.7, RT) used in the determination of K_{rel} for **II-19•II-26** and **II-19•II-22**. Conditions: **II-19** (0.5 mM), **II-26** (0.5 mM), and **II-22** (1.0 mM).

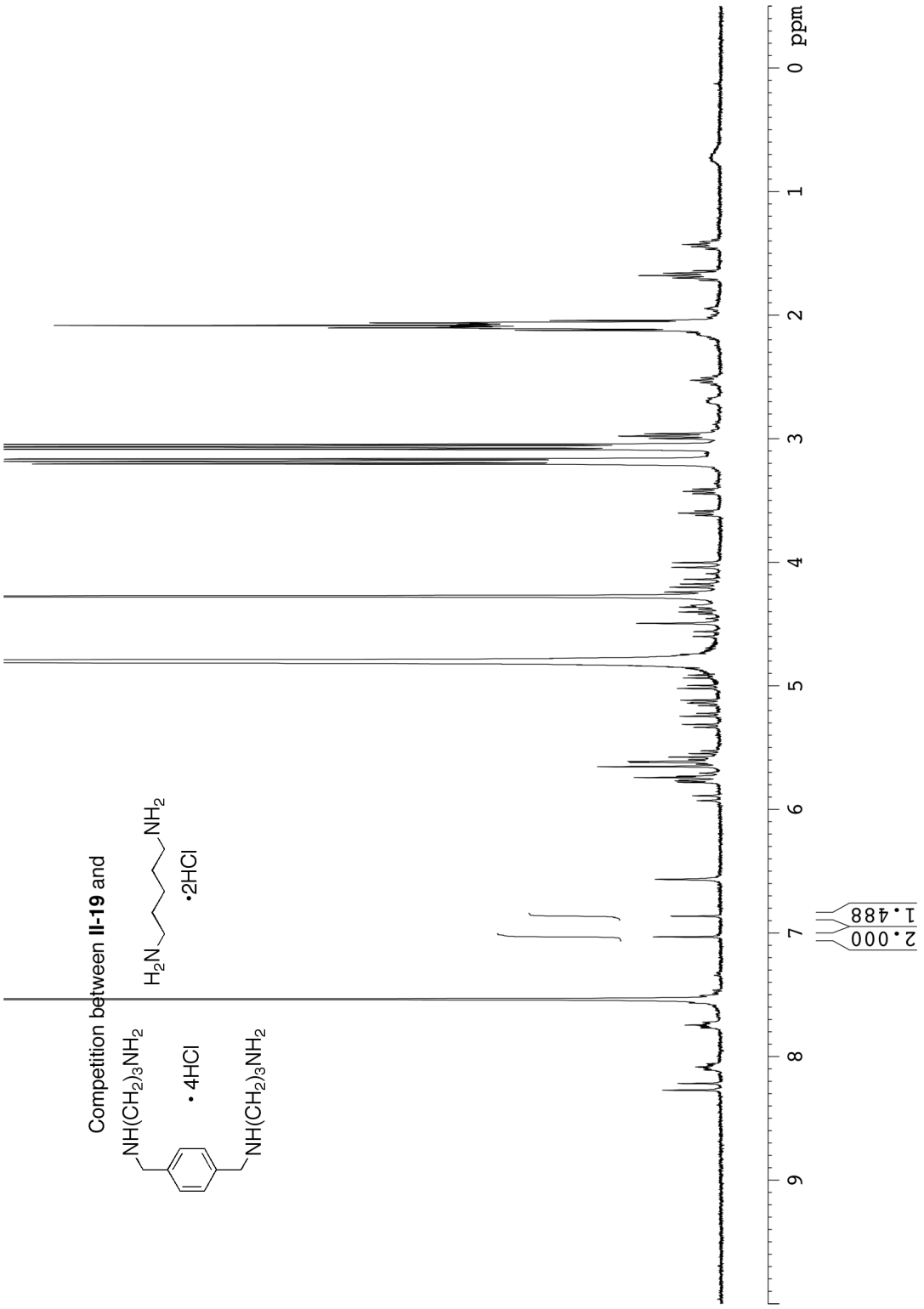

Figure II-S59. One of the ^{1}H NMR spectra (400 MHz, 20 mM $NaCO_2CD_3$ buffer, pD = 4.7, RT) used in the determination of K_{rel} for **II-19•II-26** and **II-19•II-23**. Conditions: **II-19** (0.5 mM), **II-23** (0.5 mM), and **II-26** (5.0 mM).

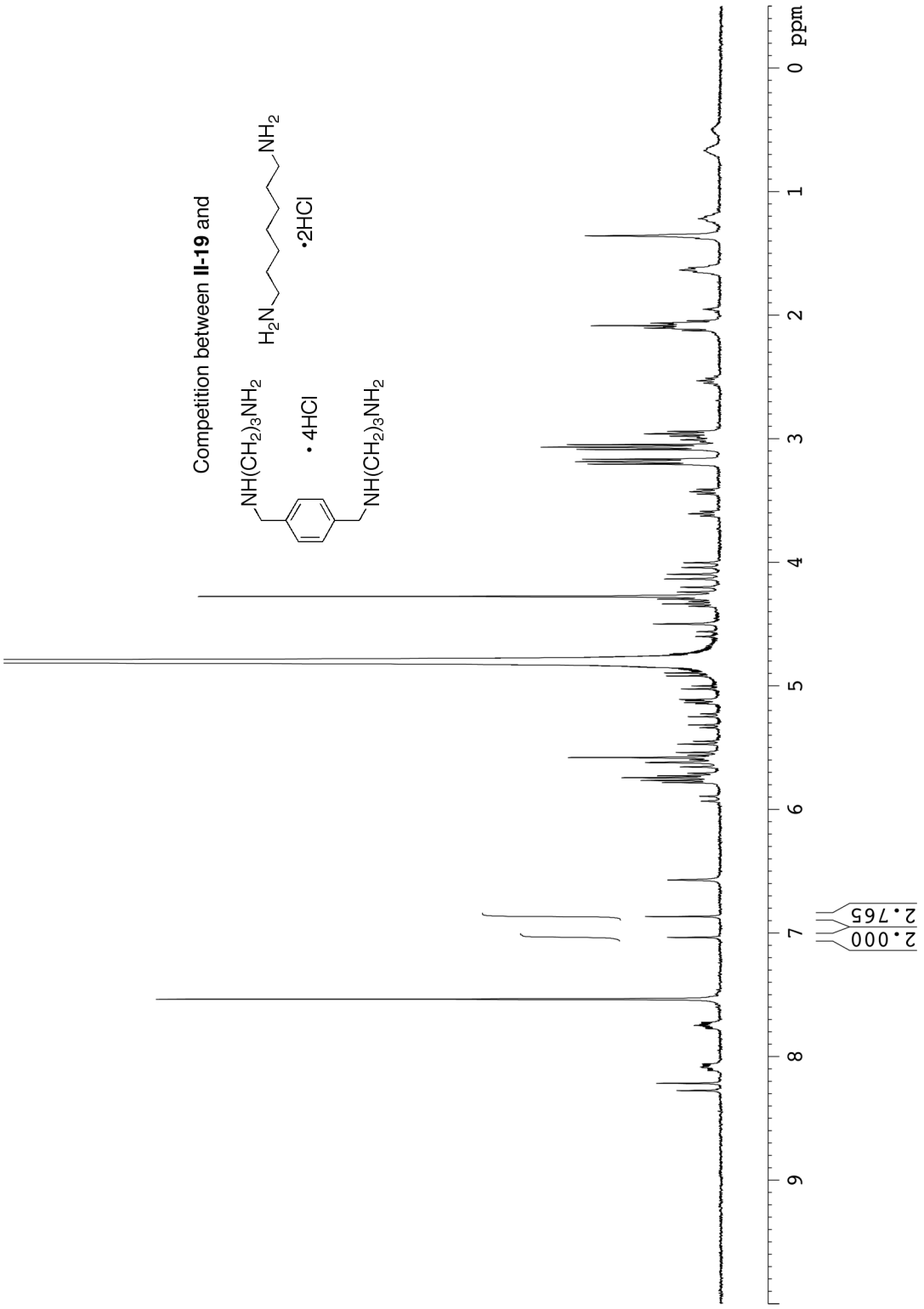

Figure II-S60. One of the ^{1}H NMR spectra (400 MHz, 20 mM $NaCO_2CD_3$ buffer, pD = 4.7, RT) used in the determination of K_{rel} for **II-19•II-26** and **II-19•II-24**. Conditions: **II-19** (0.5 mM), **II-24** (0.5 mM), and **II-26** (1.0 mM).

Experimental for kinetic study

Kinetic experiment for CB[6] ring closure (Non-templated). Concentrated HCl (0.4 mL) was added to a vial containing **6C** (0.1000 g, 0.1028 mmol) with stirring. A 2.3 M solution of paraformaldehyde in conc. HCl (0.1 mL) was subsequently added to the vial. Aliquots were taken at appropriate time points by adding the reaction mixture (2 drops) to a centrifuge tube containing methanol (5 mL). The resulting precipitate was centrifuged at 7200 rpm for 5 min. The supernatant was decanted and the precipitate was dried under high vacuum. The percentage of CB[6] was calculated by analyzing the aliquots by ^{1}H NMR in D_2O with an excess of **II-11**. The integration of the CB[6]•**II-11** binding resonance at 6.50 ppm was compared to the integration of the region between 5.29 and 5.84 ppm which allows calculation of the percentage of CB[6] in the mixture (Figure II-3).

Kinetic experiment for CB[6] ring closure (II-11 templated). Concentrated HCl (0.4 mL) was added to a vial containing **6C** (0.1000 g, 0.1028 mmol) and **II-11** (0.015 mg, 0.1131 mmol) with stirring. A 2.3 M solution of paraformaldehyde in conc. HCl (0.1 mL) was subsequently added to the vial. Aliquots were taken at appropriate time points by adding the reaction mixture (2 drops) to a centrifuge tube containing methanol (5 mL). The resulting precipitate was centrifuged at 7200 rpm for 5 min. The supernatant was decanted and the precipitate was dried under high vacuum. The percentage of CB[6] was calculated by analyzing the aliquots by ^{1}H NMR in D_2O with an excess of **II-11**. The integration of the CB[6]•**II-11** binding resonance at 6.50 ppm was compared to the integration of the region between 5.29 and 5.84 ppm which allows calculation of the percentage of CB[6] in the mixture (Figure II-3).

Kinetic Experiment for ring closure to II-13 (Non-templated). An aq. solution of H_2SO_4 (9 M aq., 0.4 mL) was added to a vial containing **6C** (0.1000 g, 0.1028 mmol) with stirring. A 1.1 M solution of **II-12** (1.1 M) in H_2SO_4 (9 M aq., 0.1 mL) was subsequently added to the vial. Aliquots were taken at appropriate time points by adding the reaction mixture (2 drops) to a centrifuge tube containing methanol (5 mL). The resulting precipitate was centrifuged at 7200 rpm for 5 min. The supernatant was decanted and the precipitate was dried under high vacuum. The percentage of **II-13** was calculated by analyzing the aliquots by ^{1}H NMR in D_2O with an excess of **II-11**. The integration of the aromatic resonance of **II-13•II-11** at 7.72 ppm or of the C-H resonance of **II-13•II-11** at 6.87 ppm was compared to the integration of the region between 4.89 and 5.95 ppm which allows calculation of the percentage of **II-13** in the mixture (Figure II-6).

Kinetic experiment for ring closure to (±)-II-21 (II-11 templated). An aq. solution of H_2SO_4 (9 M aq., 0.4 mL) was added to a vial containing **6C** (0.1000 g, 0.1028 mmol) and **II-11** (0.0154 mg, 0.1131 mmol) with stirring. A solution of **II-12** (1.1 M) in H_2SO_4 (9 M aq., 0.1 mL) was subsequently added to the vial. Aliquots were taken at appropriate time points by adding the reaction mixture (2 drops) to a centrifuge tube containing methanol (5 mL). The resulting precipitate was centrifuged at 7200 rpm for 5 min. The supernatant was decanted and the precipitate was dried under high vacuum. The

percentage of (±)-**II-21** was calculated by analyzing the aliquots by ^{1}H NMR in D_2O. The integration of the C-H resonance of (±)-**II-21•II-11** at 6.56 ppm was compared to the integration of the region between 5.11 and 5.81 ppm which allows calculation of the percentage of (±)-**II-21** in the mixture (Figure II-6).

Kinetic experiment for ring closure to II-13 (Ammonium chloride templated). A solution of H_2SO_4 (9 M aq., 0.4 mL) was added to a vial containing **6C** (0.1000 g, 0.1028 mmol) and ammonium chloride (0.0061 g, 0.1131 mmol) with stirring. A solution of **II-12** (1.1 M) in H_2SO_4 (9 M aq., 0.1 mL) was subsequently added to the vial. Aliquots were taken at appropriate time points by adding the reaction mixture (2 drops) to a centrifuge tube containing methanol (5 mL). The resulting precipitate was centrifuged at 7200 rpm for 5 min. The supernatant was decanted and the precipitate was dried under high vacuum. The percentage of **II-13** was calculated by analyzing the aliquots by ^{1}H NMR in D_2O with excess **II-11**. The integration of the C-H resonance of **II-13•II-11** at 6.87 ppm was compared to the integration of the region between 4.83 and 5.93 ppm which allows calculation of the percentage of **II-13** in the mixture (Figure II-6).

Kinetic experiment for ring closure to (±)-II-21 and II-13 (II-20 templated). A solution of H_2SO_4 (9 M aq., 0.4 mL) was added to a vial containing **6C** (0.1000 g, 0.1028 mmol) and **II-20** (0.0131 g, 0.1131 mmol) with stirring. A solution of **II-12** (1.1 M) in H_2SO_4 (9 M aq., 0.1 mL) was subsequently added to the vial. Aliquots were taken at appropriate time points by adding the reaction mixture (2 drops) to a centrifuge tube containing methanol (5 mL). The resulting precipitate was centrifuged at 7200 rpm for 5 min. The supernatant was decanted and the precipitate was dried under high vacuum. The percentage of **II-13** and (±)-**II-21** were calculated by analyzing the aliquots by ^{1}H NMR in D_2O. The integration of the C-H resonance of **II-13•II-11** at 6.95 ppm was compared to the integration of the region between 5.12 and 5.91 ppm which allows calculation of the percentage of **II-13** in the mixture. The integration of the C-H resonance of (±)-**21•11** at 6.71 ppm was compared to the integration of the region between 5.12 and 5.91 ppm which allows calculation of the percentage of (±)-**II-21** in the mixture (Figure II-6).

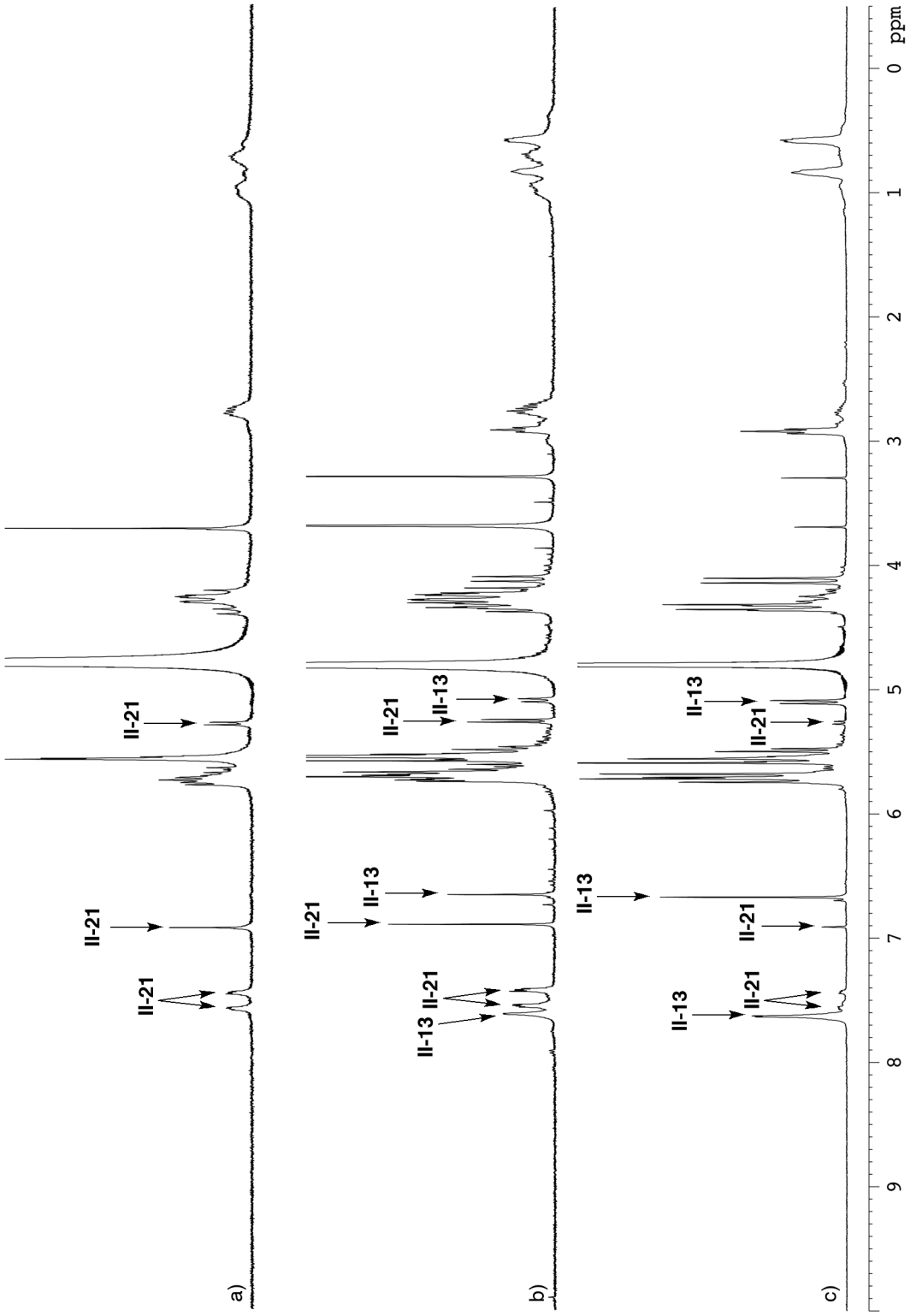

Figure II-S61. ^{1}H NMR spectrum (400 MHz, D_2O, RT) stack plot from the kinetic study of **6C**, **II-20**, and **II-12** in aq. 9 M H_2SO_4: a) Rapid conversion to (±)-**II-21** at 1 min, b) a mixture of (±)-**II-21** an **II-13** at 1245 min, c) near complete conversion from (±)-**II-21** to **II-13** at 27120 min.

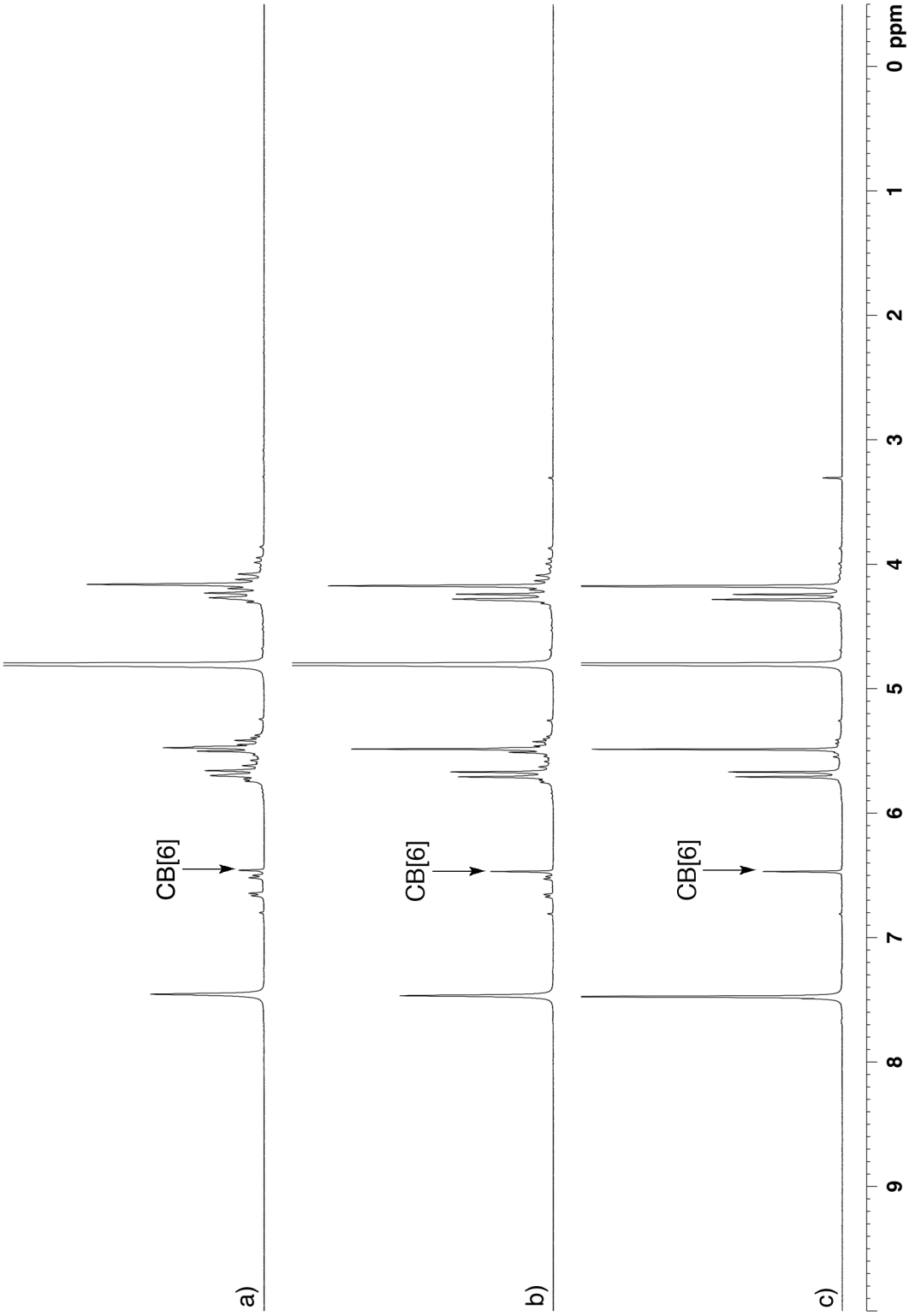

Figure II-S62. ^{1}H NMR spectrum (400 MHz, D_2O, RT) stack plot from the kinetic study of **6C** and formaldehyde in conc. HCl: a) appearance of CB[6] at 1 min, b) further conversion to CB[6] at 30 min, c) complete conversion of CB[6] at 102 min.

Recognition Properties of Acyclic Glycoluril Oligomers

Supporting Information

*by Derick Lucas and Lyle Isaacs**

Department of Chemistry and Biochemistry, University of Maryland, College Park, MD 20742

Table of Contents **Pages**

Synthesis of Glycoluril Pentamer (5C). A mixture of bis-*nor*-*seco*-CB[10] (0.750 g, 0.458 mmol) and 3,5-dimethylphenol (0.224 g, 1.834 mmol) in a 50 mL round bottom flask was treated with concentrated HCl (18 mL). The heterogeneous slurry was heated for 20 h at 50 °C with stirring. The resulting yellow slurry was poured into a stirring solution of methanol (200 mL). The mixture was then poured into a centrifuge tube and centrifuged at 7200 rpm for 5 min. The supernatant was decanted and the crude solid was dried under vacuum (0.721 g). The crude solid was then stirred with water (30 mL) containing **III-11** (0.374 g, 1.788 mmol) for 1 hour. The resulting mixture was centrifuged at 7200 rpm for 5 min and the supernatant was decanted into a clean dry round bottom flask. The water was removed by rotary evaporation and the resulting solid was mixed with a solution of 5 M NaOH: methanol (1:10, V:V; 40 mL) for 1 h. The mixture was poured into a centrifuged tube and centrifuged at 7200 rpm for 5 min. The supernatant was decanted and 0.1 M NaOH in methanol (40 mL) was added to the precipitate and mixed for 20 min. The resulting mixture was centrifuged at 7200 rpm for 5 min followed by decanting of the supernatant. The precipitate was dried under vacuum to give **5C** as a white powder (0.598 g, 0.741 mmol, 81 % yield). **Compound 5C**: M.p. >300 ^{o}C. ^{1}H NMR (400 MHz, D_2O): 5.81 (d, J = 15.6, 4H), 5.74 (s, 2H), 5.56-5.37 (m, 12H), 4.41 (d, J = 16, 4H), 4.08 (d, J = 15.6, 4H). ^{1}H NMR spectral data matches that reported in the literature.[11]

(11) Huang, W. –H.; Zavalij, P. Y.; Isaacs, L. *J. Am. Chem. Soc*. **2008**, 130, 8446-8454.

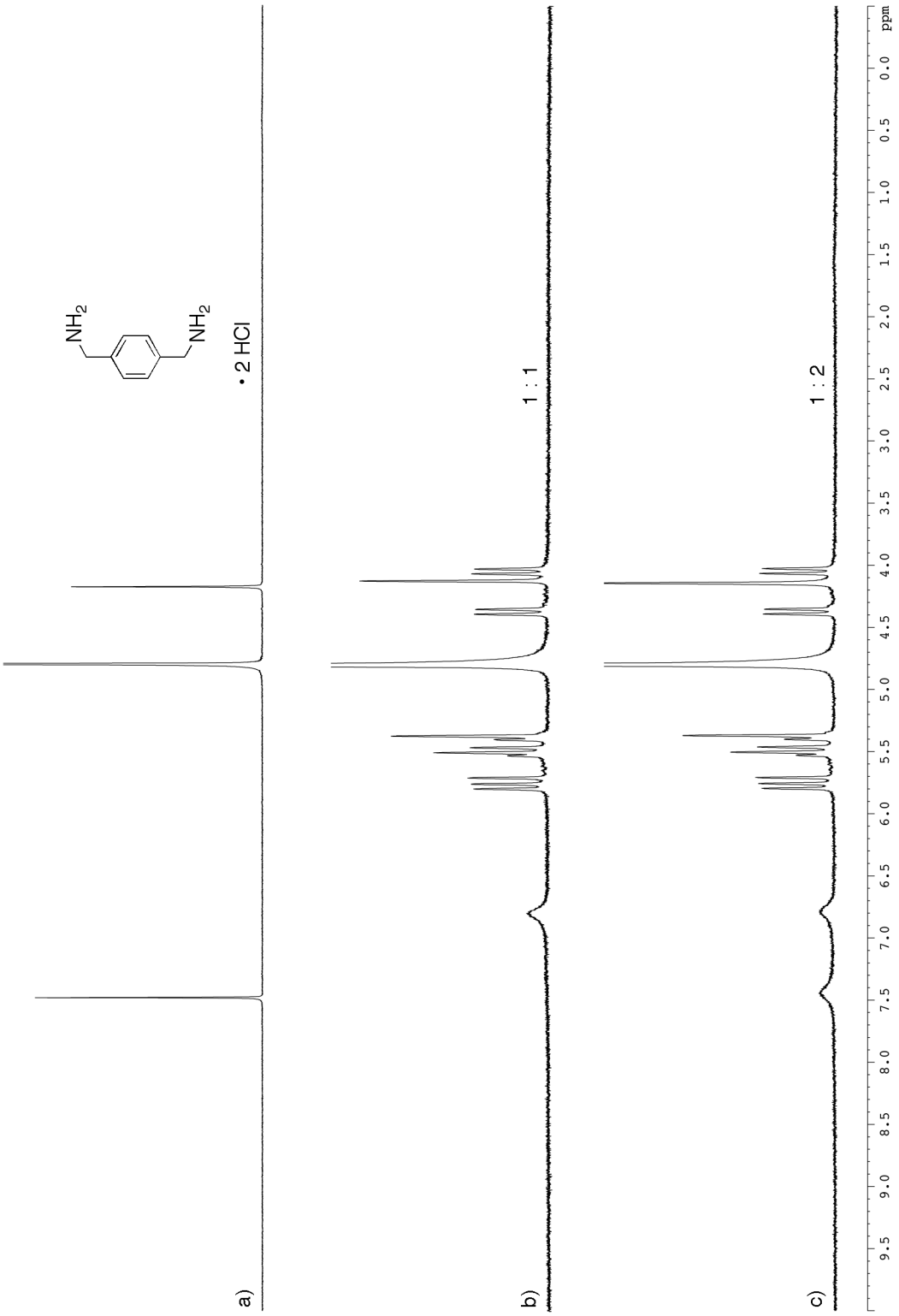

Figure III-S1. NMR spectra recorded (D_2O, 400 MHz, RT) for: a) **III-11** (1 mM), b) a mixture of **5C** (1 mM) and **III-11** (1 mM), and c) a mixture of **5C** (1 mM) and **III-11** (2 mM).

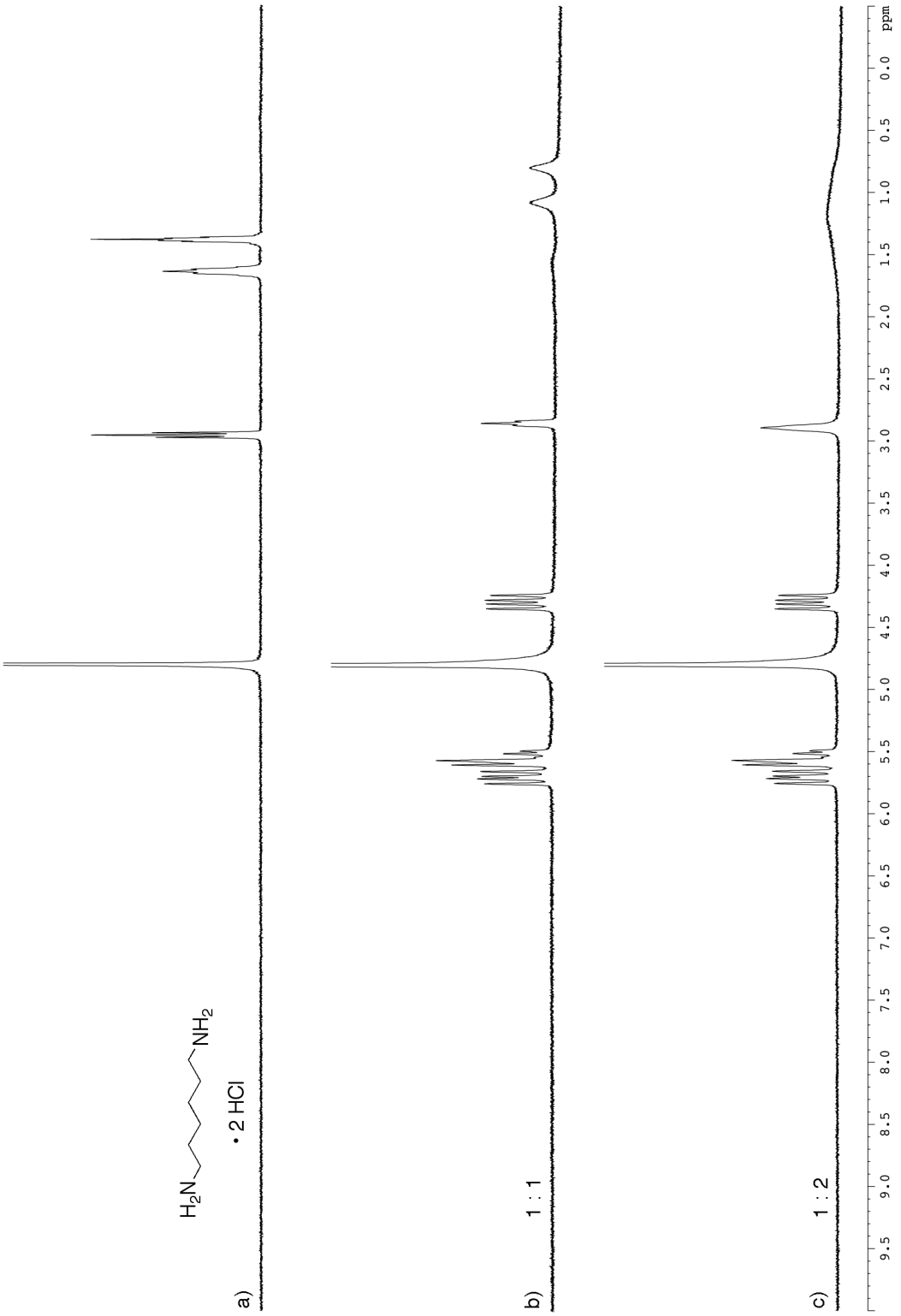

Figure III-S2. NMR spectra recorded (D_2O, 400 MHz, RT) for: a) **III-9** (1 mM), b) a mixture of **5C** (1 mM) and **III-9** (1 mM), and c) a mixture of **5C** (1 mM) and **III-9** (2 mM).

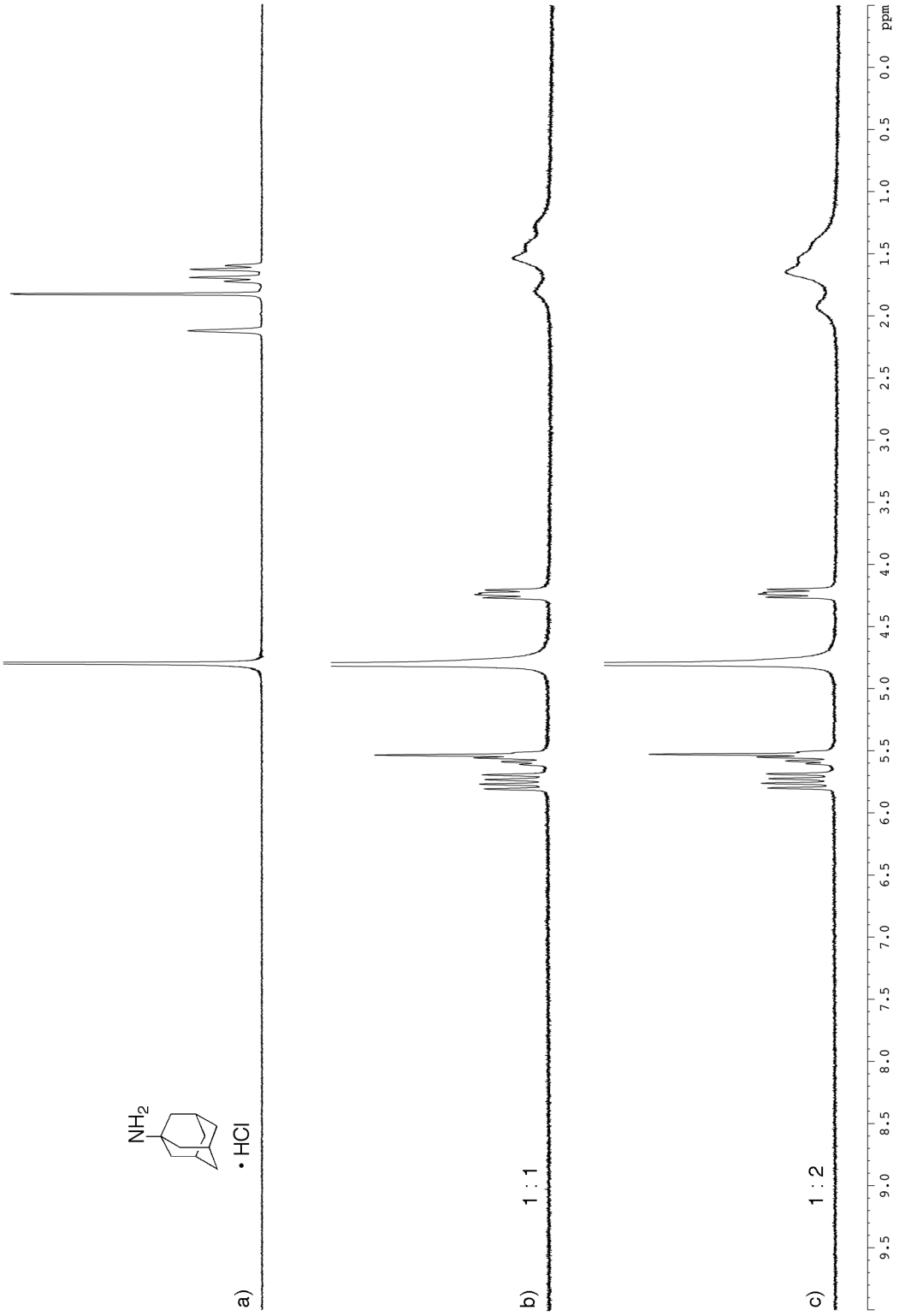

Figure III-S3. NMR spectra recorded (D_2O, 400 MHz, RT) for: a) **III-14** (1 mM), b) a mixture of **5C** (1 mM) and **III-14** (1 mM), and c) a mixture of **5C** (1 mM) and **III-14** (2 mM).

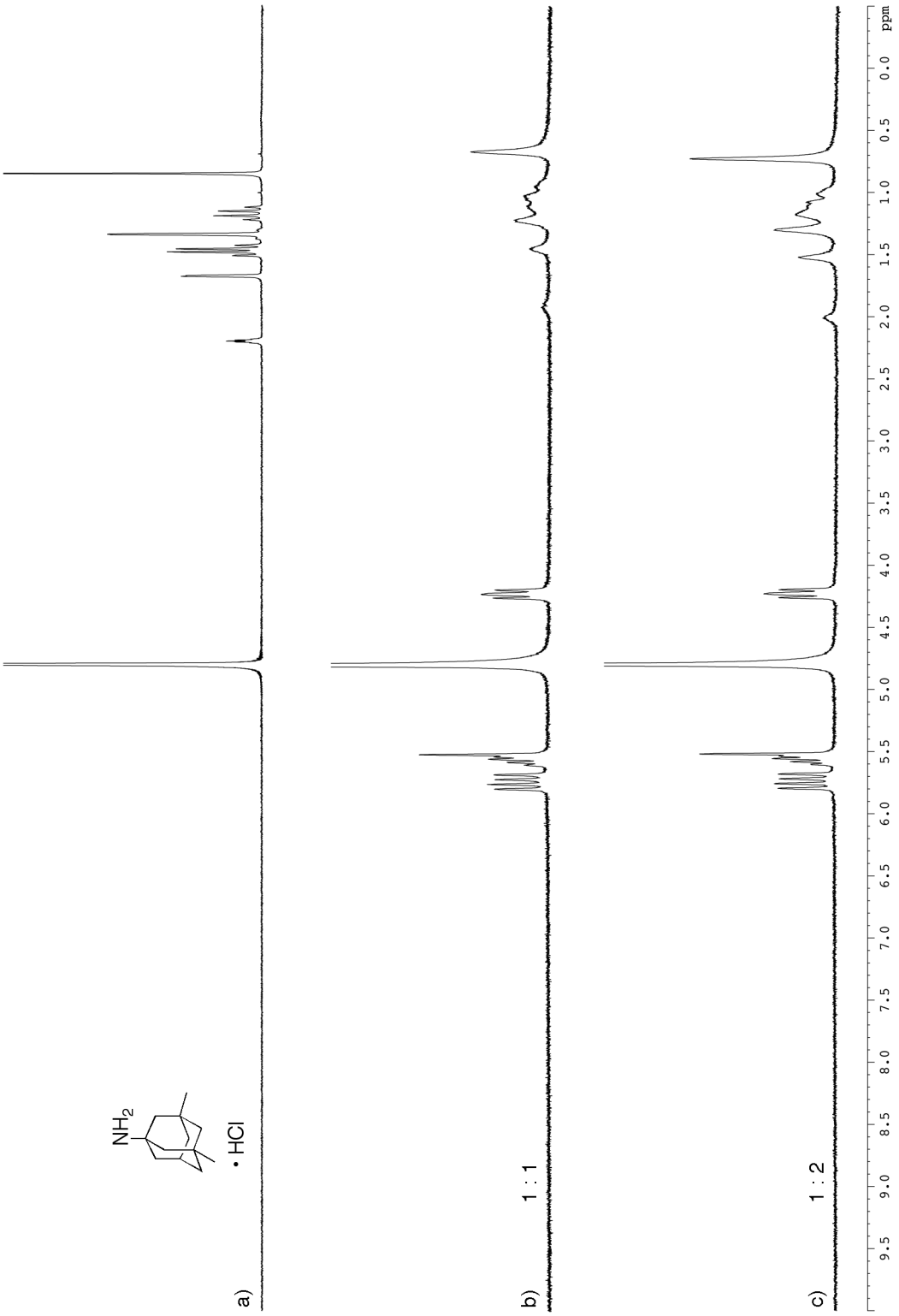

Figure III-S4. NMR spectra recorded (D_2O, 400 MHz, RT) for: a) **III-15** (1 mM), b) a mixture of **5C** (1 mM) and **III-15** (1 mM), and c) a mixture of **5C** (1 mM) and **III-15** (2 mM).

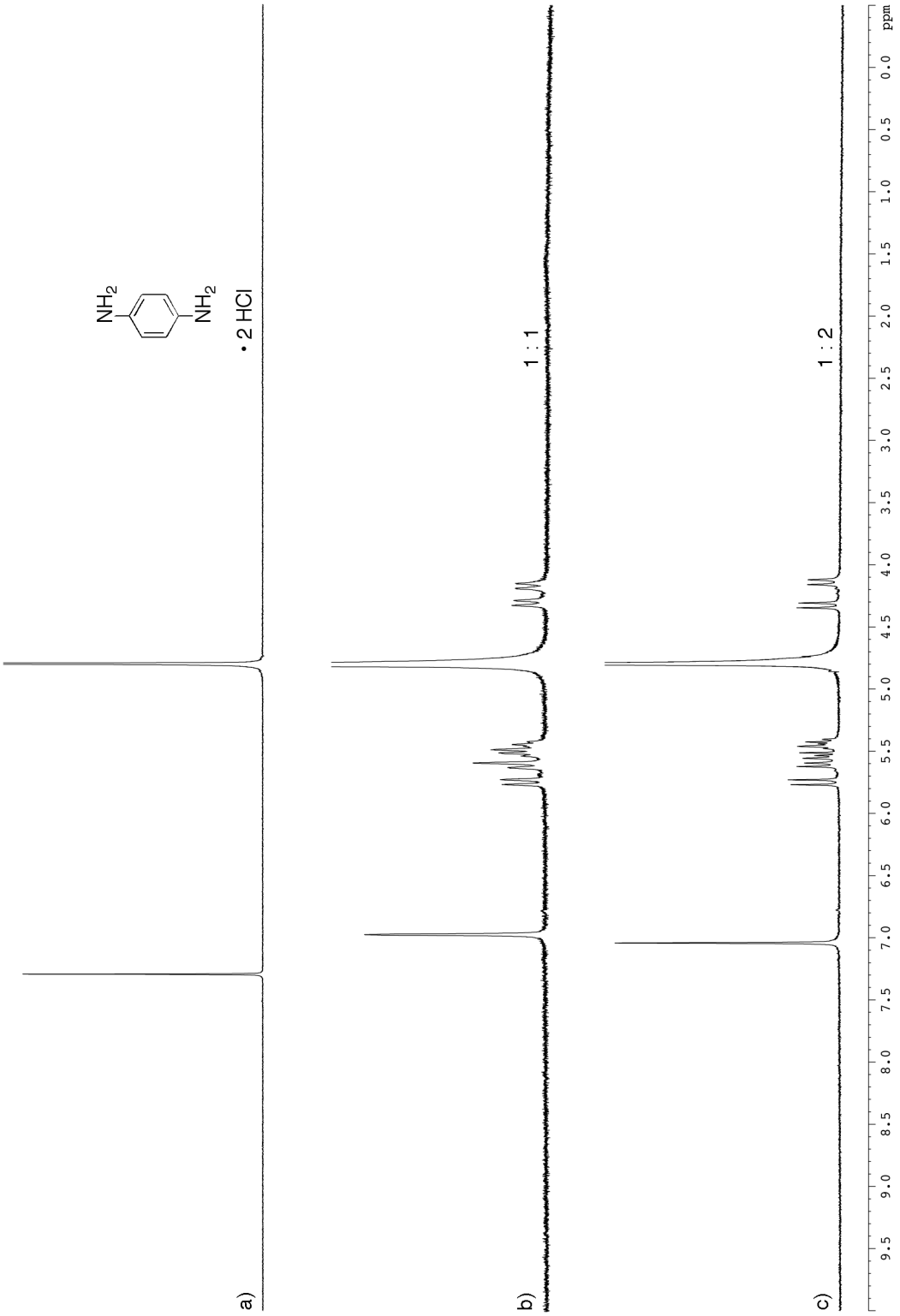

Figure III-S5. NMR spectra recorded (D_2O, 400 MHz, RT) for: a) **III-10** (1 mM), b) a mixture of **5C** (1 mM) and **III-10** (1 mM), and c) a mixture of **5C** (1 mM) and **III-10** (2 mM).

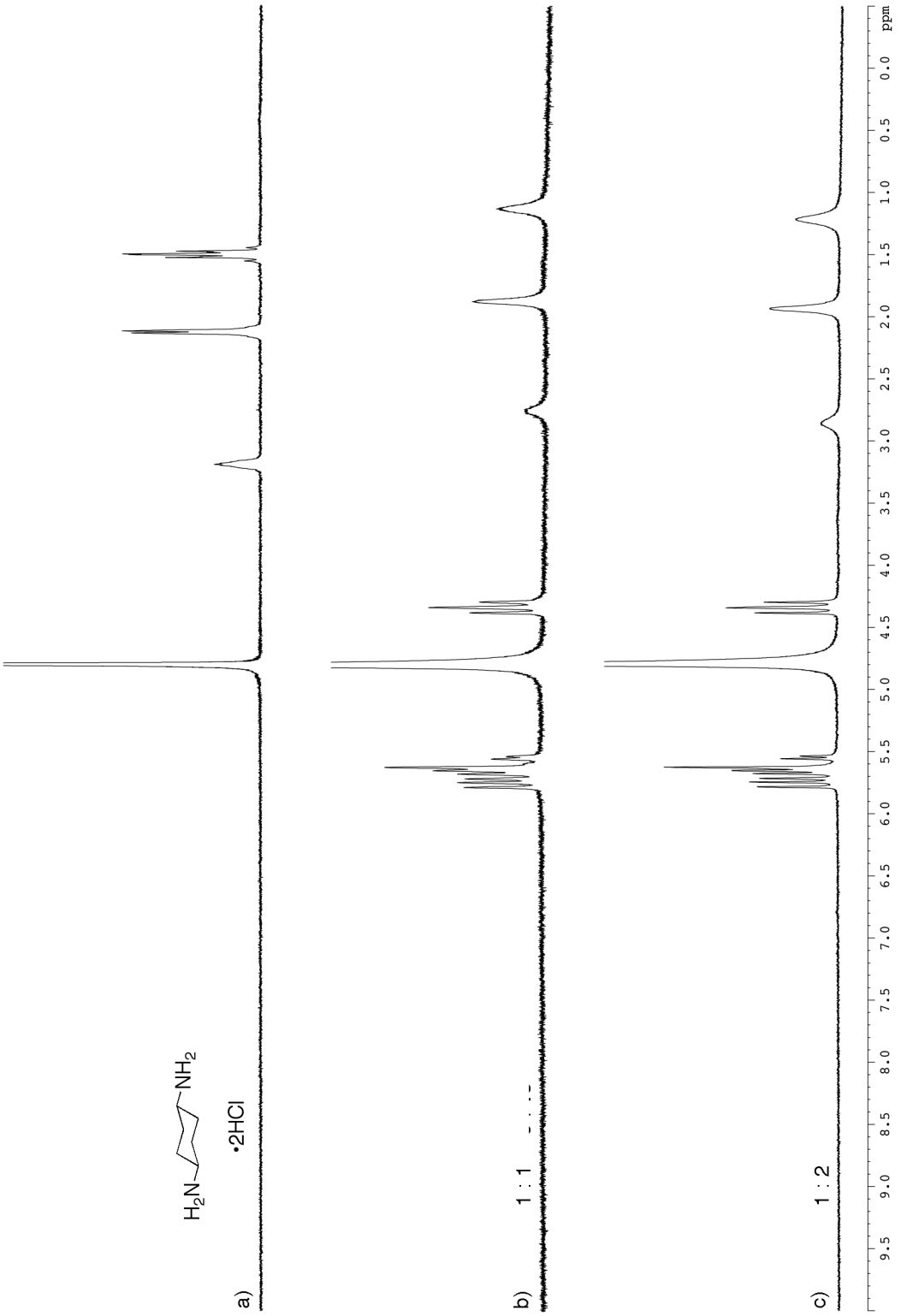

Figure III-S6. NMR spectra recorded (D_2O, 400 MHz, RT) for: a) **III-12** (1 mM), b) a mixture of **5C** (1 mM) and **III-12** (1 mM), and c) a mixture of **5C** (1 mM) and **III-12** (2 mM).

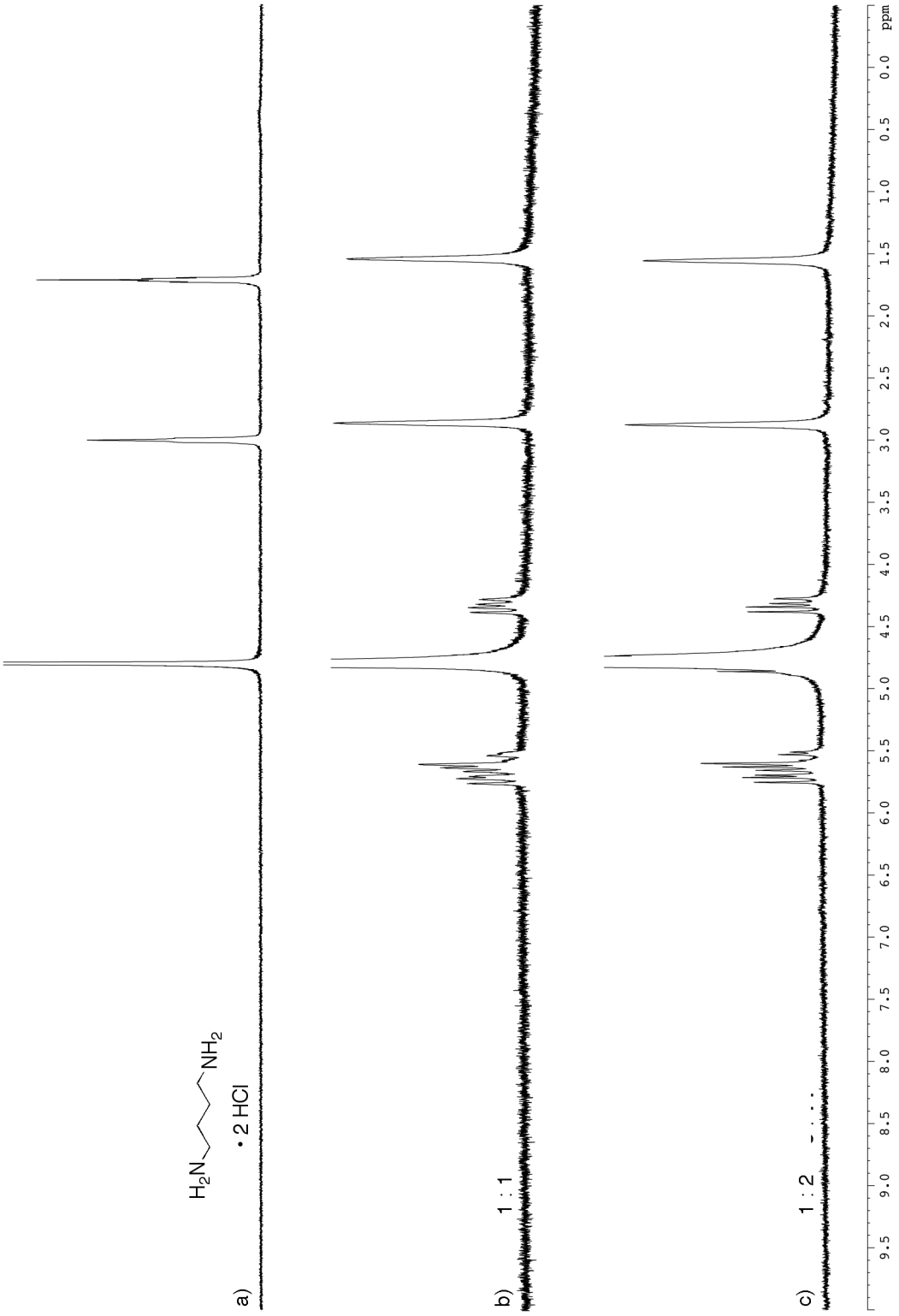

Figure III-S7. NMR spectra recorded (D_2O, 400 MHz, RT) for: a) **III-7** (1 mM), b) a mixture of **5C** (1 mM) and **III-7** (1 mM), and c) a mixture of **5C** (1 mM) and **III-7** (2 mM).

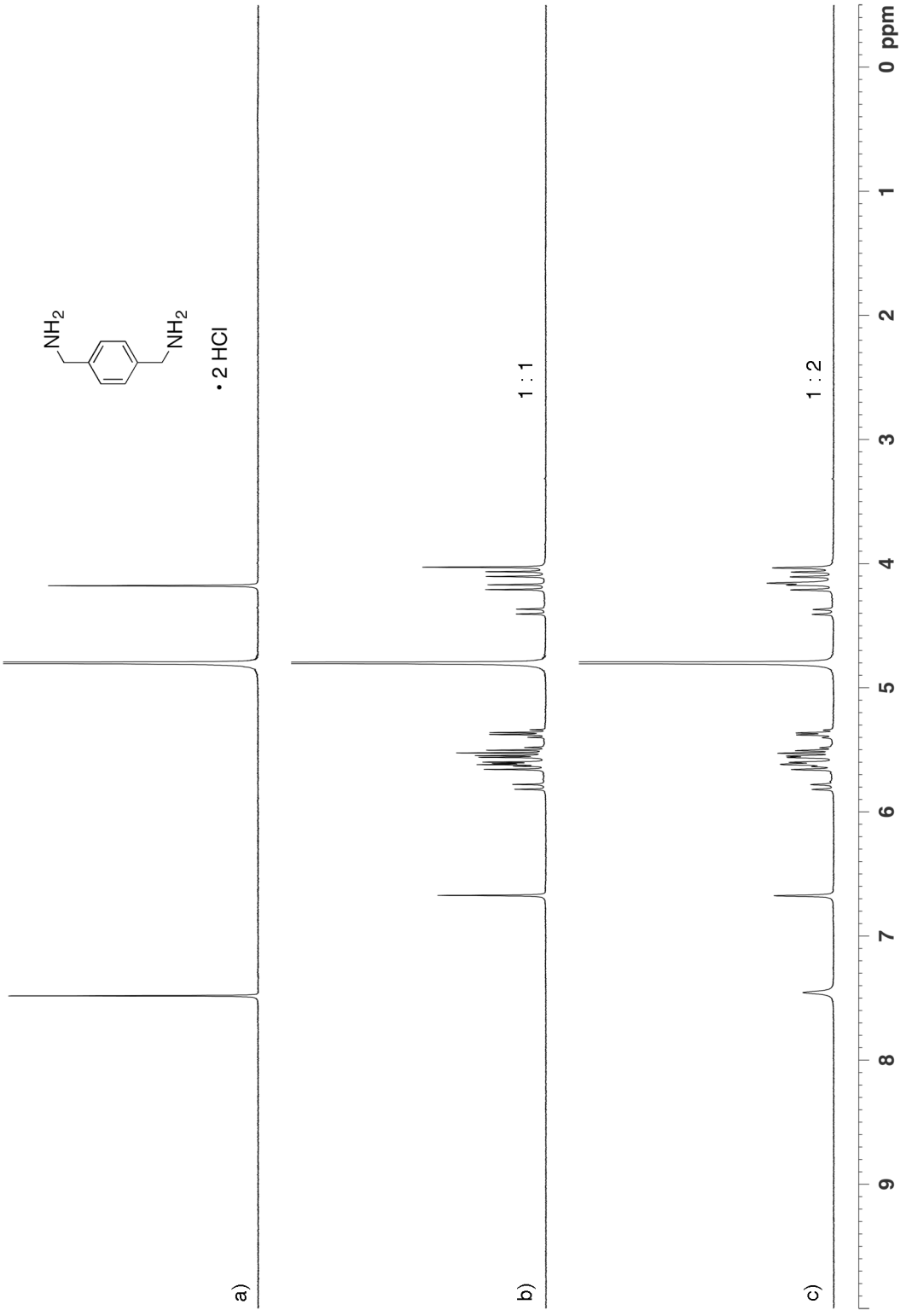

Figure III-S8. NMR spectra recorded (D_2O, 400 MHz, RT) for: a) **III-11** (1 mM), b) a mixture of **6C** (1 mM) and **III-11** (1 mM), and c) a mixture of **6C** (1 mM) and **III-11** (2 mM).

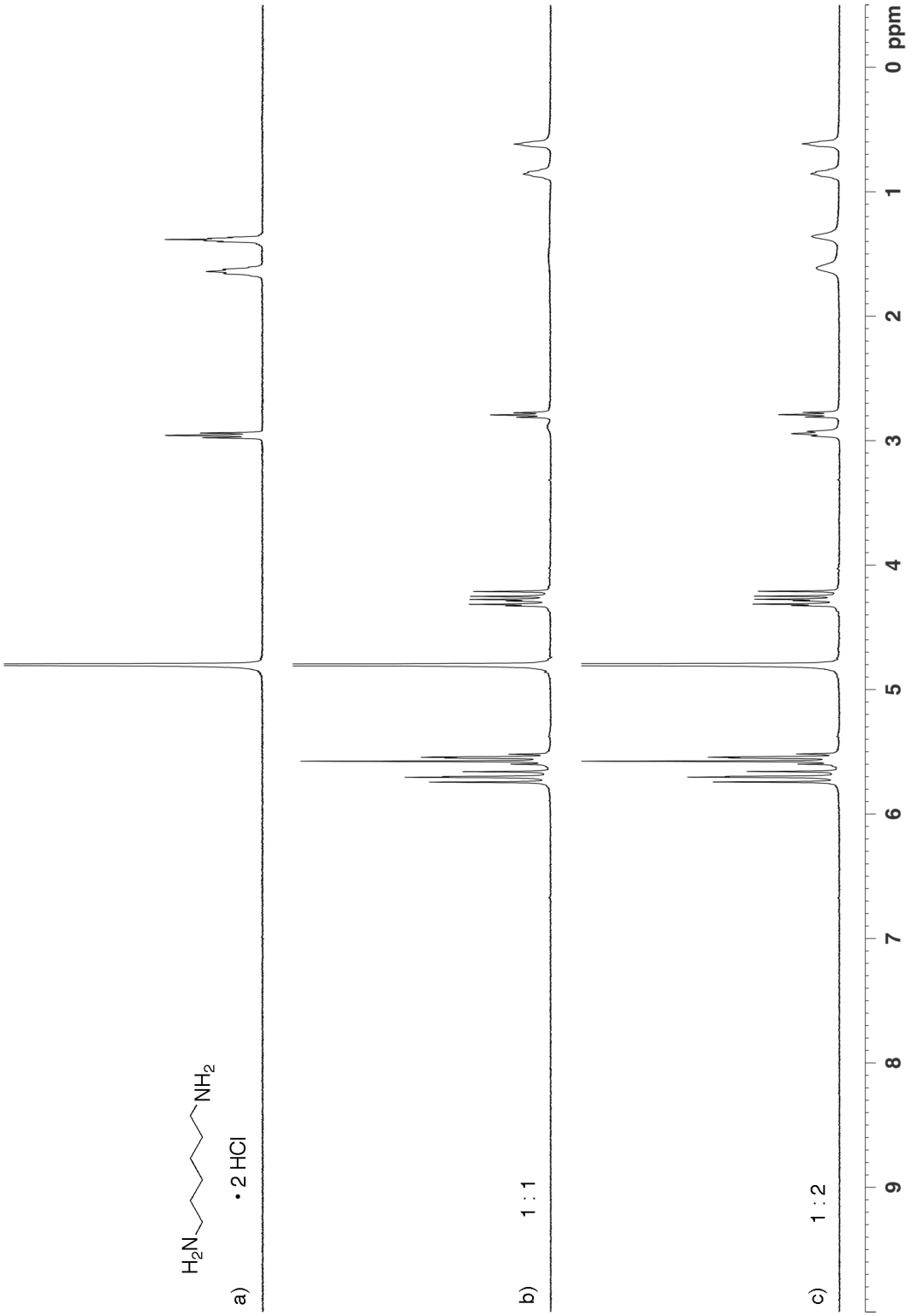

Figure III-S9. NMR spectra recorded (D_2O, 400 MHz, RT) for: a) **III-9** (1 mM), b) a mixture of **6C** (1 mM) and **III-9** (1 mM), and c) a mixture of **6C** (1 mM) and **III-9** (2 mM).

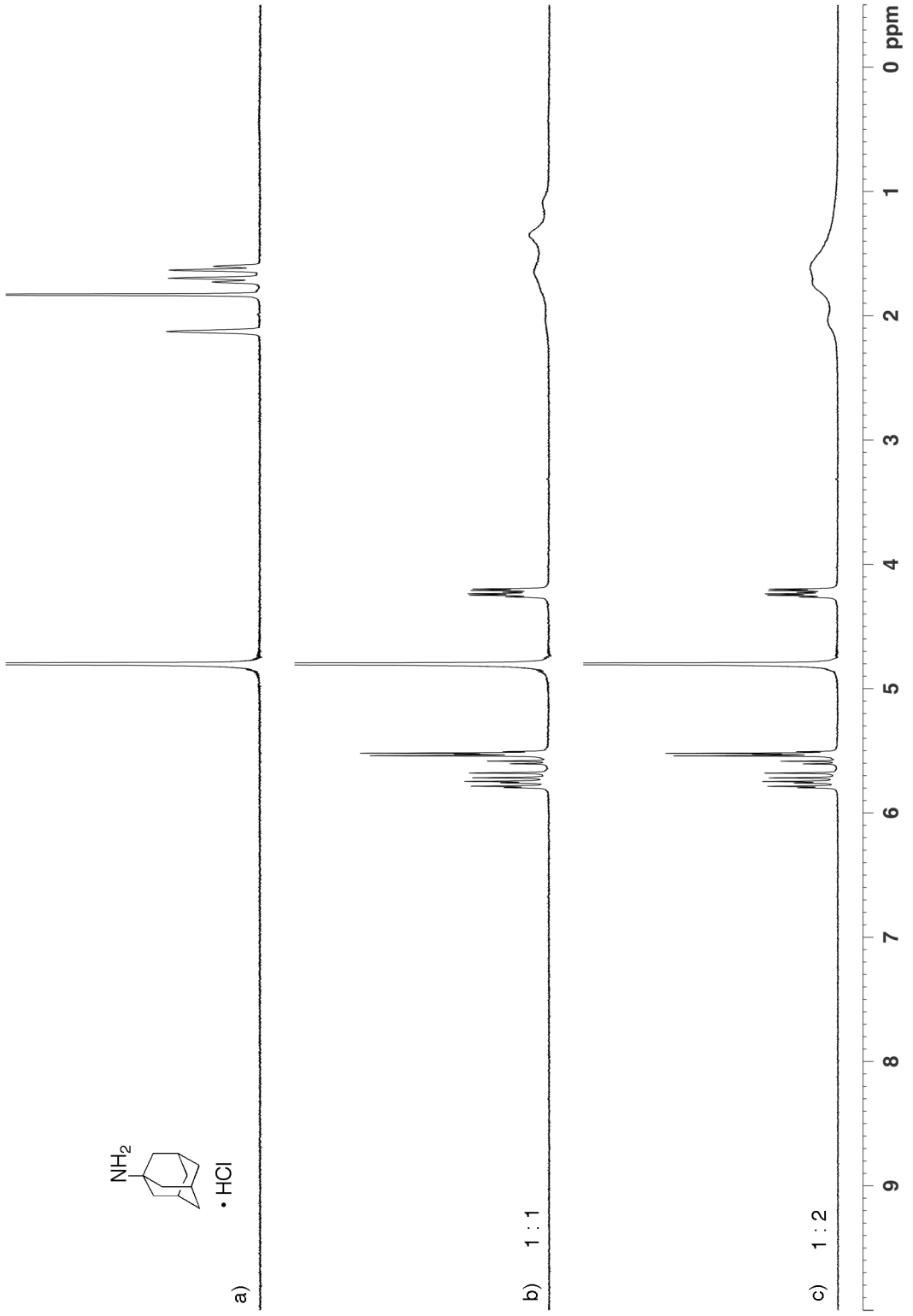

Figure III-S10. NMR spectra recorded (D_2O, 400 MHz, RT) for: a) **III-14** (1 mM), b) a mixture of **6C** (1 mM) and **III-14** (1 mM), and c) a mixture of **6C** (1 mM) and **III-14** (2 mM).

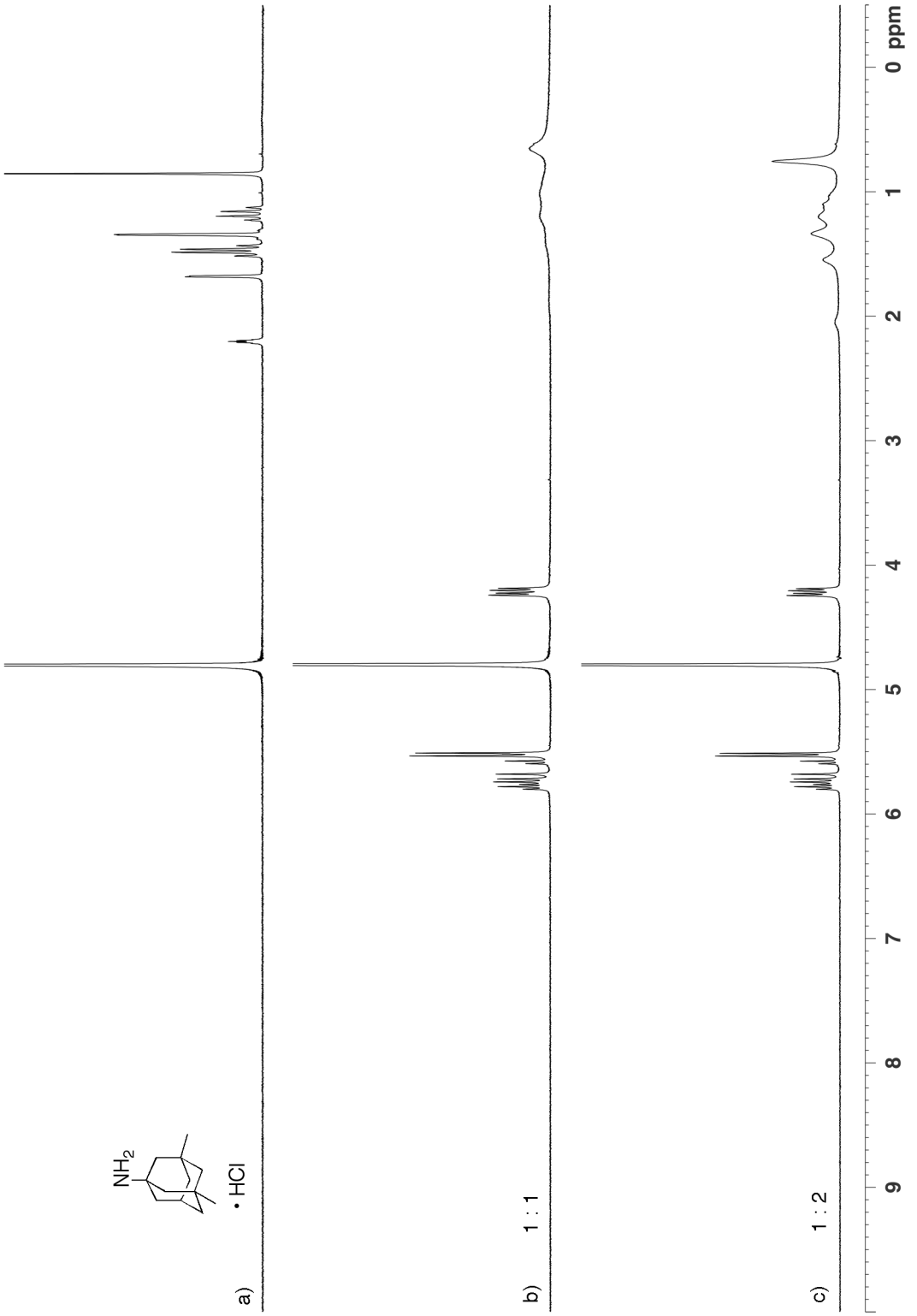

Figure III-S11. NMR spectra recorded (D_2O, 400 MHz, RT) for: a) **III-15** (1 mM), b) a mixture of **6C** (1 mM) and **III-15** (1 mM), and c) a mixture of **6C** (1 mM) and **III-15** (2 mM).

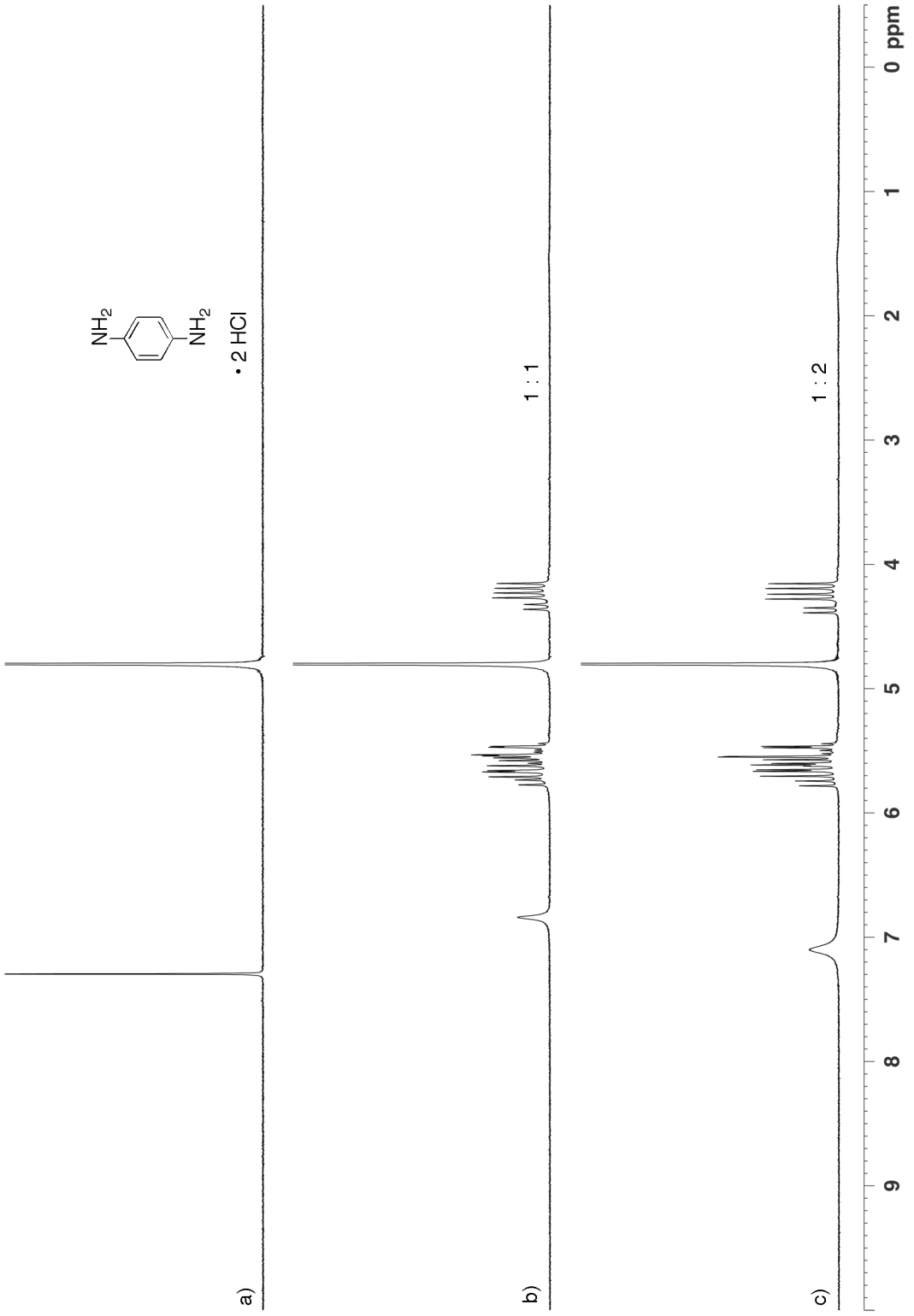

Figure III-S12. NMR spectra recorded (D_2O, 400 MHz, RT) for: a) **III-10** (1 mM), b) a mixture of **6C** (1 mM) and **III-10** (1 mM), and c) a mixture of **6C** (1 mM) and **III-10** (2 mM).

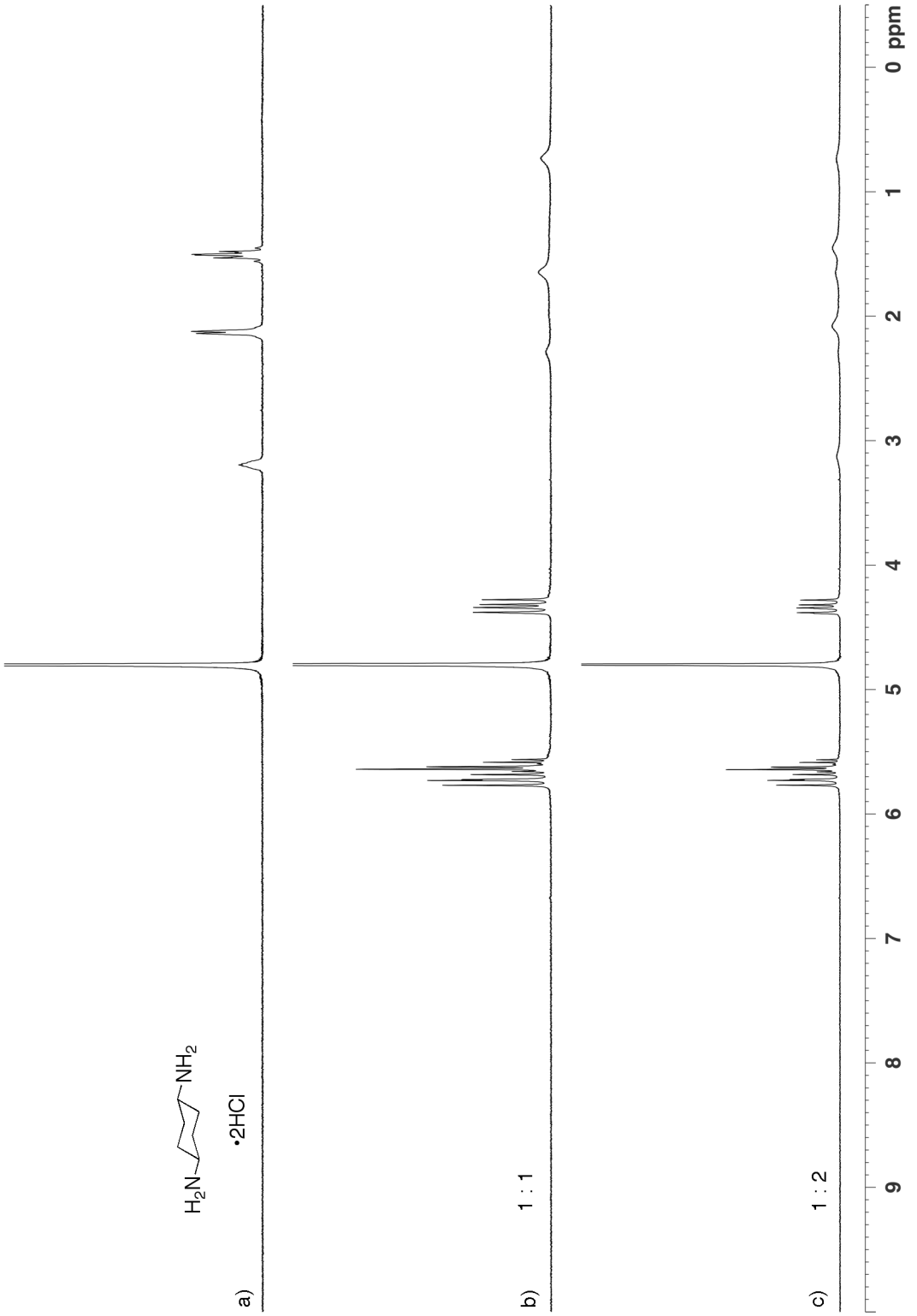

Figure III-S13. NMR spectra recorded (D_2O, 400 MHz, RT) for: a) **III-12** (1 mM), b) a mixture of **6C** (1 mM) and **III-12** (1 mM), and c) a mixture of **6C** (1 mM) and **III-12** (2 mM).

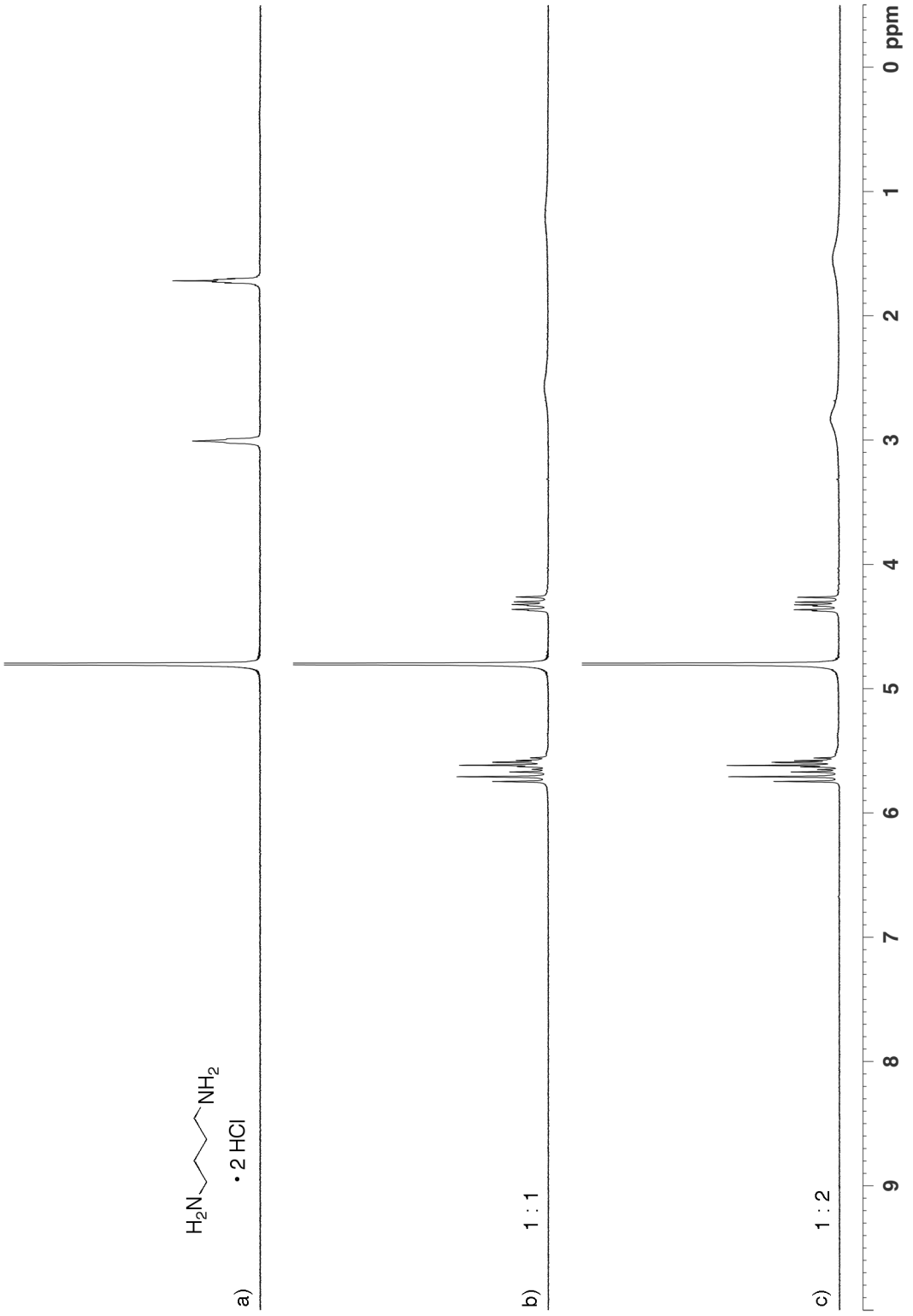

Figure III-S14. NMR spectra recorded (D_2O, 400 MHz, RT) for: a) **III-7** (1 mM), b) a mixture of **6C** (1 mM) and **III-7** (1 mM), and c) a mixture of **6C** (1 mM) and **III-7** (2 mM).

Determination of binding constants:
1:1 Binding Models Used in Scientist.
All calculations were performed on a personal computer running Scientist.

Models used to calculate the binding constant of guests **III-10** and **III-13** with hosts **5C** and **6C** using NMR titration.

```
// Micromath Scientist Model File
// 1:1 Host:Guest binding model for NMR
//This model assumes the guest concentration is fixed and host concentration is varied
IndVars: ConcHostTot
DepVars: Deltaobs
Params: Ka, ConcGuestTot, Deltasat, Deltazero
Ka = ConcHostGuest/(ConcHostFree*ConcGuestFree)
ConcHostTot=ConcHostFree + ConcHostGuest
ConcGuestTot=ConcGuestFree + ConcHostGuest
Deltaobs = Deltazero + (Deltasat - Deltazero) * (ConcHostGuest/ConcGuestTot)
//Constraints
0 < ConcHostFree < ConcHostTot
0 < Ka
0 < ConcGuestFree < ConcGuestTot
0 < ConcHostGuest < ConcHostTot
***
```

Models used to calculate the binding constant of guests and **5C** or **6C** using displacement assay.

```
// MicroMath Scientist Model File
IndVars: ConcAntot
DepVars: Absorb
Params: ConcHtot, ConcGtot, Khg, Kha, AbsorbMax, AbsorbMin
Khg = ConcHG / (ConcH * ConcG)
Kha = ConcHAn / (ConcH * ConcAn)
Absorb = AbsorbMin + (AbsorbMax-AbsorbMin)*(ConcHG/ConcGtot)
ConcHtot = ConcH + ConcHG + ConcHAn
ConcGtot = ConcHG + ConcG
ConcAntot = ConcAn + ConcHAn
0 < ConcHG < ConcHtot
0 < ConcH < ConcHtot
0 < ConcG < ConcGtot
0 < ConcAn < ConcAntot
***
```

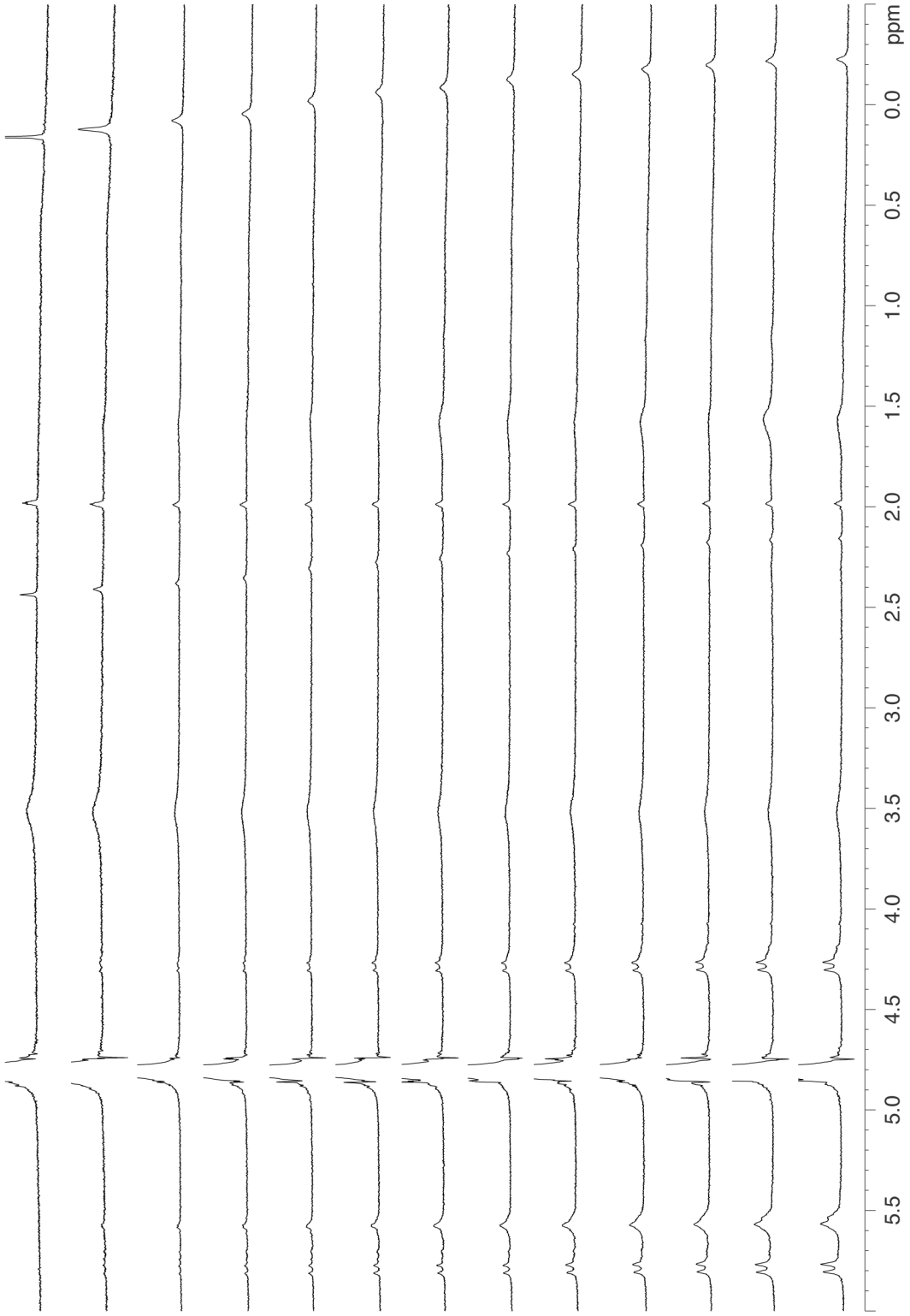

Figure III-S15. ^{1}H NMR spectra (400 MHz, 20 mM $NaCO_2CD_3$ buffer, pD = 4.74) recorded during the titration of a solution of **III-13** (0.125 mM) with **6C** of (0 – 0.591 mM).

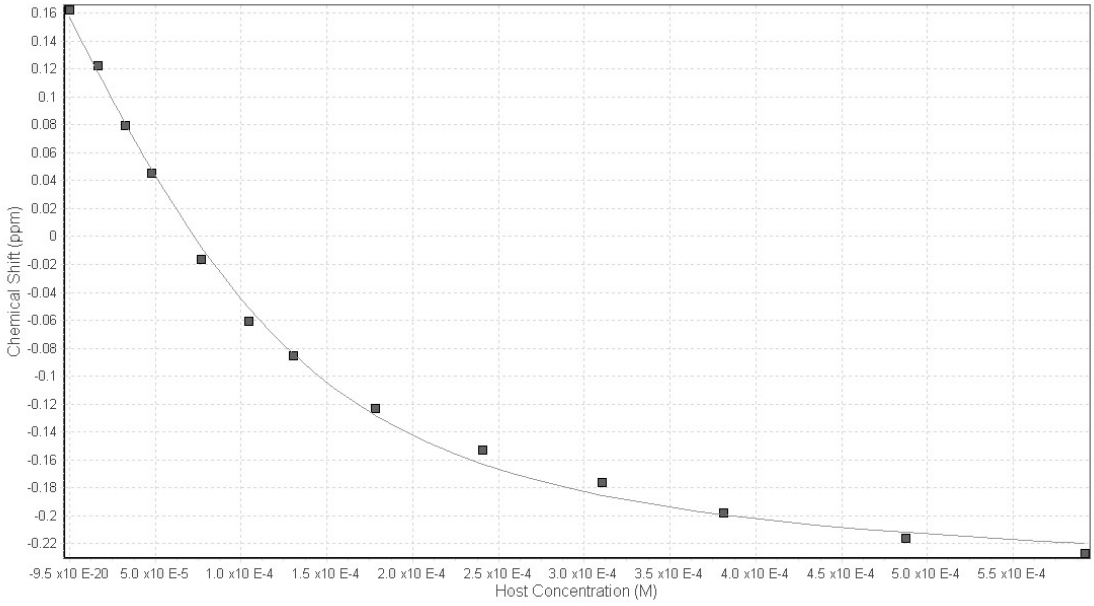

Figure III-S16. Plot of the chemical shift of the $(CH_3)_3Si$ group of **III-13** as a function of [**6C**]. The solid line represents the best non-linear fitting of the data to a 1:1 binding model ($K_a = 2.6 \pm 0.3 \times 10^4\ M^{-1}$).

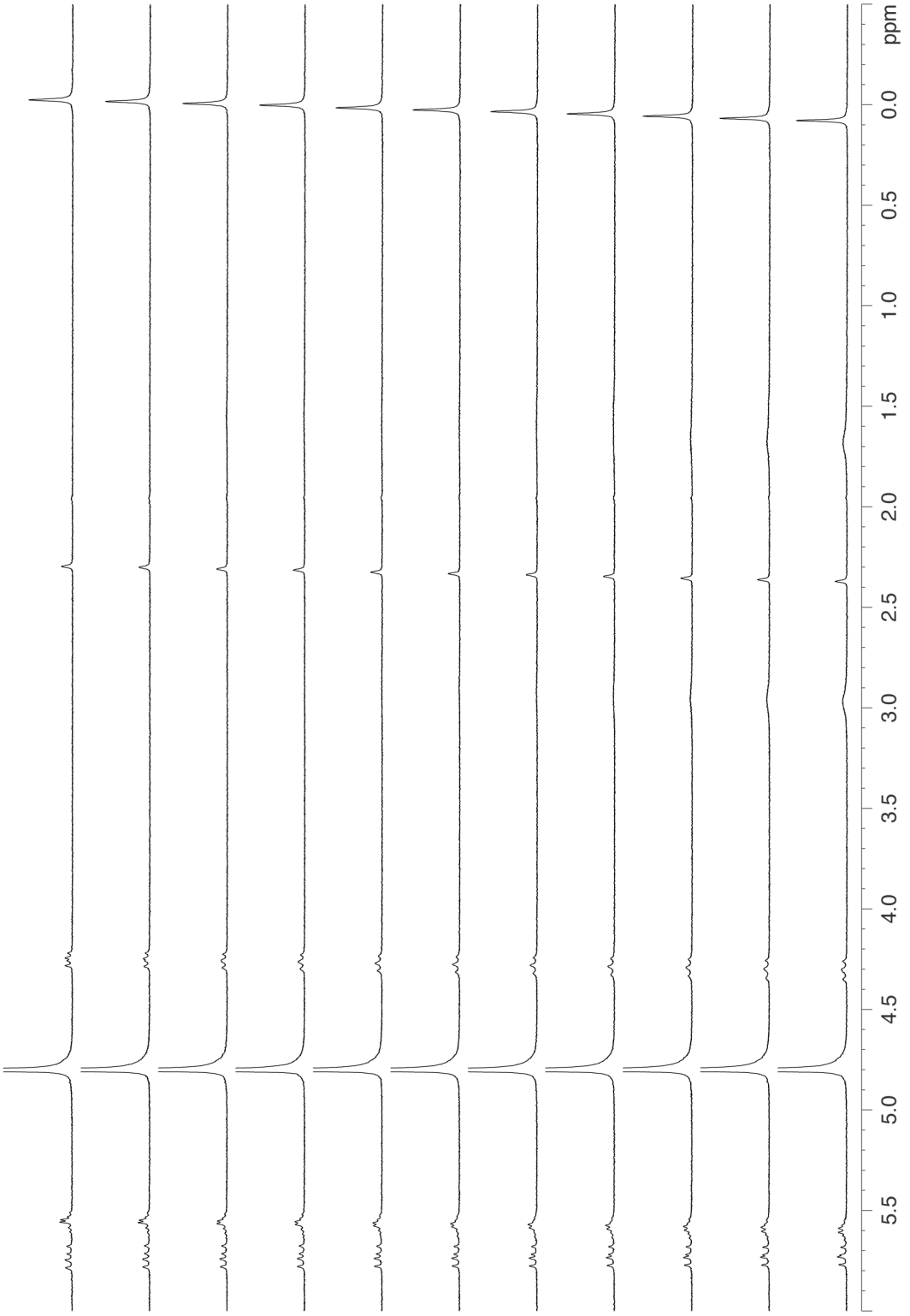

Figure III-S17. ^{1}H NMR (400 MHz, 20 mM $NaCO_2CD_3$ buffer, pD = 4.74) recorded during displacement titration of a solution **III-13** (1.0 mM) and **6C** (0.5 mM) with **III-7** (0 – 1.8 mM).

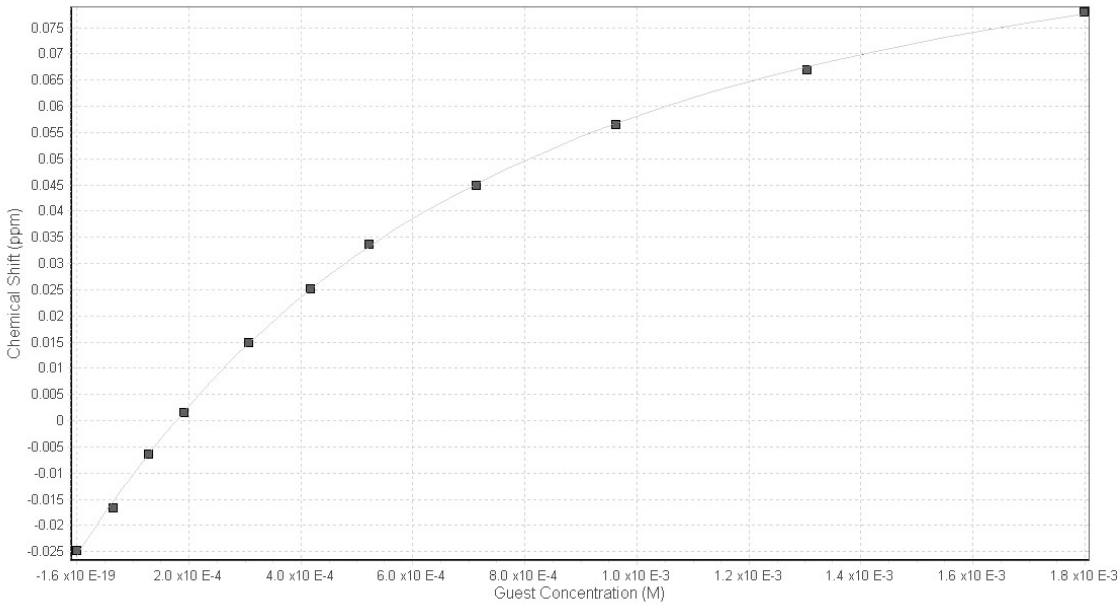

Figure III-S18. Displacement titration of a solution containing **III-13** (1.0 mM) and **6C** (0.5 mM) with **III-7** (0 – 1.8 mM) (20 mM $NaCO_2CD_3$ buffer, pD = 4.74). Non-linear fitting of a plot of chemical shift *versus* [**III-7**] with Scientist^{TM}. K_a was evaluated as 5.0 $\pm$ 0.3 $\times$ 10^4 M^{-1}.

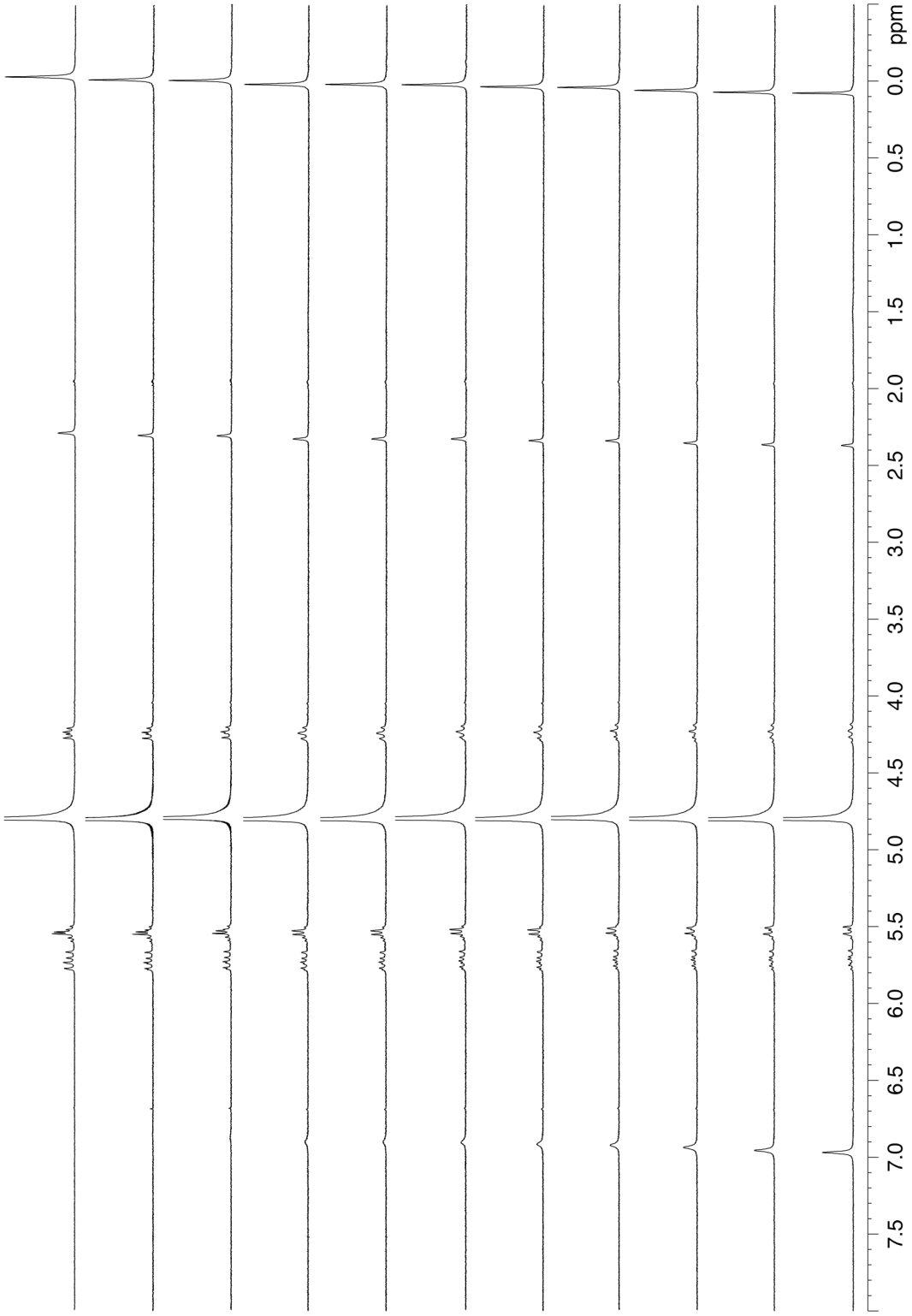

Figure III-S19. ^{1}H NMR (400 MHz, 20 mM $NaCO_2CD_3$ buffer, pD = 4.74) recorded during the displacement titration of a solution **III-13** (1.0 mM) and **6C** (0.5 mM) with **III-10** (0 – 1.8 mM).

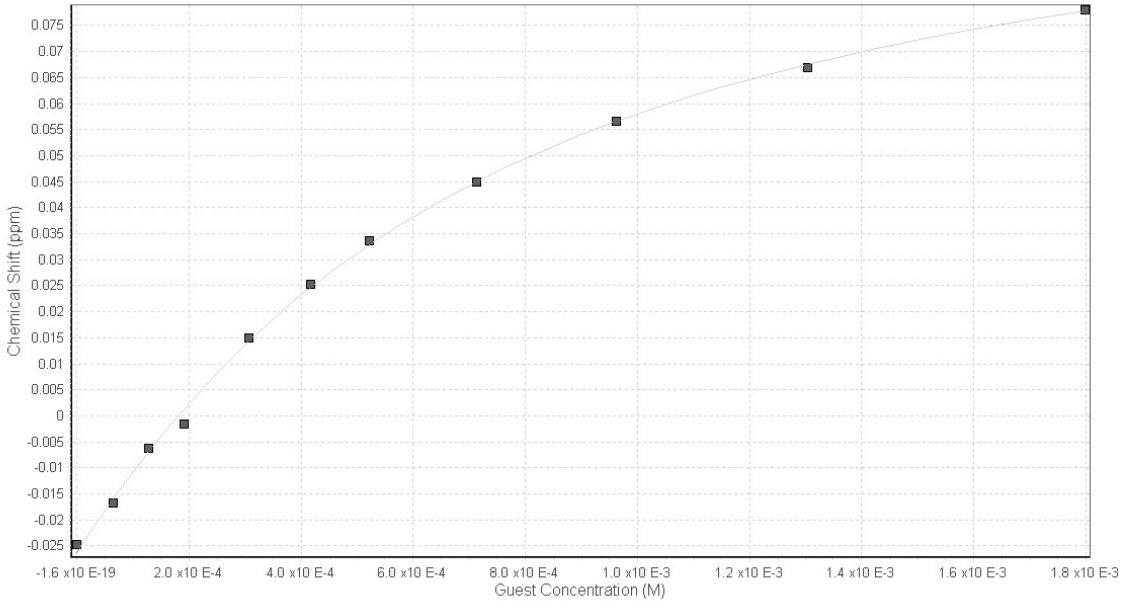

Figure III-S20. Displacement titration of a solution containing **III-13** (1.0 mM) and **6C** (0.5 mM) with **III-10** (0 – 1.8 mM) (20 mM $NaCO_2CD_3$ buffer, pD = 4.74). Non-linear fitting plot of chemical shift *versus* [**III-10**]. K_a was evaluated as $4.9 \pm 0.6 \times 10^4\ M^{-1}$.

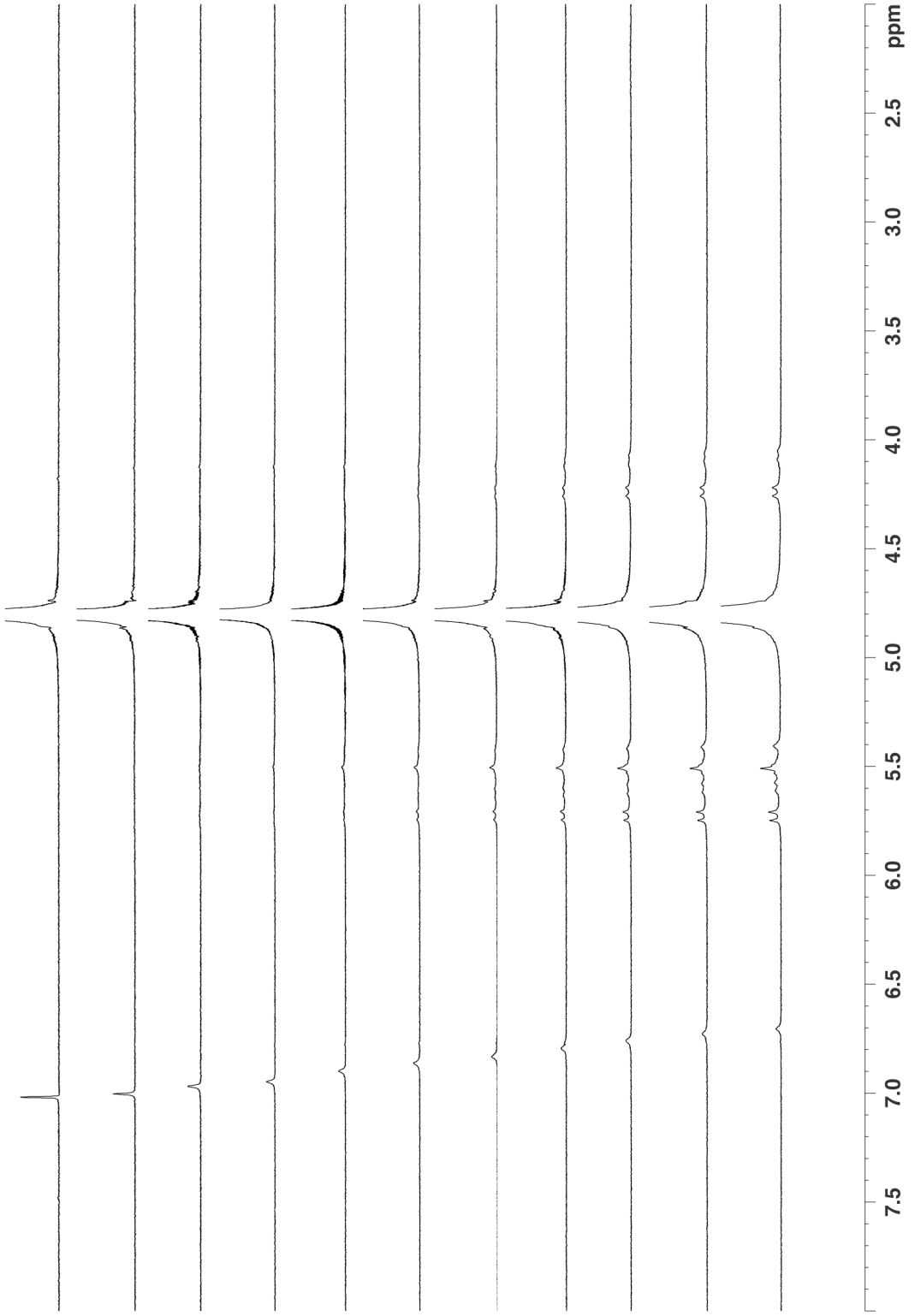

Figure III-S21. ^{1}H NMR spectra (400 MHz, 20 mM $NaCO_2CD_3$ buffer, pD = 4.74) recorded during the titration of a solution of **III-10** (0.125 mM) with **5C** (0 – 0.487 mM).

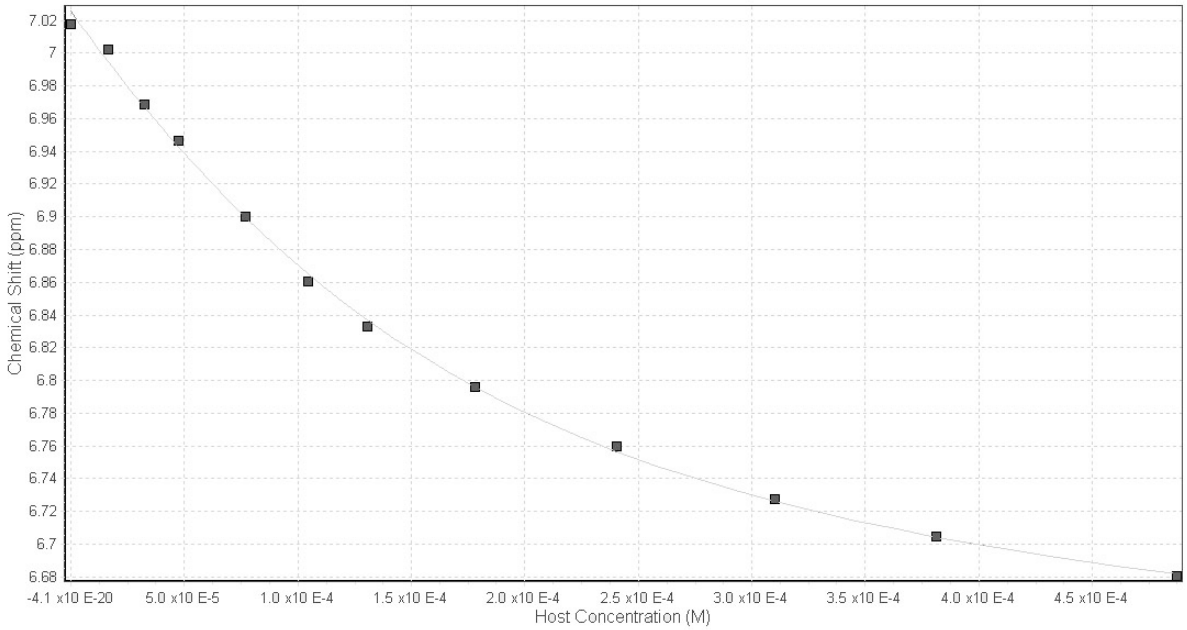

Figure III-S22. Plot of the chemical shift of the CH group of **III-10** as a function of [**5C**]. The solid line represents the best non-linear fitting of the data to a 1:1 binding model ($K_a = 1.0 \pm 0.1 \times 10^4\ M^{-1}$).

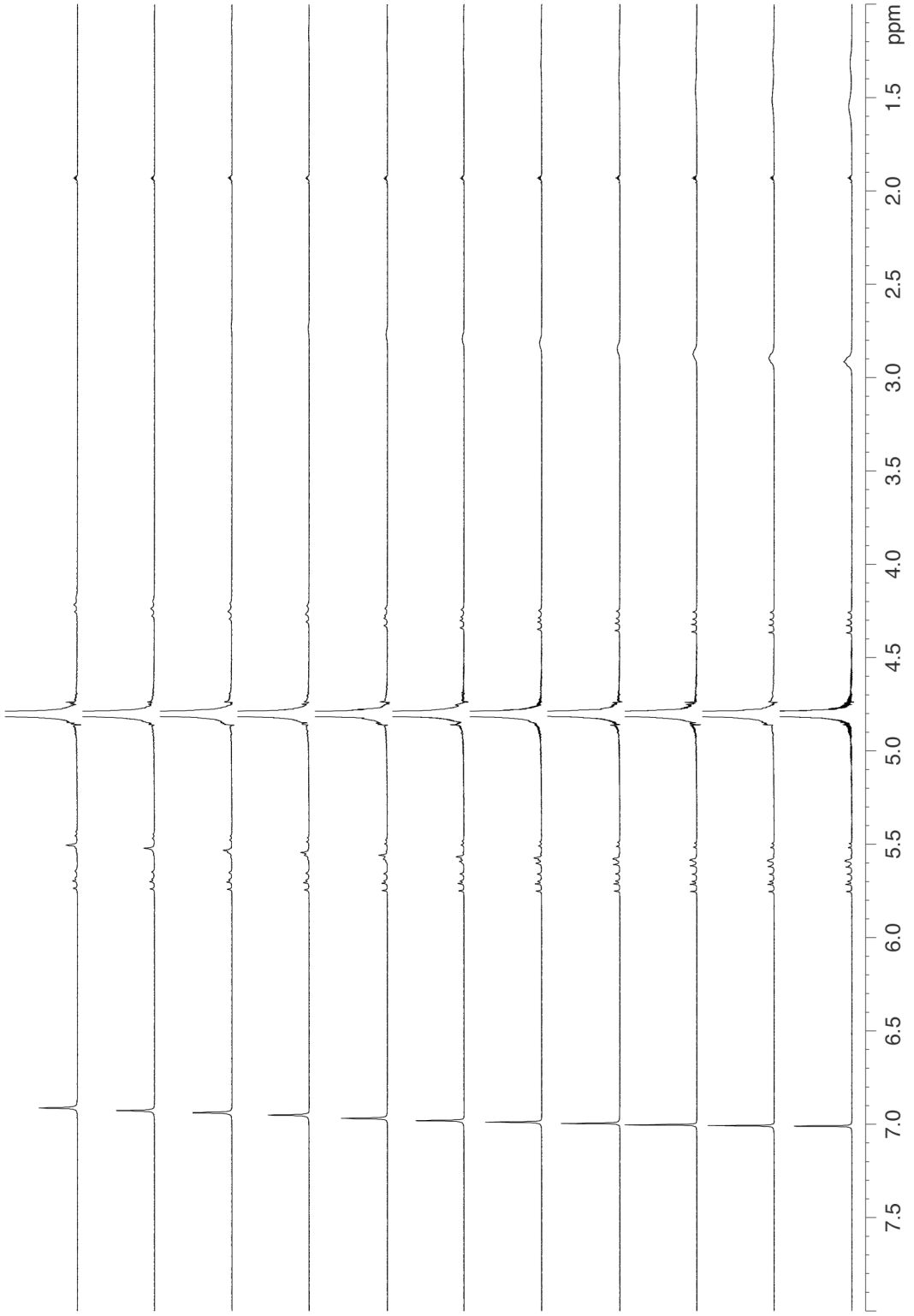

Figure III-S23. ^{1}H NMR (400 MHz, 20 mM $NaCO_2CD_3$ buffer, pD = 4.74) recorded during the displacement titration of a solution **III-10** (1.0 mM) and **5C** (0.26 mM) with **III-8** (0 – 1.3 mM).

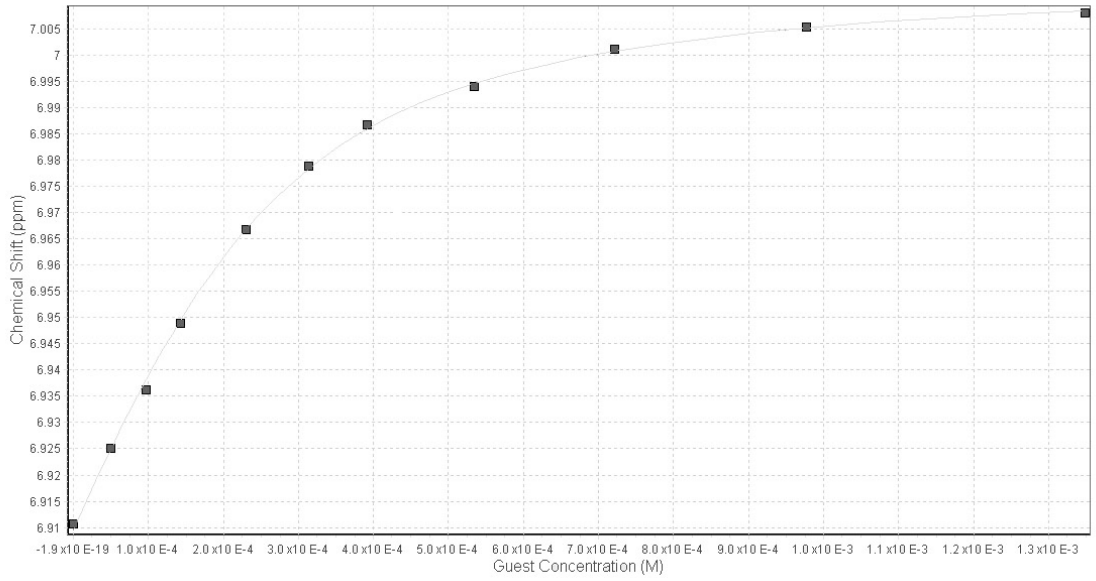

Figure III-S24. Displacement titration of a solution containing **III-10** (1.0 mM) and **5C** (0.26 mM) with **III-8** (0 – 1.3 mM) (20 mM $NaCO_2CD_3$ buffer, pD = 4.74). Non-linear fitting of a plot of chemical shift *versus* [**III-8**] with Scientist^{TM}. K_a was evaluated as 1.4 $\pm$ 0.1 $\times$ 10^5 M^{-1}.

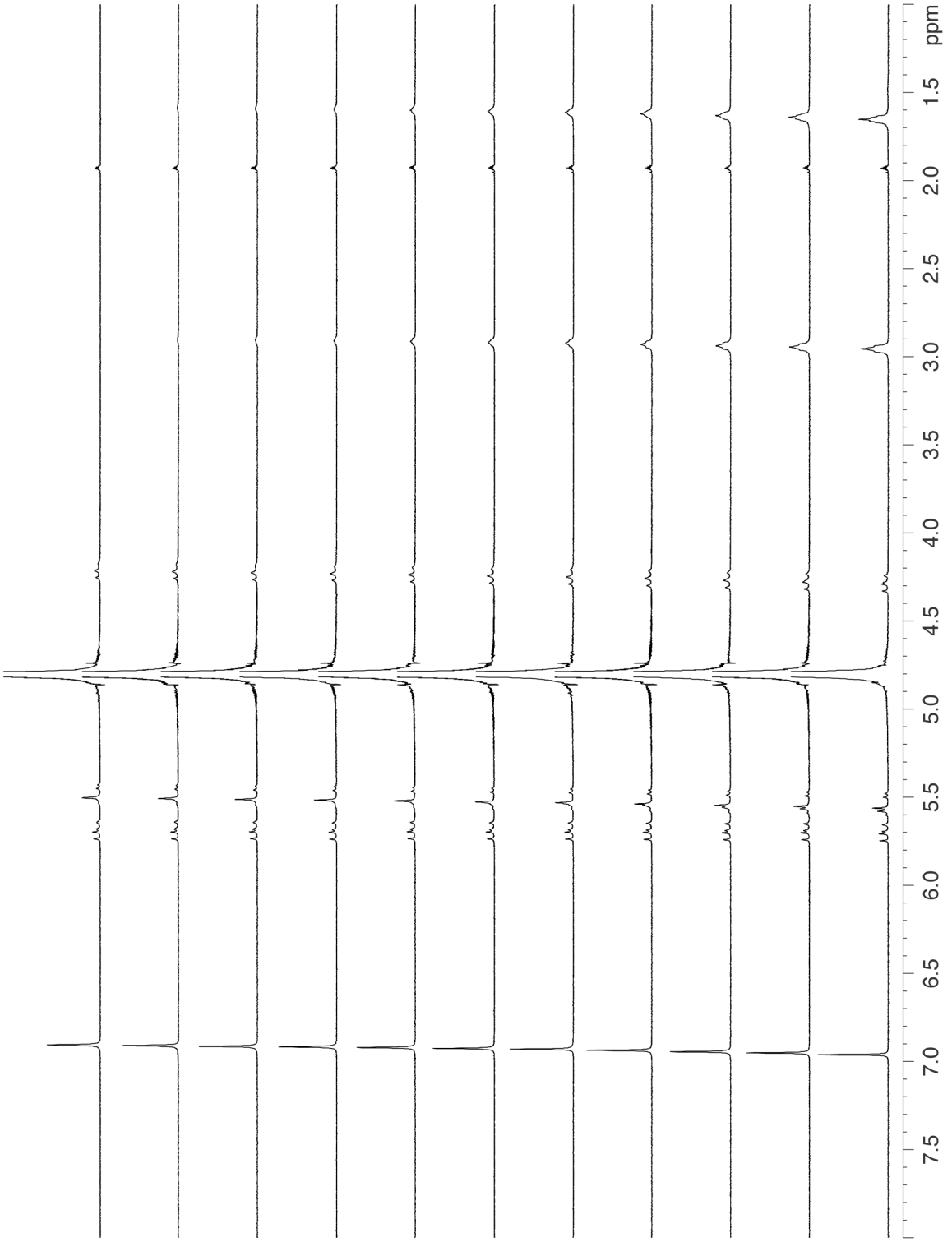

Figure III-S25. ^{1}H NMR (400 MHz, 20 mM $NaCO_2CD_3$ buffer, pD = 4.74) recorded during the displacement titration of a solution **III-10** (1.0 mM) and **5C** (0.3 mM) with **III-7** (0 – 1.8 mM).

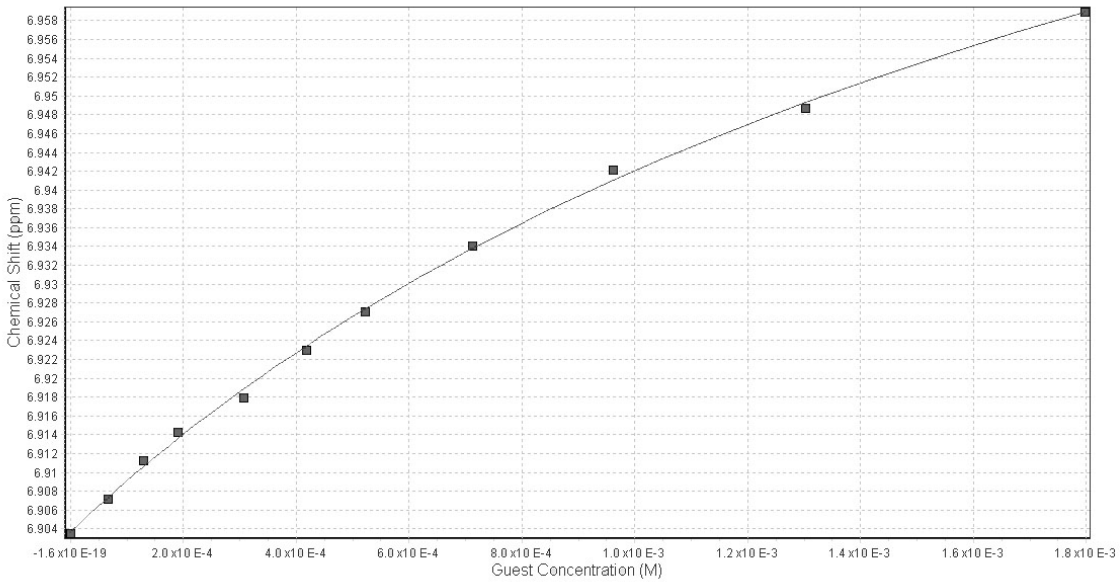

Figure III-S26. Displacement titration of a solution containing **III-10** (1.0 mM) and **5C** (0.3 mM) with **III-7** (0 – 1.8 mM) (20 mM $NaCO_2CD_3$ buffer, pD = 4.74). Non-linear fitting of a plot of chemical shift *versus* [**III-7**] with Scientist^{TM}. K_a was evaluated as 4.7 $\pm$ 0.5 $\times$ 10^4 M^{-1}.

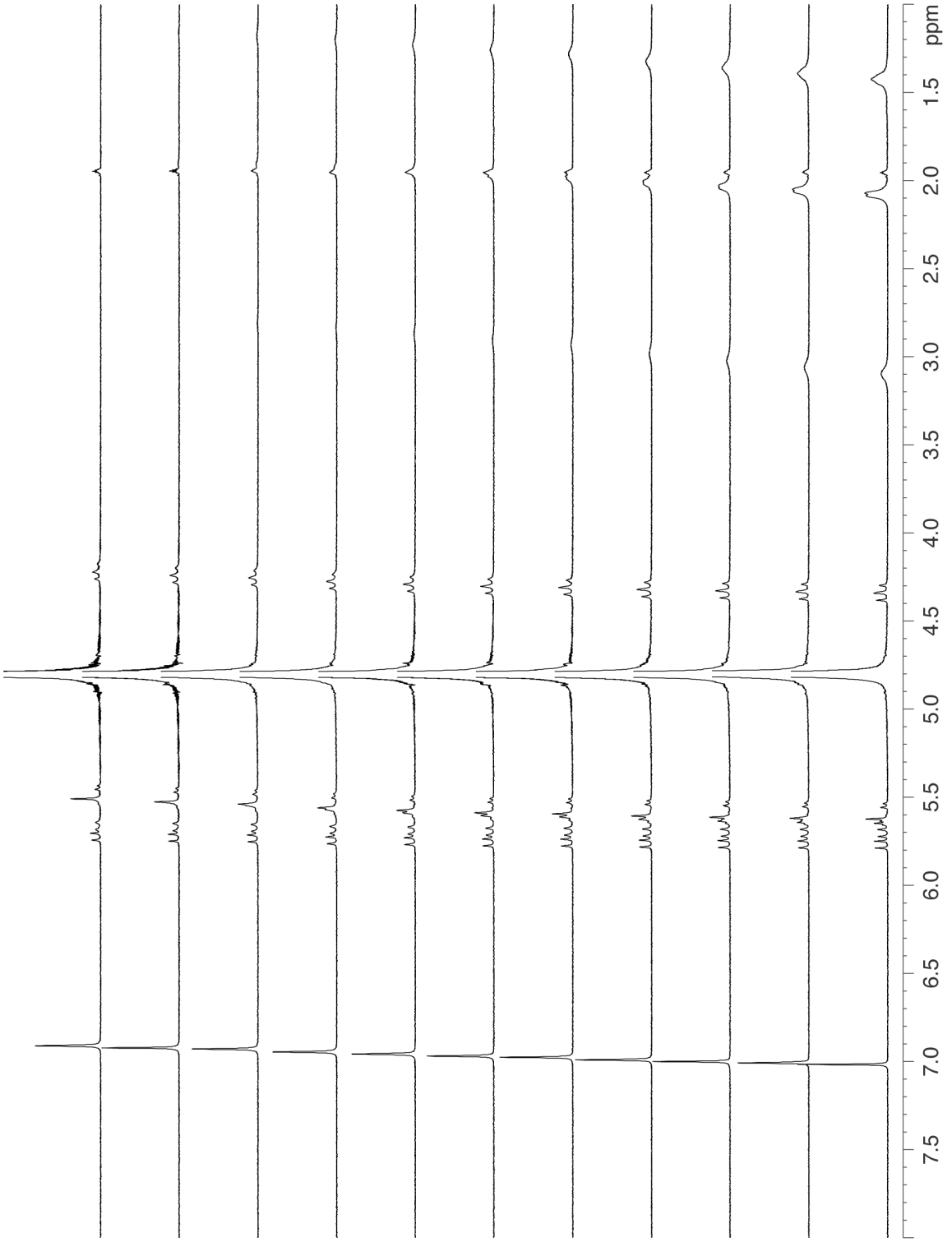

Figure III-S27. ^{1}H NMR (400 MHz, 20 mM $NaCO_2CD_3$ buffer, pD = 4.74) recorded during the displacement titration of a solution **III-10** (1.0 mM) and **5C** (0.26 mM) with **III-12** (0 – 1.8 mM).

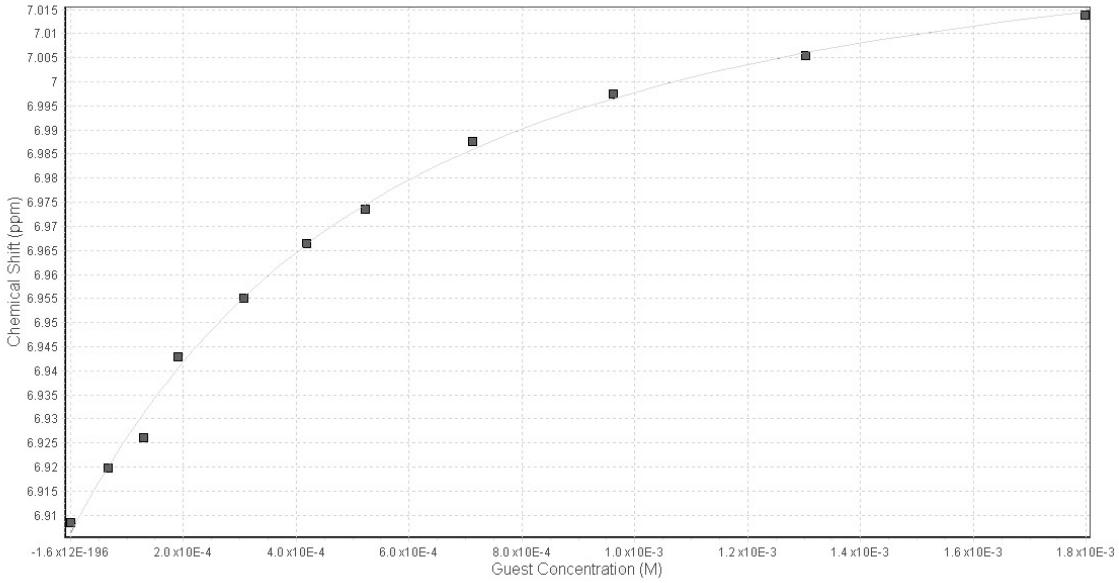

Figure III-S28. Displacement titration of a solution containing **III-10** (1.0 mM) and **5C** (0.3 mM) with **III-12** (0 – 1.8 mM) (20 mM $NaCO_2CD_3$ buffer, pD = 4.74). Non-linear fitting of a plot of chemical shift *versus* [**III-12**] with Scientist^{TM}. K_a was evaluated as 2.7 $\pm$ 0.4 $\times$ 10^4 M^{-1}.

Sample Determination of K_{rel} for the Competition Between III-11 and III-14 for 6C. We use equation 1 to determine K_{rel} for the interaction of **III-11** and **III-14** for **6C**. For this purpose, we prepared a solution containing **6C** (0.4 mM), **III-11** (0.5 mM), **III-14** (0.5 mM) and allowed it to reach equilibrium (Figure III-S32). Next, we determined the concentration of **6C•III-11** by integration of the appropriate resonances in the ^{1}H NMR spectrum (Figure III-S32: **6C•III-11**: 6.67 ppm; **III-11**: 7.47 ppm). Using the concentration and the mass balance expression (equation 2) allowed us to calculate [**III-11**]$_{free}$ = 0.2885 mM and [**6C•III-11**] = 0.2115 mM. Equation 3 is then used to calculate [**6C•III-14**] (0.1885 mM) using the known value of **6C•III-11**. Lastly, equation 4 is used to calculate [**III-14**]$_{free}$ (0.3115 mM) using the known value of [**6C •III-14**].

$$K_{rel} = ([\mathbf{6C{\bullet}III\text{-}14}][\mathbf{III\text{-}11}]_{free}) / ([\mathbf{6C{\bullet}III\text{-}11}][\mathbf{III\text{-}14}]_{free}) \quad (1)$$

$$[\mathbf{III\text{-}11}]_{Total} = 0.5\ mM = [\mathbf{III\text{-}11}]_{free} + [\mathbf{6C{\bullet}III\text{-}11}] \quad (2)$$

$$[\mathbf{6C}]_{Total} = 0.4\ mM = [\mathbf{6C{\bullet}III\text{-}11}] + [\mathbf{6C{\bullet}III\text{-}14}] \quad (3)$$

$$[\mathbf{III\text{-}14}]_{Total} = 0.5\ mM = [\mathbf{III\text{-}14}]_{free} + [\mathbf{6C\ {\bullet}III\text{-}14}] \quad (4)$$

Substitution of the values of [**6C•III-11**], [**III-11**]$_{free}$, [**6C•III-14**], and [**III-14**]$_{free}$ into equation 1 gave K_{rel} = 0.825. These determinations were done in triplicate from independently prepared stock solutions and the average values were used in the calculations of K_a and the error analysis shown below. In preparing the solutions for the above determinations we used a small excess of **III-11** (to ensure there is no free **6C**) and a small excess of **III-14**; under those conditions the errors in [**III-14**]$_{free}$, [**III-11**]$_{free}$ are small and both [**III-11**] and [**6C•III-11**] are kept in a good range for accurate measurement of their ratio by ^{1}H NMR.

Sample Error Analysis Calculation for 6C•III-9. Since the binding constants in this paper are determined by several levels of ^{1}H NMR competition experiments referenced to an absolute K_a measured for **6C•III-13** measured by ^{1}H NMR titration, a proper error analysis is critical. In this section we give a sample calculation of the error analysis used to determine the uncertainty associated with the K_a value for **6C•III-9**.

Step 1 – Estimation of the accuracy of ^{1}H NMR methods for the determination of guest and host•guest concentrations. We used ^{1}H NMR to repeatedly determine the concentration of samples of known concentration of guest and host•guest complex by monitoring guest resonances. The ^{1}H NMR based method was accurate with a standard deviation of ± 3%.

Step 2 – Determination of the Uncertainty Associated with a Single Level of Competition (K_{rel}). We propagated the above uncertainty associated with the NMR determination of concentrations (e.g. $\{(\sigma_{[CB[n]\bullet guest]})/[CB[n]\bullet guest]\} = 0.03$ and $\{(\sigma_{[Guest]})/[Guest]\} = 0.03$) of using equations 5 and equations 6 – 7 (Bevington eq. 4-11, pages 61–62). Equation 6 delivers the uncertainty associated with the weighted product (x) of two values (u and v) (e.g. x = ±a u v). Similarly, equation 7 delivers the uncertainty for dividing two numbers (e.g. x = ±(a u) / v). We make the assumption that the fluctuations in u and v are not correlated ($\sigma_{uv} = 0$) which when substituted into equations 6 and 7 delivers equation 8. Rearranging slightly yields equation 9 which allows us to

directly use the 3% uncertainty determined for our NMR method.

$$K_{rel} = ([CB[n]\bullet G2][G1]) / ([CB[n]\bullet G1][G2]) \quad (5)$$

$$\frac{\sigma_x^2}{x^2} = \frac{\sigma_u^2}{u^2} + \frac{\sigma_v^2}{v^2} + 2\frac{\sigma_{uv}^2}{uv} \quad (6) \qquad \frac{\sigma_x^2}{x^2} = \frac{\sigma_u^2}{u^2} + \frac{\sigma_v^2}{v^2} - 2\frac{\sigma_{uv}^2}{uv} \quad (7)$$

$$\frac{\sigma_x^2}{x^2} = \frac{\sigma_u^2}{u^2} + \frac{\sigma_v^2}{v^2} \quad (8) \qquad \left(\frac{\sigma_x}{x}\right)^2 = \left(\frac{\sigma_u}{u}\right)^2 + \left(\frac{\sigma_v}{v}\right)^2 \quad (9)$$

We break the uncertainty determination in K_{rel} (equation 1) into three steps: 1) Multiplying [CB[n]•G2][G1], 2) multiplying [CB[n]•G1][G2], and 3) dividing the two results. Substituting (σ[CB[n]•G2] / [CB[n]•G2]) = 0.03 and (σ[G1]/[G1]) = 0.03 into equation 9 gives equation 10 and an uncertainty of 4.24% for [CB[n]•G2][G1] (equation 11). Similarly, the uncertainty of [CB[n]•G1][G2] is 4.24%.

$$\left(\frac{\sigma_{[CB[n]\bullet G2][G1]}}{[CB[n]\bullet G2][G1]}\right)^2 = (0.03)^2 + (0.03)^2 \quad (10) \qquad \left(\frac{\sigma_{[CB[n]\bullet G2][G1]}}{[CB[n]\bullet G2][G1]}\right) = 0.0424 \quad (11)$$

With the two values of the uncertainties of [CB[n]•G2][G1] and [CB[n]•G1][G2] (4.24%) in hand we next substituted these values into equation 9 to give the uncertainty in K_{rel} (eq. 12–13) of 6%.

$$\left(\frac{\sigma_{K_{rel}}}{K_{rel}}\right)^2 = \left(\frac{\sigma\frac{[CB[n]\bullet G2][G1]}{[CB[n]\bullet G2][G1]}}{\frac{[CB[n]\bullet G2][G1]}{[CB[n]\bullet G2][G1]}}\right)^2 = (0.0424)^2 + (0.0424)^2 \quad (12) \qquad \frac{\sigma_{K_{rel}}}{K_{rel}} = 0.06 \quad (13)$$

Step 3 – Determination of the Uncertainty in the K_a value for 6C•III-10. We obtained an uncertainty in the value of K_a for **6C•III-10** ($K_a = 4.94 \pm 0.59 \times 10^4$ M^{-1}) (11.88 %) from the non- linear least squares fit of the ^{1}H NMR titration data to a 1:1 binding model (Figure III-S20).

Step 4 – Determination of K_a for 6C•III-9 by competition of* III-10 *and* III-9 *for a limiting quantity of 6C. We used ^{1}H NMR competition experiments to determine K_{rel} = 44.91 for these two guests (Figure III-S31). Substitution of $\mathbf{K_{6C\cdot III\text{-}10}} = 4.94 \pm 0.59 \times 10^4$ M^{-1} and K_{rel} into equation 14 gave $K_{6C\cdot III\text{-}9} = 2.22 \times 10^6$ M^{-1} (equation 15). The uncertainty in $K_{6C\cdot III\text{-}9}$ can be determined using equation 16. Substituting $\sigma(K_{6C\cdot III\text{-}10})/ K_{6C\cdot III\text{-}10} = 0.01188$ and $\sigma(K_{rel})/ K_{rel} = 0.10$ [Note that we are using the even more conservative 10% error in this analysis] gives the percent error in $K_{6C\cdot III\text{-}9}$ (equation 17). Substituting eq. 15 into eq. 17 gives $\sigma(K_{6C\cdot III\text{-}9})$ (equation 18) which can be combined

with eq. 15 to give a final value for $K_{\mathbf{6C\cdot III\text{-}9}}$ (equation 19).

$$K_{G2} = (K_{G1})(K_{rel}) \qquad (14)$$

$$K_{\mathbf{6C\cdot III\text{-}9}} = 2.22 \times 10^6\ M^{-1} \qquad (15)$$

$$\left(\frac{\sigma K_{\mathbf{6C\bullet III\text{-}9}}}{K_{\mathbf{6C\bullet III\text{-}9}}}\right)^2 = \left(\frac{\sigma K_{\mathbf{6C\bullet III\text{-}10}}}{K_{\mathbf{6C\bullet III\text{-}10}}}\right)^2 + \left(\frac{\sigma K_{rel}}{K_{rel}}\right)^2 \qquad (16)$$

$$\frac{\sigma K_{\mathbf{6C\bullet III\text{-}9}}}{K_{\mathbf{6C\bullet III\text{-}9}}} = 0.1553\ (15.53\%) \qquad (17)$$

$$\sigma K_{\mathbf{6C\bullet III\text{-}9}} = (0.1553)(2.22 \times 10^6\ M^{-1}) \qquad (18)$$

$$K_{\mathbf{6C\cdot III\text{-}9}} = 2.22 \pm 0.35 \times 10^6\ M^{-1} \qquad (19)$$

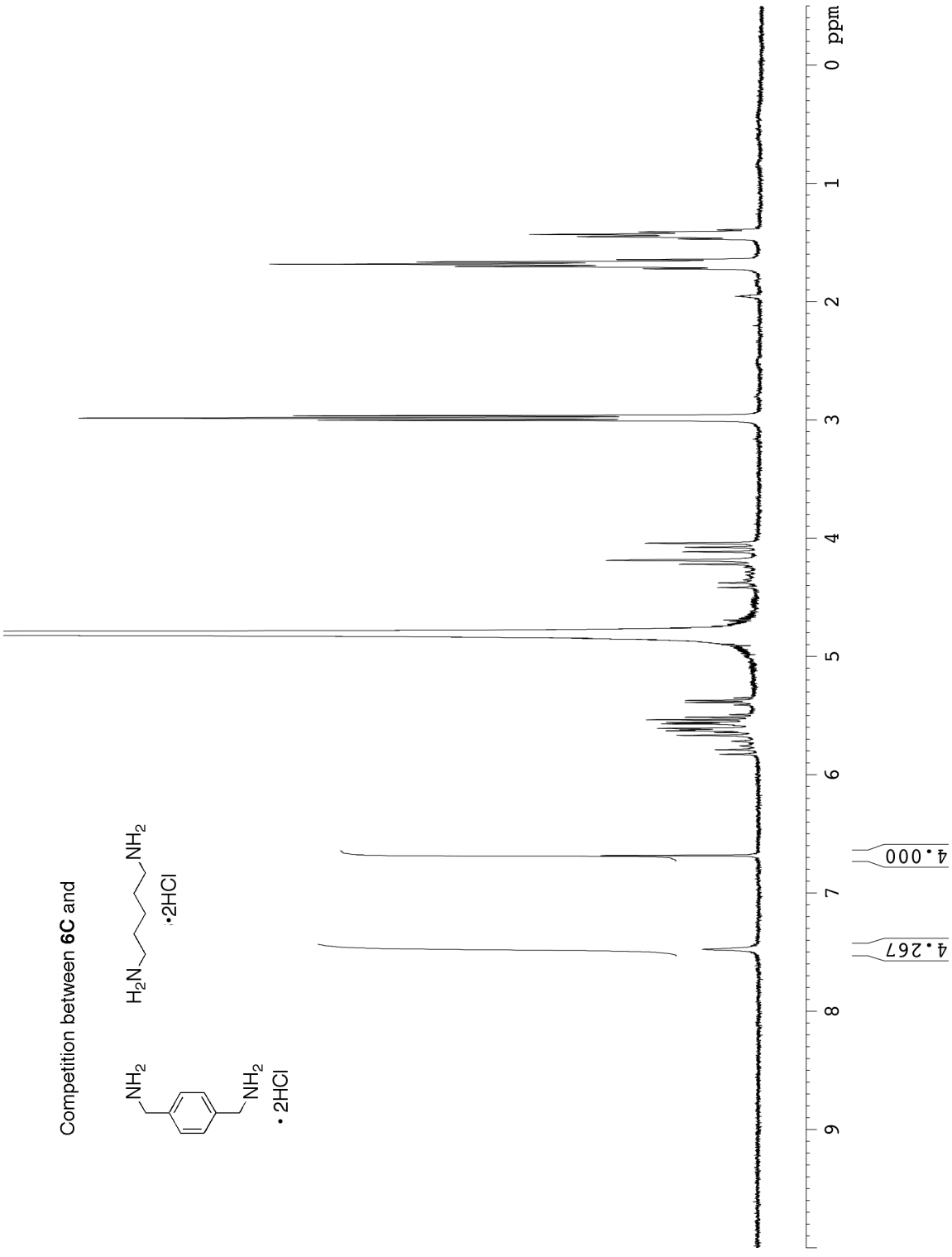

Figure III-S29. One of the ^{1}H NMR spectra (500 MHz, 20 mM $NaCO_2CD_3$ buffer, pD = 4.74) used in the determination of K_{rel} for **6C•III-11** and **6C•III-8**. Conditions: **6C** (0.4 mM), **III-11** (0.5 mM), and **III-8** (2.5 mM).

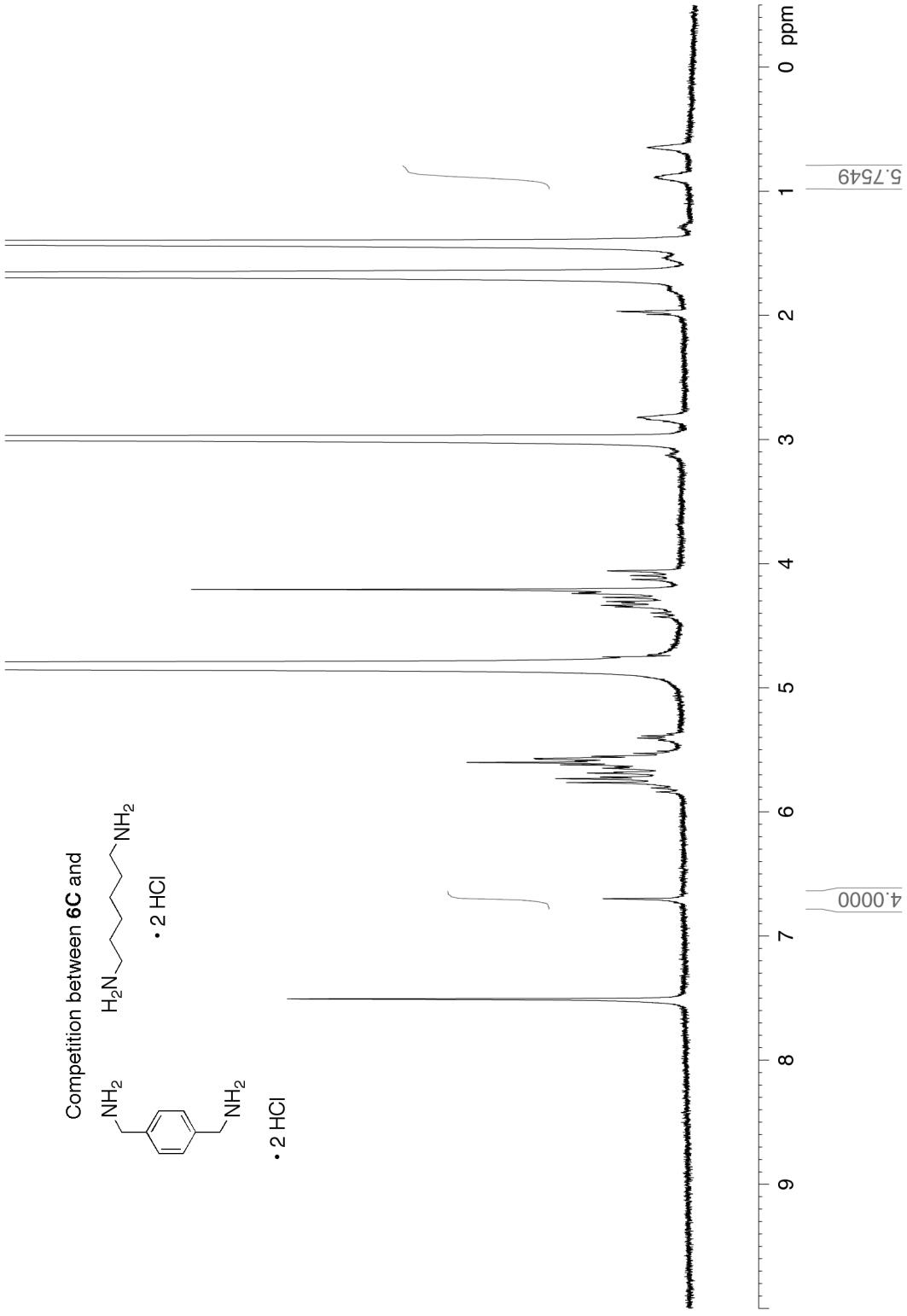

Figure III-S30. One of the ^{1}H NMR spectra (500 MHz, 20 mM $NaCO_2CD_3$ buffer, pD = 4.74) used in the determination of K_{rel} for **6C•III-11** and **6C•III-9**. Conditions: **6C** (0.4 mM), **III-11** (0.5 mM), and **III-9** (5.0 mM).

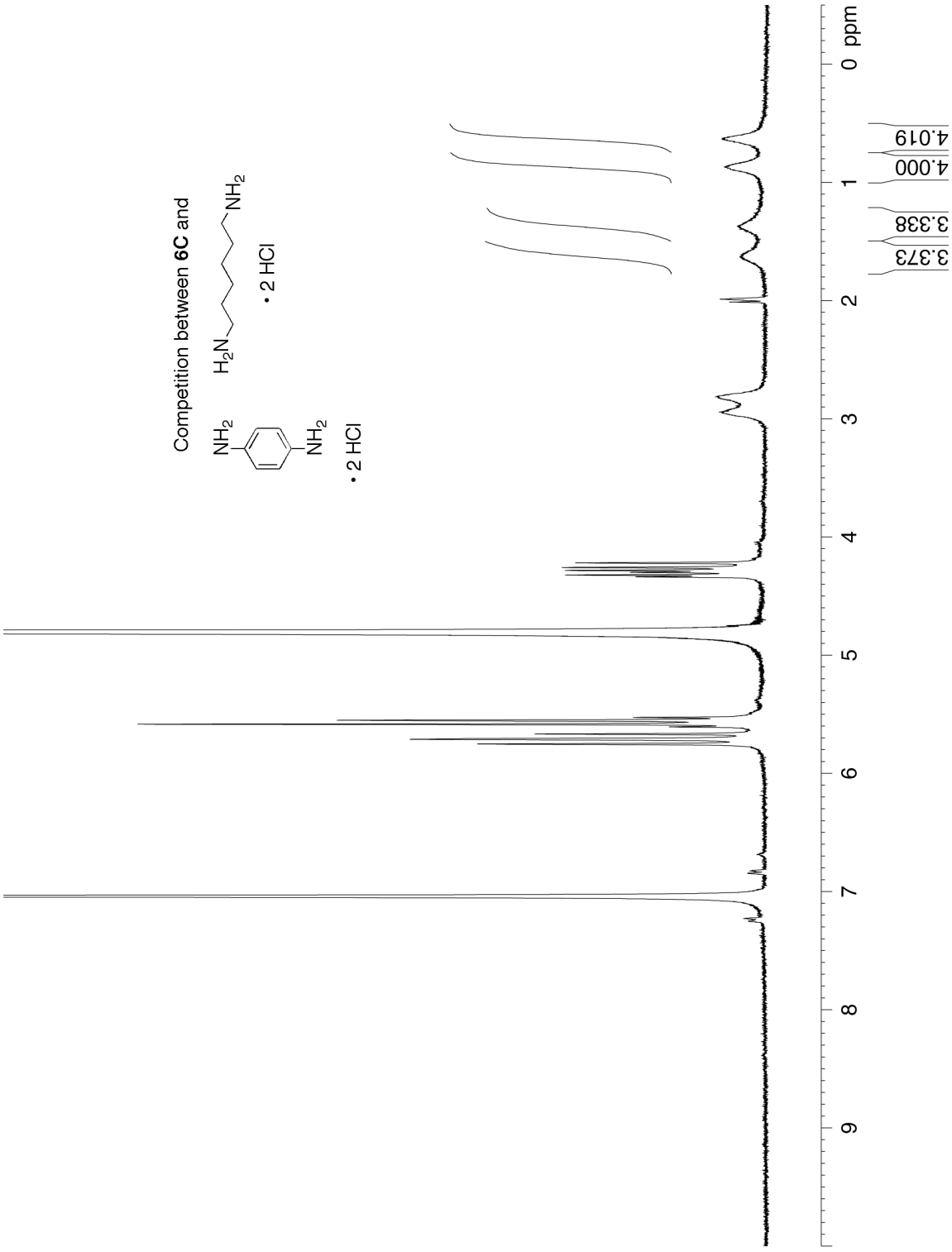

Figure III-S31. One of the ^{1}H NMR spectra (500 MHz, 20 mM $NaCO_2CD_3$ buffer, pD = 4.74) used in the determination of K_{rel} for **6C•III-9** and **6C•III-10**. Conditions: **6C** (0.4 mM), **III-9** (0.5 mM), and **III-10** (5.0 mM).

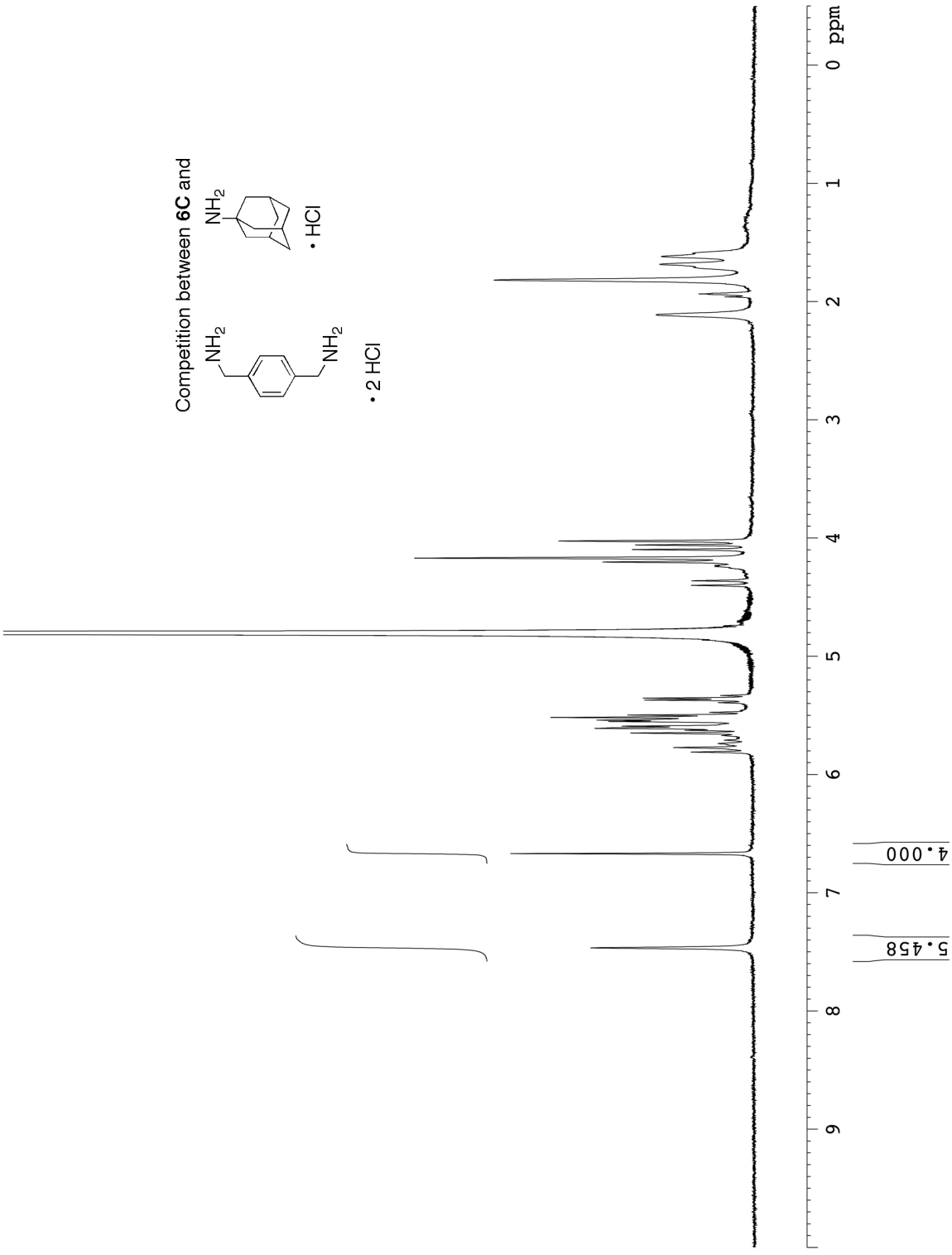

Figure III-S32. One of the ^{1}H NMR spectra (400 MHz, 20 mM $NaCO_2CD_3$ buffer, pD = 4.74) used in the determination of K_{rel} for **6C•III-11** and **6C•III-14**. Conditions: **6C** (0.4 mM), **III-11** (0.5 mM), and **III-14** (0.5 mM).

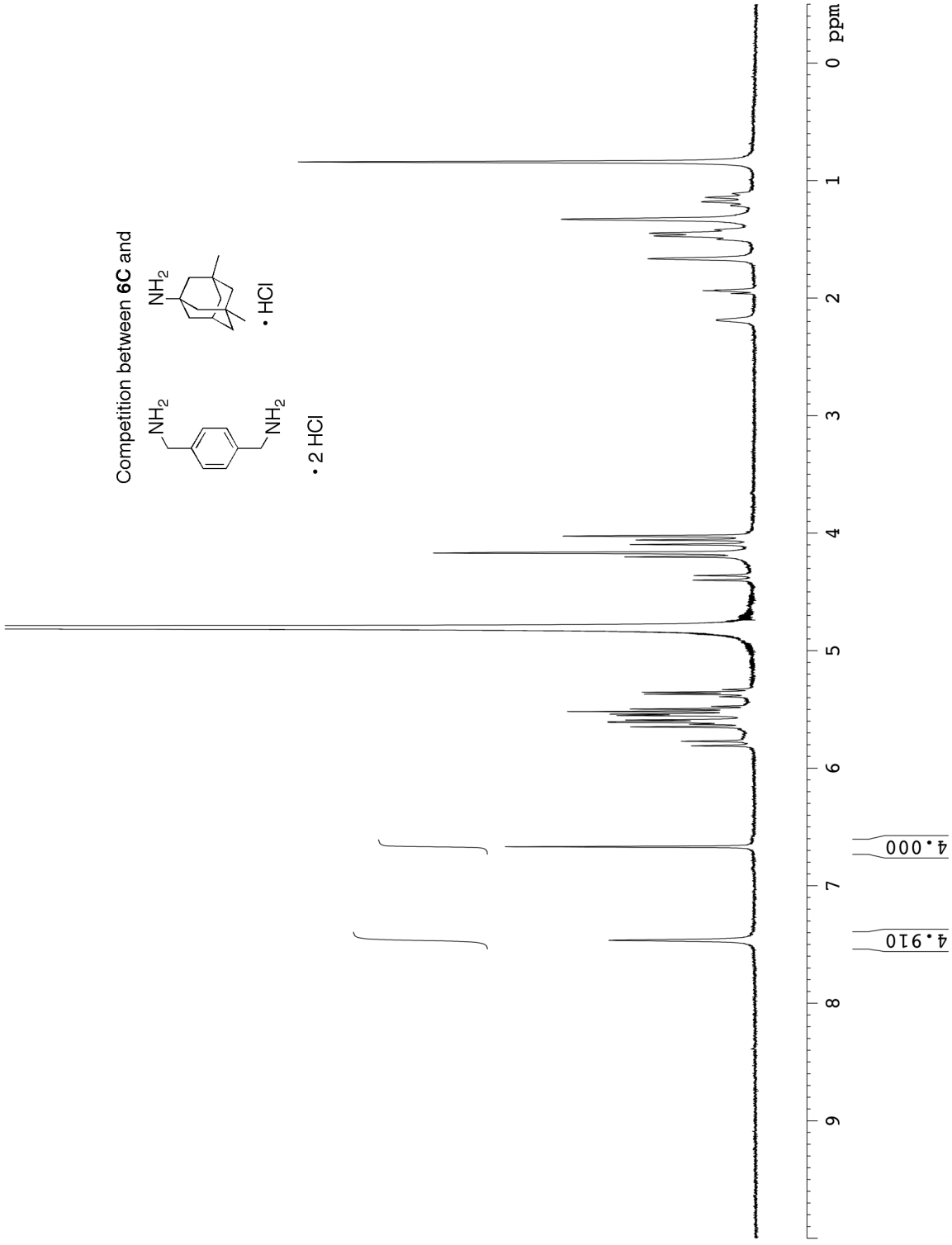

Figure III-S33. One of the ^{1}H NMR spectra (400 MHz, 20 mM $NaCO_2CD_3$ buffer, pD = 4.74) used in the determination of K_{rel} for **6C•III-11** and **6C•III-15**. Conditions: **6C** (0.4 mM), **III-11** (0.5 mM), and **III-15** (0.5 mM).

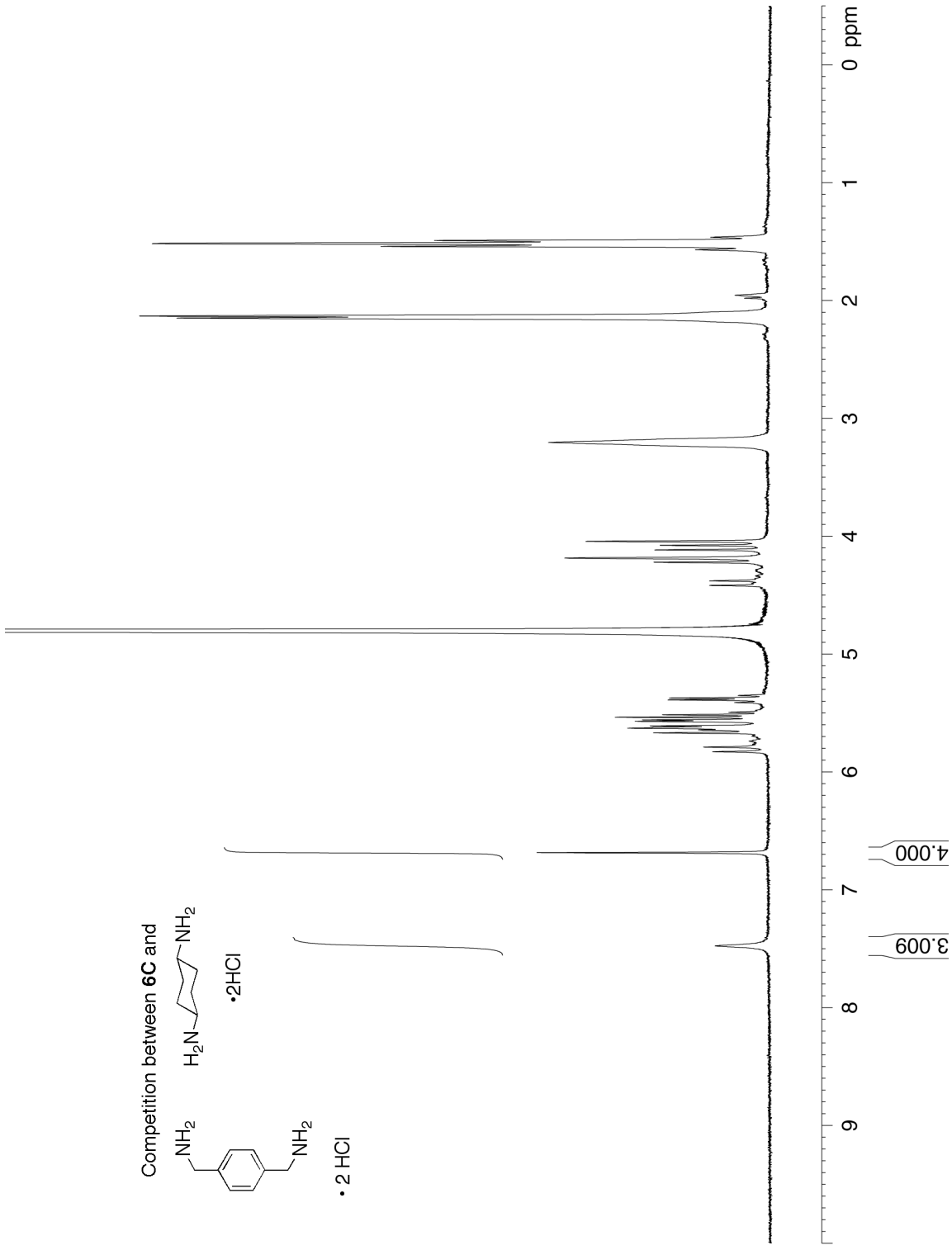

Figure III-S34. One of the ^{1}H NMR spectra (400 MHz, 20 mM $NaCO_2CD_3$ buffer, pD = 4.74) used in the determination of K_{rel} for **6C•III-11** and **6C•III-12**. Conditions: **6C** (0.4 mM), **III-11** (0.5 mM), and **III-12** (5.0 mM).

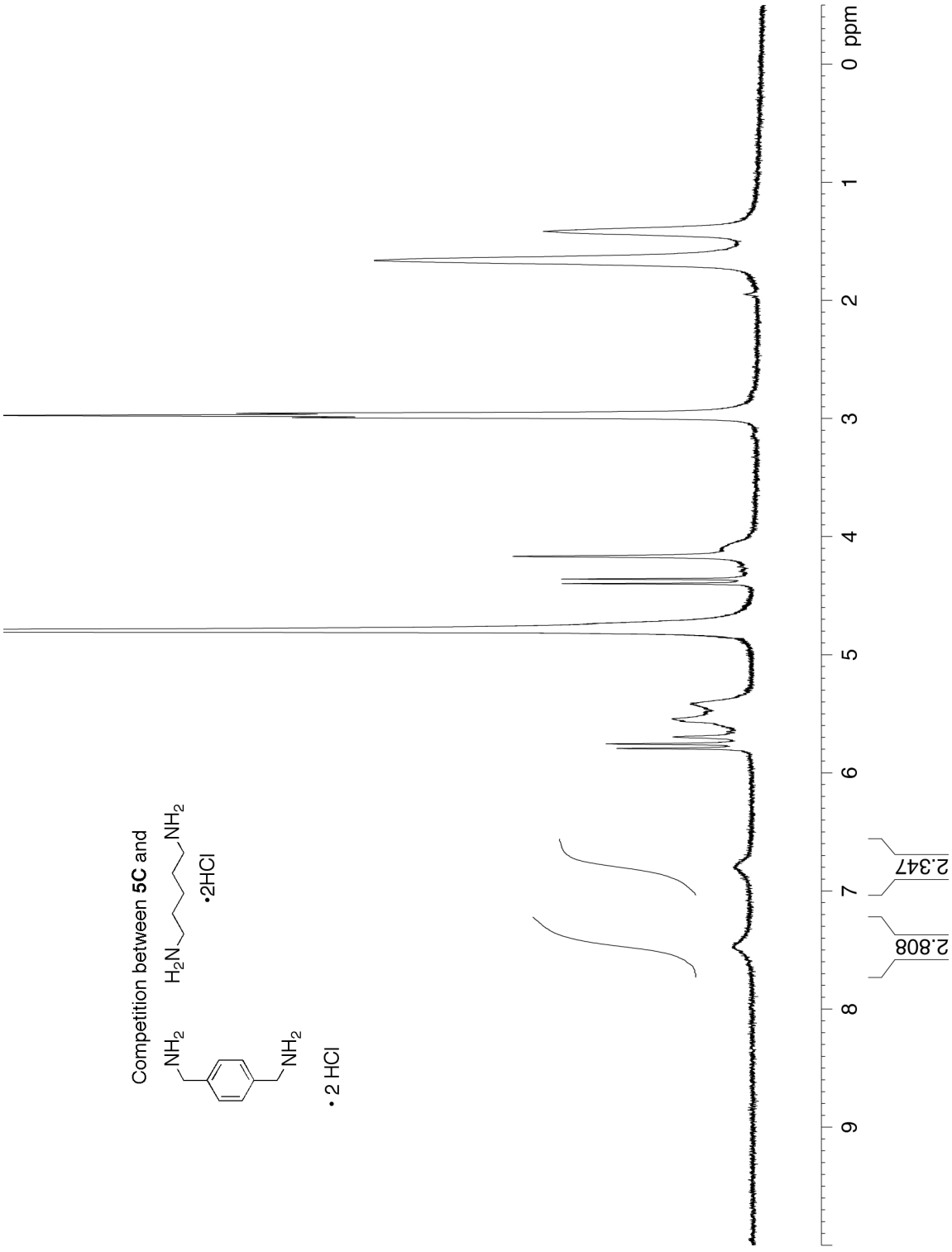

Figure III-S35. One of the ^{1}H NMR spectra (400 MHz, 20 mM $NaCO_2CD_3$ buffer, pD = 4.74) used in the determination of K_{rel} for **5C•III-11** and **5C•III-8**. Conditions: **5C** (0.4 mM), **III-11** (0.5 mM), and **III-8** (5.0 mM).

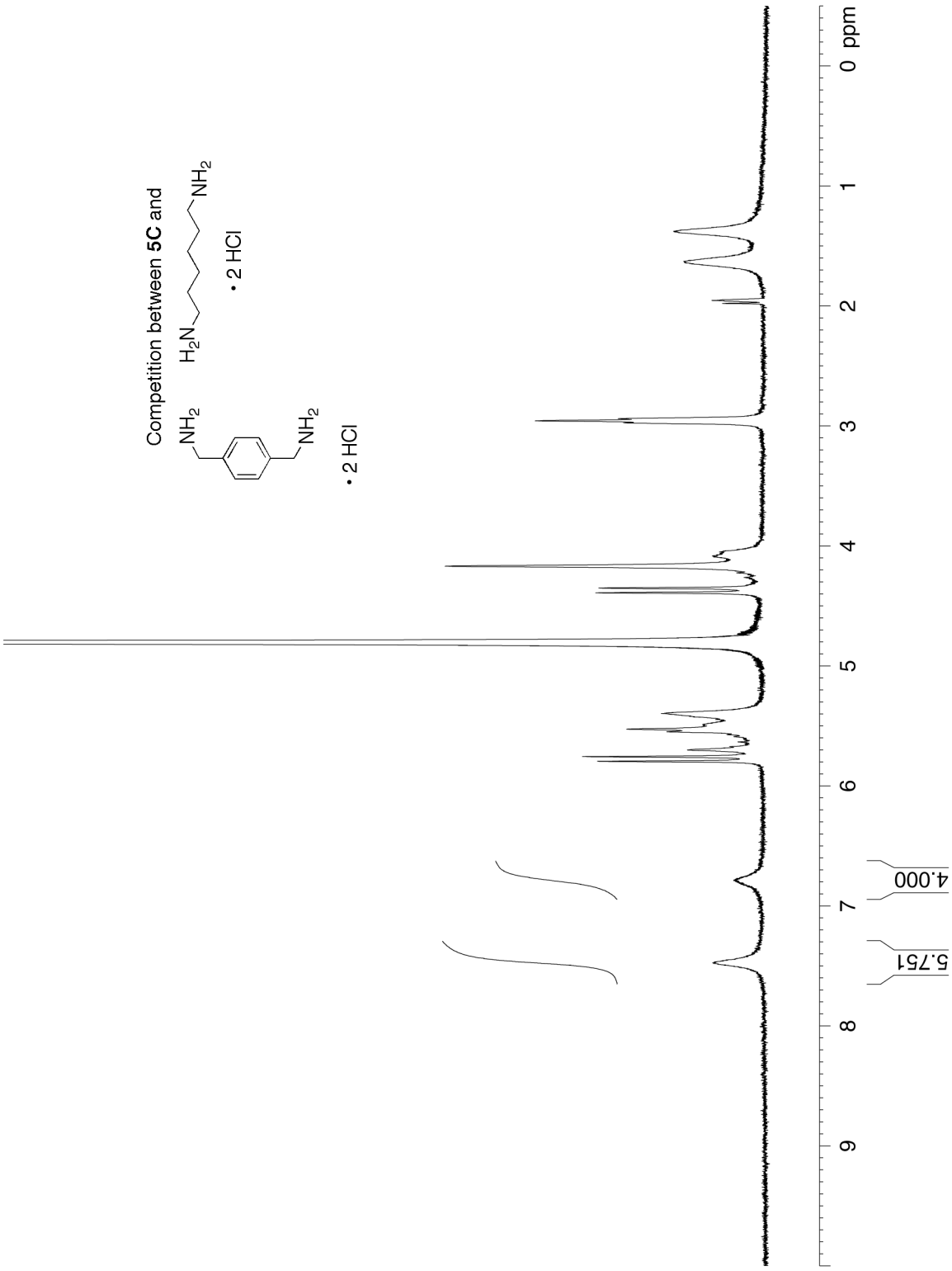

Figure III-S36. One of the ^{1}H NMR spectra (400 MHz, 20 mM $NaCO_2CD_3$ buffer, pD = 4.74) used in the determination of K_{rel} for **5C•III-11** and **5C•III-9**. Conditions: **5C** (0.4 mM), **III-11** (0.5 mM), and **III-9** (0.5 mM).

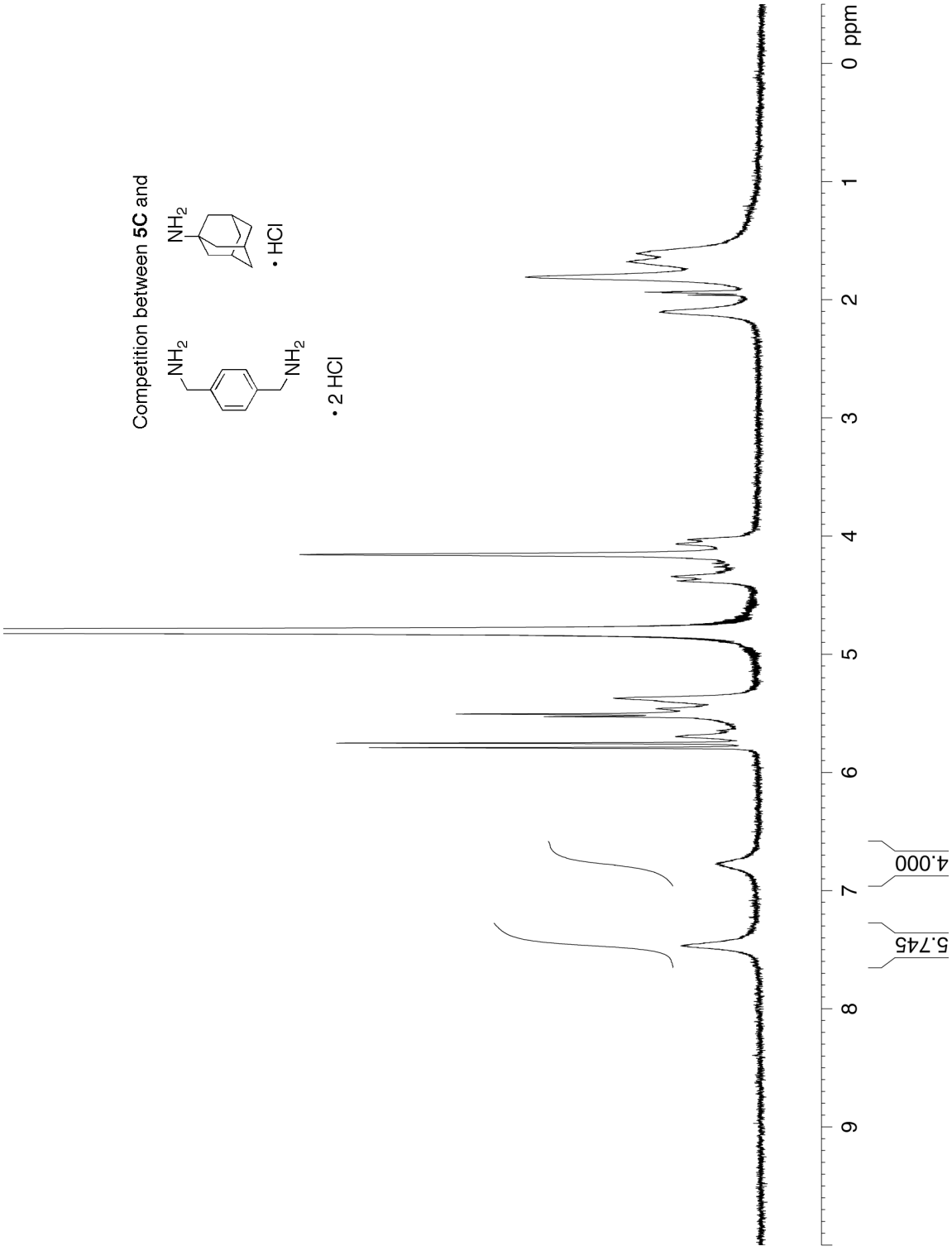

Figure III-S37. One of the ^{1}H NMR spectra (400 MHz, 20 mM $NaCO_2CD_3$ buffer, pD = 4.74) used in the determination of K_{rel} for **5C•III-11** and **5C•III-14**. Conditons: **5C** (0.4 mM), **III-11** (0.5 mM), and **III-14** (0.5 mM).

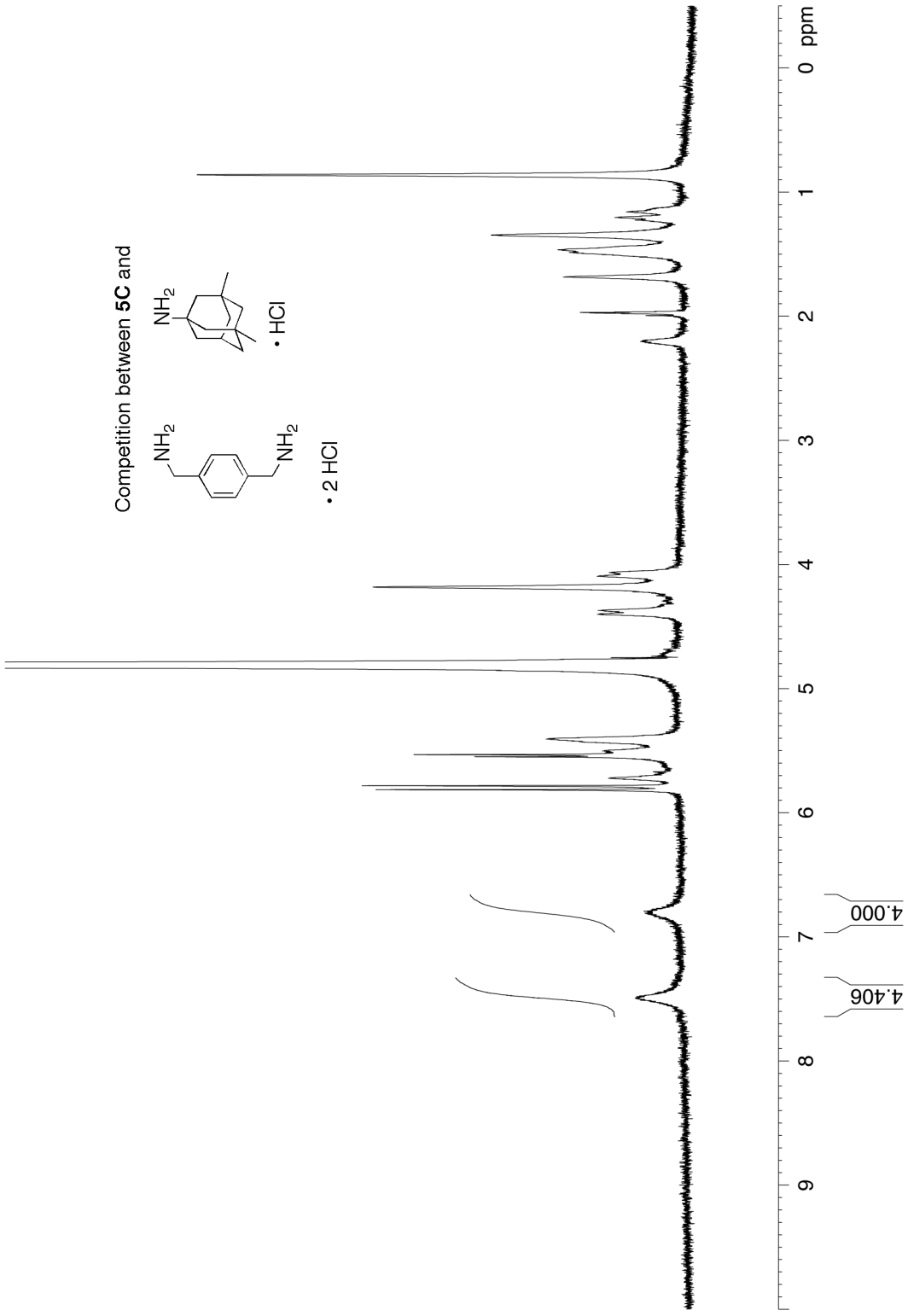

Figure III-S38. One of the ^{1}H NMR spectra (400 MHz, 20 mM $NaCO_2CD_3$ buffer, pD = 4.74) used in the determination of K_{rel} for **5C•III-11** and **5C•III-15**. Conditions: **5C** (0.4 mM), **III-11** (0.5 mM), and **III-15** (0.5 mM).

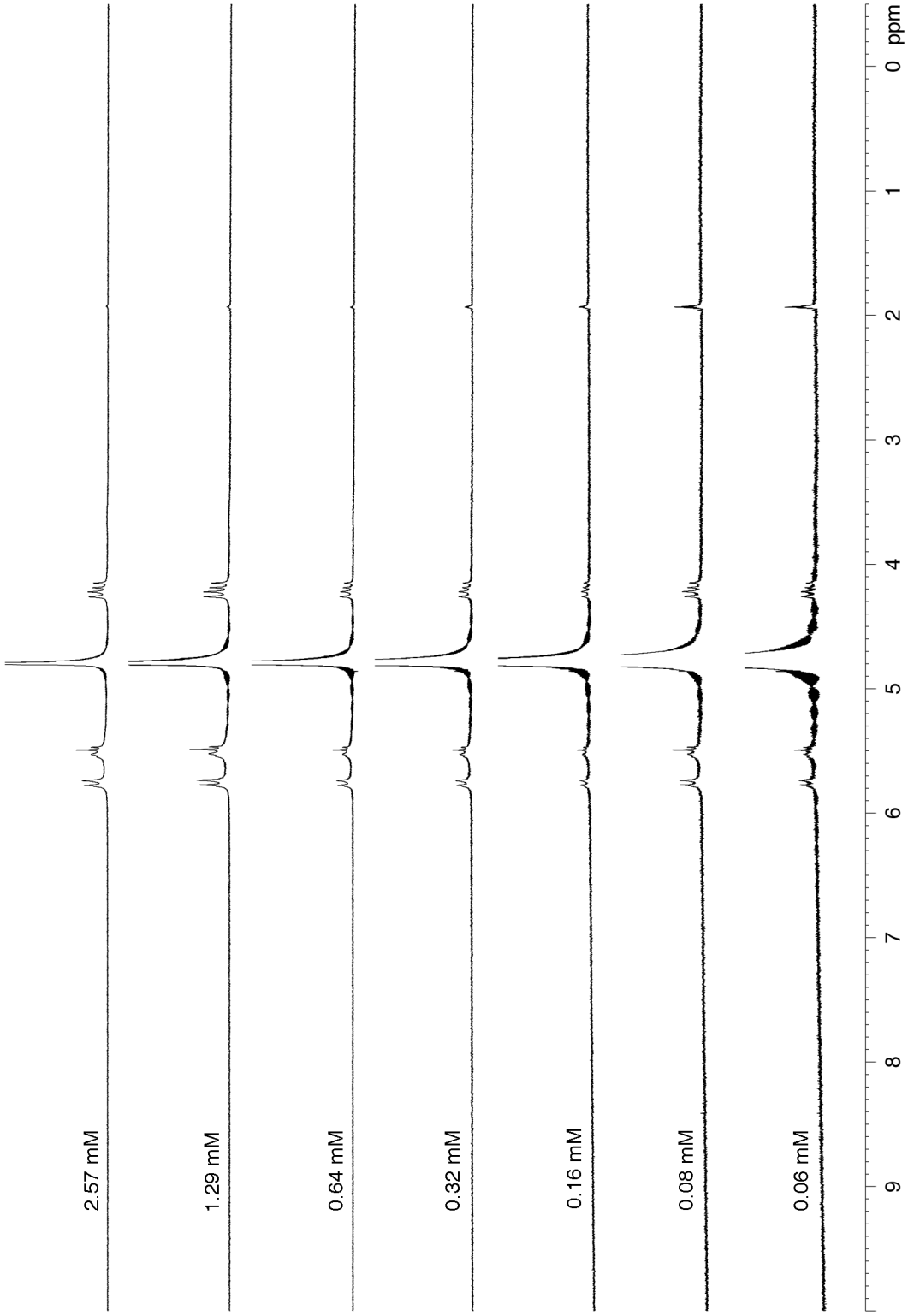

Figure III-S39. ^{1}H NMR spectra (400 MHz, 20 mM $NaCO_2CD_3$ buffer, pD = 4.74) recorded for the self-association of [**6C**] (0.06 mM – 2.57 mM).

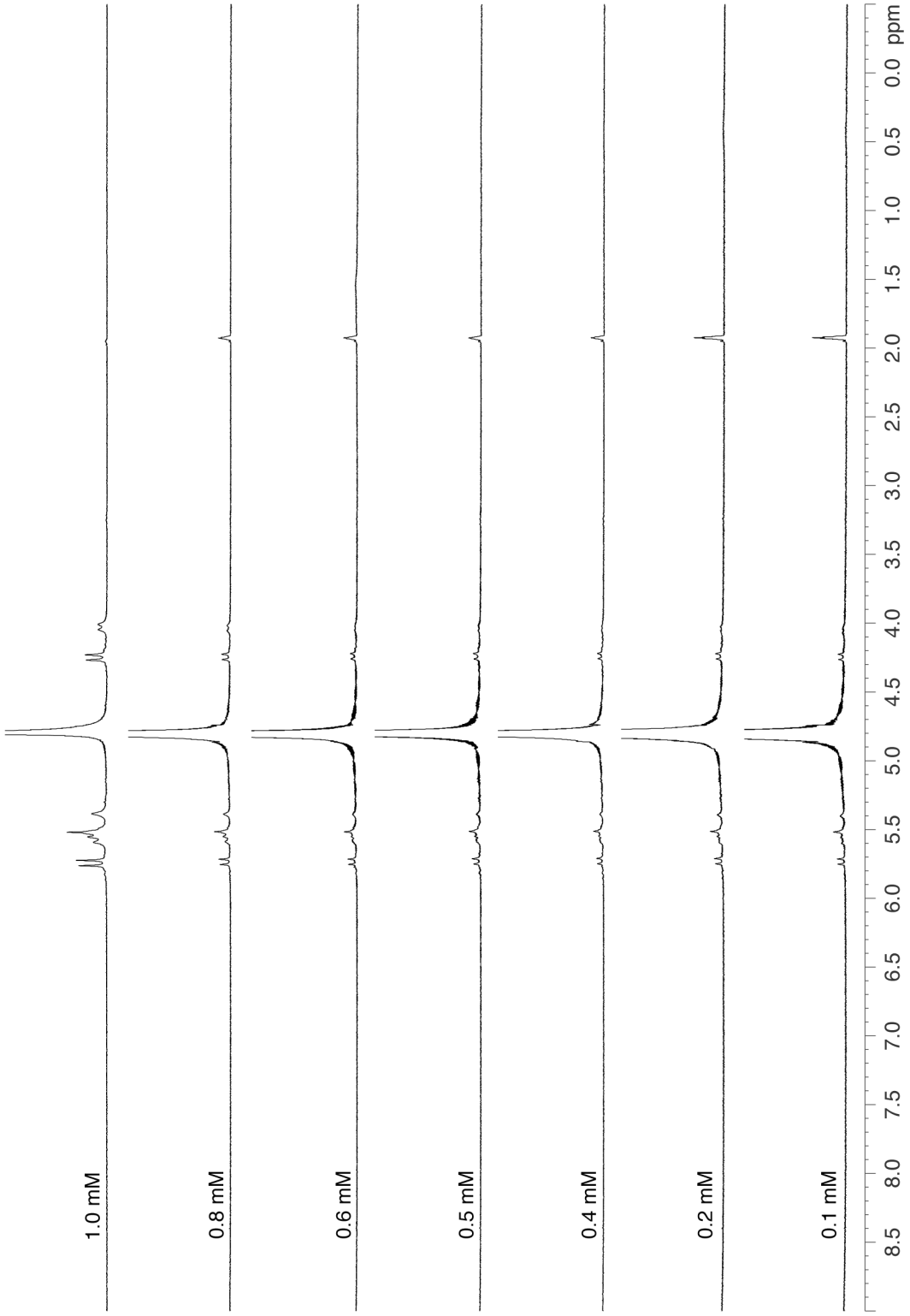

Figure III-S40. ^{1}H NMR spectra (400 MHz, 20 mM $NaCO_2CD_3$ buffer, pD = 4.74) recorded for the self-association of [**5C**] (0.1 mM – 1.0 mM).

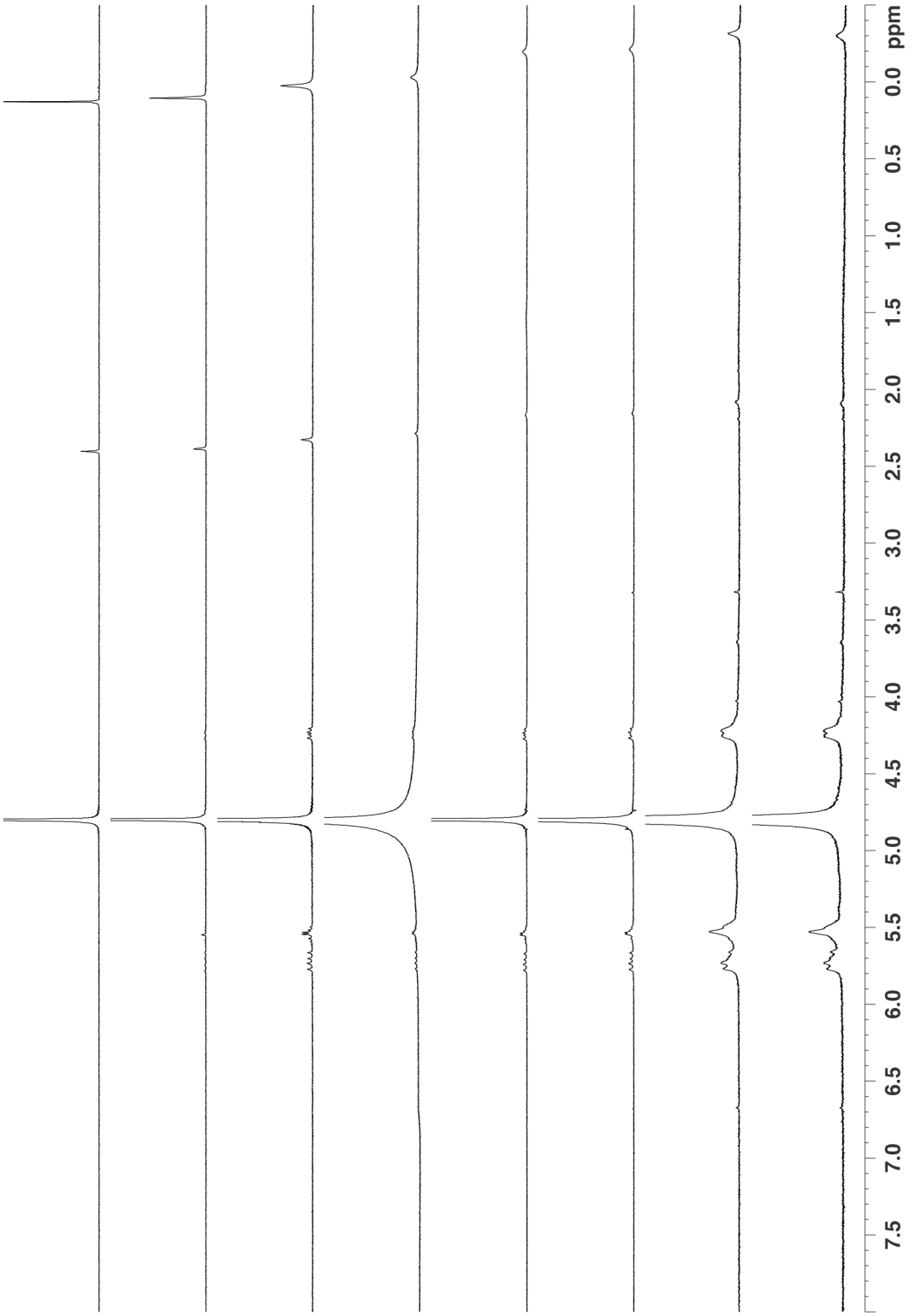

Figure III-S41. ^{1}H NMR spectra (400 MHz, 20 mM $NaCO_2CD_3$ buffer, pD = 4.74) recorded for the job plot of **6C** and **III-13** ([**6C**] + [**III-13**] = 0.5 mM).

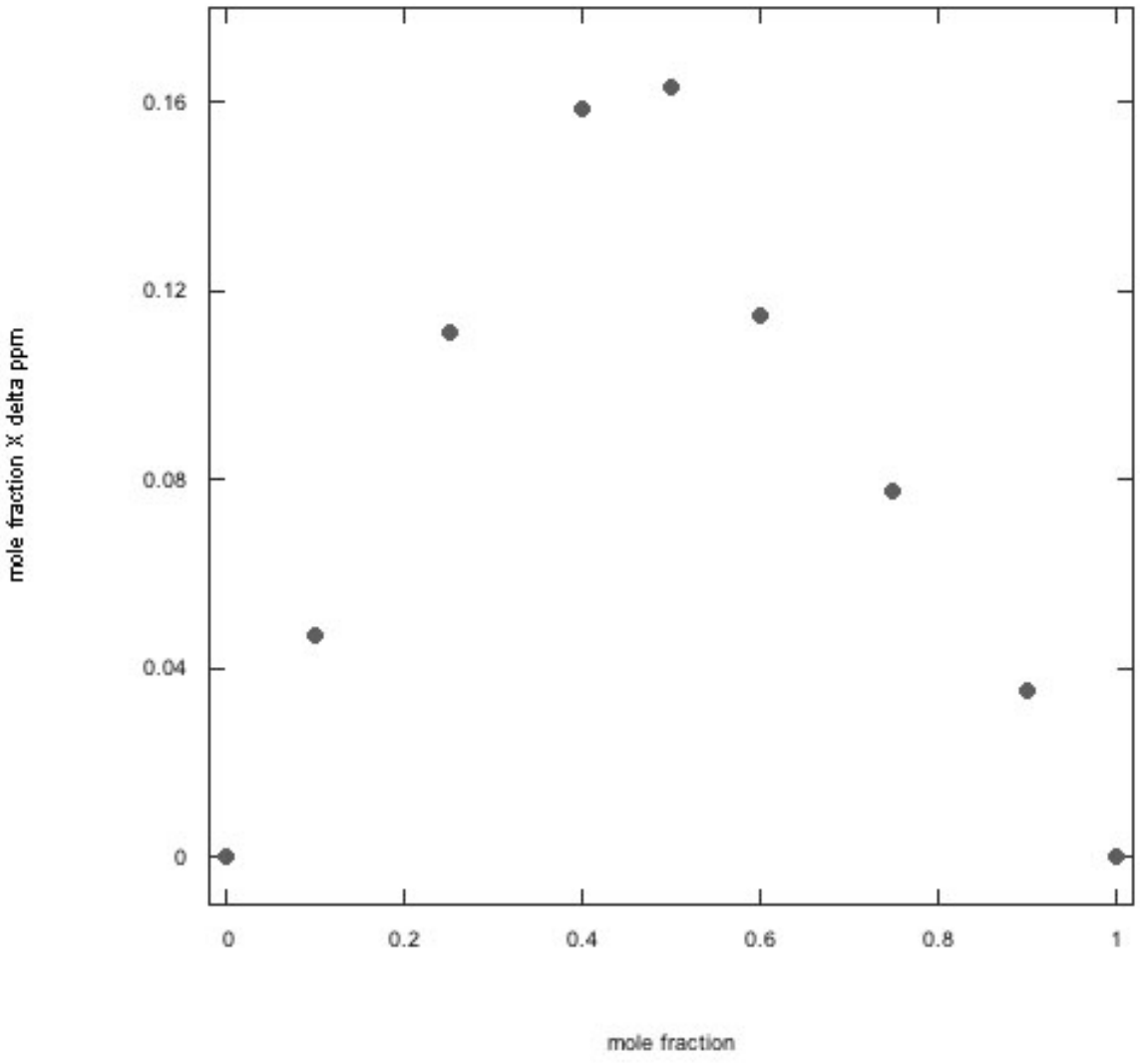

Figure III-S42. Job plot generated for **6C** and **III-13** by monitoring the $(CH_3)_3Si$ group chemical shift of **III-13** showing a 1 : 1 binding model.

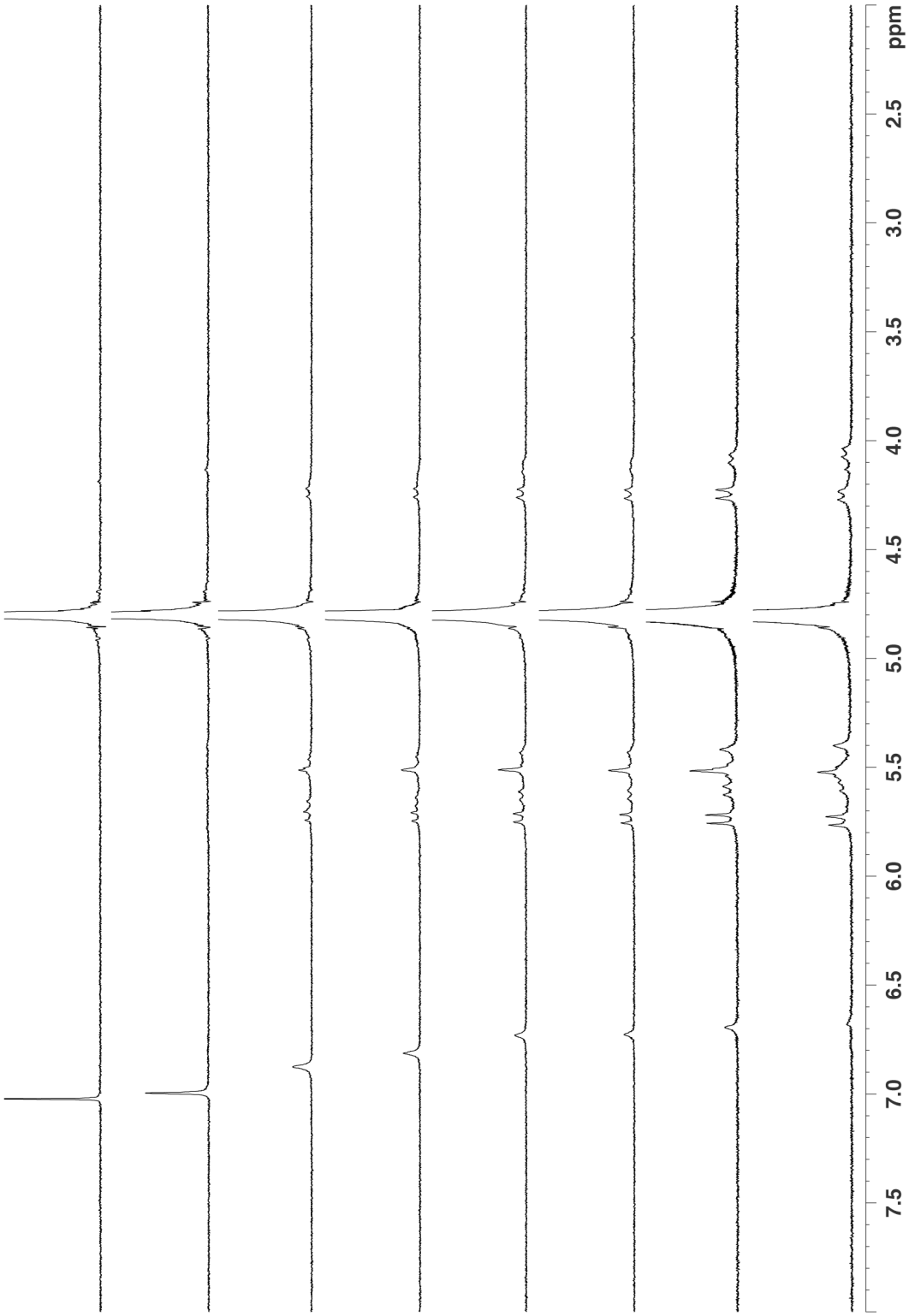

Figure III-S43. ^{1}H NMR spectra (400 MHz, 20 mM $NaCO_2CD_3$ buffer, pD = 4.74) recorded for the job plot of **5C** and **III-10** ([**5C**] + [**III-10**] = 0.5 mM).

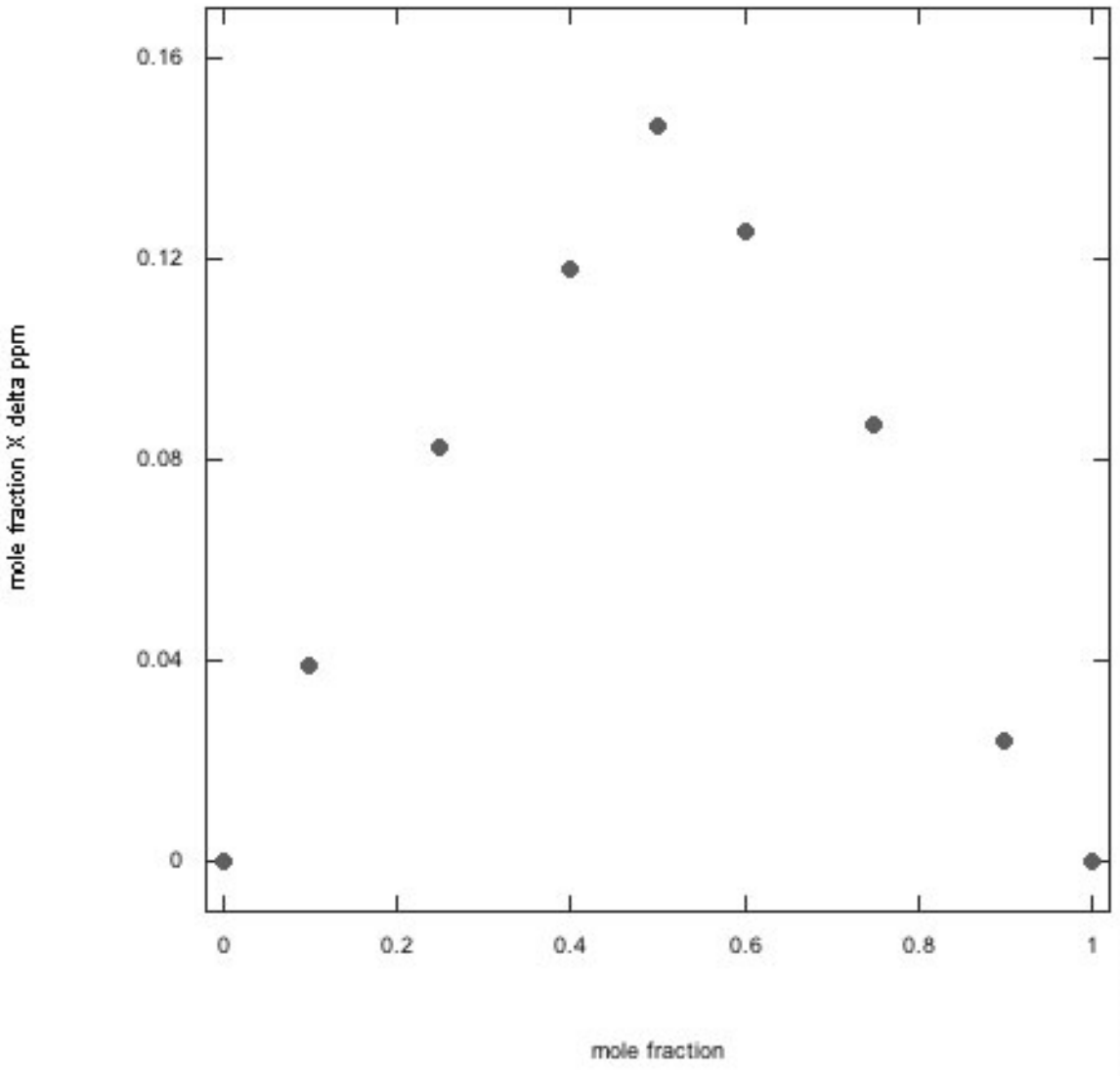

Figure III-S44. Job plot generated for **5C** and **III-10** by monitoring the Ar-H group chemical shift of **III-10** showing a 1 : 1 binding model.

Bibliography

(1) Behrend, R.; Meyer, E.; Rusche, F. *Liebigs Ann. Chem.* **1905**, *339*, 1-37.

(2) Freeman, W. A.; Mock, W. L.; Shih, N. Y. *J. Am. Chem. Soc.* **1981**, *103*, 7367-7368.

(3) Mock, W. L.; Shih, N. Y. *J. Org. Chem.* **1986**, *51*, 4440-4446.

(4) Mock, W. L.; Shih, N. Y. *J. Am. Chem. Soc.* **1989**, *111*, 2697-2699.

(5) Buschmann, H.-J.; Mutihac, L.; Jansen, K. *J. Inclusion Phenom. Macrocyclic Chem.* **2001**, 39, 1 – 11.

(6) Hoffmann, R.; Knoche, W.; Fenn, C.; Buschmann, H.-J. *J. Chem. Soc. Faraday Trans.***1994**, 90, 1507 – 1511.

(7) Day, A. I.; Blanch, R. J.; Arnold, A. P.; Lorenzo, S.; Lewis, G. R.; Dance, I. *Angew. Chem., Int. Ed.* **2002**, 41, 275 – 277.

(8) Liu, S.; Zavalij, P. Y.; Isaacs, L. *J. Am. Chem. Soc.* **2005**, 127, 16798-16799.

(9) Wu, A.; Chakraborty, A.; Witt, D.; Lagona, J.; Damkaci, F.; Ofori, M. A.; Chiles, J. K.; Fettinger, J. C.; Isaacs, L. *J. Org. Chem.* **2002**, 67(16), 5817-5830.

(10) Chakraborty, A.; Wu, A.; Witt, D.; Lagona, J.; Fettinger, J. C.; Isaacs, L. *J. Am. Chem. Soc.* **2002**, 124, 8297-8306.

(11) Huang, W.-H.; Zavalij, P. Y.; Isaacs, L. *J. Am. Chem. Soc.* **2008**, 130, 8446-8454.

(12) Kim, J.; Jung, I.-S.; Kim, S.-Y.; Lee, E.; Kang, J.-K.; Sakamoto, S.; Yamaguchi, K.; Kim, K. *J. Am. Chem. Soc.* **2000**, 122, 540-541.

(13) Lee, J. W.; Samal, S.; Selvapalam, N.; Kim, H.-J.; Kim, K. *Acc. Chem. Res.*

2003, 36, 621-630.

(14) Comprehensive Supramolecular Chemistry Vol. 1 Molecular Reconition: Receptors for Cationic Guests (Ed.: G. W. Gokel), Pergamon, Oxford, 1996.

(15) Comprehensive Supramolecular Chemistry, Vol. 2 Molecular Recognition: Receptors for Molecular Guests (Ed.: F. Vögtle), Pergamon, Oxford, 1996.

(16) Comprehensive Supramolecular Chemistry, Vol. 3 Cyclodextrins (Eds.: J. Szejtli, T.Osa), Pergamon, Oxford, 1996.

(17) Liu, S.; Ruspic, C.; Mukhopadhyay, P.; Chakrabarti, S.; Zavali, P.; Isaacs, L. *J. Am. Chem. Soc.* **2005**, 127, 15959-15967.

(18) Mukhapadhyay, P.; Zavalij, P. Y.; Isaacs, L. *J. Am. Chem. Soc.* **2006**, 128, 14093-14102.

(19) Huang, W.-H.; Liu, S.; Isaacs, L. (**2008**) Cucurbit[n]urils, in Modern Supramolecular Chemistry: Strategies for Macrocycle Synthesis (Eds.: F. Diederich; P. J. Stang; R. R. Tykwinski), Wiley-VCH Verlag GmbH & Co. KGaA, Weinheim, Germany. doi: 10.1002/9783527621484.ch4.

(20) Day, A. I.; Arnold, A.P.; Blanch, R. J.; Snushall, B. J. Org. Chem. **2001**, 66, 8094 – 8100.

(21) Isaacs, L. *Isr. J. Chem.* **2011**, 51, 578-591.

(22) Isaacs, L. *Chem. Commun.* **2009**, 619-629.

(23) Lagona, J.; Mukhopadhyay, P.; Chakrabari, S.; Isaacs, L. *Angew. Chem., Int. Ed.* **2005**, 44, 4844-4870.

(24) Ma, D.; Gargulakova, Z.; Zavalij, P. Y.; Sindelar, V.; Isaacs, L. *J. Org. Chem.* **2010**, 75, 2934-2941.

(25) Huang, W.-H.; Zavalij, P. Y.; Isaacs, L. *Angew. Chem., Int. Ed.* **2007**, 46, 7425-7427.

(26) Huang, W.-H.; Zavalij, P. Y.; Isaacs, L. *J. Am. Chem. Soc.* **2006**, 128, 14744-14745.

(27) Isaacs, L.; Park, S.-K.; Liu, S.; Liu, S.; Ko, Y. H.; Selvapalam, N.; Kim, Y.; Kim, H.; Zavalij, P. Y.; Kim, G.-H.; Lee, H.-S.; Kim, K. *J. Am. Chem. Soc.* **2005**, 127, 18000-18001.

(28) Bellia, F.; Mendola, D.; Pedone, C.; Rizzarelli, E.; Saviano, M.; Vecchio, G. *Chem. Soc. Rev.* **2009**, 38, 2756-2781.

(29) Zhou, J.; Ritter, H. *Polym. Chem.* **2010**, 1, 1552-1559.

(30) Kanamathareddy, S.; Gutsche, D.C. *J. Org. Chem.* **1995**, 60, 6070-6075.

(31) Harvey, P. O. *Coordination Chemistry Reviews*. **2002**, 233-234, 289-309.

(32) Jon, S. Y.; Selvapalam, N.; Oh, D. H.; Kang, J.-K.; Kim, S.-Y.; Jeon, Y. J.; Lee, J. W.; Kim, K. *J. Am. Chem. Soc.* **2003**, 125, 10186-10187.

(33) Kim, E.; Kim, D.; Jung, H.; Lee, J.; Paul, S.; Selvapalam, N.; Yang, Y.; Lim, N.; Park, C. G.; Kim, K. *Angew. Chem., Int. Ed.* **2010**, 49, 4405-4408.

(34) Park, K. M.; Lee, D.-W.; Sarkar, B.; Jung, H.; Kim, J.; Ko, Y. H.; Lee, K. E.; Jeon, H.; Kim, K. *Small*. **2010**, 6(13), 1430-1441.

(35) Jeon, Y. J.; Kim, H.; Jon, S.; Selvapalam, N.; Oh, D. H.; Seo, I.; Park, C.-S.; Jung, S. R.; Koh, D.-S.; Kim, K. *J. Am. Chem. Soc.* **2004**, 126, 15944-15945.

(36) Lee, D.-W.; Park, K. M.; Banerjee, M.; Ha, S. H.; Lee, T.; Suh, K.; Paul, S.; Jung, H.; Kim, J.; Selvapalam, N.; Ryu, S. H.; Kim, K. *Nature Chemistry.* **2011**, 3, 154-159.

(37) Nagarajan, E. R.; Oh, D. H.; Selvapalam, N.; Ko, Y. H.; Park, K. M.; Kim, K. *Tet. Lett.* **2006**, 47, 2073-2075.

(38) For examples of drugs formulated with the highly water soluble cyclodextrin derivative Captisol, see: http://www.cydexpharma.com/captisol.html. Access date: October 20, 2011.

(39) Wang, N. X.; Von Recom, H. A. *Macromolecular Bioscience.* **2011**, 11(3), 321-332.

(40) Nandi, S.; Debnath, S.; Manjunath, S. Y.; Mallareddy, V.; Babre, N. P.; Rao, M. G. *Int. J. Pharm. Sci. Nanotech.* **2011**, 3(4), 1263-1270.

(41) Deng, J.; Cai, W.; Jin, F. *Zhongguo Yiyao Gongye Zazhi.* **2010**, 41(11), 856-863.

(42) Kim, C.; Agasti, S. S.; Zhu, Z.; Isaacs, L.; Rotello, V. M. *Nature Chemistry.* **2010**, 2, 962-966.

(43) Wheate, N. J.; Buck, D. P.; Day, A. I.; Collins, J. G. *Dalton Trans.* **2006**, 451-458.

(44) Hettiarachchi, G.; Nguyen, D.; Wu, J.; Lucas, D.; Ma, D.; Isaacs, L.; Briken, V. *PloS ONE*. **2010**, 5, e10514.

(45) Uzunova, V. D.; Cullinane, C.; Brix, K.; Nau, W. M.; Day, A. I. *Org. Biomol. Chem.* **2010**, 8, 2037-2042.

(46) Marchetti, L.; Levine, M. *ACS Catalysis.* **2011**, 1(9), 1090-1118.

(47) Sansone, F.; Baldini, L.; Casnati, A.; Rocco, U. *New. J. Chem.* **2010**, 34(12), 2715-2728.

(48) Liu, S.; Zavalij, P. Y.; Lam, Y.-F.; Isaacs, L. *J. Am. Chem. Soc.* **2007**, 129,

11232-11241.

(49) Liu, S.; Shukla, A. D.; Gadde, S.; Wagner, B. D.; Kaifer, A. E.; Isaacs, L. *Angew. Chem., Int. Ed.* **2008**, 47, 2657-2660.

(50) Huang, W.-H.; Zavalij, P. Y.; Isaacs, L. *Org. Lett.* **2009**, 11(17), 3918-3921.

(51) Ghosh, S.; Isaacs, L. *J. Am. Chem. Soc.* **2010**, 132, 4445-4454.

(52) Urbach, A. R.; Ramalingam, V. *Isr. J. Chem.* **2011**, 51, 664-678.

(53) Biedermann, F.; Rauwald, U.; Cziterzky, M.; Williams, K. A.; Gann, L. D.; Guo, B. Y.; Urbach, A. R.; Bielowski, C. W.; Scherman, O. A. *Chem. Eur. J.* **2010**, 16, 13716-13722.

(54) Wu, J.; Isaacs, L. *Chem. Eur. J.* **2009**, 15, 11675-11680.

(55) Ghale, G.; Ramalingam, V.; Urbach, A. R.; Nau, W. M. *J. Am. Chem. Soc.* **2011**, 133, 7528-7535.

(56) Anslyn, E. V. *J. Org. Chem.* **2007**, 72, 687-699.

(57) Tian, F.; Cziferszky, M.; Jiao, D.; Wahlström, K.; Geng, J.; Scherman, O. A. *Langmir*. **2011**, 27(4), 1387-1390.

(58) Liu, J.; Du, X.; Zhang, X. *Chem. Eur. J.* **2011**, 17, 810-815.

(59) Anderson, S.; Anderson, H. L.; Sanders, J. K. M. *Acc. Chem. Res.* **1993**, 26, 469-475.

(60) Hänni, K. D.; Leigh, D. A. *Chem. Soc. Rev.* **2010**, 39, 1240-1251.

(61) Kilah, N. L.; Wise, M. D.; Serpell, C. J.; Thompson, A. L.; White, N. G.; Christensen, K. E.; Beer, P. D. *J. Am. Chem. Soc.* **2010**, 132, 11893-11895.

(62) Wisner, J. A.; Beer, P.D.; Drew, M. G. B.; Sambrook, M. R. *J. Am. Chem. Soc.* **2002**, 39, 1240-1251.

(63) Meyer, C. D.; Joiner, C. S.; Stoddart, J. F. *Chem. Soc. Rev.* **2007**, 36, 1705-1723.

(64) Glink, P. T.; Oliva, A. I.; Stoddart, J. F.; White, A. J. P.; Williams, D. J. *Angew. Chem., Int. Ed.* **2001**, 40(10), 1870-1875.

(65) Balzani, V.; Credi, A.; Raymo, F. M.; Stoddart, J. F. *Angew. Chem., Int. Ed.* **2000**, 39, 3348-3391.

(66) Kieran, A. L.; Bond, A. D.; Belienguer, A. M.; Sanders, K. M. *Chem. Comm.* **2003**, 2674-2675.

(67) Day, A. I.; Blanch, R. J.; Coe, A.; Arnold, A. P. *J. Incl. Phen. Macro. Chem.* **2002**, 43, 247-250.

(68) White, T. Supramolecular Chemistry and Synthesis of Cucurbit[n]uril. Ph.D. Thesis, University of New South Wales-Australian Defence Force Academy. School of Chemistry. **2003**.

(69) Lagona, J.; Fettinger, J. C.; Isaacs, L. *Org. Lett*. **2003**, 5(20), 3745-3747.

(70) Ma, D.; Zavalij, P. Y.; Isaacs, L. *J. Org. Chem.* **2010**, 75, 4786-4795.

(71) Zhao, Y.; Xue, S.; Zhu, Q.; Toa, Z.; Zhang, J.; Wei, Z.; Long, L.; Hu, M.; Xiao, H.; Day, A. I. *Chinese Science Bulletin.* **2004**, 49(11), 1111-1116.

(72) Flinn, A.; Hough, G. C.; Stoddart, J. F.; Williams, D. J. *Angew. Chem., Int. Ed.* **1992**, 31, 1475-1477.

(73) Huang, W.-H.; Zavalij, P. Y.; Isaacs, L. *Org. Lett.* **2008**, 10(12), 2577-2580.

(74) She, N.; Gao, M.; Cao, L.; Wu, A.; Isaacs, I. *Org. Lett.* **2009**, 11(12), 2603-2606.

(75) Lucas, D.; Minami, T.; Iannuzzi, G.; Cao, L.; Wittenberg, J.; Anzenbacher, P.; Isaacs, L. *J. Am. Chem. Soc.* **2011**, ASAP Article.

(76) Rekharsky,M.V.;Mori,T.;Yang,C.;Ko,Y.H.;Selvapalam,N.; Kim, H.; Sobransingh, D.; Kaifer, A. E.; Liu, S.; Isaacs, L.; Chen, W.; Moghaddam, S.; Gilson, M. K.; Kim, K.; Inoue, Y. *Proc. Natl. Acad. Sci. U.S.A.* **2007**, 104, 20737–20742.

(77) Kaifer, A. E.; Li, W.; Yi, S. *Isr. J. Chem.* **2011**, 51, 496–505.

(78) Nau, W. M.; Florea, M.; Assaf, K. I. *Isr. J. Chem.* **2011**, 51, 559–577.

(79) Ko, Y. H.; Kim, E.; Hwang, I.; Kim, K. *Chem. Commun.* **2007**, 1305–1315.

(80) Meschke, C.; Buschmann, H.-J.; Schollmeyer, E. *Polymer* **1998**, 40, 945–949.

(81) Tuncel, D.; Steinke, J. H. G. *Chem. Commun.* **1999**, 1509–1510.

(82) Ling, Y.; Kaifer, A. E. *Chem. Mater.* **2006**, 18, 5944–5949.

(83) Choi, S. W.; Ritter, H. *Macromol. Rapid Commun.* **2007**, 28, 101–108.

(84) Liu, Y.; Ke, C.-F.; Zhang, H.-Y.; Wu, W.-J.; Shi, J. *J. Org. Chem.* **2007**, 72, 280–283.

(85) Liu, Y.; Shi, J.; Chen, Y.; Ke, C.-F. *Angew. Chem., Int. Ed.* **2008**, 47, 7293–7296.

(86) Nally, R.; Scherman, O. A.; Isaacs, L. *Supramol. Chem.* **2010**, 22, 683–690.

(87) Das, D.; Scherman, O. A. *Isr. J. Chem.* **2011**, 51, 489–490.

(88) Chen, Y.; Zhang, Y.-M.; Liu, Y. *Isr. J. Chem.* **2011**, 51, 515–524.

(89) Bush, M. E.; Bouley, N. D.; Urbach, A. R. *J. Am. Chem. Soc.* **2005**, 127, 14511–14517.

(90) Praetorius, A.; Bailey, D. M.; Schwarzlose, T.; Nau, W. M. *Org. Lett.* **2008**, 10, 4089–4092

(91) Hennig, A.; Bakirci, H.; Nau, W. M. *Nat. Methods* **2007**, 4, 629–632.

(92) Saleh, N.; Koner, A. L.; Nau, W. M. *Angew. Chem., Int. Ed.* **2008**, 47, 5398–5401.

(93) Macartney, D. H. *Isr. J. Chem.* **2011**, 51, 600–615.

(94) Walker, S.; Oun, R.; McInnes, F. J.; Wheate, N. J. *Isr. J. Chem.* **2011**, 51, 616–624.

(95) Dong, N.; Xue, S.-F.; Zhu, Q.-J.; Tao, Z.; Zhao, Y.; Yang, L.-X. *Supramol. Chem*. **2008**, 20, 659–665.

(96) Park, K. M.; Suh, K.; Jung, H.; Lee, D.-W.; Ahn, Y.; Kim, J.; Baek, K.; Kim, K. *Chem. Commun.* **2009**, 71–73.

(97) Jeon, Y. J.; Kim, S.-Y.; Ko, Y. H.; Sakamoto, S.; Yamaguchi, K.; Kim, K. *Org. Biomol. Chem.* **2005**, 3, 2122–2125.

(98) Miyahara, Y.; Abe, K.; Inazu, T. *Angew. Chem., Int. Ed.* **2002**, 41, 3020–3023.

(99) Day, A. I.; Arnold, A. P.; Blanch, R. J. (Unisearch Limited, Australia), U.S. Patent US 2003/0140787, 2003 [Chem. Abstr. 2003, 139, 135453].

(100) Grechin, A. G.; Buschmann, H.-J.; Schollmeyer, E. *Angew. Chem., Int. Ed.* **2007**, 46, 6499–6501.

(101) Fusaro, L.; Locci, E.; Lai, A.; Luhmer, M. *J. Phys. Chem. B* **2008**, 112, 15014–15020.

(102) Lim, S.; Kim, H.; Selvapalam, N.; Kim, K.-J.; Cho, S. J.; Seo, G.; Kim, K. *Angew. Chem., Int. Ed*. **2008**, 47, 3352–3355.

(103) Huber, G.; Legrand, F.-X.; Lewin, V.; Baumann, D.; Heck, M.-P.; Berthault, P. *ChemPhysChem* **2011**, 12, 1053–1055.

(104) Kim, H.; Kim, Y.; Yoon, M.; Lim, S.; Park, S. M.; Seo, G.; Kim, K. *J. Am. Chem. Soc.* **2010**, 132, 12200–12202.

(105) Mock, W. L.; Irra, T. A.; Wepsiec, J. P.; Adhya, M. *J. Org. Chem*. **1989**, 54, 5302–5308.

(106) Jon, S. Y.; Ko, Y. H.; Park, S. H.; Kim, H.-J.; Kim, K. *Chem. Commun*. **2001**, 1938–1939.

(107) Pattabiraman, M.; Natarajan, A.; Kaanumalle, L. S.; Ramamurthy, V. *Org. Lett*. **2005**, 7, 529–532.

(108) Wang, R.; Yuan, L.; Macartney, D. H. *J. Org. Chem*. **2006**, 71, 1237–1239.

(109) Kloeck, C.; Dsouza, R. N.; Nau, W. M. *Org. Lett*. **2009**, 11, 2595–2598.

(110) Basilio, N.; Garcia-Rio, L.; Moreira, J. A.; Pessego, M. *J. Org. Chem*. **2010**, 75, 848–855.

(111) Lu, X.; Masson, E. *Org. Lett*. **2010**, 12, 2310–2313.

(112) Pemberton, B. C.; Singh, R. K.; Johnson, A. C.; Jockusch, S.; Da Silva, J. P.; Ugrinov, A.; Turro, N. J.; Srivastava, D. K.; Sivaguru, J. *Chem. Commun*. **2011**, 47, 6323–6325.

(113) Tuncel, D.; Uenal, O.; Artar, M. *Isr. J. Chem.* **2011**, 51, 525–532.

(114) Kim, K.; Selvapalam, N.; Ko, Y. H.; Park, K. M.; Kim, D.; Kim, *J. Chem. Soc. Rev.* **2007**, 36, 267–279.

(115) Ko, Y. H.; Hwang, I.; Lee, D.-W.; Kim, K. *Isr. J. Chem*. **2011**, 51, 506–514.

(116) Munteanu, M.; Choi, S.; Ritter, H. *Macromolecules* **2009**, 42, 3887–3891.

(117) Lagona, J.; Fettinger, J. C.; Isaacs, L. *J. Org. Chem*. **2005**, 70, 10381–10392.

(118) Wagner, B. D.; Boland, P. G.; Lagona, J.; Isaacs, L. *J. Phys. Chem. B* **2005**, 109, 7686–7691.

(119) Liu, S.; Kim, K.; Isaacs, L. *J. Org. Chem*. **2007**, 72, 6840–6847.

(120) Nally, R.; Isaacs, L. *Tetrahedron* **2009**, 65, 7249–7258.

(121) Wittenberg, J. B.; Costales, M. G.; Zavalij, P. Y.; Isaacs, L. *Chem. Commun*. **2011**, 47, 9420–9422.

(122) Stancl, M.; Svec, J.; Sindelar,V. *Isr. J. Chem.* **2011**, 51, 592–599.

(123) Lucas, D.; Isaacs, L. *Org. Lett*. **2011**, 13, 4112–4115.

(124) Day, A. I.; Arnold, A. P.; Blanch, R. J. (Unisearch Limited, Australia), PCT Int. Appl. WO 2000068232, 2000 [Chem. Abstr. 2000, 133, 362775].

(125) Blanch, R. J.; Sleeman, A. J.; White, T. J.; Arnold, A. P.; Day, A. I. *Nano Lett*. **2002**, 2, 147–149.

(126) Haris, S. P.; Zhang, Y.; Le Bourdonnec, B.; McCurdy, C. R.; Portoghese, P. S. *J. Med. Chem*. **2007**, 50, 3392–3396.

(127) Zhu, P. C.; Wang, D.-H.; Lu, K.; Mani, N. *Sci. China, Ser. B: Chem*. **2007**, 50, 249–252.

(128) Miao, Q.; Lefenfeld, M.; Nguyen, T.-Q.; Siegrist, T.; Kloc, C.; Nuckolls, C. *Adv. Mater*. **2005**, 17, 407–412.

(129) Samsonenko, D. G.; Virovets, A. V.; Lipkowski, J.; Gerasko, O. A.; Fedin, V. P. *J. Struct. Chem*. **2002**, 43, 664–668.

(130) Huang, W. H.; Zavalij, P. Y.; Isaacs, L. *Acta Crystallogr., Sect. E*: Struct. Rep. Online 2007, E63, o1060–o1062.

(131) Havel, V.; Svec, J.; Wimmerova, M.; Dusek, M.; Pojarova, M.; Sindelar, V. *Org. Lett.* **2011**, 13, 4000–4003.

(132) Chinai, J. M.; Taylor, A. B.; Ryno, L. M.; Hargreaves, N. D.; Morris, C. A.; Hart, P. J.; Urbach, A. R. *J. Am. Chem*. Soc. **2011**, 133, 8810–8813.

(133) Buschmann, H. J.;Cleve, E.; Schollmeyer, E. *Inorg. Chim. Acta* **1992**, 193, 93–97.

(134) Jeon, Y.-M.; Kim, J.; Whang, D.; Kim, K. *J. Am. Chem. Soc*. **1996**, 118, 9790–9791.

(135) Gerasko, O. A.; Sokolov, M. N.; Fedin, V. P. *Pure Appl. Chem*. **2004**, 76, 1633–1646.

(136) Rekharsky, M. V.; Ko, Y.-H.; Selvapalam, N.; Kim, K.; Inoue, Y. *Supramol. Chem*. **2007**, 19, 39–46.

(137) Jeon, W. S.; Kim, E.; Ko, Y. H.; Hwang, I.; Lee, J. W.; Kim, S.- Y.; Kim, H.-J.; Kim, K. *Angew. Chem., Int. Ed*. **2005**, 44, 87–91.

(138) Jeon, W. S.; Ziganshina, A. Y.; Lee, J. W.; Ko, Y. H.; Kang, J.-K.; Lee, C.; Kim, K. *Angew. Chem., Int. Ed*. **2003**, 42, 4097–4100.

(139) Nguyen, H. D.; Dang, D. T.; van Dongen, J. L. J.; Brunsveld, L. *Angew. Chem., Int. Ed.* **2010**, 49, 895–898.

(140) Tuncel, D.; Steinke, J. H. G. *Macromolecules* **2004**, 37, 288–302.

(141) Barooah, N.; Pemberton, B. C.; Sivaguru, *J. Org. Lett*. **2008**, 10, 3339–3342.

(142) Pattabiraman, M.; Kaanumalle, L. S.; Natarajan, A.; Ramamurthy, V. *Langmuir* **2006**, 22, 7605–7609.

(143) Baumes, L. A.; Sogo, M. B.; Montes-Navajes, P.; Corma, A.; Garcia, H. *Chem.; Eur. J.* **2010**, 16, 4489–4495.

(144) Appel, E. A.; Biedermann, F.; Rauwald, U.; Jones, S. T.; Zayed, J. M.; Scherman, O. A. *J. Am. Chem. Soc*. **2010**, 132, 14251– 14260.

(145) Wang, W.; Kaifer, A. E. *Angew. Chem., Int. Ed*. **2006**, 45, 7042–7046.

(146) Kim, K.; Kim, D.; Lee, J. W.; Ko, Y. H.; Kim, K. *Chem. Commun*. **2004**, 848–849.

(147) Liu, Y.; Yu, Y.; Gao, J.; Wang, Z. *Angew. Chem., Int. Ed*. **2010**, 49, 6576–6579.

(148) McInnes, F. J.; Anthony, N. G.; Kennedy, A. R.; Wheate, N. *J. Org. Biomol. Chem.* **2010**, 8, 765–773.

(149) Angelos, S.; Khashab, N. M.; Yang, Y.-W.; Trabolsi, A.; Khatib, H. A.; Stoddart, J. F.; Zink, J. I. *J. Am. Chem. Soc*. **2009**, 131, 12912–12914.

(150) Marquez, C.; Hudgins, R. R.; Nau, W. M. *J. Am. Chem. Soc*. **2004**, 126, 5806–5816.

(151) Stancl, M.; Hodan, M.; Sindelar, V. *Org. Lett*. **2009**, 11, 4184–4187.

(152) Moghaddam, S.; Yang, C.; Rekharsky, M.; Ko, Y. H.; Kim, K.; Inoue, Y.; Gilson, M. K. *J. Am. Chem. Soc*. **2011**, 133, 3570–3581.

(153) Lakowicz, J. R. *Principles of Fluorescence Spectroscopy*, Springer, New York, 3rd Ed., 2006.

(154) Biomedical Aspects of Histamine: Current Perspectives; Shahid, M., Khardori, N., Khan, R. A., Tripathi, T., Eds.; Springer: New York, 2010; Histamine: Biology and Medical Aspects; Falus, A., Ed.; S. Karger AG: Basel; **2004**.